AARHUS UNIVERSITY

UNIVERSITY of York

Key mechanisms in the formation of proteinaceous biofilm matrices in *Staphylococcus aureus* and *Staphylococcus epidermidis*

Dominique C. S. Evans

PhD Dissertation

March 2021

Department of Physics

University of York, UK

and

Interdisciplinary Nanoscience Centre

Aarhus University, Denmark

Abstract (English)

Staphylococcus aureus and *Staphylococcus epidermidis* are major human pathogens and are the leading causes of implant associated infections. After insertion into the body, implants become coated in host proteins, which *S. aureus* and *S. epidermidis* use to establish infections. They utilise many surface and secreted proteins that interact with these host proteins to increase attachment to implant surfaces, increase biofilm accumulation, and evade the immune system.

S. aureus secretes two coagulases, Coagulase (Coa) and von Willebrand factor binding protein (vWbp), which hijack the host coagulation cascade and trigger the formation of a fibrin network that is a key structure in *S. aureus* biofilms and shields bacteria from the immune system. We explored which factors cause coagulase expression, the localisation and dynamics of fibrin formation in growing biofilms, and cell-cell variation in fibrin binding using coagulation assays, time lapse confocal microscopy, and single molecule imaging of Coa:SNAP, Coa:msfGFP, and vWbp:CLIP fusion proteins. Host factors increased coagulase production and loosely associated Coa and vWbp to cell surfaces. Coa mainly localised to cell surfaces to produce a surface attached fibrin pseudocapsule, but could also form fibrin in the wider biofilm matrix. vWbp produced matrix-associated fibrin in the absence of Coa, but associated to cell surfaces to accelerate pseudocapsule production when Coa was also present. These findings indicate a more collaborative role between Coa and vWbp in building the fibrin network than previously suggested. Not all bacteria appeared to contribute to forming fibrin: we identified a slowly- or non-dividing subpopulation of bacteria that did not form a pseudocapsule. We speculated that these bacteria either lack the surface proteins required to bind fibrin, do not produce coagulases and therefore cannot produce fibrin, or both.

Extracellular matrix binding protein (Embp) is a giant surface protein expressed by *S. epidermidis* that attaches biofilms to fibronectin coated surfaces. We aimed to visualise Embp in *S. epidermidis* biofilms to further investigate its biological role in biofilm formation by constructing fusion proteins with the SNAP tag and monomeric superfolder GFP (msfGFP), but the fusion proteins could not be visualised. This was likely due to improper placement of the protein tags, which were placed before a putative cleavage site after the signal peptide. However, we demonstrated that msfGFP could be successfully secreted by *S. aureus*, either when fused to a Sec signal peptide or to Coa, which demonstrates that it is a good candidate for labelling extracellular proteins. We also visualised the SNAP tag when secreted at the cross wall during cell division by *S. aureus*, the same mechanism used to secrete Embp, and therefore envision that it is possible to visualise Embp with one of these two protein tags if the tag is placed after the cleavage site instead.

Abstract (Dansk)

Staphylococcus aureus og *Staphylococcus epidermidis* er betydningsfulde humane patogener og den hyppigste årsag til implantat-relaterede infektioner. Når et implantat indsættes i kroppen dækkes det af værtsproteiner. *S. aureus* og *S. epidermidis* interagerer med disse værtsproteiner via overfladeproteiner og udskilte proteiner. Interaktionen udnyttes til at etablere infektionen, øge fasthæftningen til implantatoverfladen, øge akkumuleringen af biofilm og undvige immunsystemet.

S. aureus udskiller to koagulaser; Coagulase (Coa) og von Willebrand factor binding protein (vWbp). Ved at kapre værtens koagulationskaskade igangsætter disse dannelsen af et fibrinnetværk og herved dannelsen af en *S. aureus* biofilm nøglestruktur der skærmer bakterierne fra immunsystemet. Vi undersøgte hvilke faktorer, der påvirkede koagulase dannelse, lokalisering og dynamik af fribrindannelsen i voksende biofilm, samt intercellulær variation i bindingen af fibrin, ved brug af koagulationsassays, time lapse konfocal mikroskopi og single molecule imaging af Coa:SNAP, Coa:msfGFP, og vWbp:CLIP fusions proteiner. Værtsfaktorer øgede produktionen af koagulase og associerede løst Coa og vWbp til overfladen af cellen. Coa lokaliserede hovedsageligt ved celleoverfladen, for produktion af en celleoverflade bundet fibrin pseudokapsel, men diffunderede også væk fra cellerne for at danne fibrin i biofilmmatrixen. vWbp dannede i fravær af Coa matrix-associeret fibrin, men med Coa til stede, associeredes vWbp ligeledes med celleoverfladen og accelererede produktionen af pseudokapsler. Disse observationer antyder et tættere samspil mellem Coa og vWbp, i dannelsen af et fibrinnetværk, end tidligere foreslået. Ikke alle bakterier virkede til at bidrage til dannelsen af fibrin: vi identificerede langsomt- eller ikke-delende subpopulationer af bakterier, der ikke dannede pseudokapsler. Vi hypotiserede at disse bakterier enten mangler de overfladeproteiner, som er nødvendige for at binde fibrin, at de ikke producerer koagulaser og derfor ikke kan producere fibrin, eller at begge dele er tilfældet.

Extracellular matrix binding protein (Embp) er et enormt overfladeprotein, udtrykt af *S. epidermidis*, der hæfter biofilm til fibronectin belagte overflader. Vi ønskede at visualisere Embp i *S. epidermidis* biofilm, og videre undersøge dens biologiske rolle i dannelsen af biofilm, ved at konstruere fusions proteiner med SNAP tagget og monomeric superfolder GFP (msfGFP). Men fusionsproteinet kunne ikke visualiseres. Dette skyldes sandsynligvis en uhensigtsmæssig placering af protein tags forinden et formodet spaltningssted efter signalpeptidet. Vi demonstrerede imidlertid, at *S. aureus* med succes kan udskille msfGFP sammensat med et Sec signalpeptid eller Coa, hvilket demonstrerer, at den udgør en oplagt kandidat for mærkning af extracellulære proteiner. Vi visualiserede desuden SNAP tagget udskilt ved tværvæggen under celledeling af *S. aureus*, via den same mekanisme som anvendes til at udskille Embp og forudser derfor en mulig visualisering af Embp med en af disse to proteinmærker, hvis mærket istedet er placeret efter spaltestedet.

Table of Contents

Acknowledgements

I will always remember my time as a PhD student. I feel lucky to have worked as part of two fantastic research groups in two different countries and for the wonderful opportunity that this PhD has been to work in such an interdisciplinary field. First of all, I would like to say a big thank you to both of my supervisors, Mark Leake and Rikke Meyer. Without you, I would not have had the opportunity to work on this project. Thank you for always believing in me and for all of the advice and encouragement you gave me throughout my work. Our meetings motivated and inspired me to do the best that I could.

Thank you as well to all members of the Leake and Biofilm groups. I learned so much from you through chatting about our work and it was a pleasure to work alongside you in the lab. It was especially daunting to move to another country for part of my PhD that I had never visited before, but both groups always welcomed me and now I can say that I feel at home in two places and that I have made some lifelong friends. A special thank you to all of the people I collaborated with throughout my project: Olatz Niembro, Melissa Eriksen, Baskhar Pradhan, Kristian Rasmussen, Lisbeth Marcussen, Amanda Khamas, Maiken Petersen, Maiken Voss, Amalie Maria Grønning, Cecilie Bach-Nielsen, Nasar Kahn, and Alex Payne-Dwyer. Also thank you to Sean Birk Bek Craig and Cindy Dreier for translating the abstract of this thesis into Danish.

Finally, I thank my family and friends, old and new, for the love and support you provided throughout this PhD and for understanding when I am away in a different place for long stretches of time.

Author's Declaration

This dissertation has been submitted to the Graduate School of Natural Sciences (GSNS) at Aarhus University for a PhD in Nanoscience awarded jointly by Aarhus University, Denmark, and the University of York, UK. The research in this PhD dissertation was conducted jointly at both universities and was supervised jointly by Prof. Mark C. Leake (University of York) and Assoc. Prof. Rikke L. Meyer (Aarhus University). This PhD was part of the Aarhus University 4 + 4 program and the midway qualifying examination was also a defence for a Master of Science in Nanoscience. In accordance with GSNS rules, parts of this thesis were also used in the progress report for the qualifying examination.

1. Introduction

1.1 Introduction to biofilms

Biofilms are the predominant form of bacterial life [1], which is no surprise because the biofilm is excellent at promoting the survival of the bacteria within [2]. Biofilms contain aggregates of bacteria (or other microorganisms like fungi, algae, or archaea) encased in an extracellular matrix, are capable of withstanding stress, and promote survival in a variety of different environments [3]. Biofilms can be found almost everywhere: in soil and on plants, on ship hulls and in pipes, as commensals of the gut flora, and in infections [2]. In fact, it is difficult to imagine a place completely free of biofilms: even highly inhospitable environments such as deep-sea vents and hot springs contain biofilms [4][5]. Biofilms have even been found in outer space, where they contaminated equipment whilst still on Earth and caused damage that led to equipment malfunction once in orbit [6].

Biofilms provide an excellent environment in which to survive by taking advantage of their surroundings and of limited nutrients. Biofilms incorporate minerals from their environment and retain them within their extracellular matrix, and retain debris from lysed cells that can be reused as a nutrient source later [3]. Biofilms are also comprised of up to 97 % water [2], and the extracellular matrix limits both the intake and loss of water, giving bacteria time to adjust to sudden environmental changes and preventing dehydration [7]. Biofilms provide the proximity to other bacteria needed for horizontal gene transfer and to facilitate cell-cell communication, which allows bacteria to respond to environmental triggers like nutrient gradients, changes in oxygen levels, or the presence of harmful chemicals [2]. Bacteria in biofilms are heterogeneous and adopt different phenotypes based on environmental cues. Bacteria in the centre of the biofilm grow more slowly due to limited nutrients [8], and other subpopulations of bacteria that serve different purposes can emerge. These include metabolically inactive persister cells that are distinct to the slow growing bacteria in the centre of biofilms, and which do not contribute to biofilm formation. Instead they benefit the population overall by surviving chemical threats like exposure to antibiotics [9].

The extracellular matrix is composed of many different molecules including polysaccharides, extracellular DNA (eDNA), and proteins [3]. Some of these components are self-produced, and others derived externally from the environment. Biofilm development usually begins with the reversible attachment of a bacterium to a surface via weak van der Waals forces [10]. This is followed by irreversible attachment by binding to environmental components via surface receptors, flagella, or secreted matrix components [10]. Next the biofilm accumulates by producing extracellular matrix while the bacteria divide and grow, and finally, biofilms degrade their matrix to disperse and release cells into the environment, allowing them to spread and establish new biofilms elsewhere [10]. It is worth noting that not all biofilms require a surface, for example, biofilms formed by *Pseudomonas aeruginosa* in infections of the lungs of cystic fibrosis patients are not surface attached [11]. Not all biofilms are comprised of the same molecules; each biofilm adapts to its own environmental niche. In addition to the above-mentioned extracellular matrix components, environmental biofilms can contain inorganic debris from the environment like clay particulates [12], and

they often contain multiple species of bacteria [13]. On the other hand, medical biofilms found in infections are simpler and are usually mono-species [13].

When bacteria colonise living tissue and form biofilms, they can cause chronic infections that evade the immune system and tolerate antibiotic treatment. Many infections involve biofilms, including endocarditis, chronic wounds, and implant infections on catheters, mechanical heart valves, shunts, and orthopaedic implants [14]. 1.5 – 2.5 % of patients with implanted medical devices get infections, which due to their chronic nature reduce quality of life as well as cause death and huge healthcare costs [15]. These biofilms are characterised *in vivo* by the presence of small, dispersed aggregates of matrix-enclosed bacteria of up to 200 nm in diameter [16], surrounded by a layer of immune cells at the biofilm surface [17], and are extremely tolerant to antibiotics. Biofilms can be up to 1000 times more tolerant to antibiotics than when bacteria are in a planktonic state [18], and these dosages are much higher than can be achieved clinically. The extracellular matrix restricts the penetration and diffusion of some antibiotics [19][20], and many antibiotics do not target the metabolically inactive cells within biofilms [8]. Furthermore, the presence of subpopulations of persister cells within biofilms complicates antibiotic treatments [21]. Most antibiotics disrupt processes carried out in metabolically active cells and therefore are ineffective against dormant persister cells. These bacteria persist after the antibiotics are removed, waking up to repopulate the biofilm and are thought to be a major reason behind chronic infections. Failure to eradicate a biofilm therefore leads to a temporary reduction in symptoms during antibiotic treatment, but the infection recurs shortly after treatment is stopped, and in the case of implant infections, the surgical removal and replacement of the infected device may be the only treatment option left [22]. Prolonged antibiotic treatment also increases the risk of acquiring genetic resistances to antibiotics [23], and therefore it is imperative to understand biofilms in order to develop better treatment options.

1.2 *Staphylococcus aureus*

Biofilm infections associated with implants are most commonly caused by Staphylococci, with *Staphylococcus aureus* and *Staphylococcus epidermidis* comprising approximately 70 % of the infections [24]. *S. aureus* is a non-motile, Gram positive, round-shaped bacteria characterised by its golden colony colour and grape like clusters of cells when visualised under a microscope. *S. aureus* colonises the skin and nares of approximately 20 – 30 % of the population as part of the normal flora [25]. However, it is an opportunistic pathogen, and causes disease when it breaches the skin and reaches the soft tissue or bloodstream [26]. It causes a large range of diseases, from superficial skin and soft tissue infections, to more serious conditions such as endocarditis, osteomyelitis, and sepsis [27]. It has numerous virulence factors that enable it to establish infections and cause disease, such as adhesins, toxins, and immune evasion factors [28].

S. aureus is one of the leading causes of implant associated infections, where bacteria colonise the surface of implants such as catheters, artificial joints, and pacemakers, and form a biofilm [27][29]. Infection of the implant can happen during insertion if *S. aureus* transfers from the patient's skin to the implant surface [30]. Once inside the body, implants get covered in numerous host proteins such as collagen, fibrinogen, and fibronectin. *S. aureus* expresses many surface receptors which recognise and bind host proteins and therefore attach

the bacteria to the implant [29][31]. Once attached, *S. aureus* divide and produce a biofilm, which helps them evade the immune system and increases tolerance to antibiotics [32]. Because the concentration of antibiotics required to eradicate a biofilm is usually higher than can be administered to a patient [32], implant infections can become chronic, and surgical removal and replacement of the infected device may be the only treatment option. Surgery is an unpleasant and risky procedure, which is best avoided. Therefore, we need to increase our understanding of biofilm infections in order to develop improved treatments and preventative measures.

S. aureus attaches to host proteins and uses them to create protein rich biofilms [33]. In the presence of plasma, *S. aureus* expresses a large family of surface proteins that bind host proteins which are called microbial surface components recognising adhesive matrix molecules (MSCRAMMs) [31][34]. Clumping factors A and B (ClfA and ClfB) are two MSCRAMMs which clump bacteria by binding fibrinogen and aid tissue colonisation [35]. Clumping is involved in several diseases including endocarditis, soft tissue infections, and osteomyelitis, and appears to protect bacteria from ingestion by immune cells once the aggregate becomes too large to ingest and increases tolerance to antibiotics by an unknown mechanism [35]. Fibronectin binging proteins A and B (FnBPA and FnBPB) not only bind fibronectin, but also fibrinogen and elastin, and therefore facilitate attachment to host tissues via a number of host proteins [35]. Collagen adhesin (Cna) facilitates attachment via collagen and helps to escape immune cells [31].

S. aureus also secretes proteins that bind to host components, called secretable expanded repertoire adhesive molecules (SERAMs). These include Extracellular adherence protein (Eap), Extracellular matrix protein-binding protein (Emp), and extracellular fibrinogen binding protein (Efp). Eap inhibits neutrophils and therefore inhibits the immune response [36], Emp binds host fibronectin, fibrinogen, and vitronectin [37], which appears to be important for virulence [35], and Efp inhibits phagocytosis [38] and decreases wound healing [39]. Overall, these SERAMs seem to be important for evading the immune system and increasing virulence.

1.3 Coagulase and von Willebrand factor binding protein

A hallmark of *S. aureus* is its ability to coagulate blood and form a fibrin clot. Fibrin, derived from host fibrinogen, is a key component of the biofilm extracellular matrix [40] and forms two concentric fibrin structures: a cell surface attached pseudocapsule, and an extended outer network, which act as mechanical barriers against immune attack [41], enhance virulence [42][4], and increase adhesion to surfaces [43]. Fibrin is the main constituent of blood clots, which serve to stop bleeding in response to an injury and promote wound healing. It is a fibrous protein formed by the enzymatic cleavage of fibrinogen, which then polymerises to form fibrin [44]. Fibrinogen is a large 340 kDa glycoprotein that exists in the blood at a concentration of about 2.5 g/l and it comprises of three pairs of chains: Aα, Bβ, and γ-chains [45]. Fibrinogen is usually converted to fibrin in response to an injury to form a blood clot by the host coagulation cascade (Figure 1). When an injury occurs, tissue factor is released into the bloodstream, which triggers a cascade reaction of clotting factors within the blood that ultimately results in the formation of a protein complex that cleaves blood protein prothrombin (fII) into its active form, thrombin (fIIa). It cleaves the N-terminus of

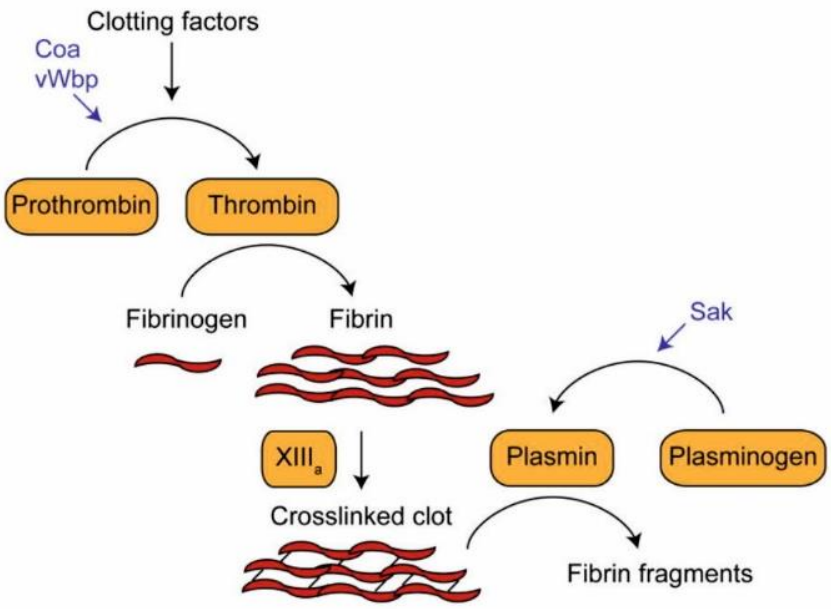

Figure 1 Simplified diagram of the coagulation cascade. In response to an injury, prothrombin is cleaved and activated. Once activated, it cleaves fibrinogen, which subsequently forms fibrin fibers. However, Coa and vWbp bind directly to prothrombin and activate it independently of the coagulation cascade. Image from [35].

prothrombin, and the new cleaved N-terminus inserts into a cleft within the protein, triggering a conformational change that exposes the active site of thrombin. Thrombin then cleaves fibrinopeptides A and B off fibrinogen to form fibrin monomers, which self assemble into fibrin fibers that form the clot. Thrombin further cleaves factor XIII (fXIII) and activates it (fXIIIa). Activated fXIIIa forms covalent cross links between adjacent fibrin fibers to stabilise the clot [46]. Fibrin clots can be subsequently broken down by plasminogen when it is activated by the tissue plasminogen activator [45].

S. aureus secretes two SERAMs, Coagulase (Coa) and von Willebrand factor binding protein (vWbp) that hijack the host coagulation cascade to trigger fibrin formation within the extracellular matrix independently of the host coagulation cascade (Figure 1). Coa and vWbp bind directly to prothrombin to form an activated complex known as Staphylothrombin, which cleaves fibrinogen and incorporates fibrin into the extracellular matrix. They both insert their first two N-terminal residues into the binding cleft of prothrombin, triggering a conformational change and activating it [47][48]. *S. aureus* also secretes Staphylokinase (Sak), which activates host plasmin to degrade fibrin and aid biofilm dispersal [49]. It is interesting that *S. aureus* secretes two proteins to produce fibrin rather than just one: it raises the question of whether Coa and vWbp serve different biological purposes, or whether their roles are redundant.

While both Coa and vWbp trigger fibrin formation, they do so with different kinetics [48], and have different binding capabilities that suggests differences in their interactions with other host proteins [50]. When Coa binds prothrombin, the complex becomes active and able to cleave fibrinogen immediately, whilst activation by vWbp requires further binding to fibrinogen and therefore occurs more slowly [48]. Coa contains a signal sequence (S) at its N-terminal, which signals Coa for export outside the cell. This is followed by the D1-D2

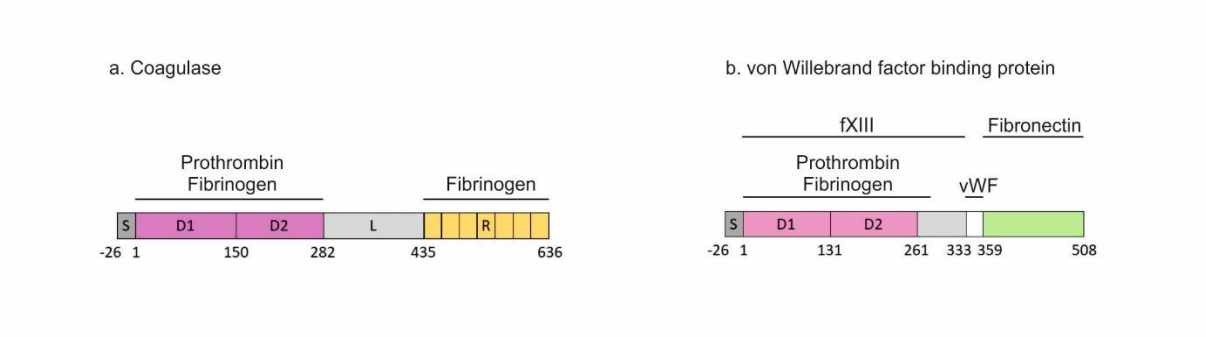

Figure 2 Domains of a) Coa and b) vWbp. Coa and vWbp both bind fibrinogen and prothrombin, and vWbp additionally binds fXIII, fibronectin, and von Willebrand factor. Image adapted from [50].

regions, which bind to the C-terminal of prothrombin, and also to fibrinogen. There is a central linker (L) region followed by the repeat (R) domain, which consists of multiple repeats of a 27 residue peptide that binds fibrinogen [51] (Figure 2a). Thomer *et al.* (2016) demonstrated that the R domain is necessary to form the fibrin pseudocapsule in *S. aureus* [50]. They compared bacteria grown in media supplemented with human plasma by wildtype *S. aureus* and *S. aureus* with Coa lacking the R domain. Only the strain with an intact R domain formed a pseudocapsule, and they hypothesised that the R domain limits the diffusion of Coa away from the bacteria to localise fibrin production to the vicinity of bacteria. However, the R domain is not required for clotting, as Coa lacking an R domain was still able to clot blood. The N-terminal of vWbp is homologous to that of Coa, and it can therefore also bind prothrombin and fibrinogen [52]. However it lacks any other fibrinogen binding capabilities, and instead has domains that bind other host proteins: fXIII [53], fibronectin [53], and von Willebrand factor (vWF) [52] (Figure 2b).

S. aureus mutants lacking Coa or vWbp are less virulent, particularly if both coagulases are lacking [42]. Inhibiting the active complex with prothrombin also decreases virulence in mice, reduces attachment to surfaces, and increases the ability of immune cells to clear the infection [54][43]. Furthermore, *S. aureus* that lacks vWbp coagulates blood more slowly than the wildtype, and *S. aureus* lacking Coa coagulates even more slowly [50]. Guggenberger *et al.* (2012) found that *S. aureus* lacking vWbp was unable to form the extended fibrin network, and *S. aureus* lacking Coa only partially formed the fibrin pseudocapsule, suggesting that Coa is primarily responsible for producing the pseudocapsule while vWbp forms the extended network [41]. Coa localises within the pseudocapsule [41][42] and accumulates at the periphery of abscess lesions [42], while vWbp is distributed throughout abscess lesions and accumulates at the periphery [42]. vWbp also has a higher affinity towards surface adsorbed fibrinogen than Coa while they both bind soluble fibrinogen equally [55].

Several biofilm treatments have been proposed that either target fibrin or the coagulases. For example, the use of fibrinolytic drugs in combination with antibiotics might break down the fibrin matrix and improve the antibiotic susceptibility of bacteria [56][57], and inhibition of Staphylothrombin reduces fibrin deposition on implants and increases antibiotic susceptibility [43]. Alternatively, vaccines and antibodies targeting Coa and vWbp trigger immune cells to kill *S. aureus* and prevent lethal infections in mice [58][50], and

coating implants in tissue plasminogen activator reduces biofilm formation and increases antibiotic susceptibility [59].

The differences found between Coa and vWbp suggest different roles for Coa and vWbp, such as Coa forming the pseudocapsule as a first line of defence against the immune system and vWbp diffusing further away to produce fibrin that attaches the biofilm to surfaces and provides a secondary barrier against immune cells. However, the mechanisms they use to carry out these distinct functions are unknown. By studying the mechanisms that Coa and vWbp use, we will further understand how they carry out different functions and deepen our understanding of why *S. aureus* produces two coagulases.

1.4 *Staphylococcus epidermidis*

Staphylococcus epidermidis is a Gram-positive, coagulase negative, non-motile cocci that was originally named *Staphylococcus albus* due to forming white colonies that distinguished it from the golden *S. aureus.* It is a generally harmless [60] and ubiquitous commensal of the skin [61]. Compared to the more pathogenic *S. aureus*, *S. epidermidis* does not express aggressive toxins that cause disease [60]. In fact, *S. epidermidis* usually has a rather benign relationship with its host and there is growing awareness that it plays a role in modulating the host immune system to promote the survival of commensals [62] and provides some protection against colonisation by pathogens such as *S. aureus* [60].

Despite its apparent harmlessness, *S. epidermidis* is the most frequent cause of implant associated infections. It causes up to 70 % of catheter related infections, over half of central nervous system shunt infections, and is the leading cause of orthopaedic implant infections [63]. *S. epidermidis* is a major source of infection because it is so abundant on our skin, but disease tends to occur in patients with predisposing characteristics such as premature birth, infection with HIV, or taking immunosuppression medication [64]. *S. epidermidis* infections are persistent and difficult to eradicate with antibiotics [64] and it is has become apparent that *S. epidermidis* main route to virulence is its ability to form biofilms [65]. Overuse of antibiotics to treat *S. epidermidis* infections has also lead to the development of numerous antibiotic resistant strains [60], and there is growing concern over *S. epidermidis* infections as the population ages and the use of implanted medical devices increases.

S. epidermidis forms biofilms with matrices comprised of a combination of polysaccharide intercellular adhesin (PIA), proteins, and eDNA, all of which are resistant to phagocytosis [60][66]. About one third of device related infections are caused by strains that do not produce PIA [66], and genes encoding biofilm forming proteins such as Accumulation associated protein (Aap) are widespread in clinical isolates [67]. Similar to *S. aureus*, *S. epidermidis* expresses a number of surface associated MSCRAMMs as well as other cell wall anchored proteins, which interact with host extracellular matrix components [68]. Aap is a cell wall anchored protein that binds fibrinogen, fibronectin, and vitronectin [60], and promotes attachment to both epithelial cells and artificial surfaces [63][69]. It promotes attachment to abiotic surfaces via its N-terminal A domain [69] and also increases biofilm accumulation when the A domain is cleaved [70]. Autolysin E (AtlE) releases eDNA from a fraction of cells within the population to aid primary attachment to abiotic surfaces [71] and might also bind surface immobilised fibronectin, fibrinogen, and fibronectin [68]. *S. epidermidis* serine-aspartate repeat protein (SdrG) initiates implant infections by binding to

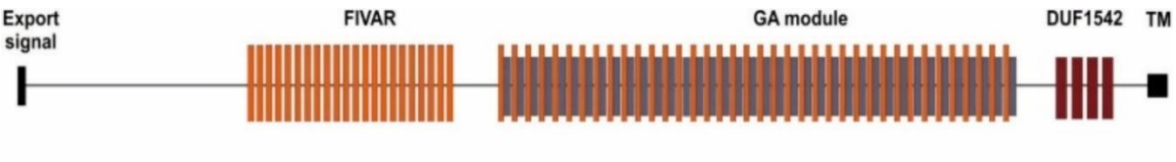

Figure 3 Diagram of Embp domains taken from [64].

immobilised fibrinogen [72] and its interaction is strengthened by shear stress, which allows it to withstand mechanical stress *in vivo* [73].

1.5 Extracellular matrix binding protein

Extracellular matrix binding protein (Embp) is a giant 1 MDa surface protein of *S. epidermidis* [74] present in 90 % of clinical isolates [64] that increases attachment to fibronectin coated surfaces, promotes biofilm accumulation, and inhibits uptake by phagocytosis [75][76]. It contains an N-terminal YSIRK/GS export signal followed by 21 found in various architecture (FIVAR) repeats and 38 repeats with alternating FIVAR and G-related albumin binding motifs (FIVAR-GA). Its C-terminal contains a domain of unknown function followed by a putative transmembrane domain [75] (Figure 3).

Overexpression of *embp* increases bacterial adhesion to fibronectin coated surfaces, but not artificial polystyrene surfaces [75]. Fibronectin is a host glycoprotein that circulates the blood in a globular conformation and exists in the host extracellular matrix in a fibrillar conformation [77]. It is involved in a variety of biological processes such as adhesion to the extracellular matrix, mobility, growth, and differentiation [78]. Embp binds surface immobilised fibronectin via its FIVAR modules [75], which probably aids bacterial colonisation of fibronectin coated implants *in vivo*. Embp is also an intercellular adhesin and promotes biofilm formation by an unknown mechanism involving interactions of the FIVAR-GA domains with adjacent cells [75]. The FIVAR domains are sufficient to bind surface immobilised fibronectin but do not promote biofilm formation alone. Embp mediated clumping also serves to protect bacteria from the immune system by inhibiting phagocytosis [76]. Embp localises to both cell surfaces and within the extracellular matrix when visualised with anti-Embp antibodies [76][79][80]. Embp has also been suggested as a potential target for biofilm prevention strategies after anti-Embp antibodies were shown to inhibit *S. epidermidis* biofilm formation [81].

Embp is only expressed at very low levels when grown in ordinary lab media [75]. This raises the question of when *embp* is expressed. Expression of *embp* increases when grown in the presence of human serum [75], the fluid component of blood with red blood cells and clotting factors removed. Therefore, exposure to host components might trigger Embp production during an infection. Sub-inhibitory concentrations of the antibiotic tigecycline also increases *embp* expression, and therefore treatments with insufficient concentrations of certain antibiotics might stimulate biofilm formation rather than treating the infection [80]. Expression also increases under osmotic stress in biofilms, but not planktonic cultures [79]. Skin has fluctuating water and salt levels and therefore fluctuating osmotic stress. This finding could therefore indicate an additional role of Embp in skin colonisation where *S. epidermidis* is a harmless commensal [79].

In vitro evidence indicates multiple biological roles for Embp in mediating attachment to surfaces and host tissues containing fibronectin, increasing biofilm formation, and evading the immune system. However, there is still much to discover about Embp. There still remain questions over the quantity of Embp that is produced and under what conditions, whether all cells produce Embp, how its localisation is related to its function, and the mechanisms that it uses to interact with host proteins, especially under *in vivo* or *in vivo*-like conditions. By answering these sorts of questions, we will further understand why *S. epidermidis* produces Embp, how it functions, its clinical significance, and might learn new ways to target Embp for biofilm treatment or prevention.

1.6 Fluorescence microscopy

Fluorescence microscopy is a valuable tool for imaging whole cells or biological molecules that are tagged with a fluorescent dye or protein. Fluorescence microscopy has allowed researchers to visualise bacteria and extracellular matrix components in both *in vitro* and *in vivo* biofilms. For example, fluorescence microscopy has been used to reveal the spatial distribution and localisation of extracellular matrix components such as extracellular DNA, polysaccharides, and proteins [82][83][56], to study the penetration of antibiotics through biofilms [84], different metabolic activities within biofilms [85], biofilm formation [86], and the distribution of multiple species of bacteria tagged by different colours [87]. Fluorescence microscopy therefore allows researchers to probe the environment of living and fixed samples in a minimally invasive way, to study several fluorescently tagged molecules simultaneously via multicolour imaging, to study structures within the extracellular matrix, and in some cases to follow dynamic processes.

Fluorescence is light emitted from atoms as their electrons transition from an excited state to the ground state, and can be described by a Jablonski diagram (Figure 4a). An electron is excited when it absorbs an incoming photon, which provides the energy required to transition to a higher energy state. Once excited, the electron loses a small amount of energy due to vibrational losses before transitioning back to the ground state by emitting a photon. The energy E of a photon is related to its wavelength λ by $E = hc/\lambda$. h is Planck's constant and c is the speed of light. Because the excited electron loses energy before de-exciting, the emitted photon therefore has lower energy and a longer wavelength than the absorbed photon. Fluorescence microscopes utilise this process to visualise samples labelled with a fluorescent tag. There are many different fluorescence microscope designs, but they share the same basic principles. A laser is used to excite samples that have been labelled with a fluorescent dye or fluorescent protein. Fluorescence emitted from the sample is collected through an objective lens and focussed onto a camera, which records an image of the fluorescence. Excitation and emission light usually passes through the same objective lens, and a dichroic mirror is used in combination with excitation and emission filters to distinguish the two. The excitation filter is placed in the excitation pathway and blocks undesired excitation wavelengths, the emission filter is placed in the imaging pathway to block excitation wavelengths and transmit emission wavelengths, and the dichroic mirror is placed between the excitation and emission filters. It reflects excitation light towards the sample whilst transmitting emission light. Imaging samples and collecting emissions through

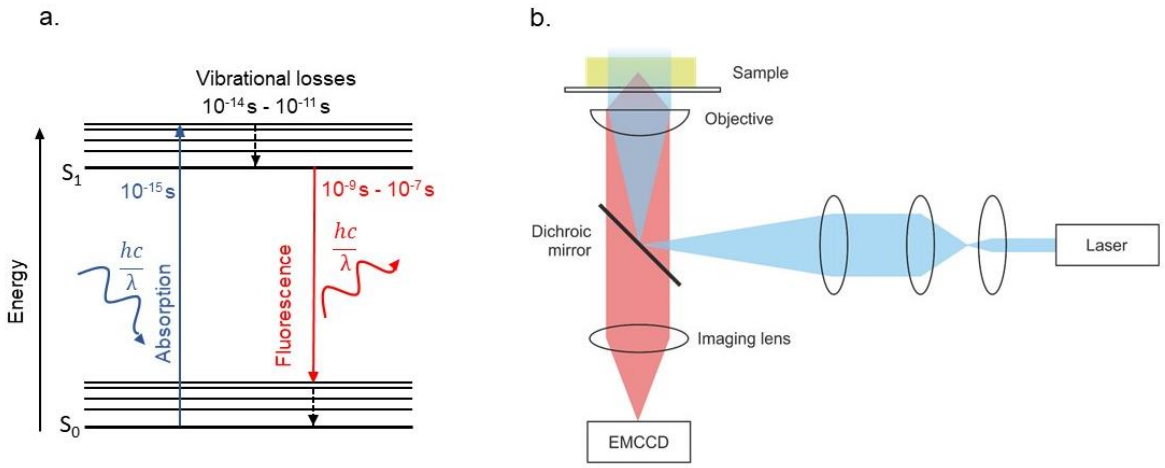

Figure 4 a) Jablonski diagram illustrating fluorescence. b) Basic optical setup of an epifluorescence microscope.

the same objective lens is called epifluorescence, and when imaging with a parallel beam of light it is called widefield microscopy (Figure 4b).

Signal to noise ratio is an important consideration in microscopy, defined as the ratio of fluorescence signal detected to noise arising from background fluorescence, variation in the incident photon flux (shot noise), and the detector itself (readout and dark noise). To get the best image quality, signal to noise ratio should be maximised. Some noise is inevitable: shot noise is present in all imaging systems because it is a fundamental property of light arising from statistical fluctuations in the number of emitted photons [88]. Readout noise is a fundamental property of charge-coupled devices (CCDs), sensors commonly used in camera chips, generated when converting charge carriers to a voltage signal [88]. Dark noise arises from thermally generated charge carriers in the CCD detector that are produced in the absence of incident light, but can be reduced by cooling the CCD [88]. One way to overcome noise and increase signal to noise ratio is to use a high numerical aperture (NA) objective lens. The NA of an objective lens is given by $nsin\theta$, where n is imaging medium refractive index and θ the half-maximum angle of a ray of light that the objective lens can capture [89]. High NA objectives improve signal by capturing more photons, with the trade-off of having a smaller depth of focus [89]. Another strategy is to use bright fluorescent dyes that provide a large fluorescent signal. Cells have intrinsic fluorescence known as autofluorescence if they contain fluorescent biomolecules such as collagen, elastin, flavins, NAD(P)H, or aromatic amino acids [90], that reduces signal to noise ratio. Most autofluorescence occurs when exciting with shorter wavelengths of approximately 300 – 500 nm and emits at approximately 350 – 550 nm [90]. Therefore, if autofluorescence is a large problem it is better to select dyes that are far red. A further source of noise arises from out of plane fluorescence. In an epifluorescence microscope, the planes above and below the focal plane are also excited, producing out of plane fluorescence and decreasing signal to noise ratio. Therefore, one major way to improve signal to noise ratio is to change the optical design of the microscope such that background from out of focus fluorescence is reduced.

Confocal laser scanning microscopy (CLSM) is a common microscope design that blocks out of plane fluorescence, and is generally considered to be the gold standard for imaging biofilms [91]. In CLSM, the laser is focussed within the sample and scanned to build up a 2D optical section. A pinhole is placed in the imaging pathway in a conjugate focal plane to block out of focus fluorescence and only allow fluorescence from the focal plane to reach the detector. A second pinhole is placed in the excitation pathway to improve optical sectioning. Therefore, CSLM has improved signal to noise ratio compared to widefield epifluorescence. An additional advantage is that optical sections taken in different Z-planes can be processed to produce a 3D image, which is particularly useful when studying a complex 3D structure such as a biofilm. A disadvantage of CLSM is that it is slow because it requires scanning to build up an image. Therefore, fast, dynamic processes cannot be measured, and it also has a limited depth of focus. It also suffers from disadvantages common to all fluorescence microscopes; fluorophores accumulate chemical damage during fluorescence that causes them to lose their ability to fluoresce, which is known as photobleaching, and extended exposure to light is phototoxic to cells [92][93]. Hence, samples cannot be imaged for long stretches of time without decreasing emissions due to photobleaching and the risk of damage to cells or cell death due to phototoxicity. Nevertheless, CLSM is an excellent tool for imaging biofilms and is widely used today.

Other microscopy techniques such as single molecule fluorescence microscopy enable the detection and quantification of single molecules and could enable researchers to study biofilms on smaller length scales. Berk *et al.* investigated the assembly of proteins and polysaccharides in the extracellular matrix of early *Vibrio cholerae* biofilms using stochastic optical reconstruction microscopy [94], a single molecule detection technique, but overall there seems to be a lack of single molecule fluorescence microscopy in biofilm research. Single molecule fluorescence microscopy has the potential however to reveal more about the molecular mechanisms and interactions that biofilms use to initiate themselves, produce their extracellular matrix, and interact with host cells and proteins.

1.7 Single molecule fluorescence microscopy

Single molecule fluorescence microscopy allows the detection and characterisation of single proteins and other biomolecules in living cells with high spatial and temporal resolution [95]. Single molecules can be detected inside cells to reveal their subcellular localisation, stoichiometry, and spatial distribution [96][97]. Single molecule trajectories can also be tracked using movies with millisecond frame rates to reveal information on dynamics, molecular interactions, diffusion properties, and binding kinetics [98][99]. Single molecule detection also provides information on protein copy number and heterogeneity within molecular subpopulations [98], which is not possible with bulk ensemble methods.

Single fluorophores do not emit a very bright signal compared to the level of background noise, and a challenge in single molecule microscopy is to detect this signal over the relatively large autofluorescence background by increasing the signal to noise ratio [100]. Signal to noise ratio can be increased with improved camera detectors and the use of bright variants of fluorescent proteins or organic fluorophores. There are also some optical designs that increase signal to noise ratio. Total internal reflection microscopy (TIRF) [101] is a common single molecule detection method in which the laser is directed towards the sample

at an angle greater than the critical angle such that it undergoes total internal reflection. This creates an evanescent field at the sample that decays exponentially with distance from the sample, and excites the sample up to a depth of about 100 nm. Because the excitation field is so thin, there is minimal out of focus fluorescence and the signal to noise ratio is large. TIRF is particularly good for imaging cell membrane proteins when the cells are immobilised on a cover glass [100]. However, a disadvantage when imaging biofilms would be that you are limited to only imaging the very bottom surface of the sample when there may be interesting features deeper within the sample. Other optical methods to increase signal to noise ratio involve shrinking the excitation beam to a diameter of about 10 μm for narrowfield epifluorescence, which increases the local beam intensity to levels sufficient for single molecule detection with millisecond sampling [102]. A similar method is slimfield epifluorescence, in which the incident laser under fills the back aperture of the objective lens to produce an expanded focus within the sample [103].

The above methods alone are still diffraction limited, that is to say that if fluorescent spots produced by single molecules are separated by less than the diffraction limited optical resolution, then they cannot be spatially resolved. Light emitted from a fluorophore diffracts as it passes through the objective lens to produce an Airy disk diffraction pattern, which has a bright central spot surrounded by concentric rings of increasing radius. The limit of optical resolution is given by the Rayleigh criterion, which approximates the minimum separation of two spots required to be spatially resolved as $d = 0.61\lambda/NA$, the distance at which the central maximum of one Airy disk aligns with the first minimum of the other [100]. λ is the wavelength of the light and NA the numerical aperture of the objective lens. This means that the optical resolution is limited to roughly half the wavelength of light (about 200 – 300 nm), which can inhibit detection of single molecules when molecules are closer together than this.

Apparent spatial resolution can be improved upon by image processing methods used after data acquisition. Light emitted from a single fluorophore appears as a blurry spot larger than its real size due to diffraction and convolution with the point spread function, a property of the imaging system that describes the shape of a point source as determined by the wavelength of light and numerical aperture of the objective lens. To process this data, an approximate of the theoretical point spread function is fitted to the spots and the positions of their centres estimated with high spatial precision that is higher than the optical resolution limit. These methods work provided that there is a relatively low concentration of single fluorophores. Complexes containing several fluorophores can sometimes still be distinguished because they will appear as single spots with higher fluorescence intensities than single fluorophores, but there is an upper limit where this analysis becomes ineffective [89].

To overcome overcrowding issues, there are imaging techniques that allow fewer fluorophores to be excited at once. TIRF delimits the excitation field to a shallow depth of around 100 nm, thus reducing the number of fluorophores detected by omitting detection outside this range. This does not improve the lateral resolution but it is often sufficient to overcome the issue. Other techniques include stochastic optical reconstruction microscopy (STORM) [104] and photoactivated localisation microscopy (PALM) [105]. These techniques both take a large number of images where a limited number of fluorophores are excited so that their spots do not overlap. PALM uses photoactivatable fluorophores that emit

light when activated by laser irradiation and bleach shortly afterwards, whilst STORM uses photoswitchable fluorophores that switch between bright and dark states. These processes are stochastic, therefore only a small subpopulation of fluorophores fluoresce at one time.

1.8 Fluorescent fusion proteins

Fusion proteins are a method of visualising proteins in which a protein tag is fused to a protein of interest and then imaged using fluorescence microscopy. Fusion proteins have enabled researchers to probe microorganisms on the subcellular level and study protein biology *in vivo* by shedding light on protein localisation, dynamics, and associations to other proteins [106]. To create a fusion protein, the gene for the protein tag is inserted in frame at the start or end of the gene for the protein of interest. The end is selected because proteins usually fold with their termini exposed [107], and if there is a functional domain at one end of the protein, the tag is inserted at the other end so that it does not impair the function of that domain. The protein and tag are usually separated by a linker, a short sequence of amino acids that provides flexibility and allows both the protein and tag to fold without steric hindrance [108]. Fusion proteins are often over-expressed from a plasmid introduced into the cell, which is separate from the cells chromosome. Over-expression ensures that there is sufficient fluorescence intensity to detect, but can cause artefacts such as aggregation [109]. Over-expression artefacts can be avoided by expressing the fusion protein from the chromosome under native expression levels [110], which allows the study of the protein of interest with expression levels more similar to their usual levels.

The first fluorescent protein tag was green fluorescent protein (GFP). GFP is a protein that emits green light when excited by blue light. It has excitation peaks at 395 nm and 475 nm and an emission peak at 509 nm. GFP is a 2 – 4 nm long, barrel shaped protein that contains a chromophore formed by three neighbouring amino acids that is responsible for fluorescence [111]. Shimomura purified GFP from the jellyfish *Aequorea victoria* in 1962, where they discovered that the protein would emit green fluorescence upon illumination with ultraviolet light [112]. In 1994 Chalfie expressed GFP in *Escherichia coli* and *Caenorhabditis elegans* and confirmed that the organisms could fluoresce, used the fusion products to monitor gene expression, and suggested that GFP could be used to study protein localisation [113]. Tsien and co-workers also engineered GFP to fluoresce at different wavelengths with enhanced spectral properties [114], and for this work combined, Shimomura, Chalfie, and Tsien were awarded the Nobel prize in Chemistry in 2008. Since then an even broader palette of fluorescent proteins have been developed, including fluorescent proteins from other marine species [115] and proteins engineered to have enhanced brightness [116], different colours [114], or other properties [117] that make up an ever growing toolbox of proteins to use for fusions [118]. Not all fusion proteins need to be fluorescent: there are also non-fluorescent protein tags such as the SNAP tag [119] and HaloTag [120], which can be labelled with a substrate conjugated to a fluorescent dye that can offer brighter fluorescence than fluorescent proteins with the trade-off of needing to be labelled before imaging.

Other methods of labelling proteins for fluorescence microscopy include antibody labelling and pre-labelled protein conjugates. Proteins can be visualised directly via primary antibodies that recognise the protein of interest and are conjugated to a fluorescent dye, or

indirectly via secondary antibodies conjugated to a fluorescent dye, which recognise a non-fluorescent primary antibody that binds the protein of interest. The organic dyes that are conjugated to antibodies are usually very bright and therefore provide a high signal, and this signal is amplified when labelling with secondary antibodies because multiple secondary antibodies can bind to one primary antibody. However, antibody staining can lead to non-specific staining [121], where the antibody binds to targets other than the protein of interest and decreases signal to noise ratio. Additionally, cells are often fixed during staining to preserve cellular structures [121], which kills cells, and therefore fast and dynamic processes cannot be monitored in living cells. Furthermore, antibodies can have difficulty penetrating a biofilm extracellular matrix due to their large size of about 10 nm [122], and therefore may not always be a suitable method. Addition of pre-labelled protein-dye conjugates avoids issues such as non-specific staining, however, results in an artificially increased quantity of protein due to the presence of both native, unlabelled protein and the added pre-labelled protein, which does not reflect the native environment of the cell. Therefore, advantages of using fusion proteins are the ability to study proteins in their native environment in living cells, the study of dynamic processes, and lack of labelling when fluorescent fusion proteins are used. The labelling efficiency when using fluorescent proteins is also 100 % because the fluorescent fusion protein is encoded into the DNA of the cell. An important disadvantage to be aware of is that fusion sometimes impairs the biological function of the protein of interest or forms aggregates [123], therefore, if possible, it is important to verify that the fusion protein functions as expected before proceeding with imaging experiments [106]. It is also possible for the protein tag itself to misfold, or, in the case of fluorescent protein tags, otherwise fail to become fluorescent in some environments [124]. The periplasm of Gram negative bacteria was a challenging environment to image because it is oxidising and promotes the formation of disulphide bonds, which prevents the use of many GFP variants as protein tags in this environment. In the periplasm, GFP gets trapped in a non-fluorescent state and the chromophore does not form correctly due to cysteine residues in GFP forming disulphide bonds with each other, cysteine residues in adjacent GFP molecules, or other cysteine containing proteins during folding [124]. However, proteins in this region have been imaged using a specific variant of GFP called superfolder GFP (sfGFP) [124], which folds quickly enough that its cysteines do not form disulphide bonds. Fluorescent proteins are also generally dimmer than organic dyes and photobleach quickly [89]. The maturation time is also an important consideration. It is the time taken for the fluorescent protein to fold into its 3D conformation and for the chromophore to form and become fluorescent, and can be a short as a few minutes to as long as several hours depending on the fluorescent protein [125]. This can be an issue when imaging fluorescent proteins in living cells; it can take up to 40 minutes for half of a population of freshly produced enhanced GFP molecules to mature, and therefore it is likely that there will be a portion of GFP that have not become fluorescent yet during imaging [89].

2. Aim

The overall aim of this project is to investigate key mechanisms of matrix formation by proteins in biofilms formed by *S. aureus* and *S. epidermidis*, specifically Coa, vWbp, and Embp, aided by advanced methods from the physical sciences. Fibrin is a major component of *S. aureus* biofilms, and it is interesting to understand why *S. aureus* secrete two coagulases to trigger fibrin formation, and whether Coa and vWbp direct fibrin production to different locations in biofilms or not. I expect that Coa is necessary to form the fibrin pseudocapsule and will therefore localise to the surfaces of bacteria to enable pseudocapsule formation, while vWbp will be required to form fibrin in the extended network and will therefore localise in the wider biofilm. Embp is present in most clinical isolates of *S. epidermidis*, yet much is still unknown about its role *in vivo*. Embp binds to fibronectin, increases biofilm accumulation, and aids immune evasion, but it is not known how abundant Embp is, when it gets expressed, or whether all cells produce Embp. Embp is a surface protein that can get cleaved off and localise elsewhere, where it might contribute to matrix formation. Visualising Embp can help address these questions, and I anticipate that Embp will localise to cell surfaces and the wider biofilm matrix, and be produced only when in the presence of host factors.

To do investigate the roles of Coa, vWbp, and Embp in matrix production, I will develop and use the tools to visualise these proteins. I will create fusion proteins and visualise them in biofilms grown under *in vivo*-like conditions using confocal and single molecule microscopy, and I will construct a novel, bespoke single molecule fluorescence microscope in order to overcome the poor signal to noise ratio that arises when imaging complex biofilms. The project is broken down into more specific aims as follows:

1. To analyse the location, dynamics, and cell-cell variation of fibrin formation in biofilms growing under *in vivo*-like conditions using time lapse confocal microscopy of wildtype *S. aureus* 29213 as well as mutants lacking Coa, vWbp, or both (Chapter 3).
2. To determine the localisation of Coa and vWbp in planktonic cultures and biofilms using coagulation assays and by constructing and visualising genomically encoded C-terminal fusion proteins with mCherry and GFP (Coa:mCherry and vWbp:GFP) (Chapters 3, 4, and 5).
3. To establish whether monomeric superfolder GFP (msfGFP) - a bright, monomeric, and fast folding GFP variant - is a suitable protein tag for secreted proteins in Gram positive bacteria. Successful secretion of msfGFP by *S. aureus* 29213 will be assessed when fused to Tat- and Sec- signal peptides and when fused to Coa (Chapter 6).
4. To create a genomically encoded N-terminal fusion protein between Embp and GFP (GFP:Embp) in *S. epidermidis* 14.1.R1 and visualise it in biofilms grown under *in vivo* mimicking conditions (Chapter 7).
5. To develop and test a novel, bespoke fluorescence microscope that is tailored towards imaging single molecules in biofilms (Chapter 8).

3. The dynamics of fibrin production during biofilm formation

In this Chapter, I investigated how Coa and vWbp direct fibrin production to different locations within biofilms, how they affect the dynamics of fibrin production, and whether there is cell-cell variation in fibrin production. The results confirmed that Coa is necessary to form the fibrin pseudocapsule, and I discovered that vWbp accelerates the formation of the pseudocapsule in the presence of Coa. A small proportion of bacteria do not form a pseudocapsule, and I hypothesise that these bacteria do not produce the surface proteins required to bind fibrin.

3.1 Introduction

The host-derived fibrin network is a key structure in *S. aureus* biofilms that protects the bacteria from host immune defences, enhances their virulence, and increases adhesion to surfaces [42][54][43]. *S. aureus* secretes both Coa and vWbp, which hijack the host coagulation cascade to trigger fibrin production and incorporate it into the extracellular matrix in two concentric structures: a surface attached pseudocapsule and an extended fibrin network [41]. It is thought that Coa produces the pseudocapsule whilst vWbp produces the extended network [41], but it is still unclear whether Coa and vWbp have different biological purposes or whether their roles are redundant.

I collaborated with a number of colleagues to tackle this question. We began by experimenting with mutants of *S. aureus* that do not produce Coa, vWbp, or both, which allowed us to monitor phenotypic changes that occurred when one coagulase was lacking. I visualised the growth of the fibrin network in *S. aureus* biofilms and compared the phenotypes to infer the roles of each coagulase individually. I investigated how removing one coagulase changed how fibrin localised within the biofilm and altered the fibrin growth dynamics. Not all of these changes could be assessed by eye, so I adapted a bespoke software written by the Leake group at the University of York [126] to analyse the data. A hallmark of *S. aureus* is its ability to coagulate blood or plasma, and *S. aureus* that lacks vWbp coagulates blood more slowly than the wildtype, and even more slowly when lacking Coa [50]. My colleagues and I also conducted similar coagulation assays to assess whether Coa and vWbp associate to cell surfaces or are secreted to cell culture supernatants to give more insight into their biological roles and mechanisms that they use to influence fibrin localisation. As the experiments progressed, I discovered that there was a subpopulation of slowly- or non-growing bacteria within biofilms that did not form a fibrin pseudocapsule, and which could be distinguished by their bright fluorescence intensity. My colleagues and I further explored why these cells did not have a pseudocapsule, why their signal was so bright, and what their biological role could be.

I contributed to all aspects of these projects. I optimised and conducted time lapse imaging experiments of fibrin growth and analysed the data. For the analysis, I adapted some MATLAB software for single particle tracking that was originally written by Adam Wollman (University of York) [126]. I adapted his code to identify bacterial cells in biofilms, to identify bacteria belonging to growing and non-growing subpopulations, and wrote additional code to quantify fibrin belonging to the fibrin pseudocapsule. Adam contributed some

additional original code to quantify the relationship between fluorescence signal from fibrin and distance to the nearest cell. Amanda Khamas (Aarhus University) transformed a plasmid with *gfp* into *S. aureus* so that the cells could be visualised with fluorescence microscopy without the need for staining, and she also conducted the coagulation assays to assess coagulase localisation. I determined that there was a subpopulation of non-growing bacteria in *S. aureus* biofilms, and Sofia Elena Muccioli (Aarhus University) performed experiments assessing the response of this subpopulation to antibiotic exposure. I had a supervisory role in Amanda and Sofia's projects.

3.2 Aim and hypotheses

The over-arching aim was to determine the different roles of Coa and vWbp in *S. aureus* biofilm formation. Based on previous research, I hypothesised that Coa was located on the cell surface and is critical for the formation of the fibrin pseudocapsule, while vWbp is released to the wider biofilm and will cause the production of fibrin that is not associated with the cells, but is nevertheless important for the formation of the wider biofilm matrix. We addressed this question by studying the dynamics of fibrin formation across whole biofilms and in association with adhered bacteria, using mutants of *S. aureus* 29213 that lack one or both coagulases.

3.3 Materials

All bacterial strains and plasmids are listed in Table 1. Assoc. Prof. Janne K. Klitgaard (University of Southern Denmark) kindly produced and provided us with mutant strains of *S. aureus* 29213 that lack one or both coagulases, or lack other surface proteins. All bacteria were stored in 15 - 25 % glycerol at -80 °C. Bacteria were plated onto brain heart infusion (BHI) (53286, Sigma Aldrich) agar plates and grown overnight at 37 °C. Liquid cultures were made by inoculating a single colony from a plate into 10 ml BHI, and grown overnight at 37 °C with 180 rpm shaking. Media was supplemented with 5 - 10 % human serum for Coa and vWbp expression, with 50 % heparin stabilized human plasma for biofilm growth and to mimic *in vivo* conditions, and with 10 µg/ml chloramphenicol (Cm) (C0378, Sigma Alrich) for plasmid selection. Blood was donated from Aarhus University Hospital and was collected in collection tubes (BD Vacutainer blood collection tubes). Plasma and serum were separated from blood by centrifugation at 2000 x *g* at 4 °C for 15 minutes. For plasma separation, blood was collected in tubes that were coated with an anticoagulant, whilst for serum separation, tubes were not coated with an anticoagulant so that the blood clotted before centrifugation. After centrifugation, the plasma or serum were pooled, divided into aliquots, and stored at -80 °C. Before use, plasma and serum were thawed in a 37 °C water bath. BHI for growing biofilms was supplemented with 2.1 mM $CaCl_2$ (C1016, Sigma Aldrich) and 0.4 mM $MgCl_2$ (M8266, Sigma Aldrich) to create modified BHI (mBHI) and further mimic physiological conditions.

Table 1 All bacterial strains and plasmids used throughout this Chapter.

Bacterial Strain	**Description**	**Reference**
Staphylococcus aureus ATCC 29213	Clinical wound isolate. Standard laboratory strain.	
S. aureus ATCC 29213 Δ*coa*	*S. aureus* 29213 *coa* deletion mutant.	Janne K. Klitgaard
S. aureus ATCC 29213 Δ*vwbp*	*S. aureus* 29213 *vwbp* deletion mutant.	Janne K. Klitgaard
S. aureus ATCC 29213 Δ*coa*Δ*vwbp*	*S. aureus* 29213 *coa* and *vwbp* double deletion mutant.	Janne K. Klitgaard
S. aureus ATCC 29213 Δ*clfA*	*S. aureus* 29213 *clfA* deletion mutant. ClfA is a fibrinogen binding MSCRAMM [31]. Contains pSB2019.	Janne K. Klitgaard
S. aureus ATCC 29213 Δ*clfB*	*S. aureus* 29213 *clfB* deletion mutant. ClfB is a fibrinogen binding MSCRAMM [31]. Contains pSB2019.	Janne K. Klitgaard
S. aureus ATCC 29213 Δ*fnbpA*	*S. aureus* 29213 *fnbpA* deletion mutant. FnbpA is a fibrinogen binding MSCRAMM [31]. Contains pSB2019.	Janne K. Klitgaard
S. aureus ATCC 29213 Δ*fnbpB*	*S. aureus* 29213 *fnbpB* deletion mutant. FnbpB is a fibrinogen binding MSCRAMM [31]. Contains pSB2019.	Janne K. Klitgaard
S. aureus ATCC 29213 Δ*fnbpAB*	*S. aureus* 29213 *fnbpA* and *fnbpB* double deletion mutant. Contains pSB2019.	Janne K. Klitgaard
S. aureus ATCC 29213 Δ*sak*	*S. aureus* 29213 *sak* deletion mutant. Sak activates human plasminogen, which in turn degrades fibrin [127]. Contains pSB2019.	Janne K. Klitgaard
S. aureus ATCC 29213 pSB2019	*S. aureus* 29213 that contains pSB2019 and produces intracellular GFP.	This study
Staphylococcus xylosus	Coagulase negative staphylococcus that contains plasmid pSB2019.	
Plasmid	**Description**	**Reference**
pSB2019	Gram positive shuttle vector, constituitive *gfp3* expression, ampicillin and chloramphenicol resistance.	[128]

3.4 Methods

3.4.1 Coagulation tests to assess whether growth phase or presence of host factors alter Coa and vWbp expression

Experiments were performed to investigate whether Coa and vWbp expression require factors from blood, and if they are affected by growth phase. Cultures of *S. aureus* 29213, *S. aureus* 29213 Δ*coa*, *S. aureus* 29213 Δ*vwbp*, and *S. aureus* 29213 Δ*coa*Δ*vwbp* were grown to

exponential (OD_{600} 0.3 - 0.4) or stationary phase (overnight) in BHI or BHI supplemented with 5 % human serum. *Staphylococcus xylosus*, which is coagulase free, was also included as a further negative control. Cells and supernatant were separated by centrifugation at 4000 x *g* for 10 minutes. The supernatant was removed and filtered through a 0.2 mm cellulose acetate filter to remove as many remaining cells as possible. 143 µl supernatant was incubated in sterile Hungate tubes with 1 ml 1:6 heparin stabilized human plasma in normal saline (0.85 %) with 10 µg/ml chloramphenicol at 37 °C without shaking, and coagulation was assessed after 4 and 24 hours. Chloramphenicol was added to inhibit the production of new Coa or vWbp after inoculation, so any coagulation seen was due Coa or vWbp from the culture only.

3.4.2 Coagulation tests to assess Coa and vWbp localisation in cell cultures

We investigated if Coa and vWbp localised to the bacterial cell surface or were secreted to the supernatant by testing the coagulation ability of cells taken directly from culture, supernatant, and cells separated from supernatant. Overnight cultures of *S. aureus* 29213 Δ*coa*, *S. aureus* 29213 Δ*vwbp*, and *S. aureus* 29213 Δ*coa*Δ*vwbp* were diluted 100 x in BHI supplemented with 5 % serum and grown to exponential phase (OD_{600} 0.3 - 0.4). Some of each culture was kept aside to use as a control in the coagulation tests, and the rest of the cells pelleted by centrifugation at 4000 x *g* for 10 minutes. The supernatant was removed and filtered through a 0.2 mm polyether sulfone membrane filter to remove remaining cells. The pelleted cells were resuspended in BHI and some kept aside. The remaining resuspension was washed twice in BHI to remove any surface-bound Coa or vWbp. 100 µl cells (culture, pelleted, or pelleted and washed) or 143 µl supernatant samples were inoculated in sterile Hungate tubes with 1 ml 1:6 heparin stabilized plasma in normal saline (0.85 %) with 10 µg/ml chloramphenicol, and incubated overnight at 37 °C without shaking. Coagulation was observed by tilting the tubes.

3.4.3 Transforming *S. aureus* for GFP expression

The plasmid pSB2019 (Table 1) was transformed using a modified version of [129] via electroporation into *S. aureus* 29213, *S. aureus* 29213 Δ*coa*, *S. aureus* 29213 Δ*vwbp*, and *S. aureus* 29213 Δ*coa*Δ*vwbp* so cells would constitutively express GFP and be visualised using confocal laser scanning microscopy (CLSM). pSB2019 was extracted from *S. xylosus* using the GeneJET Plasmid Miniprep Kit (Thermo Fisher Scientific). Electrocompetent *S. aureus* cells were prepared by first diluting an overnight culture to OD_{600} 0.5, and incubating until it reached OD_{600} 0.6. 50 ml cells were harvested by centrifugation at 4000 x *g* at 4 °C and washed 3 times in 50 ml ice-cold Milli-Q water. Cells were then harvested and resuspended in 50 ml ice-cold 0.5 M sucrose, and again in 5 ml, 2 ml, and finally 0.25 ml sucrose. 50 µl electrocompetent cells were then incubated on ice with up to 5 µg pSB2019 for 10 minutes, transferred to a chilled 1 mm electroporation cuvette, and electroporated at 2.1 kV, 25 µF, and 200 - 300 Ω using the ECM 360 BTX (Harvard Apparatus). The resistance was varied to get a time constant $\tau > 4$ ms, which indicated a successful transformation [129]. Immediately after electroporation, 1 ml preheated BHI with 0.5 M sucrose was added and incubated at 37 °C with shaking at 100 - 150 rpm for 2 hours, and then cells were plated at different dilutions onto BHI plates containing chloramphenicol

and incubated overnight. Colonies that grew were screened for GFP fluorescence expression by via CLSM (LSM700, Zeiss) using 488 nm excitation and 500 - 750 nm emission.

3.4.4 Time lapse confocal microscopy of growing biofilms

Early biofilms of GFP producing *S. aureus* 29213, *S. aureus* 29213 Δ*coa*, and *S. aureus* 29213 Δ*vwbp* containing pSB2019 were grown and visualised using time lapse CLSM. So were mutants of *S. aureus* 29213 lacking particular MSCRAMMs or Staphylokinase: Δ*clfA*, Δ*clfB*, Δ*fnbpA*, Δ*fnbpB*, Δ*fnbpAB*, and Δ*sak*. A microscope stage top incubator (Okolab) was mounted on the CLSM in which to grow samples while simultaneously imaging them. Microtiter plates (µ-Slide 8 Well, 80821, IBIDI) were mounted inside the incubator and preconditioned with 180 µl mBHI containing 50 % plasma and 0.4 µg/ml Alexa Fluor 647 conjugated fibrinogen (F35200, Thermo Fisher Scientific) by incubating at 37 °C for 30 minutes. Overnight cultures of bacteria were adjusted to OD_{600} 10, and 20 ul inoculated in the wells to reach an OD_{600} of 1. Cells were given a few minutes to settle on the bottom of the well, then located in brightfield, and time lapse fluorescence imaging was started 10 minutes after inoculation. Z-stacks were obtained automatically every 10 minutes for 160 minutes, and the setup autofocussed between each reading. 10 mW 488 nm and 5 mW 639 nm lasers were used for excitation at 2 % and 3 % power respectively, and a Plan-Apochromat 63x/1.40 oil immersion objective for imaging. The images obtained were processed with a bespoke software (see Chapter 3.4.5 below).

Because the time lapse data was intended for computational analysis and quantification, several considerations were needed. Firstly, it was imperative that the growth conditions and imaging settings were identical for each time lapse, so that the data could be compared. Secondly, the signal must not saturate, or else information about the range of fluorescence intensities would be lost. Finally, data was taken with 16-bit depth resolution in order to capture as much detail in the pixel values as possible. The master gain was adjusted in a preliminary test to ensure the signal did not saturate, that a good range of pixel values were used, and the same settings were used for each experiment. A fairly high scan speed with a pixel dwell time of 6.3 µs was used throughout in order to slow down photobleaching of the fluorophores caused by continuous imaging, at the sacrifice of a small loss of image quality. Three replicate time lapses were obtained per strain on different days to ensure that the data was reproducible.

3.4.5 Computational analysis of time lapse data

In order to analyse the time lapse data, I adapted bespoke MATLAB single particle tracking software previously written in the Leake group [126]. The purpose of the adapted algorithm was to quantify how the mean intensity of fibrin signal in the vicinity of cells (the pseudocapsule) varied over the course of the time lapses. Time lapse data was acquired as 16-bit greyscale images in two imaging channels, one for green emissions (GFP from bacteria) and one for red (Alexa-647 from fibrinogen). The green channel was used to create a cell mask: a binary matrix with the same dimensions as the original image consisting of 1s where the code detected a cell and 0 everywhere else. To do this, an intensity threshold above which cells could be differentiated from the background was calculated using Bradley's

method [130]. Bradley's method separates foreground from background by calculating a locally adaptive intensity threshold for each pixel in the image. For each pixel, it computes a threshold based on the local mean intensity in the neighbourhood of that pixel for a neighbourhood size of about 1/8 the total image size. If the pixel value is 15 % less than the local mean, it is set to 0, and otherwise it is set to 1. The sensitivity of the algorithm was decreased slightly in order to encompass slightly more pixels in the foreground because the fibrin pseudocapsule localised to the surface of cells, not within them, and a morphological opening was used to remove small fluctuations in background that were misidentified as foreground objects. After the cell mask was generated, it was used to mask the red channel and calculate the mean signal intensity from fibrin within the cell mask.

I also adapted the algorithm to segment cells based on their GFP fluorescence intensity and Adam Wollman (University of York) wrote some code to plot the sum intensity of fibrin fluorescence vs. distance from cells. To segment cells with the brightest GFP fluorescence, multilevel thresholding with Otsu's method was used. Otsu's method is a commonly used algorithm that iterates through all possible threshold values and calculates the variance of the pixel levels on either side of the threshold (background vs. foreground pixels), and aims to find the threshold where the sum of the variances on each side is at its minimum [131]. Ostu's method is a global thresholding method which analyses the pixel histogram of the entire image and usually gives a single threshold. However, it can also generate multiple thresholds when variation in pixel levels of objects in an image is of interest e.g. to separate background, dim objects, and bright objects. I calculated two thresholds and used the higher one to segment the green channel and generate a cell mask for bright cells. To plot the sum intensity of fibrin fluorescence vs. distance from cells, a distance transform was applied to the cell mask (either the mask for bright objects or the one for all objects calculated previously with Bradley's method) to generate an array where the value of each pixel is given by its distance to the nearest object. Then the distance values were binned and the sum of pixel intensities from the red channel calculated for pixels within those distance ranges.

3.4.6 Calculation of photobleaching correction factors for time lapse CLSM analysis

Correction factors were calculated for each time point in the time lapses to account for photobleaching of the fluorescently labelled fibrin. 70 ul Alexa-647 conjugated fibrinogen (1.5 mg/ml) was incubated in the dark for 1 hour on a poly-lysine coated microscope slide (Superfrost Ultra Plus, 10149870, Thermo Scientific) at room temperature. It was then washed three times with 100 µl PBS and imaged under the usual time lapse conditions. Data was processed using a bespoke MATLAB code that I wrote that calculated the mean signal intensity per frame. Signal decreased exponentially, which is described by the exponential decay equation

$$I(t) = I(0)e^{-\lambda t}, \quad (1)$$

where $I(t)$ is the mean intensity at frame t, $I(0)$ is the initial mean intensity, and λ the exponential decay constant. λ was calculated by fitting exponential functions to the signal data, and the correction factor per frame calculated using

$$\frac{I(0)}{I(t)} = e^{\lambda t}. \quad (2)$$

The mean pseudocapsule intensity data for each frame was multiplied by the corresponding correction factor, and their errors σ combined using the propagation of uncertainty equations:

$$f = AB \quad (3)$$

$$\frac{\sigma_f}{f} = \sqrt{\left(\frac{\sigma_A}{A}\right)^2 + \left(\frac{\sigma_B}{B}\right)^2}. \quad (4)$$

3.4.7 Visualising dead cells in biofilm subpopulations after antibiotic treatment

We tested what proportion of growing and non-growing bacteria in *S. aureus* 29213 pSB2019 biofilms died after antibiotic treatment by staining the dead cells after treatment and visualising them with CLSM. Microwells (µ-Slide 8 Well, 80821, IBIDI) were preconditioned with 150 µl BHI containing 50 % plasma by incubating at 37 °C for 30 minutes. The media was then removed and stored in a sterile falcon tube for use later. 100 µl of an overnight culture of *S. aureus* 29213 pSB2019 was added to the wells and incubated at 37 °C for 30 minutes to allow cells to attach to the preconditioning layer. Afterwards the culture was removed and the wells rinsed thoroughly by pipetting in 300 µl BHI and then pipetting it out again, taking care to remove as much liquid from the well as possible. 150 µl BHI containing 10 - 50 % plasma was added to the wells and incubated for 3 hours at 37 °C in order to activate the surface attached cells so they entered the exponential growth phase. Then any liquid was removed and fresh BHI containing 50 % plasma was added and the samples incubated further for up to 24 hours at 37 °C. The media was supplemented with either 50 µg/ml vancomycin (V8138, Sigma Aldrich), 3 µg/ml dicloxacillin (D9016, Sigma Aldrich), 25 µg/ml piperacillin (P8396, Sigma Aldrich) (all 25 x minimum inhibitory concentration), 1% Triton X-100 (a positive control) (T8787, Sigma Aldrich), or was not supplemented as a negative control. Dead cells were stained with either 50 µM propidium iodide (L7012, Life Technologies), 2 µM TOTO3 (T3604, Thermo Fisher Scientific), or 1 µM Sytox Orange (S11368, Life Technologies) at room temperature 30 minutes prior to imaging and samples were imaged before treatment, 1.5 hours after treatment, or 24 hours after treatment.

3.4.8 Visualising dead cells in planktonic subpopulations after antibiotic treatment

Death of growing and non-growing subpopulations of *S. aureus* 29213 pSB2019 in response to antibiotics was also assessed in planktonic cultures via dead cell staining and CSLM visualisation. Three replicate overnight cultures of *S. aureus* 29213 pSB2019 were diluted 50 x in 10 ml BHI prewarmed to 37 °C and incubated for 1.5 hours at 37 °C with 180 rpm shaking. As a positive control, cells were lysed by incubation at 85 °C for 15 minutes and then likewise incubated for 1.5 hours at 37 °C. After incubation, the cells were pelleted by

centrifugation at 4000 x *g* for 12 minutes and resuspended in 1 ml BHI and incubated for up to 8 hours at 37 °C with 180 rpm shaking. The BHI contained either 50 µg/ml vancomycin, 3 µg/ml dicloxacillin, 25 µg/ml piperacillin, or no antibiotics as a negative control. Roughly every hour, 200 µl of each sample was extracted, stained for 20 minutes with 50 µM propidium iodide, and imaged with CLSM.

3.5 Results

3.5.1 Coa and vWbp are loosely associated to the cell surface

We investigated whether Coa and vWbp associate to the cell surface or if they are secreted to the supernatant because this might reveal more about the mechanisms they use to produce different fibrin structures in *S. aureus* biofilms. We separated cells from the supernatant by centrifugation and filtration and tested the coagulation ability of *S. aureus* mutants lacking either vWbp, Coa, or both (Table 2). Chloramphenicol was added to the coagulation tests to inhibit protein synthesis and ensure that coagulation only occurred due to Coa or vWbp transferred from the culture where cells were grown to the exponential phase in BHI with 5 % serum. The culture conditions were selected based on a preliminary experiment, which revealed that host factors increased the production of Coa and vWbp, particularly in the exponential growth phase (Table 3).

As expected, the double mutant did not cause coagulation at all, confirming that Coa or vWbp were responsible for coagulation in the other samples. Coagulation occurred in samples containing either Coa or vWbp when adding either diluted bacterial culture, pelleted bacteria, or supernatant, suggesting that both coagulases partly associate with the cell surface of *S. aureus* and some are secreted into the supernatant. To test how firm the association with the cell surface was, we washed the cells by two centrifugation and resuspension steps prior to the coagulation test. After this procedure, the cells did not cause coagulation. Therefore we concluded that Coa and vWbp are only loosely associated to bacterial cells.

Table 2 Tube coagulation tests for *S. aureus* mutant strains added to human plasma containing chloramphenicol. *S. aureus* was cultured in BHI with 5 % serum until the exponential growth phase before transferring to human plasma. Samples were either taken directly from the culture, or cells were separated from the supernatant by centrifugation and filtration. In one experiment, cells were washed by two centrifugation and resuspension steps to remove loosely bound surface proteins.

	Coagulation (+/-)			
	Diluted bacterial culture	**Pelleted bacteria**	**Pelleted and washed bacteria**	**Supernatant from first centrifugation**
Δ*vwbp*	+	+	-	+
Δ*coa*	+	+	-	+
Δ*coa*Δ*vwbp*	-	-	-	-

Table 3 Tube coagulation tests for human plasma with filtered supernatant from cultures of *S. aureus*, *S. aureus* mutants lacking Coa and/or vWbp, and coagulase negative *S. xylosus*. Cultures were grown to exponential or stationary phase in either plain BHI or BHI supplemented with 5 % human serum, and coagulation assessed after 4 and 24 hours.

	Coagulation (+/-)							
	Exponential phase				**Stationary phase**			
	No serum		**5 % serum**		**No serum**		**5 % serum**	
	4 h	**24 h**	**4 h**	**24 h**	**4 h**	**24 h**	**4 h**	**24 h**
Wildtype	-	+	+	+	-	+	+	+
Δ*vwbp*	-	+	+	+	-	-	+	+
Δ*coa*	-	+	-	+	-	-	-	+
Δ*coa*Δ*vwbp*	-	-	-	-	-	-	-	-
S. xylosus	-	-	-	-	-	-	-	-

3.5.2 Coa is essential for fibrin pseudocapsule formation

Coagulation leads to the formation of a fibrin network, and in *S. aureus* biofilms the fibrin forms a pseudocapsule around cell clusters and an extended network of fibrin fibers in the wider biofilm matrix [41]. Previous studies have suggested that Coa is primarily responsible for pseudocapsule formation, while vWbp promotes the formation of the extended fibrin network, because Coa associates to cell surfaces and presumably vWbp does not [41]. Our coagulase tests did not indicate such a difference in the location of the two proteins. To explore their potentially different roles in *S. aureus* biofilms, I visualised fibrin in biofilms of *S. aureus* wildtype and mutants lacking Coa, vWbp, or both, after 160 minutes of incubation in media containing 50 % human plasma.

Fibrin fibers surrounded cell surfaces and extended in between cell clusters in *S. aureus* biofilms (Figure 5a). When vWbp was lacking, the biofilm phenotype looked similar to the wildtype, with fibers connected to cell surfaces as well as longer fibers extending in between (Figure 5a). Cell clusters likely originate from a single cell because they share a pseudocapsule: when the cells divide, they remain within the pseudocapsule rather than each producing their own pseudocapsule. However, when Coa was lacking, the phenotype was different. The cells did not form a pseudocapsule. However, some fibrin formed in between cells (Figure 5a). As expected, no fibrin formed in the double mutant (Figure 5c). This is in agreement with prior observations, namely that vWbp promotes the formation of an extended fibrin network but not a pseudocapsule [41]. In contrast to the previous study, our results indicate that Coa contributes to the formation of both the pseudocapsule and the extended fibrin network. Fluorescence from fibrin was much dimmer when Coa was lacking. This is probably because vWbp has a slower activation time than Coa [48] and it therefore did not have time to produce such a dense matrix in the short incubation time.

I additionally observed fibrin at the interface between the bottom of the biofilm and surface of the microscope slide. These fibrin fibers grew upwards into the biofilm to produce a “fibrin forest” perpendicular to the glass substrate surface (Figure 5d and 5e). Presumably, vWbp and Coa anchored this fibrin to the host factors contained within the preconditioning layer, which implicates a role in attaching biofilms to surfaces within the host. vWbp and Coa have been identified at the periphery of an *S. aureus* tissue infection in a mouse model [42]

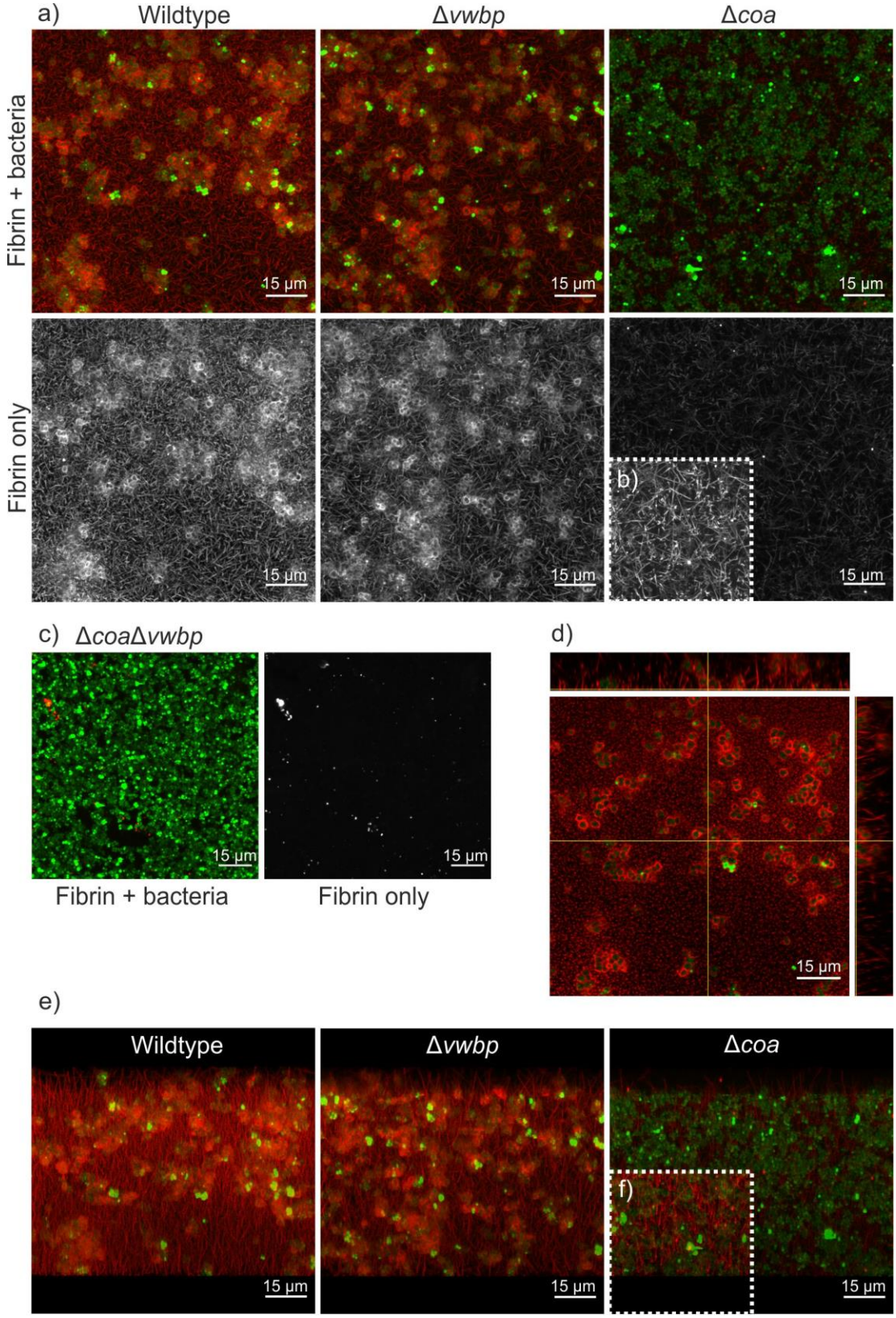

Figure 5 a) Maximum intensity Z projections of *S. aureus* biofilms formed after 160 minutes of incubation in 50% human plasma, b) enhanced fibrin brightness to compare phenotypes, c) mutant lacking Coa and vWbp after 160 minutes incubation, d) orthogonal view of wildtype, e) 3D projections tilted 60 ° around the X axis to show fibrin fibers arranged perpendicular to the glass substrate surface, and f) enhanced brightness to compare fibrin phenotypes. Bacteria are green and fibrin is red.

where it was likely to also have been interacting with host proteins like fibrinogen and fibronectin.

3.5.3 vWbp accelerates pseudocapsule formation in wildtype *S. aureus*

The kinetics of fibrin formation in different locations of the biofilm can reveal more about the roles of Coa and vWbp. Coa is required to produce the pseudocapsule, yet *S. aureus* biofilms lacking either vWbp or Coa can both produce an extended fibrin network. Fibrin growth dynamics at the cell surface would indicate whether Coa and vWbp truly play individual roles in biofilm formation, or whether there is a synergistic effect of their activity. I therefore quantified the amount of fibrin localised at cell surfaces in the pseudocapsule of growing biofilms formed by *S. aureus* wildtype and the mutants lacking either Coa or vWbp using time lapse confocal microscopy.

Fibrin formed at cell surfaces and in between cells throughout the time lapses (Figure 6a). Initial temporal analysis of cell surface associated fibrin showed that the signal intensity increased rapidly before plateauing after approximately 80 minutes (Figure 7a). However, applying a photobleaching correction to the data revealed that the fibrin signal rose continuously throughout the 160 minute time lapse (Figure 7b), which is more in line with our qualitative assessment of the images at 80 and 160 minutes (Figure 6a). However there were challenges when collecting the data to calculate the photobleaching correction factors due to large variations in the quantity of photobleaching measured in each experiment (Figure 7c), which lead to very large variation, especially as the imaging time progressed, and it is difficult to conclude how valid the photobleaching corrected data is. I troubleshooted this problem, and varying between using old vs. new stocks of fibrinogen, main room lights on vs. off, and heating vs. no heating when collecting photobleaching data did not cause this variation. Incubation times, concentrations, volumes, and imaging conditions were always the same and it is unclear why the correction factors fell into two distinct categories with apparently different rates of photobleaching.

In the mutant lacking Coa, pseudocapsule formation was absent. The signal intensity from surface-associated fibrin increased slowly and originated from fibrin fibers in the extended network which intercepted with *S. aureus* cells. Therefore, the data from this strain was much more variable than for the other strains. The strain lacking vWbp eventually reached the same signal intensity from surface associated fibrin as the wildtype, but the signal increased much more slowly. If Coa was solely responsible for pseudocapsule formation, we would expect that the increase in signal intensity from surface associated fibrin would be similar in the wildtype and the Δ*vwbp* strain. However, this was not the case. In fact, the sum of the curves from the two mutant strains Δ*vwbp* and Δ*coa* did not equal the wildtype curve during the first 2 hours of the experiment. Hence, the two coagulases appear to work synergistically to accelerate the formation of the pseudocapsule. Although vWbp did not promote pseudocapsule formation on its own, it does seem to contribute when Coa is present.

Another interesting observation from the time lapse analysis is that cell clusters with a shared pseudocapsule originated from single cells that had formed a pseudocapsule while undergoing multiple cell divisions (Figure 6b). Pseudocapsule formation therefore resulted in the formation of small aggregates during the 160 minute incubation. These pseudocapsule encased aggregates were absent in the Δ*coa* mutant, and Coa is thus essential for the

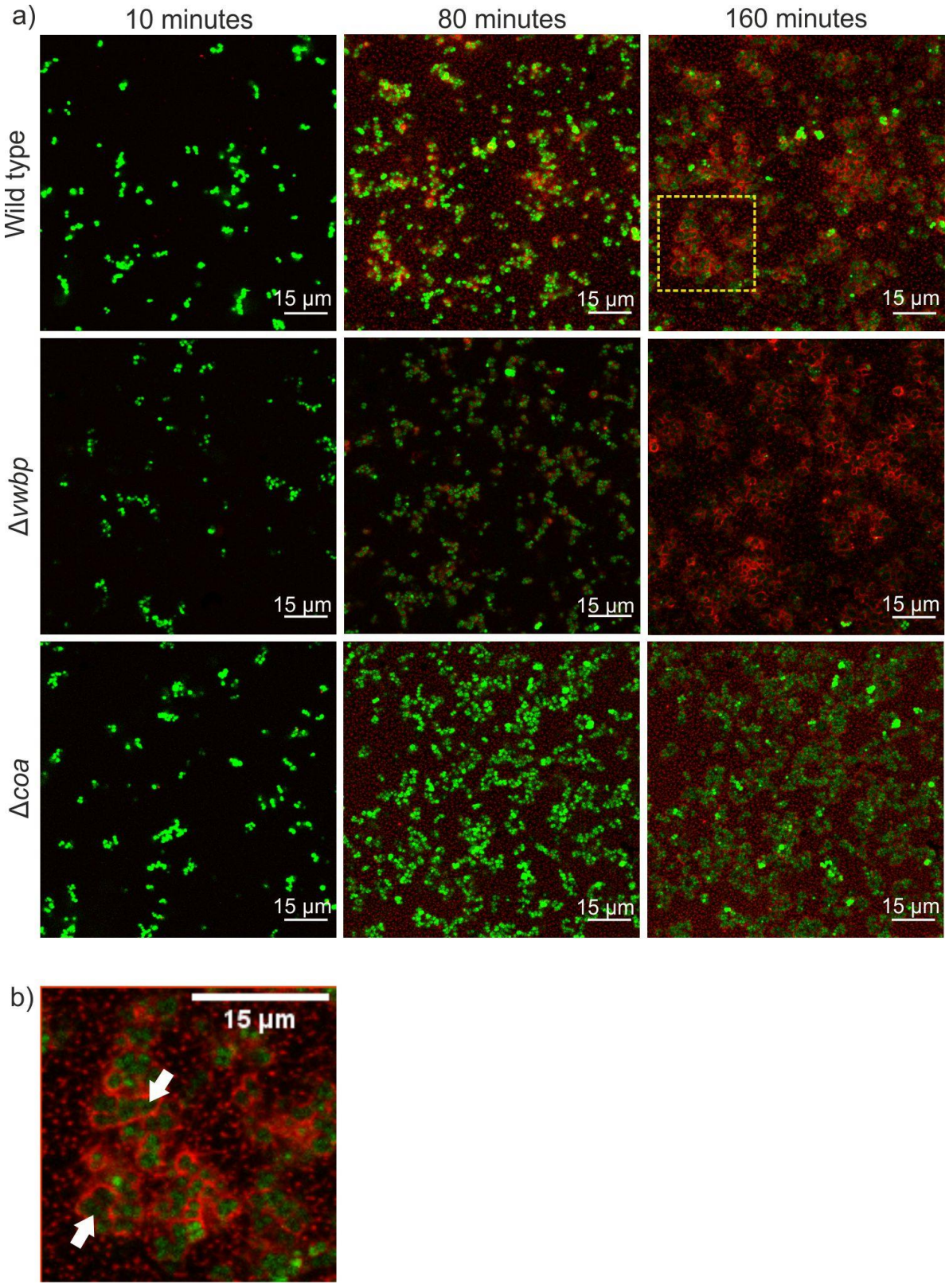

Figure 6 a) Frames from time lapses of *S. aureus* biofilms growing in media supplemented with 50 % plasma. Z slice 5/30 presented. The yellow square represents an area that is magnified in b), which shows clusters of cells residing within shared pseudocapsules indicated by white arrows. Bacteria are green and fibrin is red.

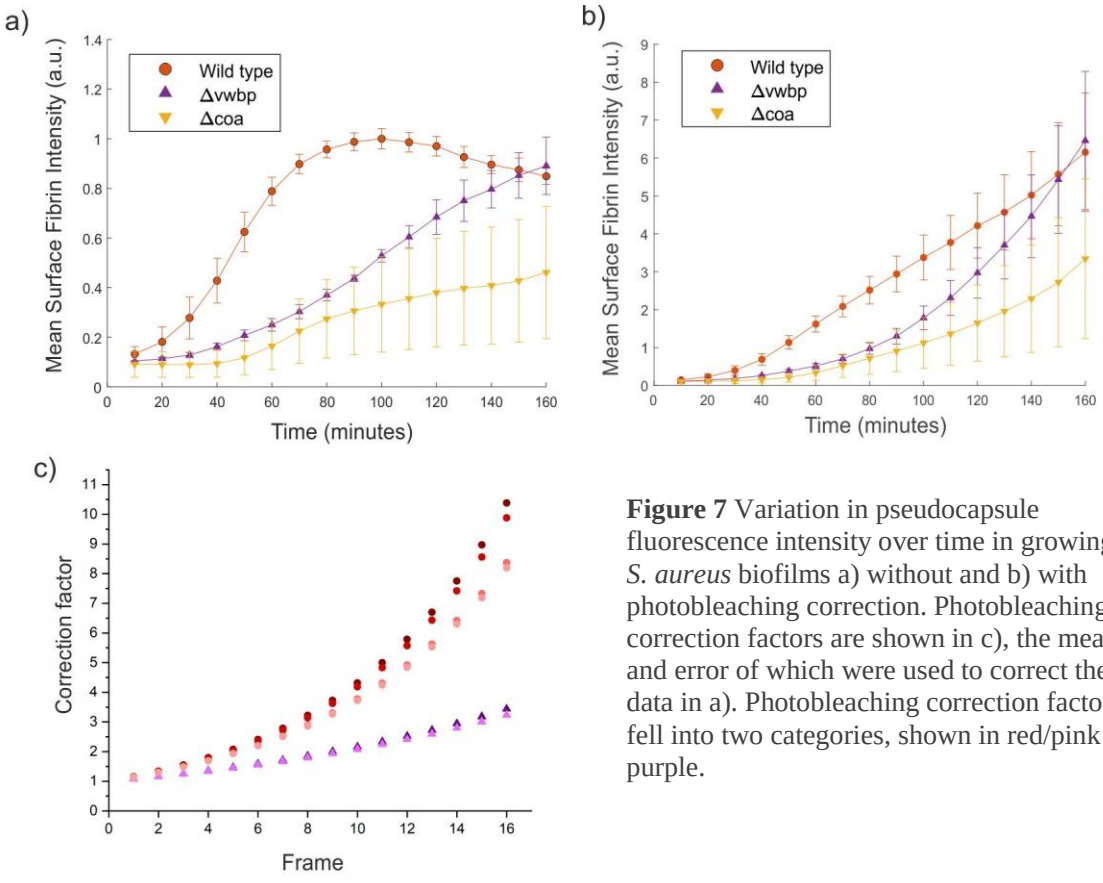

Figure 7 Variation in pseudocapsule fluorescence intensity over time in growing *S. aureus* biofilms a) without and b) with photobleaching correction. Photobleaching correction factors are shown in c), the mean and error of which were used to correct the data in a). Photobleaching correction factors fell into two categories, shown in red/pink and purple.

formation these of aggregates. Aggregating within a shared pseudocapsule may be essential for escaping phagocytosis because phagocytes cannot engulf and therefore destroy aggregates that are larger than about 5 µm in diameter [132].

3.5.4 Pseudocapsule formation does not rely on a single fibrinogen binding MSCRAMM

S. aureus produces a large family of surface receptors known as MSCRAMMs (microbial surface components recognizing adhesive matrix molecules) which bind to host proteins, including fibrinogen, fibronectin, and collagen [31]. I hypothesised that Coa associates to cell surfaces via fibrinogen that is bound to a fibrinogen binding MSCRAMM to produce the pseudocapsule. Coa contains two binding domains for fibrinogen, one at the N-terminal D1-D2 domain, and one at the C-terminal repeat domain (R domain) that consists of multiple repeats of a fibrinogen binding peptide [51]. *S. aureus* producing a mutated Coa that lacks an R domain produces fibrin, but not a pseodocapsule [50], so it most likely associates via its R domain.

To test whether Coa associates to cell surfaces via a single fibrinogen binding MSCRAMM to produce the pseudocapsule, I imaged mutants lacking particular

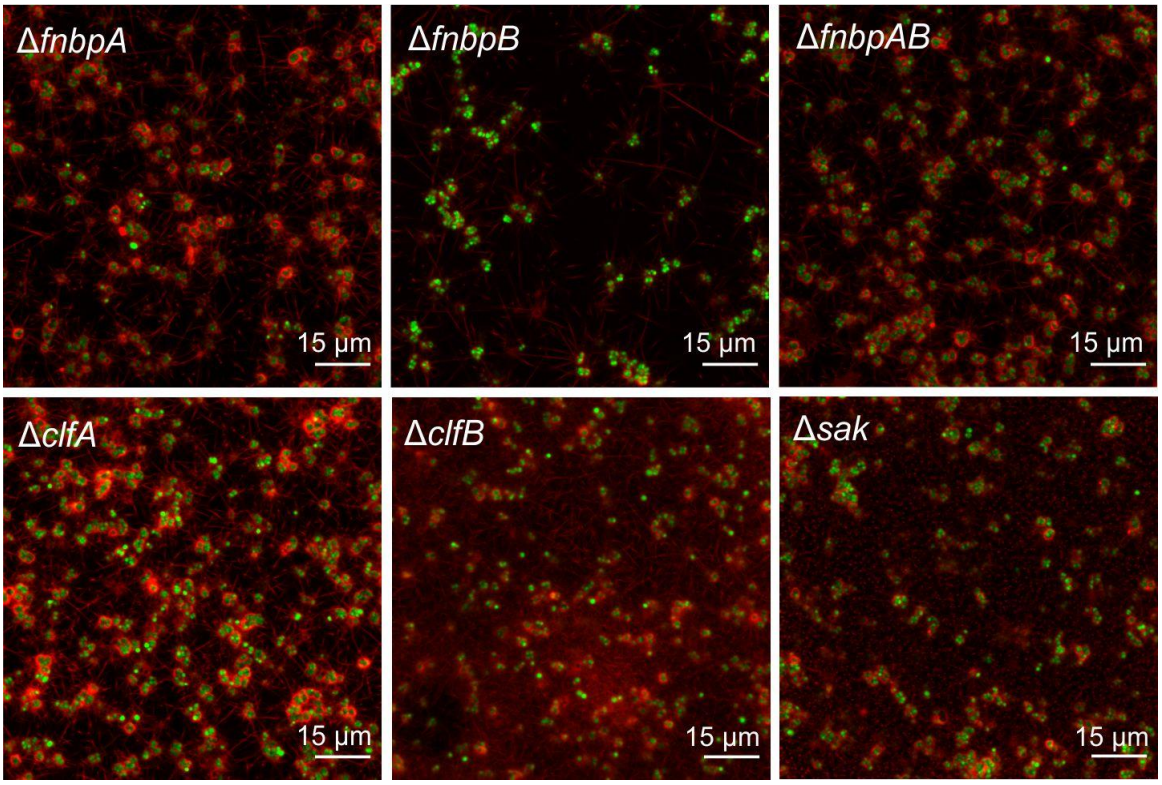

Figure 8 Biofilms formed by *S. aureus* lacking certain MSCRAMMs (ClfA, ClfB, FnbpA, FnbpB, FnbpAB), or Sak, after 100 minutes incubation in media containing 50 % plasma. Samples were imaged as time lapses and the final frame is shown here. Fibrin is red and bacteria green.

MSCRAMMs using time lapse CLSM. The deletion mutants lacked Clumping factor A or B, Fibrinogen binding protein A or B, or both (Δ*clfA*, Δ*clfB*, Δ*fnbpA*, Δ*fnbpB*, and Δ*fnbpAB*).

All strains displayed the same phenotype with the majority of cells binding fibrin by the end of the 100 minute time lapse (Figure 8), therefore a single one of these MSCRAMMs does not anchor Coa to the cell surface alone. However, it is possible that Coa associates via a combination of all of these proteins, which would not be detectable by analysing single deletion mutants. There were fewer cells and fibrin in the mutant lacking FnbpB probably due to the focus drifting upwards over the course of the time lapse.

3.5.5 Some cells do not form a pseudocapsule

The time lapse imaging of fibrin production made it apparent that some cells did not form a pseudocapsule, and that the fluorescence from GFP in these cells remained bright during the 160 minute incubation, while the signal from other cells in the biofilm became dim (Figure 9a). To quantify the absence of pseudocapsule formation in this subpopulation of cells in the biofilm, I segmented the cells in microscopy images based on their signal intensity from GFP and quantified the surface associated fibrin in the bright cells using the MATLAB code provided by Adam Wollman (University of York). This was done on the final image from each time lapse of the wildtype strain and compared to the signal intensity from surface associated fibrin for all of the cells in that frame. The majority of cells did form a pseudocapsule, and plotting the fibrin signal as a function of distance to the nearest cell

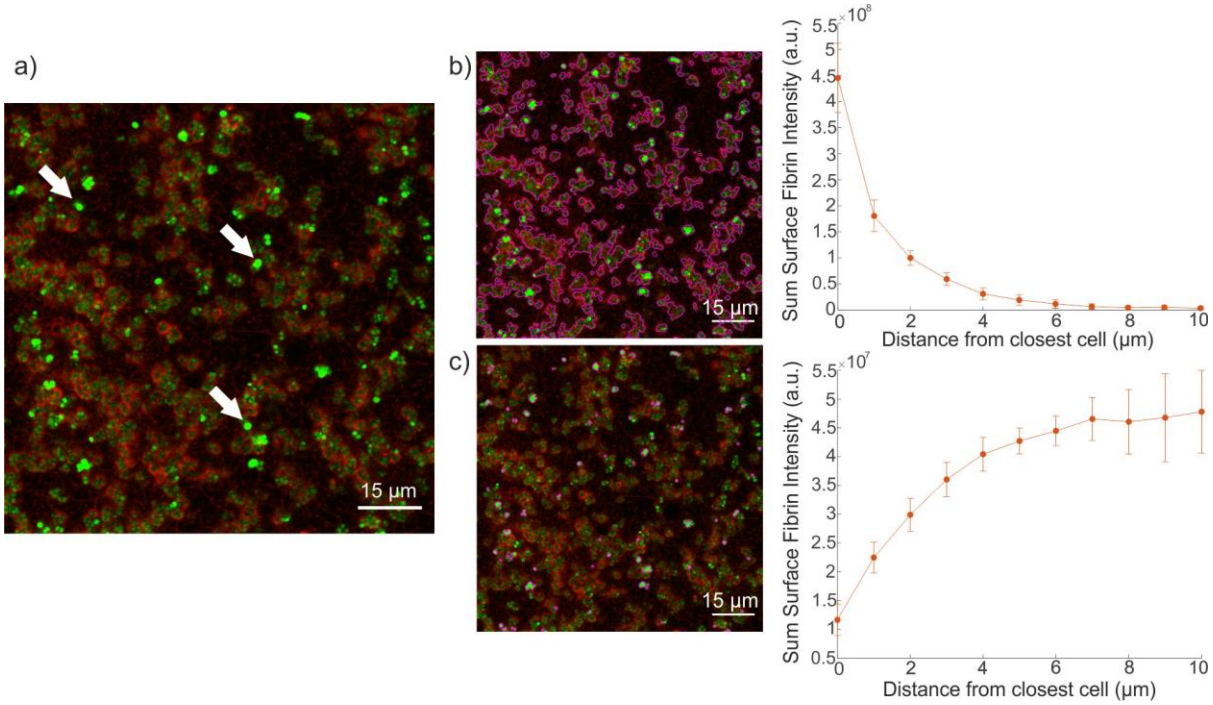

Figure 9 a) *S. aureus* wildtype splits into two distinct subpopulations after 160 minutes incubation with 50 % plasma based on GFP fluorescence intensity. Bright cells do not have a pseudocapsule (white arrows point to examples). b & c) Sum fibrin fluorescence intensity vs. distance to closest cell for a) all cells and c) bright cells only. The magenta outline indicates image segmentation based on GFP fluorescence. Cells are green and fibrin is red.

showed that the fluorescence intensity was highest at the surface of cells and decreased with distance from the cells (Figure 9b). When analysing the bright cells only, the opposite was true (Figure 9c). This confirms that the bright green cells are a distinct subpopulation that does not form a pseudocapsule.

One explanation for why some bacteria lack a pseudocapsule could be that this subpopulation produces Staphylokinase, which activates plasminogen to degrade fibrin and helps *S. aureus* establish skin infections [50]. I imaged *S. aureus* 29213 Δ*sak*, which does not produce Staphylokinase, with time lapse CLSM, but the phenotype did not differ from the wildtype strain (Figure 8). Hence, the lack of a pseudocapsule was not caused by fibrin degradation, but rather by the inability to produce or bind fibrin at the cell surface. I hypothesised that the bright subpopulation did not express the surface proteins necessary to bind fibrin/fibrinogen to cell surfaces, and turned attention instead to investigating why some cells remained bright while others turned dim.

3.5.6 *S. aureus* biofilms contain a small subpopulation of non- or slowly-dividing cells that can be distinguished by bright GFP fluorescence

To assess whether the variation in GFP fluorescence intensity reflected differences in the growth rates of the bright and dim subpopulations, I imaged *S. aureus* growing in either BHI or BHI supplemented with erythromycin, which inhibits protein synthesis and prevents cells from dividing. As expected, *S. aureus* grown in normal BHI split into the bright and dim subpopulations (Figure 10a). However, cells did not turn dim when grown with erythromycin

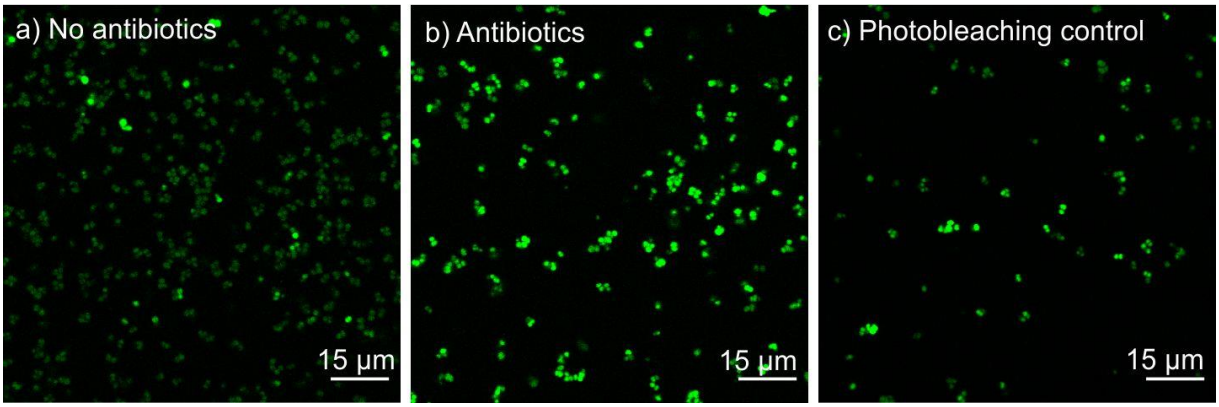

Figure 10 a) Final frame (160 minutes) of a time lapse of *S. aureus* grown in a) BHI and b) BHI supplemented with 10 µg/ml erythromycin. Cells remained bright when grown with antibiotics. c) *S. aureus* grown in BHI supplemented with 10 µg/ml erythromycin for 160 minutes and imaged only after incubation to test for photobleaching.

(Figure 10b), and a control sample of *S. aureus* grown with erythromycin but only imaged at the end of the 160 minute incubation confirmed that cell dimming did not occur due to photobleaching (Figure 10c). Hence, the bright cells were slowly- or non-dividing, whereas the other cells were dividing normally. The dividing cells became dim because they divided faster than they produced new GFP, diluting the GFP signal between the daughter cells with each division and diminishing the signal [133]. The GFP variant was GFP3, which is stable and has a half-life of over 24 hours [128], so cell division is a more likely explanation for the signal dimming rather than GFP degradation.

I confirmed in a separate experiment that the dim GFP fluorescence was not due to autofluorescence. I visualised *S. aureus* that does not produce GFP under time lapse conditions, using the same imaging settings determined in Chapter 3.4.4, and verified that no signal was seen from bacteria and that the dim signal in GFP producing bacteria was therefore not autofluorescence.

3.5.7 The non-growing subpopulation does not appear to be more tolerant to antibiotics

Many antibiotics target actively dividing cells. We therefore hypothesised that the cells with bright GFP fluorescence were an antibiotic tolerant subpopulation of persister cells that serve as a contingency plan for the entire biofilm population in the event of exposure to antibiotics. Persisters are cells that have differentiated into a metabolically dormant state and are therefore tolerant to antibiotics [134]. Persistence is not fully understood, but it is thought that when a bacterial population is exposed to antibiotics, the active cells die but the tolerant cells persist, and when the antibiotics are removed, the persisters “wake up” and switch back into a metabolically active state. Then the persisters divide and re-establish the biofilm. Persistence is therefore one explanation as to why biofilm infections become chronic and can be so difficult to treat [21]. To test the response of each subpopulation to antibiotics, we visualised biofilms after exposure to antibiotics with CLSM and identified dead cells with a fluorescent stain based on membrane integrity (usually propidium iodide). We expected that a higher proportion of dim cells would die compared to bright cells.

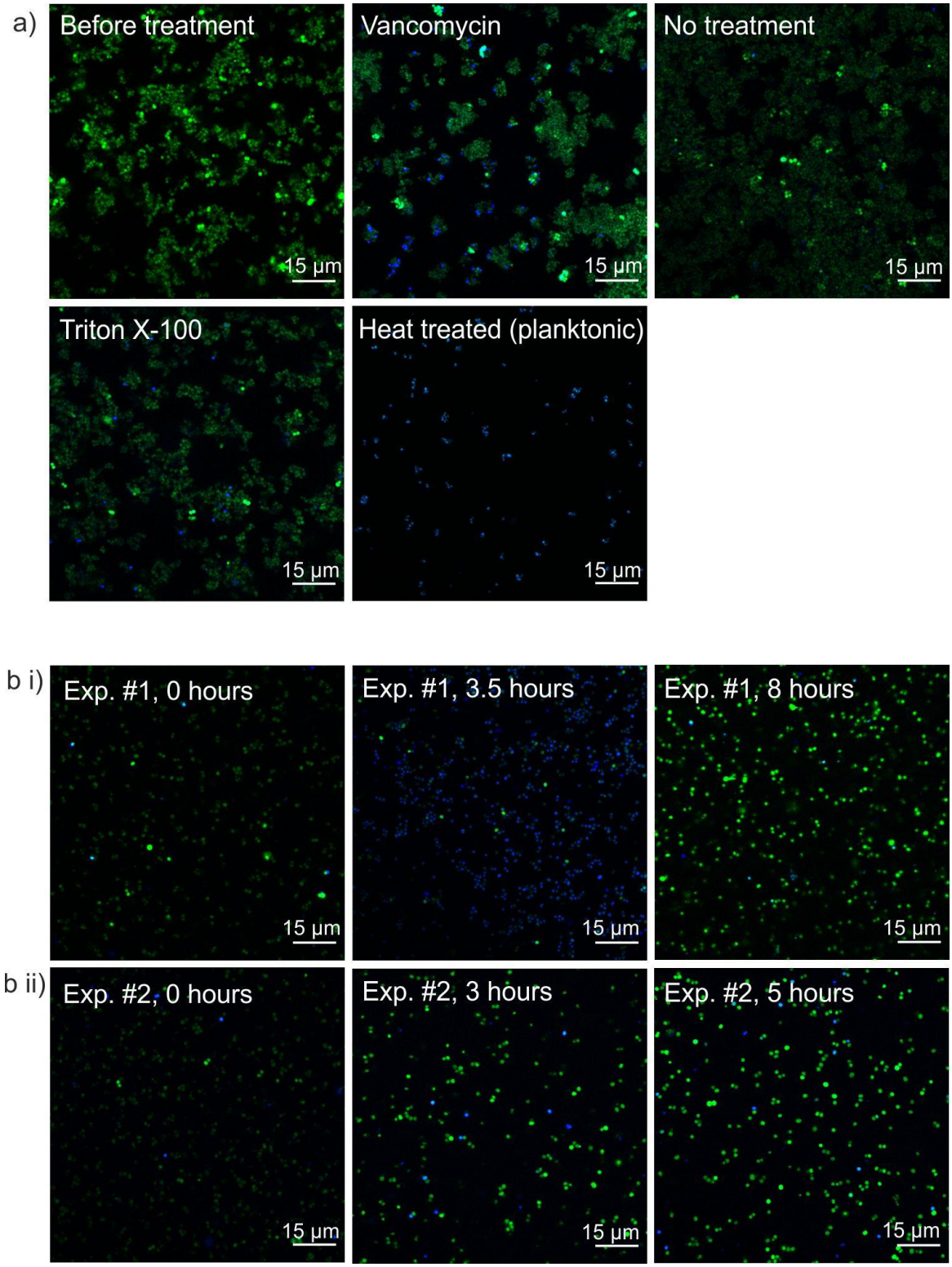

Figure 11 a) Visualisation of dead cells in biofilms after 24 hours treatment with vancomycin or 1 % Triton X-100. A planktonic culture was also lysed via heat treatment and visualised with the dead stain. b) Visualisation of dead cells in planktonic cultures in two independent experiments after treatment with vancomycin. Dead cells were stained with propidium iodide (blue).

There was only a slight increase in the number of dead cells in biofilms treated for 24 hours with vancomycin compared to a control biofilm that was left untreated (Figure 11a). It was largely dim cells within smaller aggregates that died. Treatment with Triton X-100 did not appear to kill that many cells either, despite the fact that it is a surfactant commonly used to lyse cells. We tested whether the propidium iodide was working properly in a separate experiment where planktonic cells were killed with heat treatment. Propidium iodide did indeed stain all cells in this case (Figure 11a).

In case our results were due to the biofilm phenotype protecting the bacteria from the antibiotic treatments, we simplified the experiment and treated planktonic cells with vancomycin for 5 - 8 hours, staining and visualising a small sample of the cells every hour. In one experiment, the number of dead cells rose during the first 3 hours, and then the signal from propidium iodide disappeared in the later time points (Figure11bi), and in a repeat experiment, there appeared to be no increase in dead cells over the duration of the experiment (Figure11bii). We do not know how long it takes for the cells to lose their membrane integrity after dying, and wondered whether after longer incubation times, many dead cells were unable to retain the stain due to losing their nucleic acid, and so the dead stain had nothing to bind to inside the cells and therefore failed to visualise dead cells. In the sample where many cells died after 3.5 hours (Figure 11bi), there appeared to be no significant difference in the number of dead cells from each subpopulation. Segmenting either bright or dim cells using the bespoke MATLAB software and quantifying the fraction that had a large signal from propidium iodide revealed that approximately 93 % of the bright cells and 92 % of the dim cells were dead, therefore the bright bacteria were not more tolerant to antibiotics. Interestingly, the majority of bacteria after 8 hours of incubation with antibiotics had a brighter GFP fluorescence than they did after 3.5 hours. Cells that remained bright throughout the experiment might reflect an experimental error in which the bacteria were not given sufficient time to activate after dilution into fresh media from the overnight culture prior to antibiotic treatment, or it might reflect a biological mechanism that somehow caused bacteria to become bright after the addition of antibiotics.

Both biofilm and planktonic experiments sometimes additionally included treatment with dicloxacillin and piperacillin, but neither resulted in any increase in propidium iodide signal after treatment in biofilms nor planktonic cultures. Three different dead stains were used in different experiments throughout: Sytox Orange, propidium iodide, and TOTO3. None appeared to provide clearer results than one of the others. We concluded that there were significant difficulties staining the dead cells reliably and that there seemed to be no difference in the response to antibiotics in the one sample where we did manage to stain dead cells, and hence stopped the experiment.

3.6 Discussion

The results in this Chapter show that Coa and vWbp have distinct roles in pseudocapsule formation, but their roles in forming the overall fibrin network overlap more than previously thought. Coa is essential for forming the fibrin pseudocapsule and partially the wider fibrin network, and vWbp forms the wider fibrin network but cannot form the pseudocapsule on its own. Both coagulases do however appear to associate to cell surfaces where vWbp accelerates pseudocapsule formation. These findings partially agree with the study from

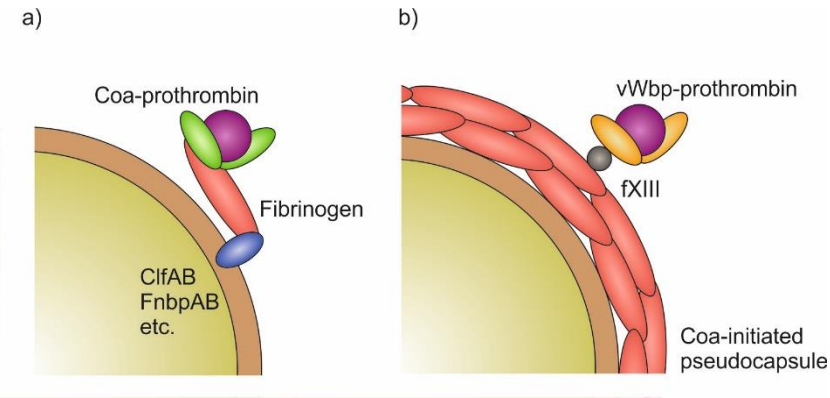

Figure 12 Models for the mechanisms that Coa and vWbp could associate to cell surfaces with to produce the fibrin pseudocapsule. a) Coa associates by binding to fibrinogen that is bound to the cell surface by an MSCRAMM. b) vWbp associates to the pseudocapsule initiated by Coa via activation of fXIII and subsequent fXIII mediated fibrin cross linking.

Guggenberger *et al.* (2012), who showed that Coa forms the pseudocapsule whilst vWbp forms the extended network [41]. It is a new result that vWbp accelerates pseuodocapsule production, which was only possible to conclude from analysis of fibrin growth dynamics, not end-point imaging of already grown biofilms where the phenotype of the wildtype and mutant lacking vWbp looked very similar. There was a "fibrin forest" at the biofilm-surface interface comprising fibrin fibers perpendicular to the glass substrate that was produced by both coagulases, where they presumably localised to increase biofilm attachment to host tissue. Cheng *et al.* (2010) found Coa within the pseudocapsule and in the periphery of *S. aureus* abscess lesions in a mouse model, while vWbp was distributed throughout the abscess as well as the peripherary [42]. In their study, both coagulases could therefore localise away from cell surfaces like we have found evidence for, and there was a tendency for Coa to accumulate at the edge of the infection whereas vWbp was distributed throughout.

Formation of the pseudocapsule is important *in vivo* because it acts as a mechanical barrier against neutrophils [41] and protects aggregates from ingestion by the immune system [135]. I observed that clusters of cells existed within a shared pseudocapsule originating from a single cell that divided within its already produced pseudocapsule. I speculate over why each cell does not form its own pseudocapsule, and it might be that initial formation of fibrin accelerates further formation in the same location rather than in new locations inside the already existing pseudocapsule. It is advantageous to share a pseudocapsule to protect the cell and its offspring, and means that the bacteria can establish an infection from relatively few cells. Coa is secreted and might be immobilised at cell surfaces to rapidly produce the pseudocapsule as a first line of defence against immune cells [41], and enables cells to divide within their protective shared pseudocapsule. Meanwhile, vWbp accelerates pseudocapsule formation, and diffuses further away to form the wider fibrin network, a second mechanical barrier against immune cells [41][50], which allows biofilms to attach to host tissues via the fibrin forest. Coa that is not used for pseudocapsule formation might also diffuse away to form the wider network and attach the biofilm to host tissues via the fibrin forest.

Because the pseudocapsule cannot form without Coa, I hypothesised that Coa associates to the surface of cells via fibrinogen that is bound to one of the many fibrinogen surface receptors of *S. aureus*, to essentially produce a "fibrin factory" that localises fibrin production to form the surface attached pseudocapsule (Figure 12a). Similarly, Thomer *et al.* (2016) found that Coa localised with bacterial cells when grown with a small amount of plasma due to association via a fibrin clot, and was otherwise secreted to the supernatant when plasma was absent [50]. We found that some Coa and vWbp were secreted to the supernatant whilst some were loosely associated to cell surfaces when grown with human serum. Perhaps Coa and vWbp were associated to cells in our experiments due to trace amounts of plasma proteins such as fibrinogen in the serum. I demonstrated that neither ClfA, ClfB, FnbpA, FnbpB were solely responsible for associating Coa to cell surfaces to form the pseoducapsule via imaging experiments with mutants lacking one of these proteins. However, this does not rule out the possibility that Coa utilises multiple fibrinogen binding proteins to associate to the surface, which would not be detected when imaging single deletion mutants. The creation, visualisation, and analysis of a mutant lacking the major, or all, fibrinogen binding MSCRAMMs would provide further support in favour of or against this hypothesis.

I also speculated on the mechanism that causes vWbp to accelerate pseudocapsule formation, and suggest that it associates to the Coa-intiated pseudocapsule via factor XIII (fXIII) (Figure 12b). vWbp binds to and activates fXIII in human plasma, but only when also bound to prothrombin and fibrinogen [53], a prerequisite for vWbp activation [48]. Activated fXIII forms cross links between adjacent fibrin strands [53], and I propose that activated vWbp is recruited to the pseudocapsule via this cross linking. vWbp also binds to fibronectin in human plasma, but it does not appear to bind to prothrombin at the same time [53], so I suggest that binding to fXIII is a more likely explanation. To test this hypothesis, one could compare the fibrin pseudocapsule formed by *S. aureus* and its mutants lacking Coa or vWbp when grown in media containing human plasma and a fXIII inhibitor such as substances which prevent fXIII cross linking [136]. If vWbp associates to cell surfaces via fXIII cross linking, it would no longer accelerate pseudocapsule production in the presence of the inhibitor. fXIII is also activated in *S. aureus* infections independently of vWbp via prothrombin in the host coagulation cascade [53], which would likely impact the structure of the fibrin network when inhibited. However because this would affect all biofilms in the experiment, including the controls, it would still be possible to detect phenotypic differences due to vWbp.

Differences in fluorescence intensity of *S. aureus* producing GFP revealed a subpopulation of bright, non- or slowly-dividing cells that did not appear to contribute to matrix production because they did not form a pseudocapsule. They either did not produce the MSCRAMMs required to bind fibrin to the surface, or they lacked the ability to form their own fibrin altogether, i.e. they did not produce the coagulases, or both. It is interesting that some cells lacked the protection from a pseudocapsule, although this subpopulation did however benefit from the protection of the extended fibrin network without contributing to its production. However, we did not consider them to be "cheaters" who benefit from the community without contributing to the common good because we hypothesised that they were a subpopulation of antibiotic tolerant persisters that benefit the overall survival of the biofilm.

Roostalu *et al.* (2008) identified a subpopulation of non-dividing cells in *E. coli* which could also be distinguished by their GFP signal, and suggested that they were persisters [133]. They verified that this subpopulation was tolerant to antibiotics by monitoring the death of the growing and non-growing subpopulations via fluorescence-activated cell sorting, and further demonstrated that the non-growing cells resumed growth after antibiotic treatment when placed into fresh media, a characteristic property of persisters. We were unfortunately not able to verify our hypothesis that bright cells are tolerant to antibiotics. In biofilms, only a very small population of mostly dim cells died after vancomycin treatment for 24 hours, though some bright cells died too. These cells resided within small aggregates, and bacteria within larger aggregates were unaffected by the treatment. 24 hours of treatment with vancomycin is sufficient to significantly reduce the number of colony forming units in planktonic cultures of our strain of *S. aureus* [137], but because we treated biofilms which are much more tolerant to antibiotics, perhaps we needed to increase the antibiotic concentration and incubation time to have a larger effect. Our results could also reflect that propidium iodide was unable to stain dead cells after they had been dead for long times due to the cell contents leaking out.

Roughly equal proportions of bright and dim planktonic bacteria died after a short 3.5 hours vancomycin treatment in one experiment, which indicates that the bright subpopulation are not more tolerant to antibiotics and are therefore not persister cells. This contradicts the findings from Roostalu *et al.* (2008) in *E. coli* [133]. We made this conclusion however from only one experiment of which the results were not replicated in a repeat experiment the next day, and there were only very few bright cells in the image, therefore further experiments might be useful to solidify this conclusion. Our experimental protocol needs adjusting. In most experiments, the majority of bacteria actually unexpectedly had bright GFP fluorescence rather than dim, which might indicate that the initial activation step when diluting bacteria from the overnight culture into fresh medium was not long enough, and therefore, antibiotics were added to cultures that had not yet reached the growing, exponential phase and were hence ineffective. The simplest way to resolve whether there is a difference in antibiotic tolerance in the two populations is to use fluorescence-activated cell sorting to separate the populations, immediately expose them to antibiotics after sorting, and subsequently determine their survival rate. An alternative experiment to identify whether bright cells are persisters would be to stain the GFP producing bacteria with a dye that indicates membrane potential such as $DiSC_3(5)$ (D306, Thermo Fisher) or $DiSBAC_2(3)$ (B413, Thermo Fisher). Metabolically active cells are expected to have a high membrane potential because they are generating ATP via the electron transport chain to produce the energy that they need to survive. Conversely, metabolically inactive or persister cells would have a low membrane potential as they do not require high levels of ATP. Together these experiments would build up a more definite conclusion of whether the bright cells are tolerant to antibiotics and whether they are persister cells.

4. Construction of fusion proteins to visualise Coa, vWbp, and Embp

In order to visualise Coa, vWbp, and Embp in biofilms formed by *S. aureus* and *S. epidermidis*, I produced fusion proteins. I produced a number of fusion proteins either individually or in collaboration with several colleagues throughout my PhD (Table 4). We often produced multiple fusion proteins simultaneously as part of our strategy, which was to to bet on multiple horses to maximise our chances of getting a successful fusion protein. Here I will present the process of making two successful fusion proteins which I used later for experiments in Chapter 5, Coa:SNAP and vWbp:CLIP, and explain how I decided to create these rather than the intended fusions with mCherry and GFP as stated in the original aim of this PhD (Chapter 2).

4.1 Introduction

To visualise Coa, vWbp, and Embp in *S. aureus* and *S. epidermidis* biofilms, I intended to create fusion proteins by inserting a protein tag next to the gene for the protein of interest in the chromosome of either *S. aureus* or *S. epidermidis*, depending on which protein was under investigation, and visualise them with confocal and single molecule microscopy. I initially intended to create fusions with fluorescent proteins, which do not require labelling, and therefore set out to create fusions with the fluorescent proteins mCherry and GFP. mCherry and GFP were chosen to allow for dual colour experiments visualising both Coa and vWbp in *S. aureus* biofilms.

I initially worked with Melissa Eriksen (Aarhus University) to produce a genomically integrated, C- terminal fusion between Coa and red fluorescent protein mCherry (Coa:mCherry) in *S. aureus*, while Olatz Niembro (Aarhus University) produced one with vWbp and green fluorescent protein GFP (vWbp:GFP) and Bhaskar Pradhan (Aarhus University) created both N- and C-terminal fusions between Embp and GFP in *S. epidermidis* (Table 4). The tags for Coa and vWbp were placed at the C-terminal so as not to interfere with the N-terminal, which is required to activate prothrombin [138][139]. Embp contains an unstructured region at its N-terminal and a domain of unknown function and a putative transmembrane domain at its C-terminal [75]. We were unsure whether fusion at the C-terminal would inhibit the domain of unknown function or the transmembrane domain and so opted to create both simultaneously. Unfortunately, once the Coa:mCherry and vWbp:GFP fusions were complete, neither Olatz nor Melissa could detect any fluorescence from them when imaging biofilms expressing these fusions with CLSM. Biofilms are not an ideal environment in which to visualise fluorescent proteins; they have a dense matrix that autofluoresces, scatters light, and reduces signal to noise ratio and perhaps the proteins were too dim to image this way. However, I also could not detect any fluorescence signal from mCherry or GFP via bulk fluorescence measurements of *S. aureus* cultures containing Coa:mCherry or vWbp:GFP nor via more sensitive single molecule fluorescence microscopy, and therefore we concluded that the fusions were either fluorescing too dimly to detect above the background or were not fluorescing at all.

Olatz later discovered that there had been a fatal error early on in the cloning process: due to a copy and paste error when ordering plasmids containing the genes for GFP and

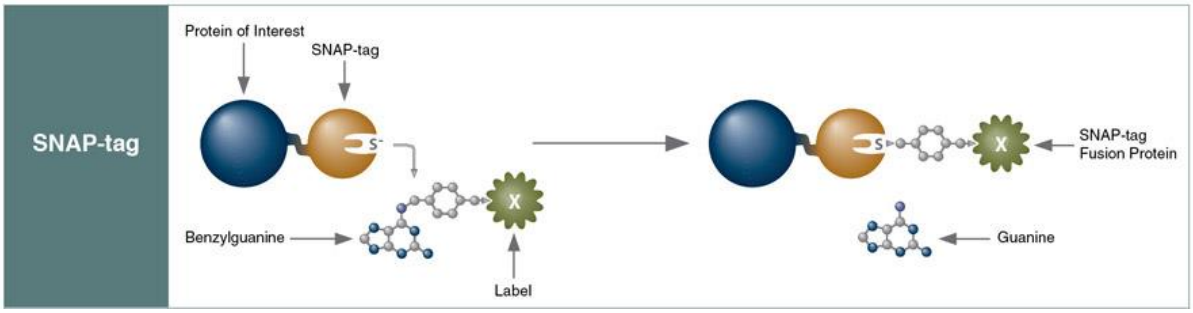

Figure 13 SNAP tag labelling reaction. Image taken from https://international.neb.com/tools-and-resources/feature-articles/snap-tag-technologies-novel-tools-to-study-protein-function, accessed on 8.12.20 at 10.36 AM.

mCherry, we ordered the wrong GFP variant by mistake. We intended to clone monomeric superfolder GFP (msfGFP), which is bright, photostable, and folds quickly [140][141], but actually cloned GFP(-30), a super negatively charged variant of super folder GFP (sfGFP) [142], which folds in minutes without molecular chaperones [117], but it has a very dim signal which was perhaps too low to detect in our experiments [123]. I did however expect to detect mCherry signal because it had been used for single molecule detection in the literature [143], albeit in less complex backgrounds such as cells in media rather than biofilms, and speculated that there were other reasons why no fluorescence was detected. The majority of secreted proteins are exported via the Secretory (Sec) pathway, in which the protein is exported in an unfolded or loosely folded state and folds in the extracellular environment [144]. Coa contains an N-terminal Sec type signal sequence and is hence exported via the Sec pathway [145]. vWbp is likely to be Sec-exported too due to its homology to Coa. Therefore, mCherry was exported whilst unfolded and needed to fold correctly in the extracellular space. This environment contains a high density of anionic polymers, such as teichoic acids, and metal cations, which affect the folding and stability of proteins, and proteases that degrade misfolded proteins [144]. Native secreted proteins have evolved to rapidly fold into their 3D conformation assisted by chaperones and metal cations [144]. Perhaps mCherry misfolded in the extracellular space and was degraded, did not fold quickly enough and was therefore degraded, or the fluorescent chromophore did not mature properly. The half time for mCherry maturation is 15 - 40 minutes [115][146], which could have been too slow to protect it from degradation by extracellular proteases before it folds.

As an alternative strategy, we began to produce fusion proteins for vWbp and Embp with the very bright fluorescent protein mNeongreen [147], but quickly discarded these projects upon realising that mNeongreen is photoswitchable and turns into a dark state when irradiated by high laser intensities [148], which was an undesired quality (Table 4). I supervised Lisbeth Marcussen and Kristian Rasmussen (Aarhus University) for this aspect of the project (Table 4). Finally, I decided to go back to our original strategy to produce fusions with msfGFP, and to bet on multiple horses by also producing fusions with the SNAP and CLIP tags. The SNAP tag is a 20 kDa mutant of the DNA repair protein O^6-alkylguanine-DNA alkyltransferase, which can be labelled with a fluorescent substrate [119]. The substrate is an O^6-benzylguanine derivative conjugated to a fluorophore, which forms a covalent bond with the active site in SNAP (Figure 13). SNAP was used to label a membrane protein in another Gram positive organism, *Bacillus subtilis*, which indicates that SNAP is able to fold in the extracellular environment and therefore might be a good candidate for labelling

Table 4 List of all fusion protein projects related to my PhD. Full names of students who worked on these projects are: Dominique Evans (me), Olatz Niembro, Melissa Eriksen, Bhaskar Pradhan, Lisbeth Marcussen, Kristian Rasmussen, Nasar Kahn, and Amalie Grønning.

Fusion Protein	**Host bacteria**	**Status**	**Comments**	**Produced by**
vWbp:GFP	*S. aureus* 29213 Δ*coa*	Completed	Fusion protein functioned normally but no GFP fluorescence detected	Olatz
Coa:mCherry	*S. aureus* 29213 Δ*vwbp*	Completed	Fusion protein functioned normally but no mCherry fluorescence detected	Me, Melissa
Embp:GFP (C-terminal)	*S. epidermidis* 14.1.R1	Discarded	Discarded due to poor GFP fluorescence from vWbp:GFP	Me, Bhaskar, Lisbeth
GFP:Embp (N-terminal)	*S. epidermidis* 14.1.R1	Discarded	Discarded due to poor GFP fluorescence from vWbp:GFP	Me, Bhaskar, Lisbeth
mNeongreen:Embp	*S. epidermidis* 14.1.R1	Discarded	Discarded due slow maturation time and photo switchable property	Me, Lisbeth, Kristian
vWbp:mNeongreen	*S. aureus* 29213 Δ*coa*	Discarded	Discarded due slow maturation time and photo switchable property	Me, Lisbeth, Kristian
Coa:SNAP	*S. aureus* 29213 Δ*vwbp* and wildtype	Completed – see Chapter 5	Coa:SNAP localised within fibrin pseudocapsule as expected	Me
vWbp:CLIP	*S. aureus* 29213 Δ*coa* and wildtype	Completed – see Chapter 5	vWbp:CLIP localised within the fibrin pseudocapsule	Me
Coa:msfGFP	*S. aureus* 29213 Δ*vwbp* and wildtype	Completed – see Chapter 6	msfGFP signal appeared to be intracellular. GFP not secreted properly	Me
SNAP:Embp	*S. epidermidis* 14.1.R1	Completed – see Chapter 7	No SNAP labelling seen	Me, Lisbeth, Nasar
msfGFP:Embp	*S. epidermidis* 14.1.R1	Completed – see Chapter 7	Alternative to SNAP:Embp, but no fluorescence seen, likely due to poor fusion protein placement	Me, Lisbeth, Amalie

secreted proteins in *S. aureus* and *S. epidermidis* [149]. Organic fluorophores used to label the SNAP substrate are brighter than fluorescent proteins, so the signal is more likely to be detectable above the background as well. CLIP is a modified version of SNAP which binds to benzylcytosine derivatives rather than benzylguanine derivatives [150], which allows different fusion proteins with SNAP and CLIP to be visualised simultaneously. I created Coa:SNAP and vWbp:CLIP, which are presented in Chapter 5, Coa:msfGFP, presented in Chapter 6, and created SNAP:Embp with Lisbeth Marcussen and Nasar Kahn (Aarhus University), presented in Chapter 7 (Table 4). I initially supervised Maiken Petersen and Maiken Voss (Aarhus University) during a short project to create Coa:SNAP, who designed the primers to create this fusion protein. I completed the rest of the work myself after their project ended. In the rest of this Chapter, I will first present the work that I contributed

towards visualising Coa:mCherry and vWbp:GFP followed the cloning process to create Coa:SNAP and vWbp:CLIP. While I will only present the data for producing Coa:SNAP and vWbp:CLIP, the process was the same for creating all other fusion proteins and any minor differences in the protocols presented here are noted in the chapter relevant to that fusion protein.

4.2 Aim

The aim was to produce genomically integrated, C- terminal fusion proteins in different *S. aureus* 29213 backgrounds. After experimenting with several protein tags, it was eventually decided to create Coa:SNAP in *S. aureus* 29213 Δ*vwbp*, vWbp:CLIP in *S. aureus* 29213 Δ*coa*, and both Coa:SNAP and vWbp:CLIP in *S. aureus* 29213 wildtype. These fusions would allow me to visualise Coa and vWbp in backgrounds lacking the other protein, as well as to visualise them jointly in the wildtype to learn about their localisation with respect to fibrin and bacteria.

4.3 Materials for cloning

All plasmids, primers, and bacterial strains used are listed in Table 5 and full mutant sequences in Appendix 1. All bacteria were stored in 15 - 25 % glycerol at -80 °C. Brain heart infusion (BHI, Sigma Aldrich, 53286) was used to culture *S. aureus*, and Luria broth (LB, Sigma Aldrich, L3522) for *E. coli*. For growth on plates, media was supplemented with 15 g/L of agar (Sigma Aldrich, A1296), and the antibiotics chloramphenicol (Cm, Sigma Aldrich, C0378) and anhydrotetracycline hydrochloride (ATc, Sigma Aldrich, 94664) if necessary. Cm was used for plasmid selection at a concentration of 25 µg/ml for *E. coli* and 10 µg/ml for *S. aureus*, and ATc at 1 µg/ml.

REDTaq ReadyMix (Sigma Aldrich, R2523) was used for standard PCR reactions according to the manufacturer's protocol, and Phusion Green Hot Start II High-Fidelity PCR Master Mix (Thermo Fisher Scientific, F566S) for high fidelity reactions according to the manufacturer's protocol. All primers used throughout this project were purchased from either Sigma Aldrich or Thermo Fisher Scientific. PCR reactions were carried out using the Thermo Fisher Scientific Arktik Thermal Cycler, and products analysed by gel electrophoresis on 0.7 - 1 % agarose in 0.5 x TBE gels. DNA was stained with SYBR Safe DNA Gel Stain (Invitrogen, S33102) and visualised using the Gel Doc EZ Imager (BioRad) and Image Lab Software (Biorad). PCR products were run alongside TrackIt 1 kb Plus DNA Ladder (Invitrogen, 10488085) to estimate the size of the products, and finally PCR products were purified either using the GenElute PCR Clean-Up Kit (Sigma Aldrich, NA1020-1KT), or the GenElute Gel Extraction Kit (NA1111-1KT). The final PCR constructs were cloned into pIMAY using the Gibson Assembly Cloning Kit (New England Biolabs, E5510S), plasmid extractions were performed using the GeneJET Plasmid Miniprep Kit (Thermo Fisher Scientific, K0502), and genomic DNA extractions with the GenElute Bacterial Genomic DNA Kits (Sigma Aldrich, NA2110-1KT). DNA was sequenced by Macrogen.

Table 5 All bacterial strains, plasmids, and primers used throughout this Chapter. Primer overhangs are lower case, while the annealing parts are in upper case text.

Bacterial Strain	**Description**	**Reference**
Escherichia coli IM08B	Derived from *E. coli* K12 DH10B. Deficient in cytosine methylation (Δ*dcm*) and methylates adenine (*hsdMS*) to bypass *S. aureus* restriction barriers.	[151]
Staphylococcus aureus ATCC 29213	Clinical wound isolate. Standard laboratory strain.	
Staphylococcus aureus ATCC 29213 Δ*coa*	*S. aureus* 29213 *coa* deletion mutant. A gift from Janne K. Klitgaard, University of Southern Denmark.	Janne K. Klitgaard
Staphylococcus aureus ATCC 29213 Δ*vwbp*	*S. aureus* 29213 *vwbp* deletion mutant. A gift from Janne K. Klitgaard, University of Southern Denmark.	Janne K. Klitgaard
Plasmid	**Description**	**Reference**
pUC57-*CLIP*	*E. coli* vector carrying *CLIP*. Ampicillin resistance.	Genscript
pUC57-*SNAP*	*E. coli* vector carrying *SNAP*. Ampicillin resistance.	Genscript
pIMAY	*E. coli*/*Staphylococci* temperature sensitive vector for allelic exchange. Cm resistance. Inducible *secY* antisense. pIMAY was a gift from Tim Foster (Addgene plasmid # 68939 ; http://n2t.net/addgene:68939 ; RRID:Addgene_68939).	[152]
Primer	**Sequence (5' – 3') and description**	**Reference**
v1F	atcaataaagtatacaatggcaaaTCAGGTGGTGGAGGAGATAA Fwd primer to amplify CLIP sequence from pUC57-*CLIP*	Me
v1R	tttgcagccatgcattaatattaaccTAAACCTGGTTTACCTAAACG Rev primer to amplify CLIP sequence from pUC57-*CLIP*	Me
v2F	tcactaaagggaacaaaagctgggtacCGTCAAACTCAGCAACAA Fwd primer to amplify upstream of *vwbp* from *S. aureus* 29213	Me
v2R	ttatctcctccaccacctgaTTTGCCATTGTATACTTTATTGAT Rev primer to amplify upstream of *vwbp* from *S. aureus* 29213	Me
v3F	cgtttaggtaaaccaggtttaggtTAATATTAATGCATGGCTGCAAA Fwd primer to amplify downstream of *vwbp* from *S. aureus* 29213	Me
v3R	gataccgtcgacctcgagggggggcccgCAAATAGCGTGCTCATAGT TAAA Rev primer to amplify downstream of *vwbp* from *S. aureus* 29213	Me
vOutF	AAAATCTAAAAATGAGTCTGTGGTT Fwd primer for screening vWbp:CLIP integration	Olatz Niembro
vOutR	TTACTAACATTTACTTTTGGCGAAT Rev primer for screening vWbp:CLIP integration	Olatz Niembro
c1F	atgggcctagagtaacaaaaTCAGGTGGTGGAGGA Fwd primer to amplify SNAP sequence from pUC57-*SNAP*	Maiken Petersen & Maiken Voss
c1R	tgtctttggatagagttataaatttaACCTAAACCTGGTTTACCTAAA Rev primer to amplify SNAP sequence from pUC57-*SNAP*	Maiken Petersen &

		Maiken Voss
c2F	cctcactaaagggaacaaaagctgggtacGCCAAGTGAAACAAACGCAT Fwd primer to amplify upstream of *coa* from *S. aureus* 29213	Maiken Petersen & Maiken Voss
c2R	ttatctcctccaccacctgaTTTTGTTACTCTAGGCCCATATGTC Rev primer to amplify upstream of *coa* from *S. aureus* 29213	Maiken Petersen & Maiken Voss
c3F	taggtaaaccaggtttaggtTAAATTTATAACTCTATCCAAAGACATACAGTCA Fwd primer to amplify downstream of *coa* from *S. aureus* 29213	Maiken Petersen & Maiken Voss
c3R	atcaagcttatcgataccgtcgacctcgaggggggggcccgTTTTAAATTTTATGAATCGAAGCCCTTTG Rev primer to amplify downstream of *coa* from *S. aureus* 29213	Maiken Petersen & Maiken Voss
OutF*	GTGAAATATAGAGATGCTGGTACA Fwd primer for screening Coa:SNAP integration	Melissa Eriksen
OutR*	TGAAGTAGGCTGAAGTTGAAGC Rev primer for screening Coa:SNAP integration	Melissa Eriksen
IM151	TACATGTCAAGAATAAACTGCCAAAGC Anneals to pIMAY multiple cloning site	[152]
IM152	AATACCTGTGACGGAAGATCACTTCG Anneals to pIMAY multiple cloning site	[152]

4.4 Methods

4.4.1 Bulk fluorescence measurements from Coa:mCherry and vWbp:GFP

Overnight cultures of *S. aureus* 29213 Δ*vwbp* expressing Coa:mCherry, *S. aureus* 29213 Δ*coa* expressing vWbp:GFP, and their parental strains were diluted to OD_{600} 0.5 in a total volume of 2 ml, and were harvested by centrifugation for 10 minutes at 4000 x *g*. Bacteria were resuspended in 2 ml PBS supplemented with 10 % plasma, incubated at 37 °C for 10 minutes with 180 rpm shaking, and then their fluorescence was measured in a fluorimeter. Samples were excited at 488 nm for vWbp and 587 nm for Coa, and emissions detected over 500 – 700 nm for vWbp and 600 – 700 nm for Coa. Assoc. Prof. Victoria Birkedal (Aarhus University) kindly let me use the fluorimeter in her lab and helped me use it.

4.4.2 Single molecule fluorescence microscopy to detect Coa:mCherry and vWbp:GFP

Overnight cultures of *S. aureus* 29213 Δ*vwbp* expressing Coa:mCherry, *S. aureus* 29213 Δ*coa* expressing vWbp:GFP, and their parental strains were incubated with growth media containing 25 % heparin stabilised human plasma, then either immobilised on an agarose pad or in a tunnel slide, and imaged using total internal reflection microscopy (TIRF) or Slimfield microscopy. To prepare tunnel slides, 1.5 ml culture was harvested by centrifugation at 4000 x *g* and washed twice in 750 µl PBS before resuspending in 750 µl CDM (chemically defined media, a low autofluorescence growth medium for staphylococci) supplemented with 25 % human plasma. The bacteria were incubated at 37 °C for 90 minutes and then 20 µl

loaded into a tunnel slide for imaging. For agarose pads, 5 µl bacteria from the overnight cultures were spotted onto a pad containing CDM supplemented with 1% agarose and 25 % plasma, and incubated at 37 °C for 90 minutes. Samples containing Coa were imaged in a bespoke TIRF microscope using a 50 mW 561 nm laser with a beam diameter of 25 µm at the sample. 100 frames per image were taken with a 50 ms frame rate using an Andor iXon 512 x 512 EMCCD camera. Samples containing vWbp were similarly imaged with a bespoke Slimfield microscope with a 20 mW 488 nm laser and 10 µm beam diameter at the sample.

4.4.3 Overview of cloning process to produce fusion proteins with SNAP and CLIP in *S. aureus*

There are several steps to produce a genomically integrated fusion protein in *S. aureus*. Firstly, to create a DNA construct containing the SNAP/CLIP sequences via polymerase chain reaction (PCR). The construct contains a linker followed by the SNAP/CLIP sequence, flanked by 400 – 600 nucleotide sequences homologous to the DNA on either side of the desired insertion site in the *S. aureus* genome, which is before the stop codon at the end of *coa* or *vwbp*. These flanking sequences allow the genomic integration of SNAP/CLIP to occur via homologous recombination later on. PCR is used to amplify the sequence of SNAP/CLIP (PCR 1), and the upstream and downstream regions around the insertion site in *S. aureus* (PCR 2/PCR 3), which are finally joined together via splicing by overlap extension PCR (SOE-PCR) (PCR 4) (Figure 14). To facilitate this, the primers contain 20 – 40 nucleotide long overhangs with sequences that match the neighbouring PCR product (Figure 14). Primers 2F and 3R add overhangs that allow PCR 4 to be cloned into pIMAY, a modified bacterial plasmid designed by Monk *et al.* for the genomic integration of DNA into staphylococci [152]. pIMAY containing the construct is transformed into *S. aureus* via an intermediate microorganism (*Escherichia coli* IM08B), and the construct integrates into the *S. aureus* genome via homologous recombination (Figure 14).

One of the challenges when cloning in staphylococci is the presence of restriction modification systems: defence mechanisms against viral infections whereby restriction enzymes cleave foreign DNA [153]. Restriction modification systems consist of a restriction endonuclease (REase) and a DNA methyltransferase (MTase). REases recognise and cleave foreign DNA that lacks methylation within specific recognition sites, while MTases protect native DNA by methylating cytosines and adenines within the recognition site [154]. Therefore pIMAY containing the SNAP/CLIP construct is first passed through *E. coli* IM08B, which methylates DNA with a profile mimicking that of *S. aureus* [151]. Then, when the DNA is transformed into *S. aureus*, the restriction modification system is bypassed. To mimic *S. aureus* methylation patterns, *E. coli* IM08B does not contain its native restriction modification system and has been engineered to contain an *S. aureus* specific adenine methyltransferase, which methylates adenines in a pattern mimicking *S. aureus* and thus blocks many restriction enzymes that cleave unmethylated adenines [151]. It also lacks DNA cytosine methyltransferase and therefore bypasses the widely spread *S. aureus* SauUSI restriction barrier which specifically targets methylated cytosines [151].

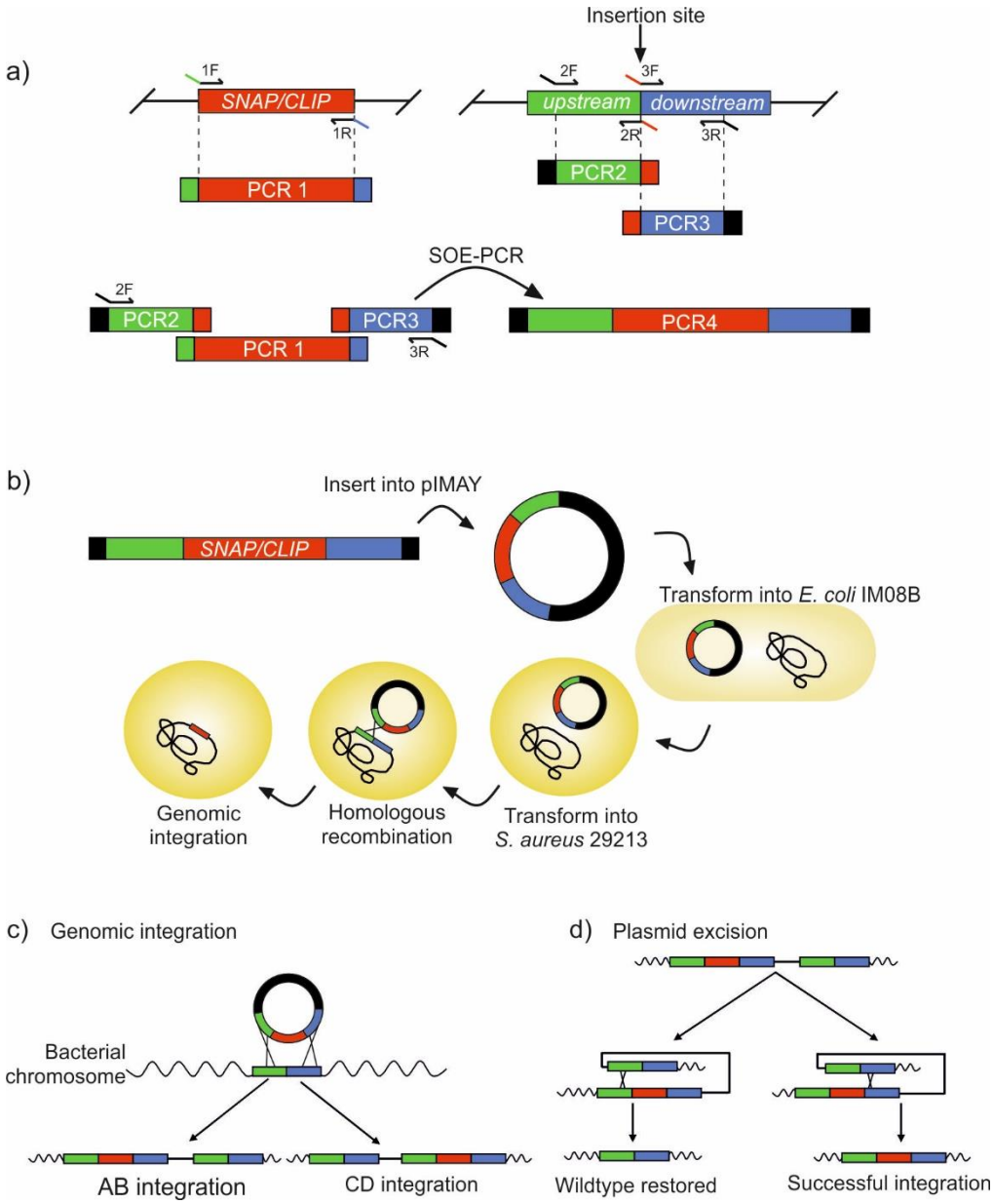

Figure 14 Diagrams of each step in the cloning process to create genomically integrated fusions of Coa:SNAP and vWbp:CLIP. a) SOE-PCR to create a DNA construct containing the sequence for SNAP/CLIP flanked by sequences homologous to the sequences on either side of the desired genome insertion site. b) Overview of the entire cloning process. c) Genomic integration of the plasmid containing the SNAP/CLIP construct. d) Plasmid excision, either restoring the wildtype genotype, or successfully integrating SNAP/CLIP.

The genomic integration of the construct occurs in two steps: integration of the entire plasmid with construct, then the excision of the plasmid, leaving the construct in the genome. pIMAY has features that help the process. It has a chloramphenicol resistance gene which allows for plasmid selection, and a temperature sensitive replicon for Gram positive bacteria, which means pIMAY only replicates at temperatures below 30 °C in staphylococci and allows for the selection of plasmid integrants [152]. Growing *S. aureus* containing pIMAY at 37 °C in media containing chloramphenicol creates selective pressure for the integration of pIMAY into their chromosome, since the chromosome can replicate at 37 °C but pIMAY cannot. This occurs via homologous recombination between one of the homologous regions between the insert and chromosome, and leads to integration in one of two orientations (Figure 14). Finally, the plasmid is excised. This occurs by another recombination event when the selection pressure for plasmid integration is removed, and results in either a successful integration of SNAP/CLIP or the restoration of the wildtype genotype (Figure 14). To screen for bacteria that have excised the plasmid, pIMAY contains *anti-secY*, a suicide gene which is activated in the presence of anhydrotetracycline. When activated, *anti-secY* produces an antisense RNA complementary to the mRNA for *secY*, blocking its translation. SecY is a housekeeping protein that cells cannot survive without. When they excise pIMAY, bacteria lose their resistance to chloramphenicol, and therefore bacteria that grow with anhydrotetracycline and are sensitive to chloramphenicol have excised the plasmid, and PCR and genetic sequencing confirm the successful integration of the SNAP/CLIP gene.

4.4.4 PCR to make SNAP/CLIP constructs

SOE-PCR was used to create DNA constructs containing the sequences for SNAP and CLIP, flanked by regions homologous to the DNA on either side of their desired insertion sites in *S. aureus*. All primers were added at a final concentration of 0.5 µM in 50 µl reactions, and annealing temperatures were calculated with the Thermo Fisher Scientific online calculator [155], omitting the primer overhangs which do not anneal to the template DNA. All PCR products, primers, annealing temperatures, and expected product sizes are listed in Table 6. 10 ng plasmid DNA was used as template to amplify SNAP/CLIP from pUC57 (PCR 1), and 166 ng *S. aureus* 29213 genomic DNA as template for PCR 2/PCR 3.The rest of the PCR conditions were calculated as stated in the manufacturer's protocol.

Table 6 PCR products, primer pairs, annealing temperatures, and product sizes when producing the construct containing SNAP/CLIP. The letter c denotes PCR products for Coa:SNAP, and v for vWbp:CLIP.

PCR product	Primer pair	Annealing temperature (°C)	Product size (base pairs)
cPCR 1	c1F/c1R	58.4	604
cPCR 2	c2F/c2R	67.8	449
cPCR 3	c3F/c3R	63.1	455
cPCR 4	c2F/c3R	62.3	1422
vPCR 1	v1F/v1R	62.8	605
vPCR 2	v2F/v2R	58.3	408
vPCR 3	v3F/v3R	60.3	422
vPCR 4	v2F/v3R	58.9	1354

4.4.5 Gibson Assembly of SNAP/CLIP constructs and pIMAY

Gibson Assembly was completed according to the manufacturer's protocol [156]. Gibson Assembly is a method for assembling DNA fragments containing 20 – 40 base pair overlapping regions. The fragments are mixed in a master mix containing three enzymes: an exonuclease to chew back the 5' ends of the DNA so the fragments can anneal, a DNA polymerase to fill in any gaps leftover, and a DNA ligase to remove nicks in the DNA. Maiken Petersen and Maiken Voss (Aarhus University) digested pIMAY using the restriction enzyme KpnI-HF (New England Biolabs, R3142S) according to the manufacturer's protocol. Then I completed the rest of the assembly. 50 ng of digested pIMAY was combined in a 20 µl reaction on ice with a 2 x excess of PCR 4 (100 ng), the provided Gibson Assembly Master Mix, and deionized water. The reactions were incubated on a heating block at 50 °C for 15 minutes and then either stored on ice for transformation immediately afterwards, or at -20 °C for use later.

4.4.6 Chemical transformation of *E. coli* IM08B

To make chemically competent cells, an overnight culture of *E. coli* IM08B was diluted in 110 ml LB media to an OD_{600} of 0.02 and incubated at 37 °C until the OD_{600} reached 0.3. The cells were divided into two 50 ml falcon tubes and transferred to ice to prevent further growth. Bacteria were harvested by centrifugation at 4000 x *g* for 10 minutes, and the supernatant discarded. Cells were then resuspended in 5 ml ice cold $CaCl_2$ (50 mM) and centrifuged again and resuspended in 1.2 ml ice cold $CaCl_2$ (50 mM). Then they were incubated on ice for 30 minutes and used immediately for transformation. Cells could however be stored for later at use at -80 °C by adding glycerol to a final concentration of 25 %.

pIMAY containing PCR 4 was transformed into chemically competent *E. coli* IM08B in the following way. Either 2 µl or 5 µl of pDNA was combined with 200 µl competent cells and incubated on ice for 20 minutes. Empty pIMAY was combined with 200 µl cells as a positive control, and 200 µl competent cells with no pDNA as a negative control. Cells were placed in a water bath at 42 °C for 90 s and then incubated on ice for a further 2 minutes. 1 ml of LB media preheated to 37 °C was added to the cells, and then incubated with gentle shaking at 37 °C for 1 hour. Cells were harvested by centrifugation at 800 x *g* for 5 minutes and 1 ml of the supernatant discarded. Cells were resuspended in the remaining supernatant and 150 µl of the mixture plated onto BHI agar plates containing 25 µg/ml Cm and incubated overnight at 37 °C.

Colonies from these transformations were screened with colony PCR using primers IM151/IM152 to verify the presence of the plasmid with the correct sized insert. IM151 and IM152 anneal to either side of the pIMAY multiple cloning site, so a small product of approximately 300 base pairs is expected when there is no insert and a larger product of approximately 1600 base pairs when there is an insert. Template DNA was prepared for PCR by touching the colony with an inoculation loop, spotting it onto a fresh plate, and mixing the remainder of the colony on the loop in 50 µl nuclease free water. The bacteria were incubated at 100 °C for 10 minutes to lyse the cells and release the DNA, and 1 - 10 µl used as template in the PCR. Empty pIMAY was used as a control. PCR products were analysed by gel electrophoresis to verify which colonies might have the correct insert, and likely candidates

sent for sequencing with IM151/IM152. *E. coli* IM08B with the correct insert were finally made into freezer stocks and plasmids extracted for transformation into *S. aureus* 29213 using a plasmid extraction kit.

4.4.7 Electroporation of *S. aureus* 29213 wildtype, Δ*coa*, and Δ*vwbp*

pIMAY containing the CLIP construst was electroporated into *S. aureu*s 29213 wildtype and Δ*coa*, while pIMAY containing the SNAP construct was electroporated into *S. aureus* 29213 Δ*vwbp* and the wildtype with vWbp:CLIP already genomically integrated. To prepare electrocompetent cells, an overnight culture of the required bacteria was diluted in 100 ml BHI to an OD_{600} of 0.5, and incubated at 37 °C until the OD_{600} reached 0.6. The cells were divided into two 50 ml tubes and harvested by centrifugation at 4 °C at 4000 x *g* for 10 minutes. The supernatant was discarded and cells resuspended in 50 ml each of ice cold 0.5 M sucrose. The harvest/resuspension steps were repeated with increasingly lower volumes of sucrose: 5 ml, 2 ml, and 0.25 ml. Then cells were ready to be transformed. 50 µl electrocompetent cells were incubated on ice with 350 - 650 ng pDNA (less than 5 µl total volume) for 1 minute, then transferred to a chilled 1 mm electroporation cuvette and electroporated using the ECM 360 BTX (Harvard Apparatus). The following electroporation parameters were used: 2.1 kV, 25 µF, and 200-300 Ω. The resistance was varied to get a time constant $\tau > 4$ ms, indicating a successful transformation [129]. 1 mL preheated BHI supplemented with 0.5 M sucrose was immediately added and incubated at 28 °C with shaking at 250 rpm for 2 hours. Afterwards, 200 µl cells were plated onto BHI plates containing 10 µg/ml Cm. Remaining cells were centrifuged for 5 minutes at 4000 x *g*, 750 µl removed, and then the cells were resuspended in the remaining supernatant and plated as well. Plates were incubated for 1 - 2 days at 28 °C until colonies grew. Colonies were screened again with colony PCR with primers IM151/IM152, analysed by gel electrophoresis, and made into freezer stocks.

4.4.8 Genomic integration of construct

Transformed bacteria were incubated overnight in 10 ml BHI containing 10 µg/ml Cm at 28 °C, a temperature permissive for pIMAY replication. 5 µl was transferred into 10 ml fresh BHI containing 10 µg/ml Cm and incubated overnight at 37 °C. When growing at 28 °C, there is a chance that a crossover event will occur between the homologous regions in the vector insert and genomic DNA, and the plasmid will incorporate into the chromosome via homologous recombination. Since pIMAY contains a resistance gene for Cm but only replicates below 30 °C, and the chromosome replicates at 37 °C, only bacteria that have incorporated pIMAY into the chromosome will survive growing at 37 °C with antibiotics. A dilution series from 10^{-3} to 10^{-6} was made from the overnight culture grown at 37 °C and plated onto BHI plates containing Cm, and incubated overnight at 37 °C. Colonies with integration were inoculated in 10 ml BHI and incubated overnight at 28 °C with 180 rpm shaking. The next day, 10 ul of the overnight culture was inoculated into 10 ml fresh BHI and incubated again at 28 °C. This was repeated for 10 days, after which serial dilutions from 10^{-1} to 10^{-8} were plated onto BHI plates and BHI plates with 1 µg/ml ATc and incubated for 1 - 2 days at 28 °C. Bacteria still containing the plasmid could not grow in the presence of ATc. 100 colonies from the ATc plates were spotted onto BHI plates with and without

10 µg/ml Cm and incubated overnight at 37 °C. Cm sensitive colonies had excised the plasmid and colony PCR was performed with OutF/OutR primers to determine if SNAP/CLIP had been integrated or if the wildtype phenotype had been restored. Successful integrants were sequenced with the OutR/OutF primers and freezer stocks made.

4.4.9 Evaluating the mutants

The genotype of the completed mutants were evaluated by sequencing with OutF/OutR primers, and the phenotype via coagulation assays and confocal laser scanning microscopy (CLSM). For the coagulation assays, overnight cultures of the mutants and their parental strains were diluted to OD_{600} 0.5 in 1 ml of 1:6 heparin stabilized human plasma in normal saline (85 %) in sterile glass tubes and incubated for 4 hours at 37 °C with no shaking. Coagulation was assessed by tilting the tubes after 4 hours. Then the tubes were left to incubate at room temperature overnight, and the coagulation assessed again after 18 more hours. A negative control with no bacteria was also included.

For CLSM imaging, microwells (µ Slide 8 well, IBIDI, 80826) were preconditioned by incubating with 180 µl mBHI supplemented with 50 % human heparin stabilized plasma, 0.4 µg/ml Alexa Fluor 647 conjugated fibrinogen, and 1 µM Syto41 for 30 minutes at 37 °C. mBHI is modified BHI that contains 2.1 mM $CaCl_2$ and 0.4 mM MgCl to mimic physiological conditions. The microwells were inoculated with bacteria to a final volume of 200 ul and OD_{600} 0.5 and incubated at 37 °C for 2 hours. The liquid over the biofilms was replaced with 200 ul fresh mBHI containing 50 % plasma, fluorescent fibrinogen, and Syto41, and incubated overnight. Samples were imaged using CLSM (LSM700, Zeiss) with 10 mW 488 nm, 5 mW 639 nm, and 5 mW 405 nm lasers operating at 2% power and a Plan-Apochromat 63x/1.40 oil immersion objective lens.

4.5 Detecting Coa:mCherry and vWbp:GFP results

4.5.1 Bulk fluorescence from Coa:mCherry and vWbp:GFP could not be detected

The first strategy to detect fluorescence from our original Coa:mCherry and vWbp:GFP fusion proteins was to measure bulk fluorescence from bacteria expressing Coa:mCherry and vWbp:GFP with a fluorimeter. The mCherry/GFP modified strains both had marginally higher intensity fluorescence emissions than the parental strains, however this was only a very slight difference (Figure 15a). Subtracting the parental signal from the Coa:mCherry/vWbp:GFP signal should yield the emission spectrum of that fluorescent protein if it produces a detectable signal. No peaks corresponding to mCherry or GFP fluorescence were found with this method (Figure 15b). Either mCherry and GFP were not fluorescing, or the signal was too dim compared to the autofluorescent background to detect with this method.

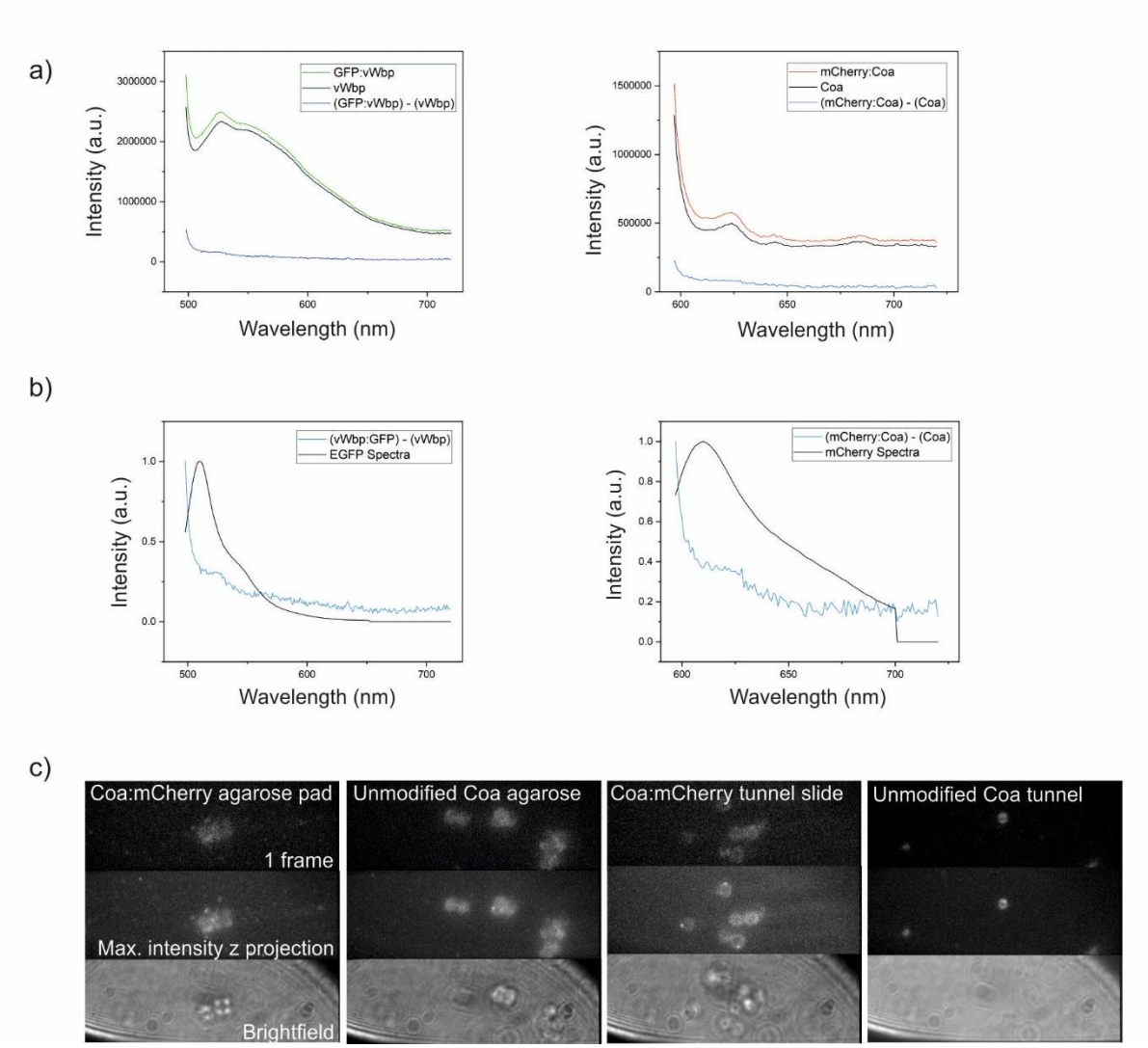

Figure 15 a) Emission spectra of *S. aureus* Δ*coa* with modified and unmodified vWbp, and *S. aureus* Δ*vwbp* with modified and unmodified Coa. b) The parental spectra subtracted from the vWbp:GFP/Coa:mCherry compared to the spectra of GFP and mCherry alone. c) TIRF images of *S. aureus* Δ*vwbp* expressing Coa:mCherry or native Coa, immobilized on an agarose pad or in CDM in a tunnel slide.

4.5.2 Coa:mCherry and vWbp:GFP signal could not be detected with single molecule microscopy

In case the fusion proteins produced a signal below the detection limit of the fluorimeter, bacteria expressing both fusion proteins were imaged with single molecule microscopy. There was no clear fluorescence from Coa:mCherry or vWbp:GFP. The cells produced a lot of autofluorescence and some bright spots appeared in areas away from the cells (Figure 15c) These spots were present in both the samples with and without mCherry/GFP, and not present at all in a blank sample containing just imaging media (data not shown), so they must originate from the bacterial samples. To determine if these spots were mCherry/GFP signal, the number of spots in the mCherry/GFP and parental samples were quantified and compared. 5 80 x 80 and 3 100 x 100 pixel regions of interest were selected at random from each sample and processed using ADEMS Code v10, a program written by the Leake group which

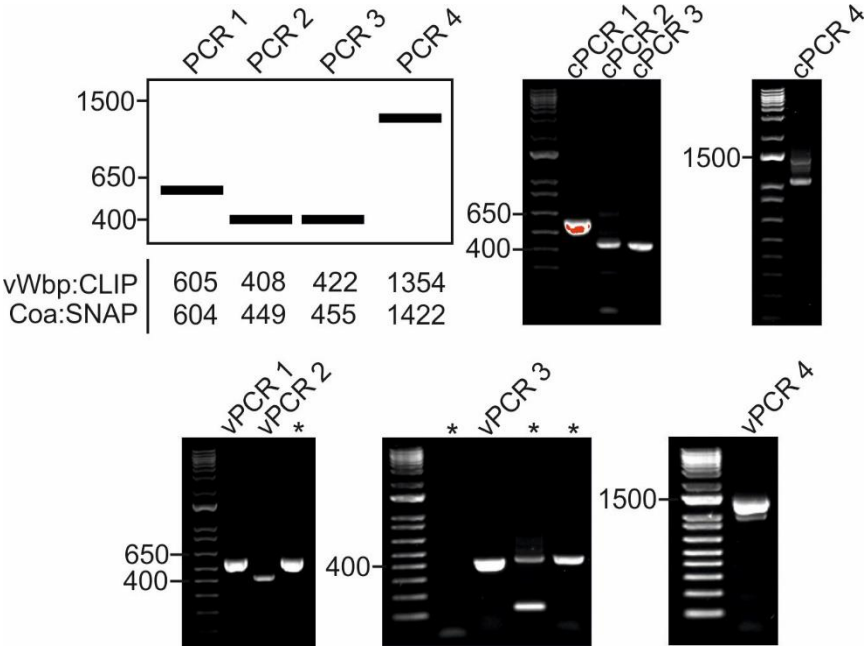

Figure 16 PCR products for producing SNAP/CLIP constructs visualised on agarose gels. The predicted product sizes are shown on the white background and the actual products on black. The letter v denotes vWbp:CLIP products and c denotes Coa:SNAP products. Red pixels are oversaturated. PCR products from an unrelated project are marked by a star. Numbers pointing to ladders on gels represent the size of the DNA ladder in nucleotides.

identifies candidate spots for single molecules and tracks them through each frame. A T-test showed that there was no significant difference in the number of spots between the mCherry/GFP and corresponding parental samples, so the spots were concluded to not be fluorescence from mCherry or GFP.

4.6 Cloning results

4.6.1 PCR to make SNAP/CLIP constructs

Constructs containing the sequences for SNAP/CLIP flanked by the sequences homologous to the intended insertion sites in *S. aureus* were synthesised via PCR and SOE-PCR. All PCR products were analysed via gel electrophoresis to verify that they were the correct approximate size. PCR products were loaded onto an agarose gel and an electric field used to move the negatively charged DNA through the gel. Smaller DNA products migrated through the pores of the gel faster than larger ones, separating the DNA products by size. A DNA ladder containing fragments of known sizes was run alongside, which allowed an estimate of size. The gel was stained with SYBR Safe (Invitrogen, S33102), so the DNA could be visualised under blue light.

All PCR products 1 – 4 for vWbp:CLIP and Coa:SNAP were approximately the correct size (Figure 16). The DNA was purified using a PCR clean up kit when there was a single band on the gel corresponding to a PCR product of a single length. When there were multiple bands, the band of the correct size was excised and purified using a gel extraction kit.

4.6.2 Chemical transformation of *E. coli* IM08B

The SNAP/CLIP constructs were assembled with pIMAY via Gibson Assembly [156] and transformed immediately into *E. coli* IM08B via chemical transformation. *E. coli* were treated with calcium chloride, incubated with the plasmid DNA, and a heat shock applied. The calcium cations bind the negatively charged plasmid DNA and cell wall to overcome the electrostatic repulsion that usually inhibits the uptake of DNA, and is thought that it could cause pores to form in the membrane. The heat shock increases pore size and causes a thermal gradient to help sweep the DNA into the cells.

To verify that the plasmid had the correct sized insert, transformants were screened with colony PCR using primers that annealed to either side of the multiple cloning site (IM151/IM152), and PCR products were visualised with gel electrophoresis. The product should be 1632 - 1636 bases if the insert was correct, and 283 base pairs if there was no insert (Figure 17a). vWbp:CLIP colony 1 produced a band of the correct size while colonies 2 and 4 had bands of the incorrect size (Figure 17a). Incorrectly sized inserts presumably arose from the smeared PCR 4 bands (Figure 16) containing products of multiple sizes that were unintentionally included in the gel extraction. Colonies for Coa:SNAP produced bands of multiple sizes, with the higher bands being most likely to have the correct size (Figure 17a). Not all colonies analysed produced bands, perhaps because the template DNA concentration in the PCR reaction was too low, or because those colonies were a contaminant.

Plasmids from multiple colonies were purified and sequenced with the IM151/IM152 primers, multiple of which had the correct sequence for the insert. Figure 17b gives an example of a plasmid containing CLIP that had the correct sequence. The forward and reverse reads were trimmed to remove poor quality sequencing data at the ends of the reads (Figure 17c) and combined into a consensus sequence, then aligned to a reference sequence using the CLC Genomics Workbench software (available at digitalinsights.qiagen.com). Bold red/green indicates where the sequence aligned to the reference and faint red/green where the data was trimmed. There were no mismatches between the consensus and reference and so the insert sequence was as expected.

4.6.3 Electroporation of *S. aureus* 29213 wildtype, Δ*coa*, and Δ*vwbp*

Plasmids containing the correct insert were transformed into *S. aureus* via electroporation. *S. aureus* were repeatedly washed with sucrose to remove ions from the growth medium. Then, the bacteria were incubated with the DNA and a brief, high voltage electric shock applied to induce pores in the membrane and allow entry of the plasmid DNA.

Transformants were again screened with colony PCR using primers IM151/IM152 to verify that they contained a plasmid with the correct sized insert. Many colonies containing the correctly sized insert were identified (Figure 17a). The template DNA for the colony PCR was more difficult to extract via cell lysis compared to when in *E. coli* due to the thick Gram positive cell wall, which may explain why no PCR product was obtained for many colonies, particularly for vWbp:CLIP in Δ*coa*. It did not matter that some lanes lacked bands because the colonies with verified inserts were used to proceed the experiment instead.

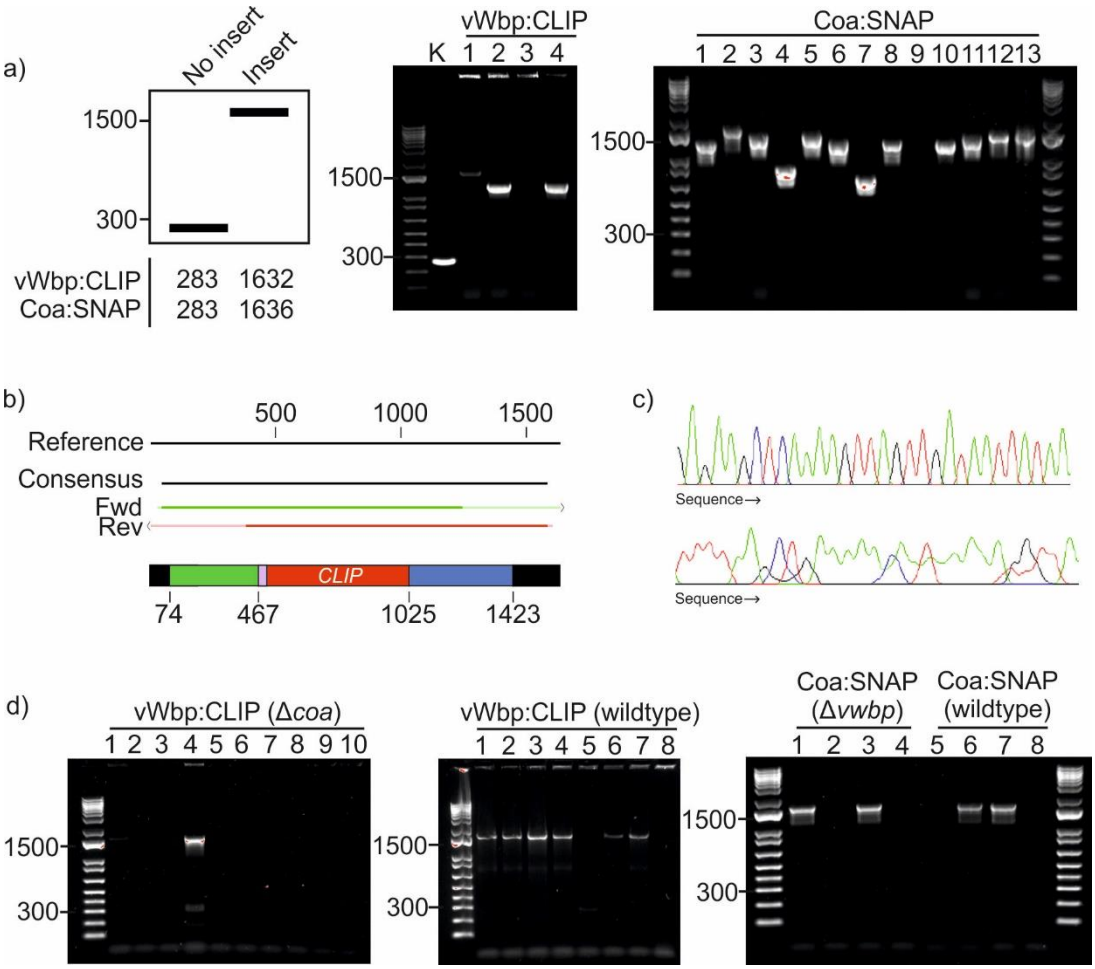

Figure 17 a) Predicted and actual product sizes when screening *E. coli* IM08B for pIMAY with the correct sized insert after transformation. b) Example of sequence alignment of sequencing data with IM151/IM152 to the reference. c) Good quality sequencing data (above) and poor quality data (below). Poor quality data was trimmed and not included in the analysis. d) Colony PCR products obtained when screening *S. aureus* transformed with pIMAY containing the SNAP/CLIP construct. Each lane contains the colony PCR product from a different colony. Numbers on gels refer to product sizes measured in number of nucleotides.

4.6.4 Genomic integration of construct

Transformants containing pIMAY with the SNAP/CLIP construct were grown under conditions permissive for plasmid replication and selection (28 °C, chloramphenicol), and then at 37 °C with chloramphenicol to select for bacteria with plasmid integration. Then the bacteria were grown at 28 °C without antibiotics for 10 days by diluting an overnight culture into fresh media to allow for plasmid excision. Bacteria were plated with anhydrotetracycline and then screened for chloramphenicol resistance to confirm that the plasmid had been excised. Chloramphenicol sensitive colonies were screened for genomic integration of SNAP/CLIP using colony PCR with the OutF/OutR primers, which anneal to either side of the insertion site. A product size of about 1100 nucleotides indicated no integration whilst a size of about 1600 nucleotides indicated a successful integration. Multiple colonies with genomic integration were identified across all strains for Coa:SNAP and vWbp:CLIP (Figure 18a).

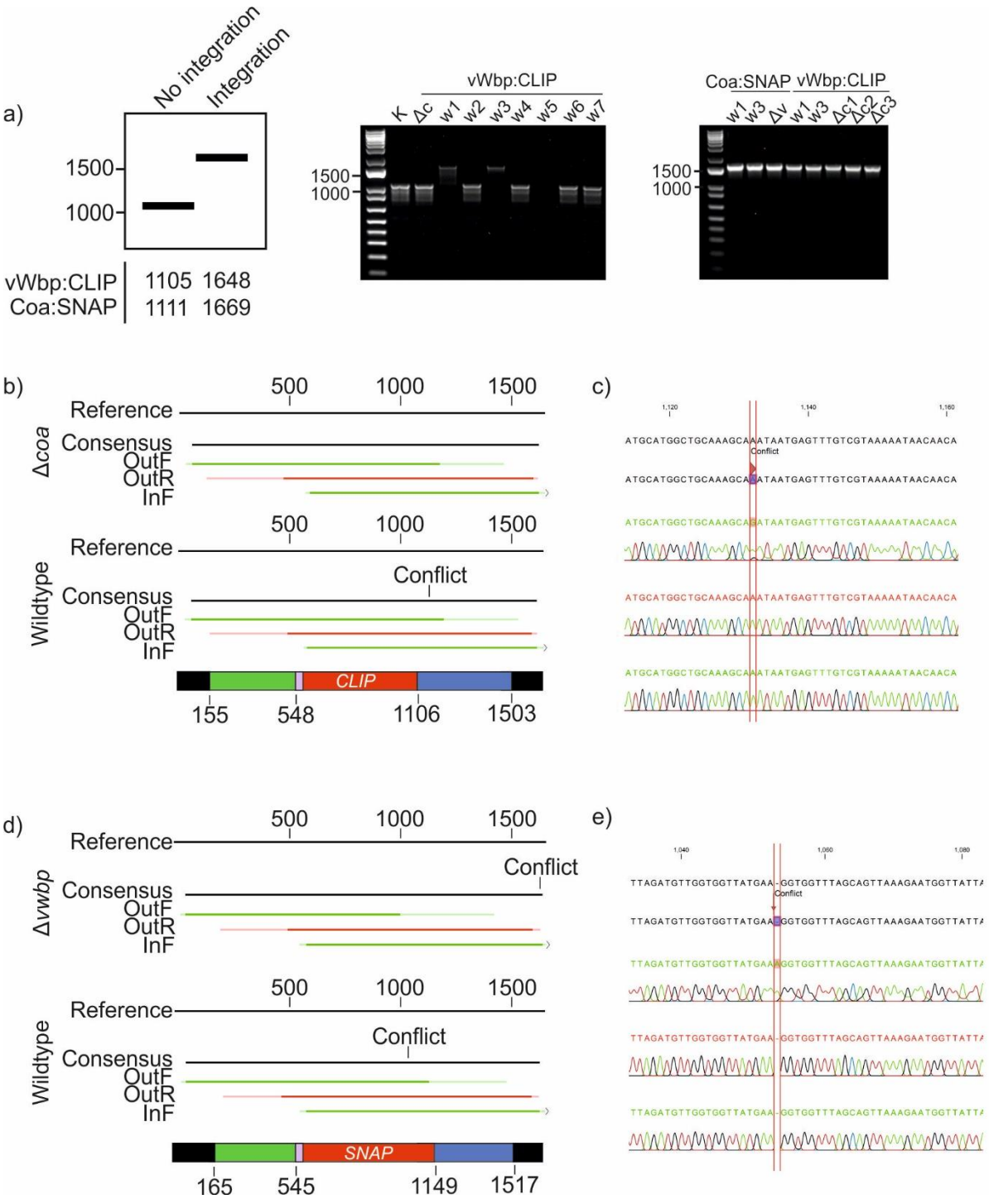

Figure 18 a) Predicted and actual PCR products when screening for genomic integration of SNAP/CLIP using the OutF/OutR primers. b) Example sequence alignments for vWbp;CLIP after genomic integration. c) A conflict in the sequencing data for vWbp:CLIP in *S. aureus* Δ*coa*. d) Example sequence alignments for Coa:SNAP after genomic integration. e) A conflict in the sequencing data for Coa:SNAP in *S. aureus* wildtype. Numbers on gels refer to product sizes measured in number of nucleotides.

4.7 Coa:SNAP and vWbp:CLIP are functional fusion proteins

4.7.1 Coa:SNAP and vWbp:CLIP modified bacteria have the predicted genetic sequence

Genomic DNA was extracted from the colonies and the region containing SNAP/CLIP was amplified with PCR using the OutF/OutR primers, which was then sequenced with OutF, OutR, and an additional InF primer which annealed to the start of the SNAP/CLIP sequence. The InF primer was introduced because initial sequencing attempts using only OutF/OutR failed to produce high quality sequencing data that spanned the entire sequence. The sequencing data from each primer was trimmed and assembled into a consensus that was compared to a reference sequence using the CLC Genomics Workbench software (available at digitalinsights.qiagen.com). There were no mismatches between the consensus and reference for vWbp:CLIP in *S. aureus* Δ*coa* (Figure 18b), indicating that CLIP was successfully inserted into the chromosome without sequence errors. A conflict arose for vWbp:CLIP in the wildtype (Figure 18c), however, upon closer inspection of the sequencing data, AAA was replaced with AGA in the OutF read whilst the other two primers indicated the correct sequence, so this was unlikely to reflect an actual error in the DNA. Conflicts also arose for Coa:SNAP in Δ*vwbp* and the wildtype (Figure 18d and 18e). However, the conflict in Δ*vwbp* was outside the homologous region and did not correspond to a sequence where any changes were made to the DNA, and this error was due to poor sequencing data at the end of the read and not an error in the DNA. The error in the wildtype was also a sequencing error rather than a mistake in the DNA; the OutF read was lower quality and introduced an extra base where there was none on the other two reads nor the reference.

4.7.2 Coa:SNAP and vWbp:CLIP modified bacteria coagulate human plasma

Coa and vWbp both hijack the host coagulation cascade to produce a fibrin clot [157]. Therefore the ability of the modified proteins to coagulate human plasma was compared to the native proteins to assess whether the proteins functioned correctly when fused to SNAP/CLIP. Bacteria containing either modified or unmodified Coa/vWbp were incubated with human plasma and the coagulation was assessed after 4 and 24 hours. All strains coagulated plasma by 4 hours, apart from a double mutant lacking both Coa and vWbp (Table 7), which confirmed that coagulation occurred due to Coa and vWbp alone. Therefore Coa and vWbp could still function to coagulate plasma when fused to SNAP and CLIP.

Table 7 Coagulation of *S. aureus* strains with modified and unmodified Coa and vWbp.

	Coagulation (+/-)							
	vWbp:CLIP		**Coa:SNAP**		**Parental strains**			
	wt	**Δ*coa***	**wt**	**Δ*vwbp***	**wt**	**Δ*coa***	**Δ*vwbp***	**Δ*coa*Δ*vwbp***
4 h	+	+	+	+	+	+	+	-
24 h	+	+	+	+	+	+	+	-

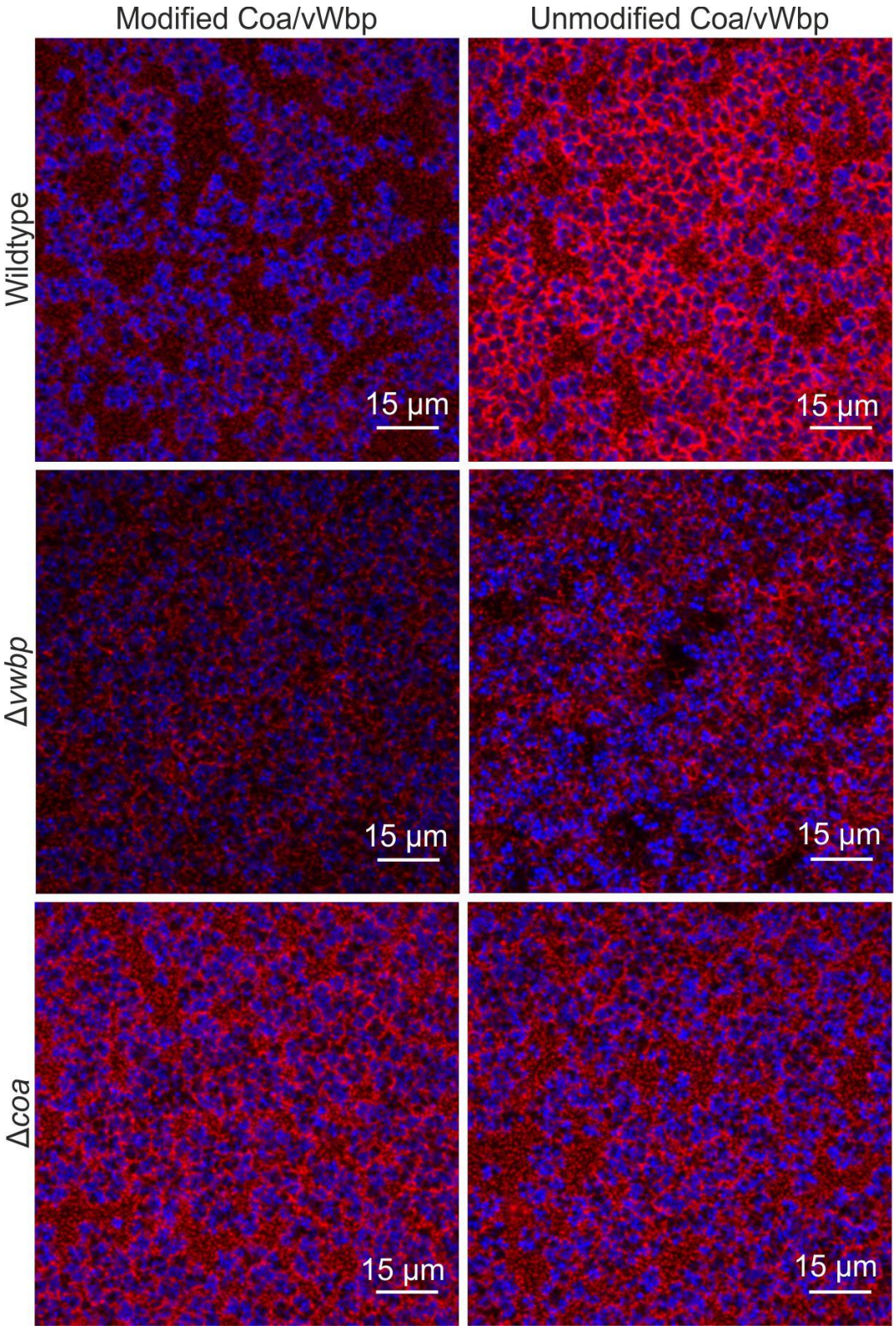

Figure 19 CLSM images of *S. aureus* biofilms formed with modified and unmodified Coa/vWbp. Cells are blue and fibrin is red.

4.7.3 Coa:SNAP and vWbp:CLIP modified bacteria produce biofilms with the same phenotype as the parental strains

Coa and vWbp cause a fibrin network to form in the biofilm extracellular matrix. As an additional check to verify that the fusion proteins functioned as expected, the phenotype of the fibrin matrix was assessed via CLSM in bacteria with modified and unmodified Coa/vWbp. The fibrin networks of all modified strains resembled the parental strains. In the wildtype and mutant lacking Coa, there was a thick extended network of fibrin (Figure 19). There were no clear differences between the modified and parental strains, except for a large increase in fibrin signal in the parental wildtype, which could have been due to a pipetting or mixing error resulting in an increased concentration of fluorescent fibrinogen during sample preparation since this increase in signal was not present in any of the other parental strains. Overall, the modified bacteria produced a fibrin network as expected and the fusion proteins functioned correctly.

4.8 Discussion

I could not detect any fluorescence from bacteria that produce Coa:mCherry or vWbp:GFP. The GFP variant that we accidentally used, GFP(-30), is very dim [123] and might not have been bright enough to detect even with single molecule microscopy. mCherry has been used to tag proteins for single molecule microscopy in the literature [143], and I therefore expected to be able to detect fluorescence from this fusion protein. However, I did not, and I hypothesised that mCherry failed to become fluorescent in the extracellular environment. Perhaps interactions with ions in the extracellular environment prevented mCherry from folding correctly, or perhaps mCherry was simply degraded by restriction enzymes before folding [144]. Therefore I decided to create fusion proteins with the SNAP and CLIP tags instead because the SNAP tag had previously been used to label an extracellular protein in a species of Gram positive bacteria in the literature [149], which indicates that it is able to fold correctly in the extracellular environment.

I assessed the ability of the completed Coa:SNAP and vWbp:CLIP fusion proteins to coagulate plasma and form a network of fibrin in biofilms. The completed Coa:SNAP and vWbp:CLIP fusion proteins caused coagulation the same as unlabelled Coa and vWbp. The sequences of the gene inserts and surrounding homologous regions were correct, and modified Coa and vWbp produced fibrin networks in *S. aureus* biofilms as expected. These results are a good indication that fusion with SNAP or CLIP did not impair the successful secretion and function of Coa and vWbp, and therefore I can progress onto doing imaging experiments with these fusion proteins. These functional assays are vital because protein tags can cause artefacts like aggregation and mislocalisation [123], so it is important to assess whether the fusion protein behaves normally compared to the native unlabelled protein before proceeding with imaging experiments [106]. Coa and vWbp have functions that can be assessed fairly easily, but in the case of proteins where this is not possible, it is a good idea to compare the distribution of the labelled fusion protein to the distribution of the native protein by another method such as antibody labelling to check that the fusion localises correctly [106]. The placement of the protein tag can affect the functionality of the fusion protein. Placing SNAP/CLIP at the C-terminal did not impair the ability of Coa and vWbp to activate prothrombin, which is the function of the N-terminal [138][139], nor did it seem to interfere

with the ability of Coa and vWbp to direct fibrin production to different biofilm locations. Creating a C-terminal fusion was a deliberate decision to avoid impairing binding to prothrombin. Sometimes the functional domains of a protein of interest are unknown, and in this case both N- and C-terminal fusions should be made to maximise the chances of success, although that was not necessary here.

Coa:SNAP and vWbp:CLIP were integrated into the genome of *S. aureus* and are therefore under the control of the native promoter, which allows for the study of Coa and vWbp under their native expression levels. Fusion proteins can alternatively be over expressed from an expression vector, which increases fluorescence intensity. It is an advantage to increase signal when the protein of interest normally has low expression levels or the protein tag has a dim fluorescence signal, which may otherwise render the signal too low to detect. Expression can also be controlled via an inducible promoter. However, over expression can cause artefacts such as aggregation [109], which is circumvented under native expression levels [110]. The levels of Coa and vWbp expression in biofilms are unknown, so it is not possible to ascertain at this stage whether it will be possible to detect fluorescence signal from the SNAP and CLIP tags above the background noise in the biofilm. However, the SNAP and CLIP substrates can be labelled with organic dyes that are much brighter than traditional fluorescent proteins, and therefore are more likely to produce a detectable signal than fluorescent proteins. It is also not possible to conclude whether the SNAP and CLIP tags function correctly from the data in this Chapter, but the imaging experiments in later Chapters would reveal this.

5. Coa:SNAP and vWbp:CLIP localisation in *S. aureus* biofilms

In order to determine the localisation of Coa and vWbp in *S. aureus* biofilms, I visualised the Coa:SNAP and vWbp:CLIP fusion proteins that I produced in Chapter 4. I anticipated that both Coa and vWbp would localise within the fibrin pseudocapsule because Coa is necessary to form the pseudocapsule and vWbp accelerates its formation, as I demonstrated in Chapter 3. My data showed that Coa and vWbp both localised within the fibrin pseudocapsule, but it was unclear to what extent they localised within the wider biofilm.

5.1 Introduction

In Chapter 3, I showed that Coa is essential for forming the fibrin pseudocapsule, one of the characteristic fibrin structures in *S. aureus* that encases aggregates of bacteria and protects them from immune cells. This was in accordance with previous research [41]. However, I also showed that vWbp accelerates pseudocapsule formation in the presence of Coa even though it does not produce a pseudocapsule by itself, which is a new discovery. I also found that Coa and vWbp both contribute to forming the wider fibrin network, a second characteristic fibrin structure, and that they both form a fibrin structure perpendicular to the biofilm-surface interface, albeit that the process is faster with Coa than vWbp. It was previously thought that Coa is primarily responsible for pseudocapsule formation whilst vWbp is primarily responsible for forming the wider network [41], but my results suggest more overlap between their roles.

To support my findings, I wanted to visualise Coa and vWbp in *S. aureus* biofilms. In Chapter 4, I developed fusion proteins for Coa and vWbp with the SNAP and CLIP tags, and verified that fusion to SNAP and CLIP did not impair the biological function of the two coagulases and could therefore be used for imaging experiments. SNAP and CLIP are genomically encoded protein tags that require labelling with a fluorescent substrate [119][150]. They recognise different substrates, which allows for dual labelling of both coagulases within the same biofilm. I expected that Coa would localise to cell surfaces to trigger pseudocapsule formation, and it has been shown previously that Coa localises within the fibrin pseudocapsule [41][42]. I expected that vWbp would localise within the fibrin pseudocapsule in the presence of Coa and would also localise to the wider biofilm.

I performed all the work in this Chapter. My initial labelling attempts showed large fluorescent backgrounds from the SNAP and CLIP substrates that inhibited the detection of signal from Coa and vWbp. To troubleshoot my labelling protocol, Assoc. Prof. Phil Hill (University of Nottingham) kindly provided me with a plasmid that he had been working with in *S. aureus* to use as a positive control. The plasmid expressed SNAP preceded by the YSIRK/G-S secretion sequence for *S. aureus* protein A (SpA) and followed by an LPXTG motif. When transformed into *S. aureus*, SNAP was secreted and covalently anchored to the cell wall via Sortase A, which recognises and cleaves the LPXTG motif. It cleaves between the threonine (T) and glycine (G) residues, and then the new C-terminal of the motif covalently binds to the cell wall peptidoglycan [158]. After transforming this into *S. aureus* and developing a labelling protocol for those bacteria, I was able to adapt my protocol and image Coa:SNAP and found that it localised within the fibrin pseudocapsule as expected. I

also demonstrated that vWbp localised within the fibrin pseudocapsule as expected, but it was unclear to what extent it localised within the wider biofilm too.

5.2 Aim and hypothesis

I aimed to visualise Coa:SNAP and vWbp:CLIP fusion proteins in *S. aureus* biofilms and assess where the two coagulases localise with respect to fibrin in the extracellular matrix. I expected that Coa would primarily localise within the pseudocapsule, and that vWbp would localise to both the pseudocapsule and extended fibrin network.

5.3 Materials

All bacteria and plasmids used throughout this Chapter are listed in Table 8. Bacteria were stored in BHI containing 25 % glycerol in cryo tubes at -80 °C. Bacteria were cultured in brain heart infusion (BHI, 53286, Sigma Aldrich) for *S. aureus* or Luria broth (LB, L352, Sigma Aldrich) for *E. coli.* Overnight cultures were prepared by inoculating 10 ml media with a single colony from an agar plate and incubated overnight at 37 °C with 180 rpm shaking. Media was supplemented with 10 μg/ml erythromycin (E5389, Sigma Aldrich) for plasmid selection in *S. aureus* and 150 μg/ml in *E. coli*. For biofilm growth, media was supplemented with 50 % heparin stabilised human plasma, which was separated from blood donated by Aarhus University Hospital by centrifugation for 15 minutes at 2000 x *g* at 4 °C. Plasma from each patient was pooled, divided into aliquots, and stored at -80 °C. Before use, plasma was thawed in a 37 °C water bath. For confocal microscopy experiments, bacteria were stained with the nucleic acid stain Syto41 (S11352, Life Technologies), and the SNAP and CLIP tags were stained with either SNAP-Surface Alexa Fluor 647 (S9136S, New England Biolabs), SNAP-Surface Alexa Fluor 546 (S9132S, New England Biolabs), CLIP-Surface 488 (S9232S, New England Biolabs), or CLIP-Surface 547 (S9233S, New England Biolabs), which are referred to as SNAP-647, SNAP-546, CLIP-488, and CLIP-547 throughout. Prior to staining, biofilms were blocked with 5 % bovine serum albumin (BSA, A9418, Sigma Aldrich) dissolved in 1 x phosphate buffered saline (PBS, 28348, Thermo Fisher Scientific).

5.4 Methods

5.4.1 Transformation of pUNK-*snap* into *S. aureus* 29213

The plasmid pUNK-*snap* was transformed into *S. aureus* 29213 using a modified version of Monk's protocol [159], which was explained in detail in Chapter 4. First, the plasmid was transformed into *E. coli* IM08B via heat shock, which methylates DNA with a pattern mimicking *S. aureus* to bypass its restriction barriers when transforming *S. aureus* later on. *E. coli* IM08B was engineered by Monk and co-workers to be deficient in a DNA cytosine methytransferase and therefore bypasses the widely spread *S. aureus* SauUSI restriction barrier which specifically targets methylated cytosines [159][19]. It also contains an *S. aureus* specific adenine methyltransferase encoded by *hsdMS* [159]. Then the plasmid was extracted

Table 8 All bacterial strains and plasmids used throughout this Chapter.

Bacterial Strain	**Description**	**Reference**
Staphylococcus aureus ATCC 29213	Clinical wound isolate. Standard laboratory strain.	
S. aureus ATCC 29213 Δ*coa*	*S. aureus* 29213 *coa* deletion mutant.	Janne K. Klitgaard
S. aureus ATCC 29213 Δ*vwbp*	*S. aureus* 29213 *vwbp* deletion mutant.	Janne K. Klitgaard
S. aureus ATCC 29213 *coa:snap vwbp:clip*	Wildtype *S. aureus* 29213 producing both Coa:SNAP and vWbp:CLIP fusion proteins.	Chapter 4
S. aureus ATCC 29213 Δ*vwbp coa:snap*	*S. aureus* 29213 lacking vWbp that produces Coa:SNAP.	Chapter 4
S. aureus ATCC 29213 Δ*coa vwbp:clip*	*S. aureus* 29213 lacking Coa that produces vWbp:CLIP	Chapter 4
S. aureus ATCC 29213 *snap:lpxtg*	Wildtype *S. aureus* 29213 with cell wall anchored SNAP. Contains pUNK-*snap*.	This study
Escherichia coli IM08B	Methylates DNA to mimic methylation pattern of *S. aureus.* DNA cytosine methyltransferase deficient (Δ*dcm*) with added *S. aureus hsdMS* genes to methylate adenine residues.	[159]
Plasmid	**Description**	**Reference**
pUNK-*snap*	Plasmid containing SNAP preceded by an SpA secretion sequence and followed by an LPXTG motif. Erythromycin resistance. Tet repressor.	Phil Hill

with the GeneJet Plamid Miniprep kit (Thermo Fisher Scientific) and transformed into *S. aureus* 29213 via electroporation. The only changes to the protocols in Chapter 4.5.3 and 4.5.4 were the use of 10 μg/ml erythromycin for plasmid selection, and all incubations were carried out at 37 °C.

5.4.2 Optimisation of SNAP labelling protocol

I employed two strategies to visualise SNAP on the surface of *S. aureus snap:lpxtg*. Firstly, biofilms were stained after 24 hours of growth. Secondly, planktonic bacteria were immobilised and stained on a microscope slide as a control in case the SNAP substrate was unable to penetrate the biofilm matrix or bound non-specifically to the matrix rather than to the SNAP tag.

For biofilm samples, microwells (μ-Slide 8 Well, 80821, IBIDI) were preconditioned with 180 μl BHI media supplemented with 50 % plasma by incubation for 30 minutes at 37 °C. Biofilms were inoculated with 20 μl overnight culture of either *S. aureus* 29213 or *S. aureus* 29213 *snap:lpxtg* to a final OD_{600} 0.5 and incubated for 2 hours at 37 °C. Then the media over the biofilms was replaced with fresh BHI containing 50 % plasma and they were

further incubated overnight at 37 °C. The next day, biofilms were incubated with 200 µl BHI supplemented with 5 µM SNAP-647 and 1 µM Syto41 at 37 °C for 30 minutes. The media was removed and the biofilms washed twice for 3 hours with 200 µl PBS before visualisation with confocal laser scanning microscopy (CLSM) (LSM700, Zeiss) with 405 nm and 639 nm excitation with a Plan-Apochromat 63x/1.40 oil immersion objective lens.

For surface immobilised planktonic bacteria, overnight cultures of *S. aureus* 29213 and *S. aureus* 29213 *snap:lpxtg* were adjusted to OD_{600} 10 and 50 µl pipetted onto a poly-lysine coated microscope slide (Superfrost Ultra Plus, 10149870, Thermo Scientific) and incubated at room temperature for 30 minutes. The liquid was replaced with 50 µl BHI supplemented with 5 µM SNAP-647 and 1 µM Syto41 and incubated at room temperature for 30 minutes. The media was removed and the samples washed 3 times for 5 minutes with 50 µl PBS, covered with a microscope glass cover slip, and imaged with CLSM.

5.4.3 Confocal microscopy of Coa:SNAP and vWbp:CLIP in *S. aureus* biofilms

S. aureus 29213 Δ*vwbp*, Δ*vwbp coa:snap*, Δ*coa*, Δ*coa vwbp:clip* biofilms were initially prepared in the same way as above (Chapter 5.4.2), only with 2.5 hours of incubation rather than 24 hours and no wash step, but there were large levels of non-specific staining by the SNAP and CLIP substrates and the protocol needed to be modified. Biofilms were made much thinner by inoculating with a single layer of bacteria attached to the preconditioning layer, the substrate concentration was reduced, and a blocking step was added to prevent non-specific staining where possible. The protocol went through multiple rounds of improvements and the final one is presented here.

Microwells (µ-Slide 8 Well, 80821, IBIDI) were incubated with 180 µl BHI media with 50 % plasma for 30 minutes at 37 °C to create the preconditioning layer. This step was essential, and without it, bacteria did not adhere strongly enough to the surface and were washed away during the later steps of this protocol. The liquid was removed and the wells were rinsed with 200 µl BHI by pipetting gently into the corner of the well and pipetting out again, taking care to remove as much liquid as possible. When exchanging liquid, the pipette was always directed into the corner of the well and only very gentle force used. 100 µl overnight cultures adjusted to OD_{600} 10 were added to the wells and incubated at 37 °C for 30 minutes to allow bacteria to attach to the preconditioning layer. The cultures were removed and the wells rinsed again with 200 µl BHI to remove unbound cells, taking care to remove as much liquid as possible. 100 µl BHI containing 50 % plasma and 0.4 µg/ml Alexa Fluor 488 conjugated fibrinogen (F13191, Thermo Fisher Scientific) (or Alexa Fluor 647 conjugated fibrinogen (F35200, Thermo Fisher Scientific), depending on the spectra of the SNAP/CLIP substrate so as not to overlap) was added and incubated at 37 °C for 30 minutes. Then it was replaced with 100 µl blocking buffer (5 % BSA in 1 x PBS) and blocked for 30 minutes at room temperature. Afterwards the blocking buffer was replaced with staining buffer (5 % BSA in 1 x PBS with 1 µM Syto 41 and 0.5 µM SNAP-647, SNAP-546, CLIP-488, or CLIP-547) and incubated for a further 30 minutes at 37 °C. The staining buffer was removed and the biofilms washed with 100 µl blocking buffer by incubating at room temperature for 1 hour. The wash step was repeated and finally biofilms resuspended in 100 µl blocking buffer and imaged with CLSM. Signal from the SNAP and CLIP substrates

was dim, and the CLSM settings were carefully adjusted to improve the fluorescence signal. This included turning up the gain and laser power, decreasing scanning speed, and increasing line averaging.

In additional experiments with vWbp:CLIP, the blocking, staining, and wash buffers were further supplemented with either 0.1 – 1 % Triton X-100 (X100, Sigma Aldrich), 0.1 – 1 % Tween-20 (P9416, Sigma Aldrich), 200 mM NaCl (S7653, Sigma Aldrich), or the blocking buffer was replaced with 10 % BSA, or replaced with 2 M glycine (G7126, Sigma Aldrich) and the staining and washing buffers replaced by 200 mM glycine. The staining buffer still included 1 µM Syto 41 and 0.5 µM CLIP substrate. In one experiment, the CLIP substrate concentration was reduced to 0.2 µM.

5.5 Results

5.5.1 SNAP labelling was clear when SNAP was anchored to the *S. aureus* cell wall

Initial labelling attempts of *S. aureus* biofilms producing Coa:SNAP and vWbp:CLIP had large fluorescent backgrounds and no clear specific labelling of the SNAP and CLIP tags. Biofilms with Coa:SNAP and vWbp:CLIP appeared the same as biofilms with unmodified Coa and vWbp that were labelled in the same way (Figure 20a), and I concluded that this fluorescent background was either caused by non-specific staining within the biofilm matrix or an inability to label the SNAP and CLIP tags, or both. I therefore troubleshooted my labelling protocol with a control strain of *S. aureus* that produced cell wall anchored SNAP tag that was not fused to any protein to ensure that I could label the SNAP tag correctly. I began by adding a wash step to the labelling protocol in order to remove background fluorescence.

Signal from SNAP staining in the control strain was very clear in both planktonic and biofilm samples. SNAP staining produced a strong, ring-shaped signal at cell surfaces corresponding to cell wall anchored SNAP tag, and produced very little signal in samples that did not produce any SNAP tag (Figure 20b). Therefore, my protocol was sufficient to label the SNAP tag. It is unknown how much Coa each cell produces; if cells produce much less Coa:SNAP than cell wall anchored SNAP, the signal from Coa:SNAP in my initial experiments could have been lower than the background and therefore not detected.

When applying this protocol for visualising Coa:SNAP, I could still not detect any signal from Coa, and there was still some background fluorescence corresponding to non-specific staining of the biofilm extracellular matrix. The fibrin network was also removed, indicating that the wash step was too long. Hence, I reduced the wash incubation time from 2 x 3 hours to 2 x 1 hour and added a blocking step to prevent non-specific staining. Samples were blocked with BSA before staining, which occupies the non-specific binding sites and therefore inhibits the SNAP substrate from interacting with them. To further reduce background, the SNAP substrate concentration was reduced, and the biofilm matrix was made as thin as possible. I devised a new protocol for growing biofilms in which biofilms were inoculated with a single layer of bacteria attached to the microwell glass surface and grown in media containing plasma for just 30 minutes.

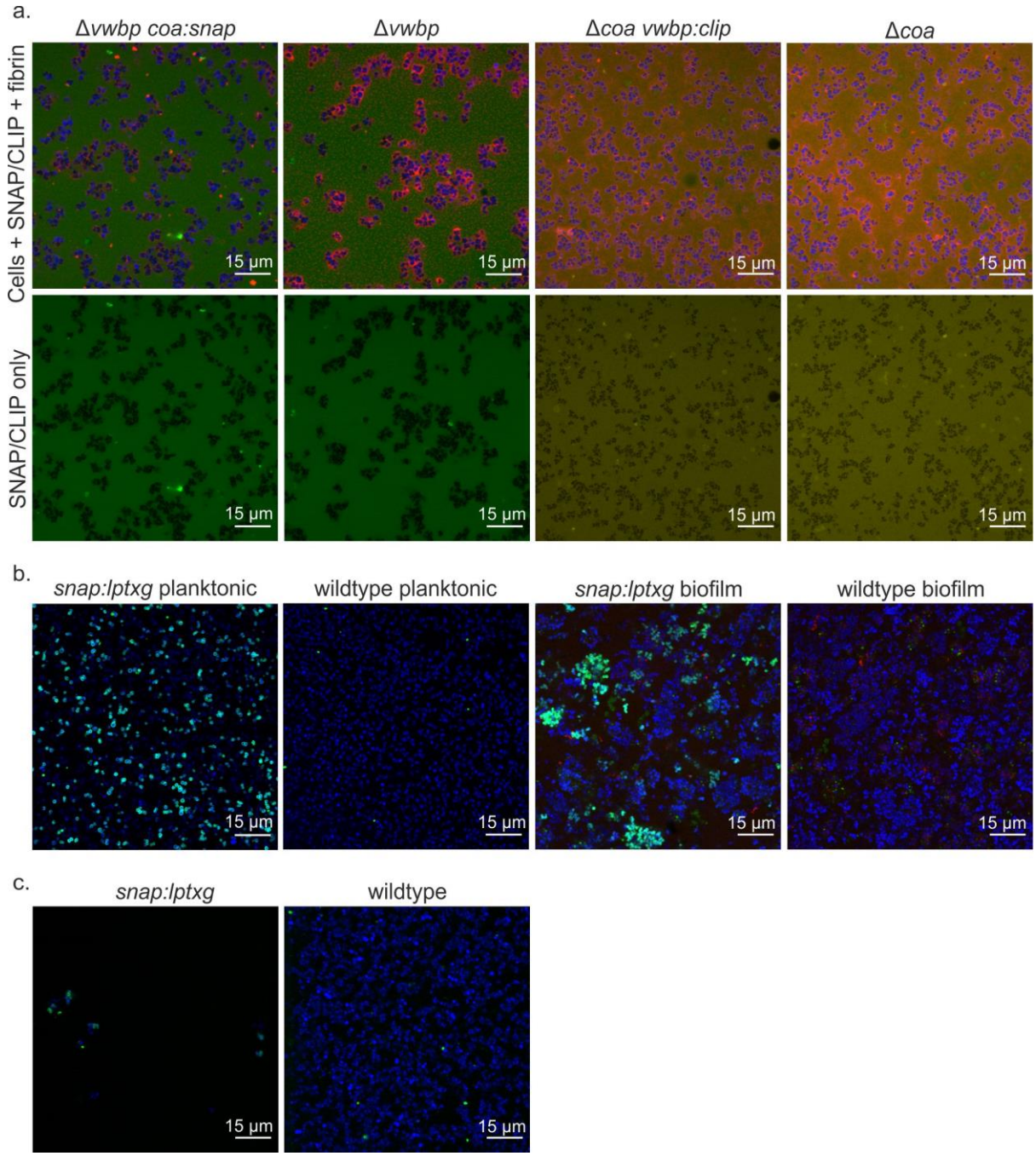

Figure 20 a) Initial labelling attempts of biofilms producing Coa:SNAP or vWbp:CLIP. Biofilms with unmodified Coa and vWbp were labelled as negative controls. b) Labelled *S. aureus* with and without cell wall anchored SNAP. Fibrin (red) was degraded and therefore not present in the biofilm matrix. c) Labelled *S. aureus* with and without cell wall anchored SNAP (alternative protocol). Fluorescent fibrin was omitted from this experiment. Bacteria are blue, fibrin is red, SNAP substrate is green, and CLIP substrate is yellow.

I tested this new protocol on *S. aureus* with cell wall anchored SNAP. As expected, SNAP staining still produced ring-shaped patterns of expression at cell surfaces with little background fluorescence (Figure 20c). However, cells easily detached from the microwell surface whenever media was pipetted onto or off the biofilm, leaving very few cells behind to image in some cases. My protocol lacked a preconditioning layer, in which media containing

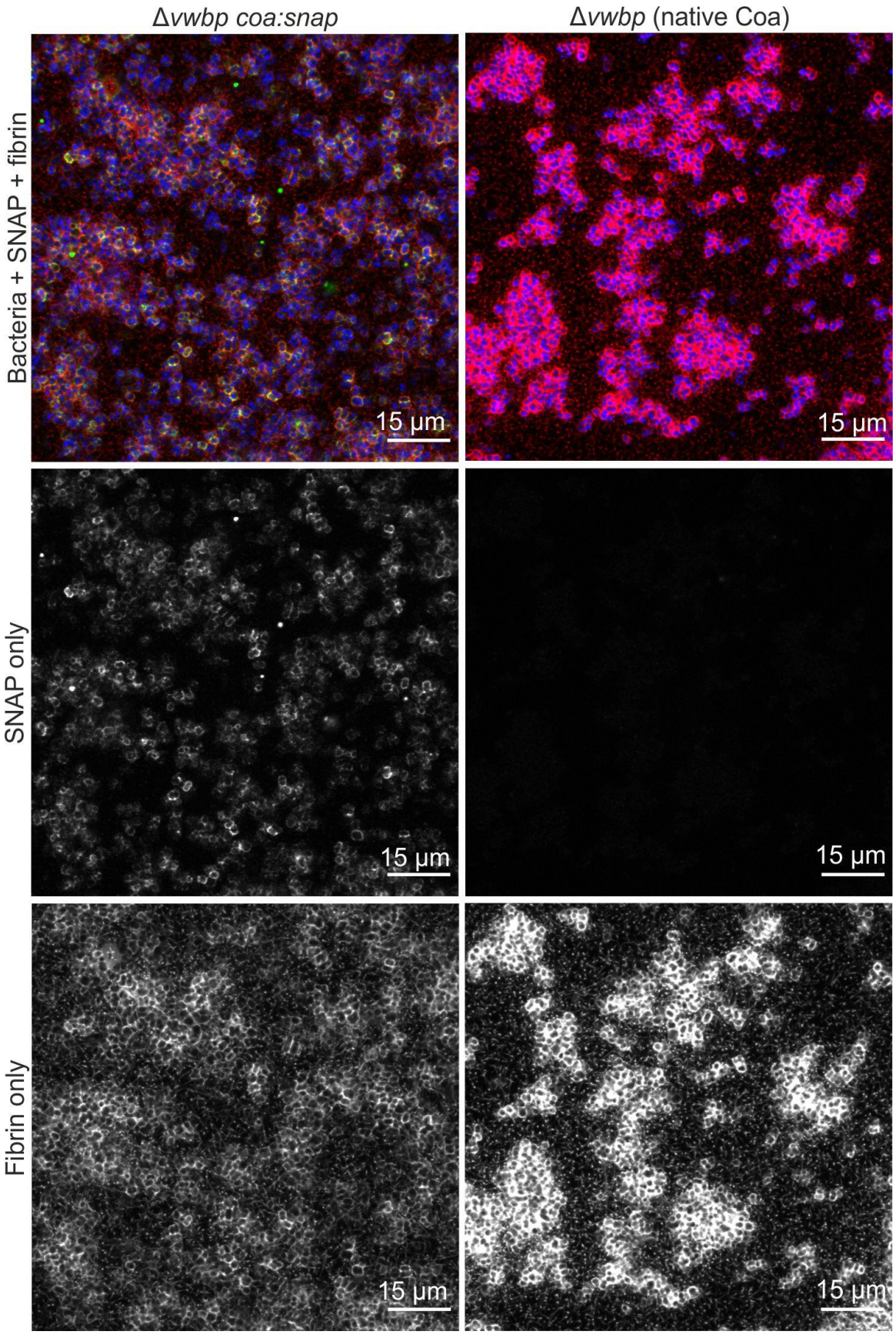

Figure 21 SNAP labelling of *S. aureus* biofilms lacking vWbp. Biofilms either produce Coa:SNAP or unmodified, native Coa. Coa:SNAP localised to the fibrin pseudocapsule. Fibrin is red/grey, bacteria are blue, and SNAP is green/grey.

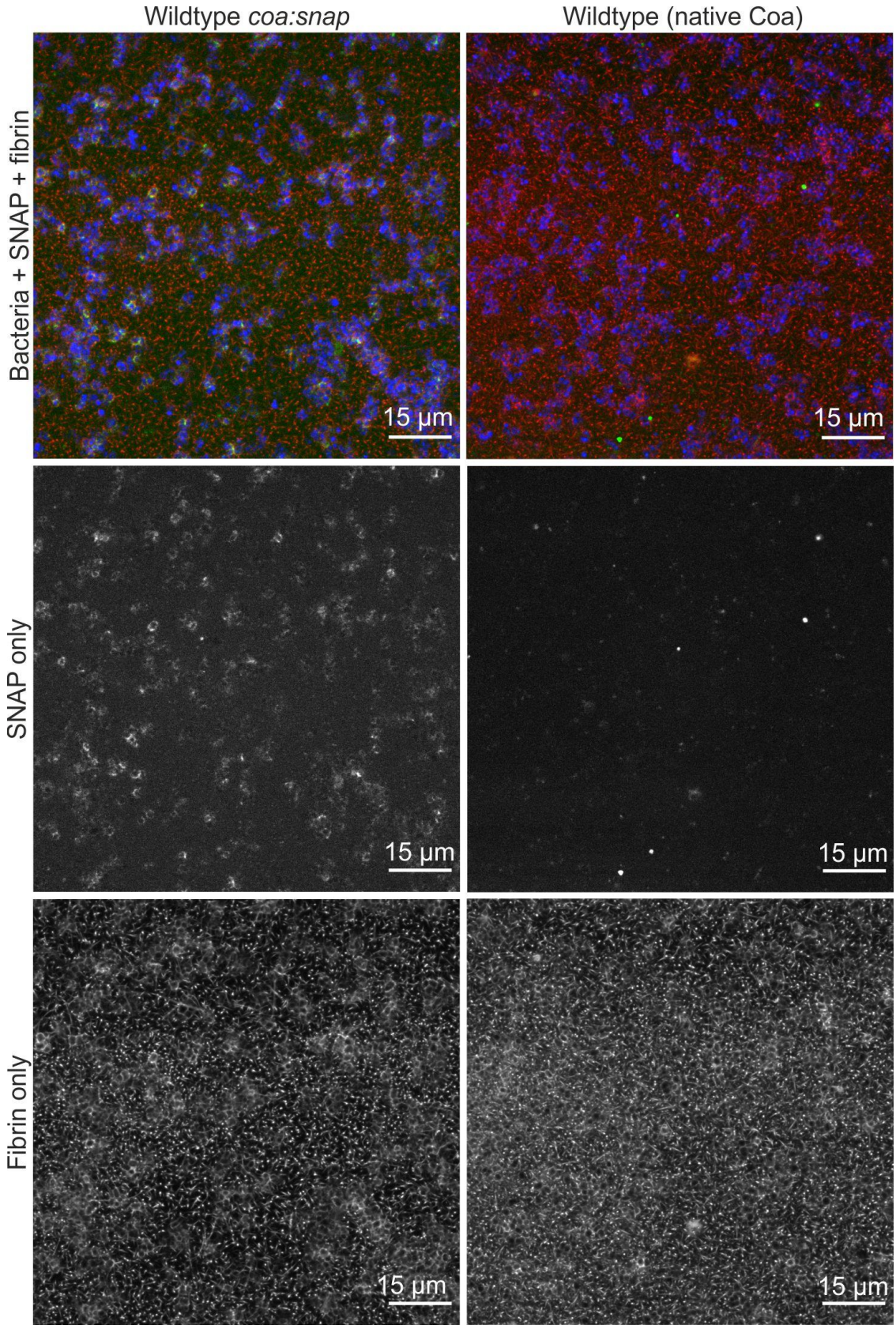

Figure 22 SNAP labelling of wildtype *S. aureus* biofilms. Biofilms either produce Coa:SNAP or unmodified, native Coa. Coa:SNAP localised to the fibrin pseudocapsule. Fibrin is red, bacteria are blue, and SNAP is green/grey.

plasma is incubated in the microwells prior to inoculation with bacteria. While *S. aureus* do adhere weakly to glass [160], this preconditioning layer provides the host proteins that *S. aureus* require to adhere strongly enough to remain attached during repeated blocking, staining, and washing steps. I therefore added a preconditioning step to the protocol and proceeded to image Coa:SNAP.

5.5.2 Coa:SNAP localises to the fibrin pseudocapsule

I visualised Coa:SNAP using the improved protocol in wildtype *S. aureus* biofilms as well as the mutant that does not produce vWbp. Coa:SNAP localised within the fibrin pseudocapsule, as seen when the colours for SNAP (green) and fibrin (red) overlap (Figure 21 and Figure 22). The absence of such signal in biofilms with unmodified Coa verifies that this signal arose from specific interactions between the SNAP substrate and SNAP tag rather than non-specific staining. The signal was however fairly dim and required some optimisation of the imaging settings to achieve the best signal to noise ratio possible, namely, increasing the gain, laser power, and line averaging, and decreasing the scanning speed. The signal from Coa:SNAP was also dimmer in the wildtype compared to the mutant lacking vWbp, presumably because the extracellular matrix is thicker when both coagulases are present, and a thicker matrix scatters emissions more strongly and decreases signal to noise ratio. Nevertheless, my results show that Coa localises to the fibrin pseudocapsule in biofilms where I hypothesised that it facilitates fibrin production at the cell surface.

5.5.3 vWbp:CLIP localises close to cells, possibly within the fibrin pseudocapsule

I visualised vWbp:CLIP in wildtype *S. aureus* biofilms as well as in the mutant lacking Coa using the same protocol that we used to successfully visualise Coa:SNAP. However, no difference was seen between biofilms producing vWbp:CLIP or unmodified vWbp (Figure 23a). The CLIP substrate appeared to bind non-specifically to the fibrin, or alternatively there was cross talk in the CLIP imaging channel with the fluorescent fibrin. To verify whether this was a non-specific interaction with the fibrin from the plasma or was cross talk, I visualised biofilms without pre-labelled fibrin. I also supplemented the blocking, staining, and washing buffers with additional reagents to increase blocking to test whether potential non-specific interactions could be prevented.

The fibrin-shaped CLIP signal could not be prevented by supplementing the buffers with any additional blocking reagent (Triton X-100, Tween-20, NaCl, or glycine) (data not shown), but it could be reduced by omitting pre-labelled fibrin from the experiment (Figure 23b), and therefore was caused by cross talk with the fluorescent fibrin. When fluorescent fibrin was omitted, there was a difference in the CLIP signal from biofilms with vWbp:CLIP vs. those without. vWbp:CLIP localised close to the surface of the cells (Figure 23c), possibly within the fibrin pseudocapsule, although it is difficult to specify precisely where without an image of the fibrin too. I previously found that vWbp accelerates pseudocapsule formation and my data here suggests that it does so by associating to the pseudocapsule. However, there was still a lot of background in these images, including non-specific staining of fibrin in the extracellular matrix (Figure 23b and 23d), which makes it difficult to

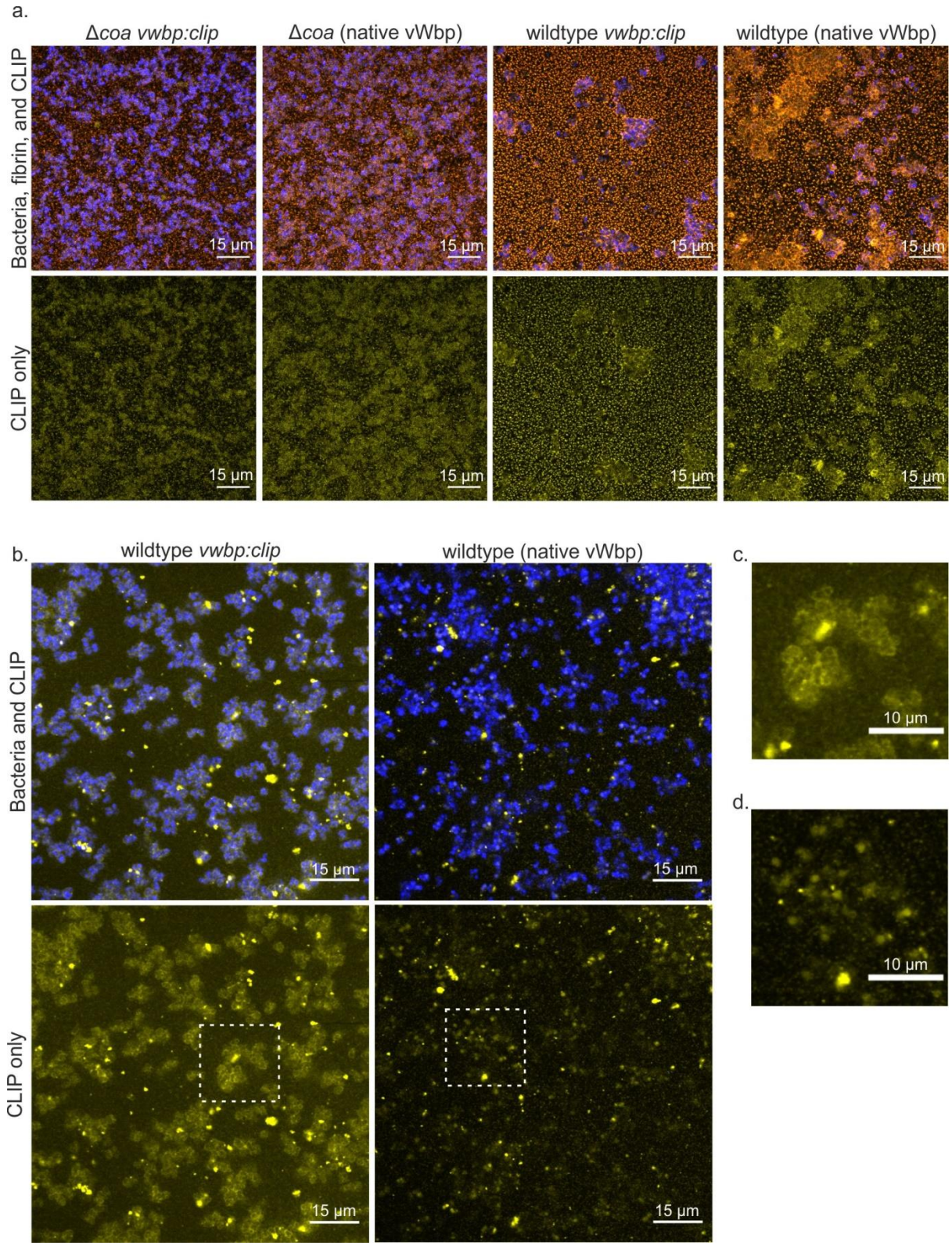

Figure 23 a) *S. aureus* biofilms that produce either vWbp:CLIP or native, unmodified vWbp. Biofilms were stained using the successful Coa:SNAP protocol, however only cross talk with the fluorescent fibrin was seen. b) *S. aureus* biofilms with and without vWbp:CLIP when the fluorescent fibrinogen was not added. c) and d) are zoomed in images of the regions marked by boxes in b). Bacteria are blue, fibrin is red, and CLIP substrate is yellow.

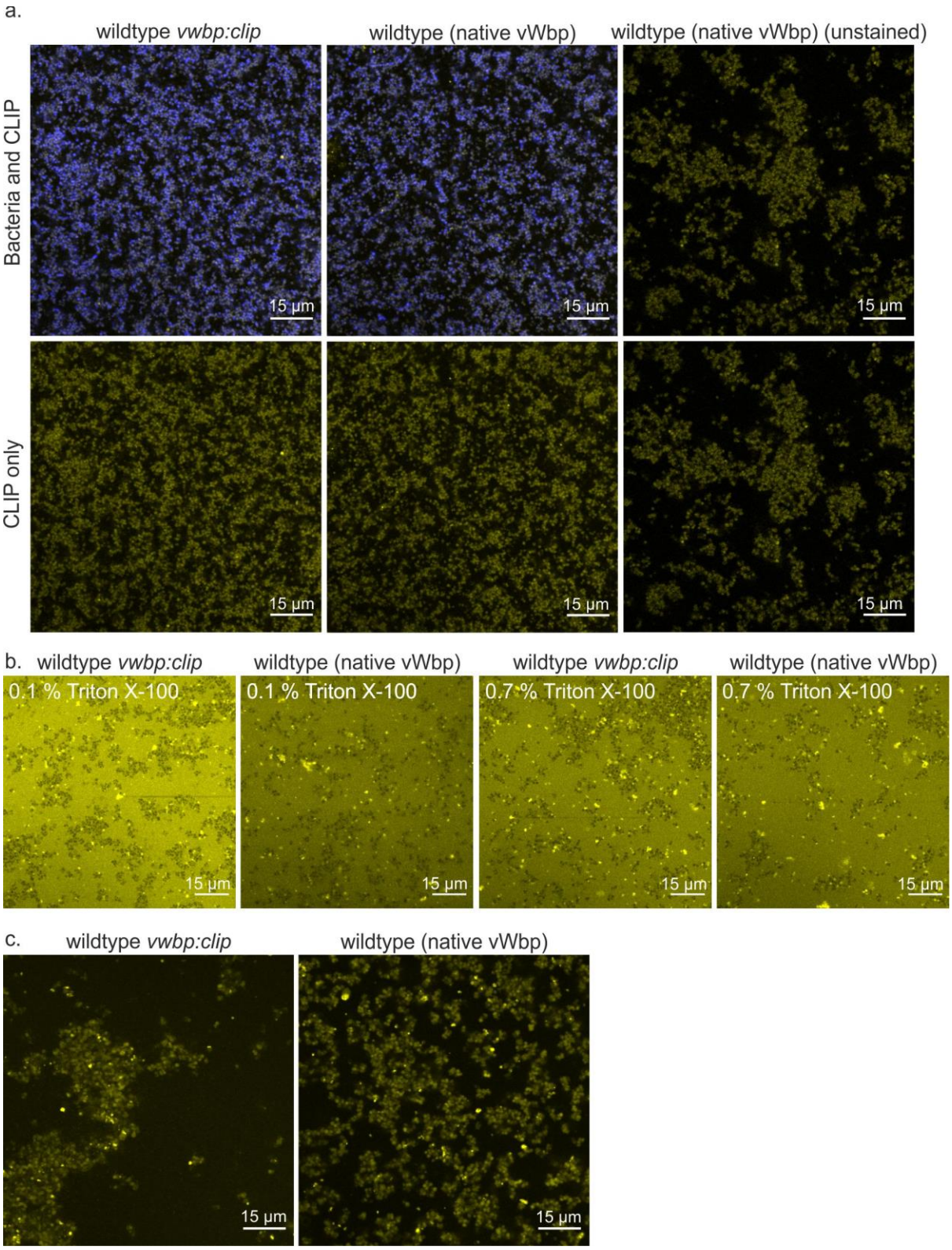

Figure 24 a) Biofilms with either vWbp:CLIP or native vWbp had no CLIP staining when the blocking, staining, and washing buffers were supplemented with 1 % Triton X-100. Only autofluorescence was seen. b) Supplemented Triton X-100 concentration was varied from 0.1 – 0.7 %, but was ineffective due to an experimental error (only CLIP signal shown). c) 10 % BSA was sufficient to block all CLIP staining. Again, only autofluorescence was seen. (Only CLIP signal shown). Bacteria are blue and CLIP substrate is yellow.

analyse whether vWbp localises elsewhere in the matrix. While the background signal in the wider biofilm matrix appears brighter in the sample containing vWbp:CLIP (Figure 23c) than the sample without (Figure 23d), it is possible that this difference was caused by variation in fibrin quantity and thus non-specific staining rather than by detection of vWbp in the wider matrix. I decided to experiment further with different blocking conditions to try and eliminate the non-specific staining in the extended fibrin network.

In one experiment, I supplemented the blocking buffer with 1 % Triton X-100, and no CLIP signal was seen at all (Figure 24a). The cell-shaped signal in the CLIP channel in these images is autofluorescence that occurred due to increasing the imaging power to search for any CLIP emissions: imaging an unstained sample under the same imaging settings produced the same result. Therefore, I concluded that 5 % BSA supplemented with 1 % Triton X-100 blocked the specific and well as the non-specific interactions of the CLIP substrate. I imagined that there must be a threshold concentration of Triton X-100 at which the specific interactions are not blocked, yet non-specific interactions are blocked sufficiently to enable a good enough signal to noise ratio for clear vWbp:CLIP detection. I performed a series of experiments in which the Triton X-100 concentration was increased from 0.1 – 0.7 % in the presence of 5 % BSA.

Unfortunately, there was a high CLIP background in all biofilms when varying Triton X-100 concentration (Figure 24b). This was due to an error during the sample preparation in which removing the microwell lid caused Triton X-100 solution that had slipped into the joint between the lid and microwell to foam and contaminate neighbouring wells, transferring CLIP substrate with it and causing the high backgrounds seen here. It was very difficult to avoid getting this error, and I spent a lot of time double checking that the initial autofluorescence results were correct and optimising the protocol to reduce foaming. Eventually I had to discard this experiment due to time constraints and prioritise other experiments. In one final experiment, the BSA concentration was increased to 10 % rather than 5 %, which resulted in only autofluorescence (Figure 24c). There may be a threshold between 5 – 10 % BSA which enhances vWbp:CLIP detection, but given that there is already autofluorescence in samples blocked with 5 % BSA, perhaps this is unlikely to significantly improve upon the data that I already have without compromising the signal from vWbp:CLIP. Perhaps fewer molecules of vWbp associate to the fibrin pseudocapsule compared to Coa, which is why the signal to noise ratio is so low. My results nevertheless support the findings from the time lapse analysis in Chapter 3 that vWbp accelerates pseudocapsule formation and demonstrates that it does this by associating to the pseudocapsule.

5.6 Discussion

I demonstrated that Coa localises within the fibrin pseudocapsule in *S. aureus* biofilms. This agrees with the study by Guggenberger *et al*. (2012) [41], who found Coa within the fibrin pseudocapsule via antibody labelling, and with Cheng *et al*. (2010) [42], who identified Coa within the pseudocapsule surrounding *S. aureus* in an abscess model. This finding also supports my time lapse CLSM results from Chapter 3, where I confirmed that the pseudocapsule cannot form without Coa. Therefore, Coa accumulates at the surface of cells, perhaps by association via the fibrinogen binding MSCRAMMs on the surface of *S. aureus*,

and localises fibrin production close to cells to facilitate pseudocapsule formation. Then the bacteria can divide within shared pseudocapsules that protect them from immune cells once the aggregate reaches a critical size.

I also demonstrated that vWbp localises to the fibrin pseudocapsule or cell surfaces in wildtype *S. aureus* biofilms. In Chapter 3, I discovered that vWbp accelerates the formation of the pseudocapsule when Coa is present and my results here suggest that it does so by associating to the pseudocapsule. While Coa is essential for facilitating pseudocapsule formation, my results suggest that the role of vWbp is to accelerate it, which increases the protection that the bacteria get from the immune cells by the pseudocapsule more quickly.

It was not possible to conclude whether Coa or vWbp also localise within the wider biofilm matrix from my data. No signal from Coa:SNAP was seen in the wider matrix, possibly because the quantity of Coa was too low and the signal was hence too dim to detect above the background. While the signal from biofilms producing vWbp:CLIP was brighter than in biofilms that produce native vWbp, I am uncertain whether this occurred due to staining of the CLIP tag or non-specific staining. I do expect that some Coa is present in the wider biofilm because I demonstrated in Chapter 3 that Coa does form an extended fibrin network in the absence of vWbp. I do also expect that vWbp is present in the wider biofilm for the same reason. Producing fibrin further away from bacteria likely benefits them by attaching biofilms to surfaces within the host to initiate biofilm formation, possibly by interacting with other host proteins. vWbp has a domain that binds fibronectin, and has been shown to only bind fibronectin in plasma when it is not bound to prothrombin and therefore cannot cleave fibrinogen to trigger fibrin formation [53]. However, fibronectin exists in two different conformations: a globular conformation in plasma and a fibrillar conformation in the host extracellular matrix and on implant surfaces [77]. Perhaps vWbp attaches to fibrillar host fibronectin when bound to prothrombin rather than globular fibronectin in plasma to localise fibrin formation to host surfaces. Hence it would be interesting to use the vWbp:CLIP fusion protein to further investigate whether vWbp binds to fibrillar fibronectin.

I had some difficulties visualising vWbp in the wider biofilm matrix clearly due to issues with non-specific staining of the extracellular matrix by the CLIP substrate and possibly due to low concentrations of vWbp in the biofilm. The high background from non-specific staining combined with low signal from a low protein abundance caused a small signal to noise ratio. Non-specific staining occurs when the substrate binds non-specifically to sites other than the site of interest. Many forces, including hydrophobic, electrostatic, and van der Waals interactions, govern this. These can occur for example due to hydrophobic interactions between hydrophobic amino acid side chains, due to attractive forces between carboxyl and amino groups with opposite charges, or due to ionic interactions between dipolar molecules. The biofilm matrix is a complex environment containing many bacteria, proteins, and biomolecules for the substrate to interact with non-specifically. There are a number of strategies to reduce non-specific staining. Protein blockers such as BSA are large proteins with hydrophobic and hydrophilic subgroups, which can be added to compete for non-specific binding sites. Likewise, Triton X-100 and Tween-20 are amphiphilic, containing both hydrophobic and hydrophilic groups, and can therefore occupy non-specific binding sites, and addition of ions such as NaCl reduces non-specific binding due to charge interactions by producing a shielding effect.

The level of non-specific staining by SNAP and CLIP substrates varies in the literature and my work. The brochure that came with the SNAP and CLIP substrates recommended blocking with 0.5 % BSA, which was ineffective for my experiments. 5 % BSA was sufficient to block the SNAP substrates I used, but not entirely for the CLIP substrates. Landgraf *et al.* (2012) found that BSA was insufficient to block non-specific staining in their experiment [123], and recommended the use of glycine instead because it had been shown to effectively block non-specific binding of SNAP substrates to glass [161]. They devised a complex and extensive protocol in which planktonic *E. coli* with an intracellular SNAP tag were stained and washed in a buffer consisting of glycine, BSA, and Tween-20, and washed 10 times with 1 hour incubations in between. Other studies reported labelling SNAP tags in bacteria seemingly without such difficulty [162][163][164].
Bosch *et al.* (2014) labelled live human cells with 22 SNAP substrates conjugated to different dyes and reported variable levels of non-specific staining [165]. Many substrates had high levels of non-specific staining to either cellular substructures or glass surfaces. Therefore, the dye conjugate determines non-specific interactions. However, the staining characteristics were unpredictable. Dyes with net neutral or negative charge bound less to cellular substructures, but there were several exceptions to this, and there was no correlation between chromophore family and non-specific staining. They suggested that staining behaviours were determined by a complex combination of local charges and lipophilicity that cannot currently be predicted.

Although all dyes used in my experiments (Alexa 647, ATTO 488, and Dyomics 547) have a net negative charge, and therefore have a slight tendency to cause less non-specific staining according to the study by Bosch *et al.* (2014), they all caused some level of non-specific staining. This was not a problem when imaging Coa:SNAP (Alexa 647) because non-specific staining could be blocked effectively. However, it was a problem when visualising vWbp:CLIP in the wider biofilm matrix (ATTO 488 and Dyomics 547). Unfortunately, none of my attempts to completely block non-specific staining worked, presumably due to interactions with the complex biofilm matrix. My results were however still clear enough to conclude that vWbp associated to the fibrin pseudocapsule.

6. Monomeric superfolder GFP as a tag for extracellular proteins

In Chapter 4, I was unable to visualise fusion proteins with mCherry and GFP(-30) and hypothesised that they could not fold and become fluorescent in the extracellular space. Monomeric superfolder GFP (msfGFP) is an ideal candidate for extracellular fusion proteins because it is bright, photostable, and folds quickly. In this Chapter, I worked with my colleagues to discover whether msfGFP could be secreted from *S. aureus* when fused to Tat and Sec signal peptides. After confirming that msfGFP could be secreted via the Sec pathway, I produced and analysed a Coa:msfGFP fusion protein. The fusion functioned correctly, and I used it to quantify colocalisation with fibrin in *S. aureus* biofilms.

6.1 Introduction

Green fluorescent protein (GFP) has been used for decades as an intracellular reporter for gene expression and as a fluorescent tag to visualise single proteins in the cytoplasm of bacteria. An advantage of fluorescent proteins is that samples don't need to be stained and incubated to visualise the protein. GFP and other fluorescent proteins have therefore been instrumental for studies into protein localisation, visualising subcellular compartments, monitoring gene expression, tissue labelling, and DNA and RNA labelling [166].

While GFP fusion proteins have taught us much about intracellular proteins, little research has been done on extracellular proteins, such as surface-bound proteins or other secreted proteins. Some GFP variants have been successfully secreted to the periplasm and outer membrane of Gram negative bacteria [167][168][169], however there are few literature examples of this for Gram positive bacteria. GFP secretion has been achieved in *Corynebacterium glutamicum* [170], but no others to our knowledge. GFP secretion is challenging and there are a multitude of reasons why it may not work. The fusion protein may not be successfully secreted, secreted GFP may not fold and become fluorescent in the extracellular environment, it may misfold, or the chromophore may not mature properly [170][171]. The level of transcription and translation, protein turnover rate, and photobleaching may additionally complicate imaging GFP fusions [171].

Most extracellular proteins are secreted via the Secretory (Sec) pathway, where they are exported across the cytosolic membrane in an unfolded state into the periplasm in Gram negative bacteria or outside the cell in Gram positives [172]. It is a highly conserved pathway present in all classes of bacteria [173]. Sec-routed proteins have a signal peptide at their N-terminus that directs them towards the SecYEG membrane protein channel and are driven stepwise across the membrane by the ATPase molecular motor SecA [174]. The protein then folds on the trans side of the membrane. In many Gram negatives, SecB stabilizes and targets the unfolded protein to SecA, while in other Gram positive and negative bacteria, general chaperones maintain the protein in an unfolded state [174]. Another common secretion pathway is the Twin Arginine Translocation (Tat) pathway, in which proteins are exported in a folded state [175]. Not all bacterial species have a Tat pathway [176]. Tat-routed proteins have an N-terminal signal sequence containing a twin-arginine motif that gives the pathway its name [177], and they usually need to fold in the cytoplasm to function correctly, such as proteins with cofactors that bind to cytoplasmic proteins [178]. The Tat pathway contains three subunits TatA, TatB, and TatC in Gram negative bacteria and two subunits TatA and

TatC in Gram positives, which bind the signal peptide and form a membrane spanning channel [173]. Folded proteins are exported outside of the cell in Gram positives, and to the periplasm in Gram negatives, where they may be exported across the outer membrane via other mechanisms [173].

The aim of this study was to investigate whether monomeric superfolder GFP (msfGFP) would be a good candidate for tagging extracellular proteins in *S.aureus*, which has both Sec and Tat secretion pathways [173][176]. My initial intention was to use fluorescent proteins to visualise Coa and vWbp, which avoid issues with labelling and non-specific staining. However, after failing to detect mCherry and GFP(-30), I decided to pursue two strategies and produced fusions with both non-fluorescent protein tags as well as the fluorescent GFP. msfGFP was chosen as a target fusion protein due to its brightness and enhanced folding properties [179][141], and it has been previously been shown to fold in traditionally challenging environments such as the Gram negative periplasm [141]. While there were concerns over whether msfGFP could be exported and become fluorescent in the extracellular environment, previous reports of using momoneric superfolder GFP (msfGFP) for the visualisation of periplasmic proteins encouraged us to continue working with this protein. We decided to first address these concerns by demonstrating if msfGFP can be exported from *S. aureus* and become fluorescent. We fused msfGFP to Sec and Tat signal peptides and measured the fluorescence from cultures and supernatants separated from cultures of *S. aureus* expressing these fusions. After confirming that msfGFP is suitable to visualise secreted proteins, I constructed Coa:msfGFP. Coa is predicted to have a Sec-type signal peptide [180], and I have previously visualised it with the SNAP tag, therefore could assess whether it localised correctly in biofilms. I used the Coa:msfGFP fusion to quantify the fraction of Coa that colocalises within the fibrin pseudocapsule and extended fibrin network in *S. aureus* biofilms.

I worked together with Lisbeth Marcussen and Amanda Khamas for parts of the work in this Chapter. Lisbeth created two expression vectors containing msfGFP fused to Tat and Sec signal peptides. Amanda added Shine-Dalgarno sequences to these vectors, transformed them into *S. aureus*, and analysed whether msfGFP was secreted when fused to a signal peptide. I created Coa:msfGFP and analysed whether the fusion protein functioned as expected. I also performed a colocalisation analysis using images of the fusion protein to assess the level of colocalisation between Coa and fibrin in biofilms. To do so I adapted a MATLAB algorithm previously written by the Leake group (University of York) [126] and used it to analyse images taken with single molecule microscopy. I took the single molecule microscopy data and Alex Payne-Dwyer helped set up the microscope.

6.2 Aim and hypothesis

The aim was to investigate whether msfGFP can be exported out of *S. aureus* when fused to Tat or Sec signal peptides. The aim was also to test whether fusion to msfGFP inhibited the correct functioning and localisation of Coa, and compare these results to the prior results with Coa:SNAP. A successful fusion protein would be used to assess Coa colocalisation with fibrin in the extracellular matrix. I hypothesised that msfGFP would be exported and become fluorescent when secreted by both Tat and Sec pathways, and that the Coa:msfGFP fusion

protein would primarily associate to bacterial cell surfaces and colocalise with fibrin in the pseudocapsule.

6.3 Materials

All bacterial strains, plasmids, and primers used are listed in Table 9 and all additional sequences in Appendix 2. Bacteria were stored in 25 % glycerol and stored at -80 °C. Bacteria were plated onto agar and incubated overnight at 37 °C. Liquid cultures were made by inoculating a single colony into 10 ml either Luria Broth (LB) or Brain Heart Infusion (BH) media and incubated overnight at 37 °C with 180 rpm shaking. Media was supplemented with either 25 µg/ml or 10 µg/ml chloramphenicol (Cm), or 100 µg/ml ampicillin (Amp) for plasmid selection. Biofilms were grown in modified BHI (mBHI) supplemented with 50 % heparin stabilised human plasma to mimic physiological conditions. Plasma was separated from blood donated by Aarhus University Hospital by centrifugation at 2000 x *g* for 15 minutes at 4 °C and stored in aliquots at -80 °C. Before use, plasma was immediately thawed in a water bath at 37 °C. mBHI is BHI supplemented with 2.1 mM $CaCl_2$ and 0.4 mM $MgCl_2$. Expression of fusions proteins with signal peptides were induced with the addition of 320 ng/µl anhydrotetracycline (ATc).

Table 9 Bacterial strains, plasmids, and primers used in this study. Annealing sequence of primers given in upper case, and overhangs in lower case text.

Bacterial Strain	**Description**	**Ref.**
Escherichia coli IM08B	Derived from E. coli K12 DH10B. Deficient in cytosine methylation (Δ*dcm*) and methylates adenine (*hsdMS*) to bypass *S. aureus* restriction barriers.	[159]
Staphylococcus aureus ATCC 29213	Clinical wound isolate. Standard laboratory strain.	
S. aureus ATCC 29213 *coa:msfgfp*	*S. aureus* 29213 with Coa:msfGFP genomically integrated fusion protein.	This study
S. aureus ATCC 29213 Δ*vwbp coa:msfgfp*	*S. aureus* 29213 lacking vWbp and with Coa:msfGFP genomically integrated fusion protein.	This study
Plasmid	**Description**	**Ref.**
pRMC2	*E. coli*/*S. aureus* shuttle vector. Inducible $P_{xyl/tetO}$ promoter. Amp and Cm resistance. pRMC2 was a gift from Tim Foster (Addgene plasmid # 68940 ; http://n2t.net/addgene:68940 ; RRID:Addgene_68940).	[181]
pUC57-*msfGFP*	*E. coli* vector carrying *coa:msfGFP*. Amp resistance.	Genscript
pIMAY	*E. coli*/*Staphylococci* temperature sensitive vector for allelic exchange. Cm resistance. Inducible *secY* antisense. pIMAY was a gift from Tim Foster (Addgene plasmid # 68939 ; http://n2t.net/addgene:68939 ; RRID:Addgene_68939).	[182]
Primer	**Sequence (5' – 3') and description**	**Ref.**
FwdRMC2	CTCTTCGCTATTACGCCAGC Anneals to pRMC2 multiple cloning site.	This study
RevRMC2	TGGATCCCCTCGAGTTCATG Anneals to pRMC2 multiple cloning site.	This study

1Fa	ttctgaattcttaTTTATATAATTCATCCATACCATGTG Anneals to msfGFP. EcoRI overhang.	This study
1Rsg	gtatcattcagcacatgcaTCAGGTGGTGGAGGATC Anneals to msfGFP. Sec SP overhang.	This study
2Fsg	gatcctccaccacctgaTGCATGTGCTGAATGATAC Anneals to Sec SP. msfGFP overhang.	This study
2Ra	ttctggtaccATGAAAAAATGTATTAAAACATTATTTTT Anneals to Sec SP. KpnI overhang.	This study
1Rtg	gtgttgcaattggtgcaTCAGGTGGTGGAGGATC Anneals to msfGFP. Tat SP overhang.	This study
2Ftg	gatcctccaccacctgaTGCACCAATTGCAACAC Anneals to Tat SP. msfGFP overhang.	This study
2Rb	ttctggtaccATGACAAATTATGAACAAGTTAATGA Anneals to Tat SP. KpnI overhang.	This study
1Rc	ttctggtaccatgTCAAAAGGTGAAGAATTATTTAC Anneals to msfGFP (excluding linker). KpnI restriction site.	This study
MutF	cctcctCATCAAGCTTATTTTAATTATACTC Mutagenic primer containing Shine-Dalgarno sequence.	This study
GfpR	GTACCATGAAAAAATGTATTAAAAC Reverse mutagenic primer for msfGFP control.	This study
SecR	GTACCATGACAAATTATGAAC Reverse mutagenic primer for Sec:msfGFP.	This study
TatR	GTACCATGAAAAAATGTATTAAAAC Reverse mutagenic primer for Tat:msfGFP.	This study
Coa:msfGFP_F	actaaagggaacaaaagctgggtacGGTACCGCCAAGTGAAAC Anneals to Coa:msfGFP construct. pIMAY overhang for Gibson Assembly.	This study
Coa:msfGFP_R	tcgacctcgaggggggcccggtacGGTACCAAATTTTATGAATCGAAG Anneals to Coa:msfGFP construct. pIMAY overhang for Gibson Assembly.	This study
IM151	TACATGTCAAGAATAAACTGCCAAAGC Anneals to pIMAY multiple cloning site.	[182]
IM152	AATACCTGTGACGGAAGATCACTTCG Anneals to pIMAY multiple cloning site.	[182]

Figure 25 Visual schematics of fusion proteins under control of the inducible Pxyl/tetO promoter in pRMC2. a) Tat:msfGFP, b) Sec:msfGFP, and c) msfGFP control. SD = Shine-Dalgarno sequence, SP = signal peptide, and L = linker.

6.4 Methods

6.4.1 Construction of pRMC2 vector carrying signal peptide:msfGFP constructs

Tat and Sec signal peptides were fused to msfGFP to create Tat:msfGFP and Sec:msfGFP in the vector pRMC2 (Figure 25) [181]. A positive control was also constructed consisting of msfGFP with no signal peptide (Figure 25c). Note that the Shine-Dalgarno sequences were added later as described in Section 6.4.2.

Sequences for msfGFP [140][141], and Tat [176] and Sec signal peptides [183] were reverse translated with an *S. aureus* USA300 codon usage table. The RNA polymerase α and β subunits are highly conserved, and their nucleotide sequences were used to predict codon usage in *S. aureus* USA300 and *S. aureus* 29213, and an *S. aureus* USA300 codon usage table deemed suitable. Signal peptides were ordered as oligos (Thermo Fisher Scientific) and msfGFP with a linker (SGGGG) at its N-terminal on a high copy plasmid (pUC57, Genscript). The signal peptides and msfGFP were amplified with PCR with Phusion polymerase. The primers contained overhangs to join fragments and add KpnI and EcoRI restriction sites at the 5' and 3' ends. Primers 2Ftg/2Rb and 2Fsg/2Ra were used to amplify Tat and Sec signal peptides respectively, and msfGFP with 1Fa/1Rsg. The signal peptides were joined to msfGFP via SOE-PCR to create Tat:msfGFP (primers 1Fa/Rtg) and Sec:msfGFP (primers 1Fa/2Ra). msfGFP was also amplified alone with no signal peptide to be used as a control. PCR products were analysed by gel electrophoresis and purified with the GenElute Gel Extraction Kit (Sigma Aldrich). All PCR products and pRMC2 were digested by KpnI (FastDigest, Thermo Fisher Scientific) and EcoRI (FastDigest, Thermo Fisher Scientific), and PCR products were ligated into pRMC2 with T4 DNA ligase (Invitrogen), according to the manufacturer's protocols.

6.4.2 Insertion of Shine-Dalgarno sequence via site directed mutagenesis

In order that msfGFP could be translated, the Shine-Dalgarno sequence was inserted upstream of the signal peptides and msfGFP via site directed mutagenesis [184]. The consensus sequence was chosen [185] and inserted 5 nucleotides upstream of the start codons of Tat:msfGFP, Sec:msfGFP, and msfGFP to ensure maximum translation efficiency [186]. To do this, the entire plasmids from 6.4.1 were amplified with PCR using primers with overhangs to add the Shine-Dalgarno sequence in the desired place (MutF/TatR for Tat:msfGFP, MutF/SecR for Sec:msfGFP, and MutF/GfpR for msfGFP). Then the new PCR products were digested with DpnI to remove remaining template DNA, and ligated back into a whole plasmid, according to the manufacturer's instructions (Phusion Site-Directed Mutagenesis Kit, Thermo Fisher Scientific).

6.4.3 Transformation into *E. coli* IM08B

The pRMC2 constructs (Tat:msfGFP, Sec:msfGFP, msfGFP, and empty pRMC2) were transformed via heat shock into *Escherichia coli* IM08B in order to gain a methylation profile mimicking *S. aureus* [159]. To prepare chemical competent cells, an overnight culture of *E. coli* IM08B was diluted to OD_{600} 0.02 and grown to OD_{600} 0.3, then chilled on ice for 10 minutes. Cells were harvested by centrifugation at 4000 x *g* for 10 minutes at 4 °C and

resuspended in 5 ml ice cold 0.5 M $CaCl_2$. The centrifugation was repeated and the cells resuspended in 1.2 ml $CaCl_2$ before incubating on ice for 30 minutes. For transformation, either 1 µl, 2 µl, or 3 µl of each pRMC2 construct was incubated for 30 minutes on ice with 50 µl of competent cells. A heat shock was applied at 42 °C for 90 seconds and then cells were transferred to ice for a further 2 minutes. 950 µl of prewarmed LB media (37 °C) was added and then cells incubated with 180 rpm shaking for 1 hour at 37 °C. Cells were finally plated with Amp and incubated at 37 °C overnight. Plasmids were extracted from positive transformants with the GeneJET Plasmid Miniprep Kit and sent for sequencing with Macrogen Europe with primers FwdRMC2/RevRMC2.

6.4.4 Transformation into *S. aureus* 29213

Plasmids with the correct sequence were transformed into *S. aureus* 29213 via electroporation. To prepare electrocompetent cells, an overnight culture was diluted to OD_{600} 0.5 and grown to OD_{600} 0.6. Cells were harvested by centrifugation at 4000 x *g* for 10 minutes at 4 °C and washed in 50 ml ice cold MilliQ H_2O three times. Cells were then centrifuged and resuspended in 50 ml, then 5 ml, 2 ml, and finally 0.25 ml 0.5 M sucrose. Up to 1 µg plasmid DNA was incubated on ice with 50 µl fresh competent cells for 10 minutes before being transferred to a chilled 1 mm electroporation cuvette and electroporated at 2.1 kV, 200 Ω, and 25 µF in an ECM 630 BTXTM (Harvard Apparatus). Afterwards, 1 ml BHI supplemented with 0.5 M sucrose was immediately added to cells, which were then incubated at 37 °C with 150 rpm shaking for 2 hours. Cells were finally plated with Cm and incubated overnight at 37 °C.

6.4.5 Screening for msfGFP fluorescence in cell cultures and supernatants

To verify if msfGFP was successfully secreted by the Tat and Sec pathways, cell cultures and supernatants from *S. aureus* 29213 expressing Tat:msfGFP, Sec:msfGFP, msfGFP, or no msfGFP were screened for fluorescence in a VarioScan Flash Plate Reader (Thermo Fisher Scientific). Overnight cultures were diluted to OD_{600} 0.1 in mM9 media and incubated at 37 °C with 180 rpm shaking until OD_{600} 0.5. mM9 is a minimal media comprising of M9 salts supplemented with 2 mM $MgSO_4$, 0.1 mM $CaCl_2$, 1 % glucose, 1 % casamino acids, 1 mM Thiamine-HCl, and 0.05 mM nicotinamide [187]. It was used in place of BHI because it has a lower autofluorescent background. Then 340 ng/ml ATc was added to the cultures and incubated for a further 60 minutes to induce the $P_{xyl/tetO}$ promoter and msfGFP expression. Final OD_{600} was recorded and 2 ml of each sample taken. 200 µl of which was added directly into a 96 well plate (Nunc F96 MicroWell Black-bottom plate, Thermo Fisher Scientific) and the remaining 1.8 ml centrifuged at 2600 x *g* for 10 minutes. The supernatant was removed, sterile filtered, and 200 µl added to the plate. 3 biological and 3 technical replicates were tested per construct, and mM9 media used to blank the machine. Fluorescence was measured with 488 nm excitation, 510 nm emission, and 1000 ms exposure time.

6.4.6 CLSM of *S. aureus* expressing signal peptide fusions

To visualise whether msfGFP was retained within cells, all constructs were also imaged with confocal laser scanning microscopy (CLSM). Overnight cultures were diluted to OD_{600} 0.1 in

mM9 and were grown to OD_{600} 0.5, then incubated for a further 2 hours with 340 ng/ml ATc and imaged with the LSM700 confocal microscope (Zeiss) with a 10 mW 488nm laser at 2 % power and a Plan-Apochromat 63x/1.40 oil immersion objective lens.

6.4.7 Construction and evaluation of Coa:msfGFP fusion protein

A C-terminal fusion Coa:msfGFP was created via allelic replacement via the protocol in Chapter 4. Primers Coa:msfGFP_F/Coa:msfGFP_R were used to amplify Coa:msfGFP from a pUC57 plasmid and add overhangs for Gibson Assembly. pIMAY was digested using restriction enzyme KpnI and then ligated to Coa:msfGFP via Gibson Assembly [156]. The ligated construct was first transformed via chemical transformation into *E. coli* IM08B to gain a methylation profile mimicking that of *S. aureus* [159], and then extracted and transformed via electroporation into *S. aureus* 29213 wildtype and Δ*vwbp* as described in Chapter 4. The plasmid was then integrated into the chromosome and finally the backbone excised as described in Chapter 4. Appendix 2 contains the sequence of the fusion and primer annealing sites. The genotype of the fusion protein was assessed via sequencing and the phenotype via coagulation assays and CLSM according to the protocols in Chapter 4.

6.4.8 CLSM of *S. aureus* expressing Coa:msfGFP

S. aureus expressing either Coa:msfGFP or unmodified Coa were grown overnight in BHI and then diluted to OD_{600} 5. Microwells (µ-Slide 8 Well, IBIDI) were preconditioned with 180 µl BHI supplemented with 50 % plasma, 10 µM Syto41, and 0.4 µg/ml Alexa Fluor 647 conjugated fibrinogen (20 %) by incubating at 37 °C for 30 minutes. Then 20 µl OD_{600} 5 cultures were added and incubated for a further 2 hours. The biofilms were imaged with 405 nm, 488 nm, and 639 nm excitation in the LSM700 confocal microscope (Zeiss). The signal from the GFP was dim, so the gain and power were increased until signal was seen, and then the line scan speed decreased and averaging increased to further increase signal and reduce noise. The Alexa Fluor 647 conjugated fibrinogen unexpectedly fluoresced with a peak at about 650 nm when excited at 488 nm, which prevented the detection of GFP emissions. This unwanted signal was removed by using a 640 nm short pass filter and limiting the range of emission detection to a 600 nm cut-off with the software.

6.4.7 Single molecule microscopy of *S. aureus* expressing Coa:msfGFP

Biofilms formed by *S. aureus* expressing either Coa:msfGFP or unmodified Coa were prepared in the same way as described above (Chapter 6.4.8), except with an initial OD_{600} of 0.2 rather than 0.5 to reduce the density of bacteria within the biofilm and within the field of view of the microscope. The pre-labelled fibrinogen concentration was also reduced 100 times to 4 ng /ml.

Samples were imaged with a bespoke single molecule fluorescence microscope with HILO (highly inclined and laminated optical sheet) illumination, in which lasers excited the sample at a 45 ° angle to reduce out of plane background fluorescence and increase signal to noise ratio. The laser profile was reduced to approximately 25 µm in diameter in order to increase the intensity and enable single molecule sensitivity, and fluorescent emissions were

split with a dual channel simultaneous imaging system (DV2, Photometrics) according to wavelength into separate green and red channels that were displayed side by side on the same image. Prior to imaging biofilms, a control sample of fluorescent beads (Tetraspeck Microspheres 0.2 µm, T7280, Invitrogen) was diluted 1:100 in 1 x PBS and 50 µl pipetted into a tunnel created by two pieces of double-sided tape on a conventional microscope slide and with a plasma cleaned microscope cover glass on top. The beads were alternately excited at a 50 ms frame rate for 10 frames by 640 nm and 488 nm wavelength lasers (OBIS 640 nm LX 40 mW and OBIS 488 nm LX 50 mW) operating at 1 mW. These data were used to verify that the lasers were aligned onto the sample correctly and later used to align the red and green channels during image analysis. Then, the biofilms were alternately excited at a 50 ms frame rate for 300 frames by 640 nm and 488 nm wavelength lasers operating at 1 mW and 40 mW respectively. Fibrin was visualised by the addition of 0.2 % fibrinogen pre-labelled with Alexa Fluor 647, which was very bright and only required excitation at 1 mW, whereas Coa:msfGFP was dimmer and was therefore excited at 40 mW.

6.4.8 Coa and fibrin colocalisation analysis

Single molecule microscopy data was analysed to quantify if, and to what degree, Coa and fibrin colocalise within biofilms, specifically in the pseudocapsule and wider biofilm matrix. To do this, I adapted some code previously written in the Leake group [126][188] and added some original code to it. The overall concept was to mask regions of interest in the images i.e. to mask the signal from fluorescent fibrin and from Coa:msfGFP, and quantify the fraction of pixels from the GFP mask that were also contained within the fibrin mask. The fraction of colocalised pixels were quantified separately in the pseudocapsule and extended network regions by masking signal from fluorescent fibrin and Coa:msfGFP in these regions only and quantifying the overlap.

Microscopy data was split into red and green channels, which displayed emissions from the same spatial location within the sample separated based on wavelength and displayed side by side on the image. There is a small spatial shift between the red and green channels due to slight differences in the optics for each channel, spherical, and chromatic aberrations, which means that corresponding pixels in each channel do not match perfectly. Therefore, to accurately assess which pixels were colocalised between channels, the red channel (containing signal from fluorescent fibrin) was transformed to align to the green channel (containing signal from Coa:msfGFP) using a geometric affine transformation on a frame average of the fluorescent beads data (Figure 26a). The transformation corrected for shifts in the X and Y directions, and differences in scale, shear, and rotation between the two images, and the transformation calculated from the beads data was used to correct the biofilm data. The fluorescence from Coa:msfGFP photobleached quickly, and therefore the following analysis was performed on frame averages of the first 10 frames of the image acquisitions before the GFP bleached. Adaptive thresholding with Bradley's method [130] was applied to mask the signal from either GFP (Figure 26d) or fluorescent fibrin (Figure 26c) in a 250 x 250 pixel region of interest.

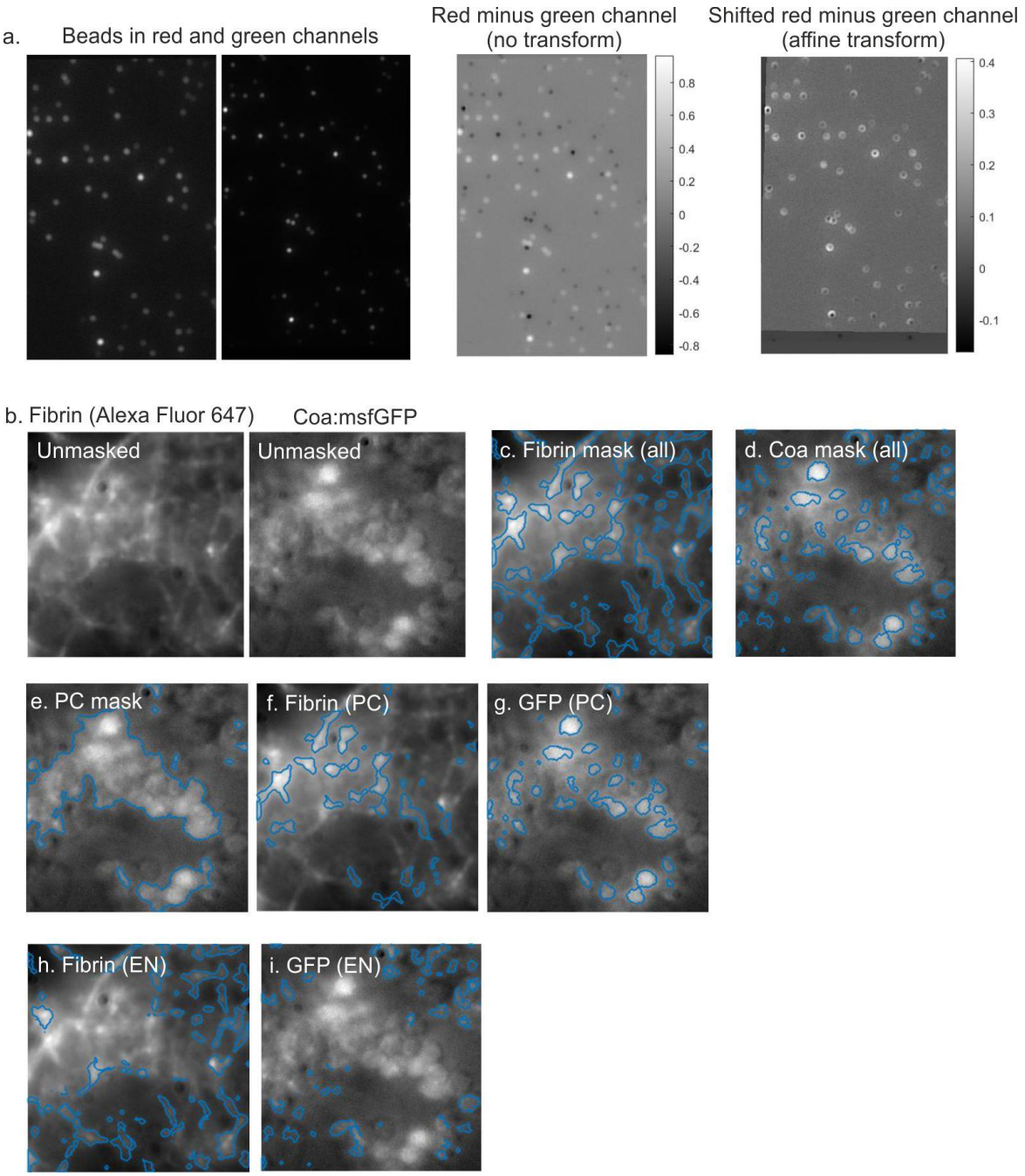

Figure 26 a) Alignment of red to green channel using images of fluorescent beads that appear in both channels. Subtracting the normalised green channel from the normalised red reveals that the channels are not aligned, but that they are after applying an affine transformation. The heat bars indicate pixel values. b) Example 250 x 250 region of interest divided into separate imaged containing fluorescently labelled fibrin and Coa. c-i) Masks overlaid on the image of Coa or fibrin that mask particular regions for analysis – either all fibrin or Coa, the pseudocapsule (PC), fibrin or Coa within the PC, or fibrin or Coa within the extended network (EN).

Rather than analysing the entire 512 x 256 pixel images, a slightly smaller region of interest was chosen because it improved the image segmentation. To mask the pseudocapsule region, a global threshold was applied to the green channel containing GFP fluorescence using

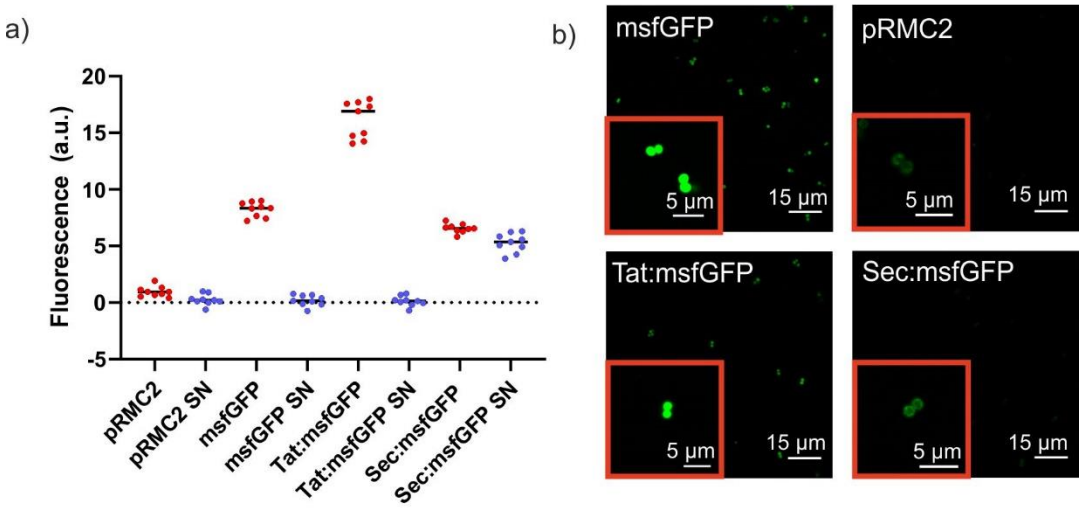

Figure 27 a) Fluorescence of cell cultures or supernatants (SN) of *S. aureus* expressing msfGFP fusions. msfGFP was fused to either Tat or Sec signal peptides, no signal peptide, or not expressed at all (pRMC2). Black bars indicate group medians. Red dots represent fluorescence from the bacterial cultures while blue dots represent fluorescence from the supernatant after separating the bacteria by centrifugation and filtration. b) Confocal microscopy images of *S. aureus* cells expressing msfGFP fusions. Red boxes indicate zoomed in images that had their brightness increased equally.

Otsu's method [131] (Figure 26e), and this mask was then combined with either the GFP (Figure 26g) or fibrin masks (Figure 26f) in order to mask either the GFP or fibrin within the pseudocapsule region only. The mask is a matrix of the same size as the region of interest that equals 1 within the masked regions and 0 outside. When combining two masks, the new mask only contains 1s where both input masks contained a 1 and is 0 everywhere else. Finally, the two new GFP/fibrin pseudocapsule masks were combined to create a mask containing just the pixels that were colocalised between the two masks. By quantifying the number of 1s in these masks, the code calculated the fraction of GFP colocalised with fibrin in the pseudocapsule. Similarly, the inverse of the pseudocapsule region mask was combined with the GFP (Figure 26i) and fibrin (Figure 26h) masks to quantify colocalisation of GFP with the extended fibrin network. Eight different images were analysed and the means and standard deviations of the colocalised fractions were calculated.

6.5 Results

6.5.1 msfGFP is secreted to cell culture supernatants via Sec, but not when secreted via Tat

msfGFP is a good candidate for an extracellular protein tag in Gram positive bacteria, but it depends on whether msfGFP can be secreted to the extracellular space and fold properly. We tested the ability of msfGFP to be secreted via the Tat and Sec pathways in *S. aureus* and then to fold properly by fusing msfGFP to Tat and Sec signal peptides. We measured the fluorescence of cultures and supernatant separated by centrifugation and filtration of bacteria expressing either Tat:msfGFP, Sec:msfGFP, msfGFP with no signal peptide, or not expressing msfGFP at all. Expression was induced by the addition of ATc.

msfGFP was successfully secreted via Sec and folded correctly, as its fluorescence was detected in the supernatant from bacterial cultures (Figure 27a). The fluorescence from the culture was at a similar level to the supernatant alone, so this fluorescence was assumed to come from the supernatant. Fluorescence was not detected in the other supernatants. msfGFP was retained within the cells expressing Tat:msfGFP or just msfGFP alone (Figure 27a). msfGFP could fold correctly within cells and fluoresce, but was unable to be secreted via the Tat pathway. Our findings indicate that msfGFP could be secreted by the Sec pathway and become fluorescent in the extracellular environment.

6.5.2 msfGFP is retained within *S. aureus* when fused to a Tat signal peptide, and partially associates to cell surfaces when fused to a Sec signal peptide

Our bulk fluorescence measurements demonstrated that Sec:msfGFP was secreted to the supernatant whereas Tat:msfGFP could not be secreted and was retained within cells. We verified this via CLSM imaging of cell cultures expressing Tat:msfGFP, Sec:msfFP, msfGFP with no signal peptide, and no msfGFP expression at all. Expression was induced with ATc. We expected to see fluorescence signal within cells expressing Tat:msfGFP and msfGFP, but not for those expressing Sec:msfGFP or no msfGFP.

As expected, msfGFP fluorescence was detected inside cells expressing Tat:msfGFP and msfGFP with no signal peptide (Figure 27b). While there was no bright intracellular fluorescence in *S. aureus* expressing Sec:msfGFP and no msfGFP, interestingly, dim rings of fluorescence at cell surfaces were seen when the brightness of the images were increased. Some of this is likely due to autofluorescence from ATc [189], which was present in all samples but cannot be distinguished from the intracellular fluorescence in the Tat:msfGFP and msfGFP samples. However, the higher level of cell surface fluorescence for Sec:msfGFP might indicate that some secreted msfGFP associated to cell surfaces.

6.5.3 Coa:msfGFP modified bacteria have the correct genetic sequence, coagulate human plasma, and have an unchanged biofilm phenotype

msfGFP was successfully secreted via the Sec pathway, so to verify whether it could be a suitable tag for extracellular proteins, it was fused to Coa from *S. aureus* as an example. The fusion Coa:SNAP previously localised correctly to the fibrin pseudocapsule, which provided a system to compare these results to. Modified *S. aureus* expressing Coa:msfGFP had the correct genetic sequence (Figure 28a), coagulated plasma the same as the parental strains (Table 10). Therefore, fusion to msfGFP did not inhibit the function of Coa.

Table 10 Coagulation of *S. aureus* 29213 wildtype and Δ*vwbp* expressing either Coa:msfGFP or unmodified Coa after 4 hours incubation with human plasma at 37 °C.

	Coagulation (+/-)			
	Coa:msfGFP		**Parental strains**	
	wt	**Δ*vwbp***	**wt**	**Δ*vwbp***
4 h	+	+	+	+

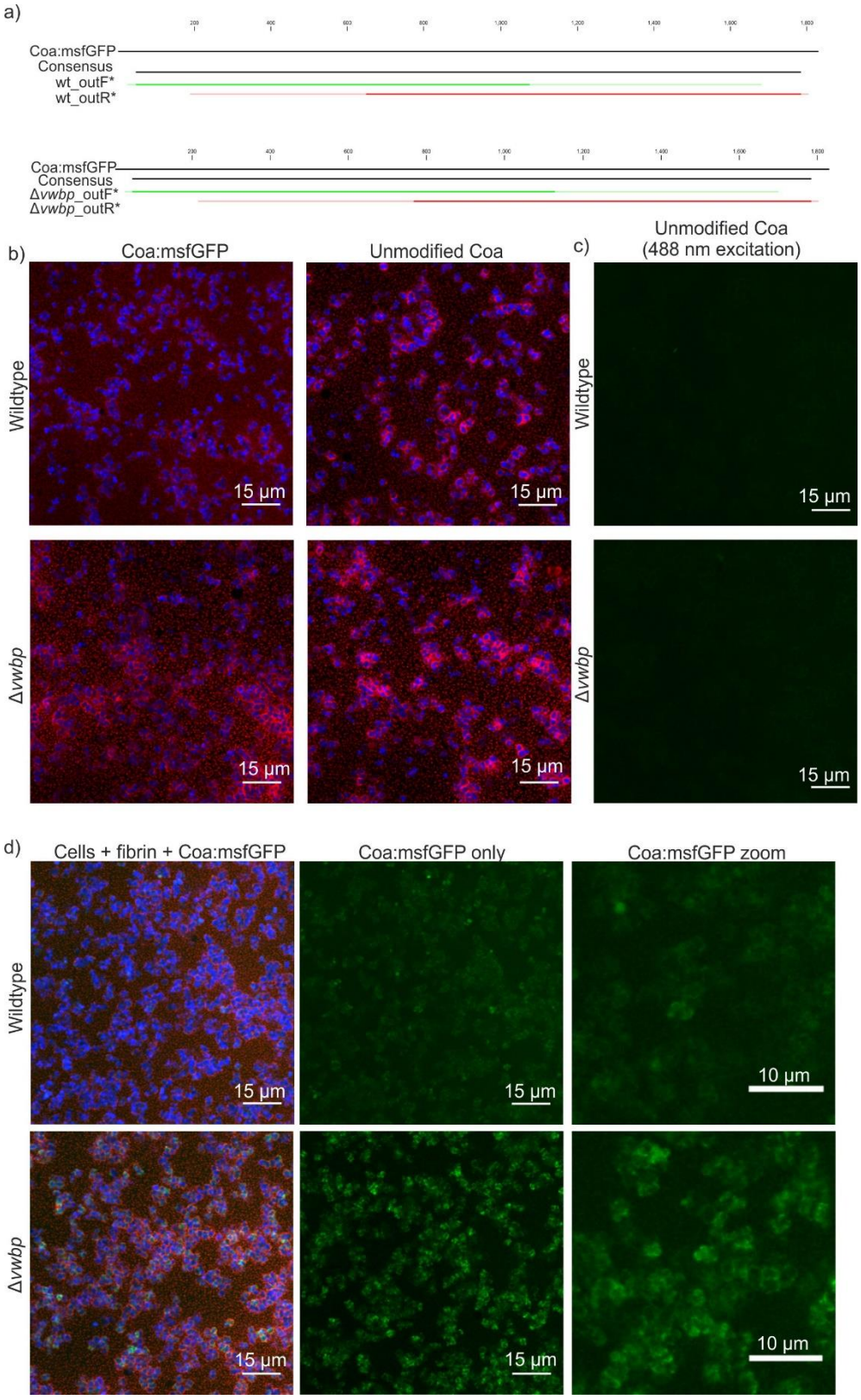

Figure 28 a) Sequence alignments for Coa:msfGFP in *S. aureus* wildtype and Δ*vwbp*. b) Fibrin phenotypes of *S. aureus* with msfGFP modified and unmodified Coa visualised with CLSM. c) Parental *S. aureus* with unmodified Coa excited under GFP conditions identical to Figure 4d). d) *S. aureus* Coa:msfGFP fluorescence. Cells are blue, fibrin is red, and Coa:msfGFP is green.

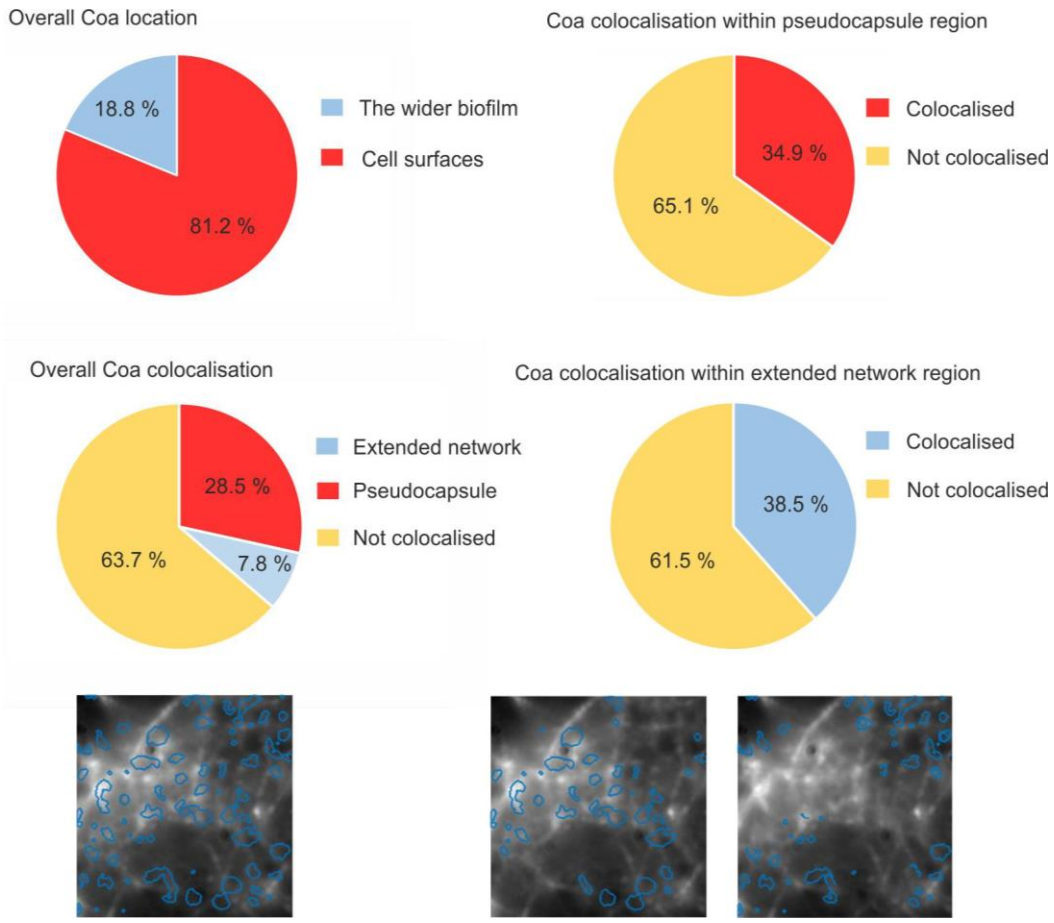

Figure 29 Coa localisation in biofilms and colocalisation with fibrin in the pseudocapsule and extended fibrin network. Masks mark an example of Coa locations in regions of interest and are overlaid over the fibrin image. Fractions of Coa localisation were averaged from data of 8 individual images. The masks for all Coa throughout the biofilm (left) were used to calculate the overall localisation/colocalisation, and the masks for Coa in the pseudocapsule region (middle) and extended network region (right) were used to calculate percentage colocalisation within the pseudocapsule and extended network regions respectively.

6.5.4 Coa:msfGFP correctly localises within biofilms

To assess if Coa:msfGFP localised correctly in biofilms, I imaged *S. aureus* biofilms expressing Coa:msfGFP with CLSM. Coa:msfGFP appeared to localise correctly. There was GFP signal close to the surface of cells, where Coa localises to produce the fibrin pseudocapsule (Figure 28d), which agrees with my findings when visualising the Coa:SNAP fusion protein in Chapter 5. However, it is difficult to assess from these images alone whether Coa truly colocalises with fibrin in the pseudocapsule and I therefore quantified the percentages of Coa colocalising with fibrin in the pseudocapsule and extended network using the msfGFP fusion.

Analysis of high resolution HILO images revealed that some Coa colocalised with fibrin within both the pseudocapsule and extended fibrin network, but more so within the pseudocapsule. 81.2 ± 9.5 % of the total Coa localised close to the surface of cells, and of that, 34.9 ± 3.7 % colocalised with the fibrin pseudocapsule. The remaining 18.8 ± 9.5 % of

Coa was located in the wider biofilm matrix, and of that, 38.5 ± 10.6 % colocalised with fibrin in the extended network. Overall, 28.5 ± 5.3 % of all Coa colocalised with the fibrin pseudocapsule, 7.8 ± 4.7 % colocalised with the extended network, and 63.7 ± 3.2 % did not colocalise with either (Figure 29). Upon close inspection of the cell masks presented in Figure , it does however appear that the masks are a little inaccurate in places, which will have impacted on the calculated percentages. In the example I provided in Figure 26, some Coa that lies close to bacteria was included in the extended network calculation, when I believe that it should have belonged to the pseudocapsule calculation. The algorithm also omitted a small number of bacteria from the pseudocapsule calculation and included them in the extended network instead. This likely artificially increased the calculation of percentage of Coa localised within the wider biofilm, and therefore the percentages I calculated may not accurately reflect the true distribution of Coa in biofilms. I can however conclude from these data that the majority of Coa is retained close to cells but does not exclusively colocalise with fibrin.

6.6 Discussion

msfGFP was secreted from *S. aureus* when fused to a Sec signal peptide, but not a Tat signal peptide. When fused to Coa, msfGFP did not hinder the biological function of Coa, and the fusion protein correctly localised to the fibrin pseudocapsule. Our findings agree with previous data from visualising Coa fused to the SNAP tag in Chapter 5 and indicate that fusion to both of these proteins does not seem to cause the Coa to mislocalise or malfunction. Therefore, msfGFP is a good candidate for tagging proteins exported by the Sec pathway. I further used the Coa:msfGFP fusion protein to quantify the proportions of Coa that colocalise with fibrin in the pseudocapsule and extended network.

Most Coa localised to cell surfaces in biofilms, while approximately one third colocalised with the fibrin pseudocapsule where it most likely bound to cell surfaces in order to facilitate the production of the pseudocapsule. In Chapter 3, I hypothesised that Coa associates to the surface of bacteria via fibrinogen that is bound to the surface, from where it localises fibrin production to the surface of bacteria to form the pseudocapsule. It was therefore surprising that more Coa did not colocalise with fibrin/fibrinogen and I speculate whether single fibrinogen molecules bound to cell surfaces could not be detected due to the large fluorescent signal from fibrin and low imaging power (1 mW) required to prevent the fibrin fluorescence signal from saturating the camera. A much higher power would be required to visualise single molecules of fibrinogen bound to cell surfaces, which would not be possible in my current experiment because the signal from fibrin would saturate and obscure the image. A small proportion of Coa appeared to localise to the wider biofilm rather than being retained on the cell surface. It might be beneficial to the bacteria to lose some Coa to the wider network, because there it can contribute to building the extended network that acts as a mechanical barrier against immune cells [41], and to potentially attach the biofilm to surfaces within the host.

Construction of the Coa:msfGFP was instrumental to the above analysis, and msfGFP is a good candidate when considering which protein tag to use for creating fusion proteins. msfGFP has a superfolding mutation that means it folds quickly, without chaperones, even when fused to another protein, and exhibits a high level of brightness [179][141] that I

thought would make it ideal for fusion proteins in the extracellular environment. Correct folding is essential for chromophore formation and fluorescence, while fast folding is also important for the protein to fold into its 3D conformation before it is cleaved by extracellular restriction enzymes that clear unfolded or misfolded proteins away from the cell surface. msfGFP is also monomeric, which makes it less likely to aggregate and cause artefacts. I do not know whether msfGFP would be exported correctly via the Sec pathway in other bacterial species. Past studies into GFP export via Tat in Gram positive bacteria revealed that their particular GFP variant was exported in some, but not all, species tested [170]. The authors speculated that this was due to differences in the physical or chemical structure of the cell wall, or in the quality control mechanisms of the Tat translocases. Such interspecies differences may also affect the outcome when using msfGFP for Sec exported proteins, and this is an important factor to bear in mind. While signal from msfGFP was dimmer than signal from the SNAP tag labelled with a substrate conjugated to Alexa Flour 647 in Chapter 5, it is advantageous because it does not require labelling procedures that can cause non-specific labelling within the extracellular matrix. Many bacteria establish infections, causes disease, and evade the immune system through a number of secreted and cell surface associated proteins. The MSCRAMM family of surface proteins expressed by *S. aureus* all contain a Sec signal peptide and interact with host proteins during infections [31] and would therefore benefit from a reliable protein tagging system, along with many others. While it is not possible to predict whether a fusion protein will always function as intended [106], msfGFP is a good candidate to consider first.

7. Visualising Embp in *S. epidermidis*

In this Chapter I present some work into visualising Embp in *S. epidermidis* biofilms via fusion to the SNAP tag or msfGFP. I intended to use these fusion proteins to analyse the localisation and cell-cell variation in Embp production under *in vivo* mimicking conditions, however was unable to visualise either of the fusion proteins. After failing to visualise both fusion proteins and failing to detect SNAP:Embp with anti-Embp antibodies, I concluded that poor protein tag placement might explain why the fusion proteins could not be visualised. Both SNAP and msfGFP were unintentionally placed before a putative cleavage site after the Embp signal peptide, and hence the protein tag may have been cleaved off or prevented protein secretion by inhibiting the signal peptide.

7.1 Introduction

Extracellular matrix binding protein Embp is a giant surface protein of *S. epidermidis* [74] present in 90 % of clinical isolates [64]. A major part of the protein contains the FIVAR and FIVAR-GA domains, which bind fibronectin when expressed recombinantly [75]. Fibronectin is a host protein involved in a variety of biological processes such as adhesion to the extracellular matrix, mobility, growth, and differentiation [78]. It usually circulates in plasma in a globular conformation or exists in the host extracellular matrix in a fibrillar conformation [77]. Overexpression of Embp increases bacterial adhesion to surface immobilised, fibrillar fibronectin *in vitro* [75], although Embp cannot bind globular fibronectin [190]. Expression of Embp requires the presence of serum, where it promotes cell clumping and biofilm formation by a mechanism involving interactions between the FIVAR-GA domains and ligands on the surface of adjacent cells [75]. Embp-mediated clumping also protects bacteria from phagocytosis [76]. Therefore, it seems that Embp could promote bacterial adhesion to host tissue and implants via fibronectin, increase biofilm formation *in vivo*, and help evade attack by the immune system. However, more research is required to confirm this, and the mechanisms Embp uses are currently unknown. I wanted to visualise Embp by creating a genomically encoded fusion protein and imaging it via fluorescence microscopy. By visualising Embp, I aimed to address questions such as under what conditions Embp is expressed, how much Embp is produced, its localisation within biofilms, and whether there is cell-to-cell variation in Embp production. By answering these questions, we gain new insight into why *S. epidermidis* produce Embp and its clinical significance.

My colleagues and I produced a number of Embp fusion proteins as part of our strategy to bet on multiple horses and maximise the chance of getting a successful fusion protein. All fusion protein projects are summarised in Table 4 in Chapter 4. We initially worked on both N- and C-terminal fusions with GFP and mNeongreen. The N-terminal of Embp contains a YSIRK/GS signal peptide which signals the protein for export out of the cell. The middle contains the fibronectin binding FIVAR and FIVAR-GA domains, and the C-terminal contains a domain of currently unknown function and a putative transmembrane domain [75]. Fusion proteins are usually placed at the terminus away from functional domains so as not to interfere with protein function [106], so we initially produced both N- and C-terminal fusions because we did not know whether fusion at the C-terminal would inhibit the domain of unknown function and putative transmembrane domain. The fusion was

placed after the signal peptide cleavage site at the N-terminal, or before the stop codon at the C-terminal. However, we discarded these projects before completing them. There was an error with the GFP: we intended to use msfGFP, a bright and fast folding GFP variant [179][141], but due to a copy and paste error, cloned GFP(-30) [142] instead, which is very dim [123], and was too dim to visualise when fused to vWbp in an earlier project. We chose mNeongreen as an alternative because it fluoresces much brighter than GFP [147], however discarded the project when we realised that mNeongreen is photoswitchable [148], an unwanted fluorescent property.

My colleagues and I therefore produced N-terminal fusions with msfGFP and the SNAP tag. We omitted C-terminal fusions in case the fusion inhibited the domain of unknown function. Unfortunately, I struggled to stain the SNAP tag and visualise Embp, and could not visualise msfGFP:Embp either. There are no functional assays to verify Embp production and secretion similar to the coagulation assays used to confirm the presence of Coa and vWbp. Hence, I was unable to verify whether fusion to SNAP or msfGFP impaired the secretion or function of Embp. Embp is secreted via a different mechanism to Coa, and so it is unsure whether the pathway used by Embp can secrete SNAP. Coa is secreted by the Secretory pathway, in which proteins are exported out of the cell in an unfolded state and fold in the extracellular space [180][172]. Ebh is an *S. aureus* surface protein homologous to Embp that is directed to the cross wall during cell division [191]. The cross wall is a compartment formed during cell division between the plasma membranes of two daughter cells where cell wall synthesis occurs [192]. When peptidoglycan synthesis is complete, the cross wall splits down the middle and separates the two daughter cells, thus exposing proteins directed to the cross wall on the cell surface. While the mechanism of directing proteins to the cell wall is unknown, several other proteins with YSIRK/GS motifs have been shown to be secreted at the cell wall, such as sortase-anchored proteins [193]. Due to its homology to Ebh, Embp is probably secreted via this pathway too. To assess whether SNAP:Embp was secreted successfully, my colleague and I labelled SNAP:Embp with an antibody against a recombinant Embp kindly provided by Prof. Holger Rohde (University of Hamburg) that was later confirmed to also recognise full length Embp, but were unable to verify the presence of Embp. It was later realised that the proteins tags were unintentionally placed before a putative cleave site after the signal peptide, and therefore reasons for failure to detect the fusion proteins could be that the protein tag was cleaved off, or that the fusion protein prevented the secretion of Embp out of bacteria by interfering with the signal peptide.

All fusion proteins were produced according to the modified version of Monk's protocol [159] presented in Chapter 4. Because we did not complete the initial GFP and mNeongreen fusions, this Chapter will begin at the stage of producing and visualising SNAP:Embp. I will also present the work we did trying to visualise Embp when stained with anti-Embp antibodies and with msfGFP:Embp. I collaborated with a number of colleagues to produce the work in this Chapter. Lisbeth Marcussen (Aarhus University) and Nasar Khan (Aarhus University) created SNAP:Embp, Amalie Maria Grønning (Aarhus University) produced msfGFP:Embp with Lisbeth and performed the antibody labelling experiments. I supervised these projects. Nasar kindly provided protocols for antibody labelling. I developed labelling protocols for SNAP:Embp and visualised it with CLSM. I also visualised msfGFP:Embp with single molecule microscopy, and Alex Payne-Dwyer (University of York) helped me set up the single molecule microscope. Cecilie Siem Bach-Nielsen (Aarhus

University) performed a bioinformatic analysis of *embp* in *S. epidermidis* 14.1.R1 and identified the putative cleavage site, and I realised that this might explain why we could not visualise the fusion proteins.

7.2 Aim and hypothesis

The aim was to produce a fusion protein for visualising Embp in *S. epidermidis* 14.1.R1. I intended to use the fusion protein to answer fundamental questions regarding Embp, such as its localisation, quantity of Embp, production under different conditions, and whether Embp is produced equally by all cells. By addressing these questions, I would learn more about the biological role of Embp. I expected that host factors would be required for the expression of *embp,* and that Embp would localise to the surface of bacteria and the wider biofilm matrix.

7.3 Materials

All bacterial strains and plasmids used throughout this Chapter are given in Table 11. Bacteria were stored in 25 % glycerol at -80 °C. Liquid cultures were made by inoculating a single colony from an agar plate into 10 ml brain heart infusion broth (BHI, Sigma Aldrich, 53286) and incubating overnight at 37 °C with 180 rpm shaking. Media was supplemented with either 5 µg/ml erythromycin (Erm, Sigma Aldrich, E5389), 10 µg/ml chloramphenicol (Cm, Sigma Aldrich, C0378), or 100 µg/ml ampicillin (Amp, Sigma Aldrich, A9393) for plasmid selection, 0.1 µg/ml anhydrotetracycline (ATc, Sigma Aldrich, 94664) to induce Embp expression from *S. epidermidis* 1585 $P_{xyl/tet}$ *embp,* and 50 % human serum for native Embp expression. For biofilm growth, BHI was supplemented with 50 % heparin stabilised human plasma to mimic *in vivo* conditions. Serum and plasma were separated from blood donated by Aarhus University Hospital by centrifugation at 2000 x *g* for 15 minutes. Separated serum and plasma were pooled and divided into aliquots and kept at -80 °C for long term storage. Aliquots were thawed in a 37 °C water bath prior to use. For microscopy experiments, bacteria were stained with either one of the DNA binding stains Syto41 (Life Technologies, S11352) or Syto9 (Life technologies, S34854). The SNAP tag was stained by SNAP-Surface Alexa Flour 647 (New England Biolabs, S9136S), referred to as SNAP-647 in the text. Prior to staining, samples were blocked with 5 % bovine serum albumin (BSA, Sigma Aldrich, A9418) in 1 x phosphate buffered saline (PBS, Thermo Fisher Scientific, 28348).

7.4 Methods

7.4.1 Creation of SNAP:Embp and msfGFP:Embp fusion proteins

In order to visualise Embp, a gnomically encoded N-terminal fusions between SNAP or msfGFP and Embp was produced in *S. epidermidis* 14.1.R1 (SNAP:Embp, msfGFP:Embp) using a modified version of Monk's protocol [159], which was presented in detail in Chapter 4. A DNA construct containing the sequence for SNAP flanked by 400 – 600 nucleotide long sequences homologous to the insertion site in *S. epidermidis* was made by SOE-PCR. The DNA construct was inserted into the shuttle vector pIMAY [182] by restriction enzyme digestion and ligation using restriction enzyme KpnI-HF (New England Biolabs, R3142S)

Table 11 Bacterial strains and plasmids used in this Chapter.

Bacterial Strain	**Description**	**Reference**
Staphylococcus epidermidis 14.1.R1	Isolate from human skin. High antimicrobial activity. *icaADBC* deficient.	[194]
S. epidermidis 14.1.R1 *snap:embp*	Genomically encoded, N-terminal *snap:embp* fusion.	This study
S. epidermidis 14.1.R1 *msfgfp:embp*	Genomically encoded, N-terminal *msfgfp:embp* fusion.	This study
S. epidermidis 1585 Δ*embp*	Clinical isolate that does not produce polysaccharides (*icaADBC* deficient), engineered to lack Embp.	[190]
S. epidermidis 1585 $P_{xyl/tet}$ *embp*	Expression of *embp* from the chromosome with inducible $P_{xyl/tet}$ promoter.	[75]
Escherichia coli DC10B	Bypasses *S. epidermidis* restriction barrier. Deficient in cytosine methylation (Δ*dcm*).	[182]
Plasmid	**Description**	**Reference**
pUC57-*snap*	*E. coli* vector carrying *snap*. Ampicillin resistance.	Genscript
pUC57-*msfgfp*	*E. coli* vector carrying *msfgfp.* Ampicillin resistance.	Genscript

and T4 DNA ligase (Thermo Fisher Scientific, EL0011). The construct was transformed into *E. coli* DC10B via heat shock, which methylates its DNA with a profile similar to *S. epidermidis* [182]. The plasmid was extracted using the GeneJET Plasmid Miniprep Kit (Thermo Fisher Scientific, K0502) and transformed into *S. epidermidis* via electroporation. To integrate the plasmid into the chromosome, positive transformants were first grown under conditions permissive for plasmid replication (28 °C, with Cm), and then diluted into fresh media and incubated at 37 °C with Cm to select for colonies with plasmid integration. Then to excise the plasmid backbone, all selection pressure for retaining the plasmid was removed, and bacteria were diluted into fresh media without Cm and incubated at 28 °C. This process was repeated for up to 14 days. Bacteria were then incubated with ATc to kill bacteria still containing the plasmid and were screened for Cm resistance to confirm plasmid backbone excision. Cm sensitive colonies were screened with colony PCR to verify if *snap* or *msfgfp* were successfully inserted into the chromosome and then sequenced with Macrogen to confirm the correct genotype. The sequences of the fusion proteins and primers used for cloning are given in Appendix 3.

7.4.2 Visualising SNAP:Embp in biofilms

This staining protocol is based on the one used to label Coa:SNAP in *S. aureus* in Chapter 5, but includes some modifications because *S. epidermidis* did not adhere strongly to the micowell surface, especially when grown with plasma. Bacteria were therefore easily removed from the surface through repeated blocking, staining, and washing steps. This

protocol went through multiple rounds of optimisation, and the final protocol is presented here.

Overnight cultures of *S. epidermidis* 14.1.R1 *snap:embp* or wildtype were diluted to OD_{600} 0.5 in BHI. 50 µl was inoculated into a microwell (µ-slide Angiogeneis, IBIDI, 81501) and incubated for 6 hours at 37 °C to allow the bacteria to attach to the microwell surface. Then the media was replaced with 50 µl BHI supplemented with 50 % plasma and incubated overnight to induce *embp* expression. The next day, the media was replaced with 50 µl fresh BHI with 50 % plasma and incubated overnight again. Then the biofilms were blocked with 50 µl blocking buffer (5 % BSA in 1 x PBS) for 30 minutes at room temperature, then stained with 50 µl staining buffer (5 % BSA in 1 x PBS supplemented with 1 µM SNAP-647 and 1 µM Syto41) for 30 minutes at 37 °C. Biofilms were washed for 1 hour at room temperature with 50 µl blocking buffer before resuspension in PBS and imaging with CLSM (LSM700, Zeiss). Biofilms were imaged with 405 nm and 639 nm excitation with a Plan-Apochromat 63x/1.40 oil immersion objective lens.

7.4.3 Visualising SNAP:Embp in planktonic cultures

Overnight cultures of *S. epidermidis* 14.1.R1 *snap:embp* or wildtype were diluted 100 times in BHI and incubated for 6 hours at 37 °C with 180 rpm shaking. 1 ml culture was harvested by centrifugation in a microcentrifuge at 2000 x *g* for 5 minutes. The supernatant was discarded and the pellet resuspended in 1 ml blocking buffer (5 % BSA in 1 x PBS) and incubated at room temperature with 180 rpm shaking for 30 minutes. Then the culture was harvested again and resuspended in 1 ml staining buffer (5 % BSA in 1 x PBS supplemented with 1 µM SNAP-647 and 1 µM Syto41) and incubated at 37 °C with 180 rpm shaking for 30 minutes. Finally, the culture was resuspended in 1 ml blocking buffer and washed for 1 hour at room temperature with 180 rpm shaking, resuspended in 1 ml PBS, and imaged with CLSM (LSM700, Zeiss). For imaging, 5 µl of each sample was pipetted onto a poly-lysine coated microscope slide (Superfrost Ultra Plus, Thermo Scientific, 10149870) and a glass microscope coverslip placed on top. Samples were imaged with 405 nm and 639 nm excitation with a Plan-Apochromat 63x/1.40 oil immersion objective lens.

7.4.4 Antibody labelling of SNAP:Embp

After struggling to label SNAP:Embp, Embp was visualised with an anti-Embp antibody in order to verify whether SNAP:Embp was actually produced. A number of strains were visualised: *S. epidermidis* 14.1.R1 *snap:embp* and wildtype, *S. epidermidis* 1585 Δ*embp,* and *S. epidermidis* 1585 $P_{xyl/tet}$ *embp*, which has inducible *embp* expression in the presence of ATc. Single colonies of each strain were inoculated in 100 µl either BHI or BHI supplemented with 50 % human serum in a microwell (µ-Slide 8 well, IBIDI, 80821) and incubated overnight at 37 °C. The next day, the cultures were collected in eppendorfs, centrifuged for 5 minutes at 2000 x *g*, and resuspended in 1 x PBS. Cultures were adjusted to an OD_{600} 1 and 100 µl pipetted onto a poly-lysine coated microscope slide (Superfrost Ultra Plus, Thermo Scientific, 10149870) inside a ring drawn with a hydrophobic marker. All the following steps were carried out at room temperature and all volumes were 100 µl. The slides were washed 3 times with 1 x PBS and then blocked with 3 % BSA in 1 x PBS for

45 minutes. Then the slides were washed 3 times with 1 x PBS supplemented with 0.05 % Tween-20 (Sigma Aldrich, P9416). The primary Anti-Embp antibodies were diluted 1:300 in in 3 % BSA in 1 x PBS, and incubated on the slides for 60 minutes. The slides were washed 5 times with 1 x PBS supplemented with 0.05 % Tween-20 before incubation with the secondary antibody (Alexa Fluor 635 goat anti-rabbit IgG (H + L), Thermo Fisher Scientific, A-31576) diluted 1:1000 in 3 % BSA for 60 minutes. Slides were washed again with 1 x PBS supplemented with 0.05 % Tween-20, stained with 10 µM Syto9 for 10 minutes, washed once more with 1 x PBS, and finally visualised with CLSM (LSM700, Zeiss) with 488 nm and 639 nm excitation and a Plan-Apochromat 63x/1.40 oil immersion objective lens.

7.4.5 Visualisation of msfGFP:Embp in biofilms with single molecule microscopy

Microwells (µ-Slide 8 Well, IBIDI) were preconditioned with 180 µl BHI supplemented with 50 % human plasma by incubating at 37 °C for 30 minutes. Overnight cultures of *S. epidermidis* 14.1.R1 *msfgfp:embp* and wildtype were diluted to OD_{600} 2 in BHI, and then 20 µl was added to the microwells to reach an overall OD_{600} 0.2. The samples were incubated for a further 2.5 hours at 37 °C and then imaged. Biofilms were imaged with a bespoke single molecule HILO [195] microscope, which illuminates samples obliquely at a 45 ° angle in order to reduce background noise arising from out of plane fluorescence. A 488 nm laser (Coherent Obis 488 nm LX 50 mW) operating at 40 mW was used for excitation with a 50 ms frame rate. The laser profile was reduced to a diameter of 25 µm in the sample to increase the intensity and enable single molecule detection with high temporal resolution. Fluorescence emissions were split into red and green channels with dual-channel imaging system (DV2, Photometrics).

7.5 Results

7.5.1 No labelling of SNAP:Embp was seen in biofilms nor planktonic cultures

To visualise Embp in *S. epidermidis* biofilms, we created a genomically encoded N-terminal fusion with the SNAP tag (SNAP:Embp) and I visualised it with CLSM. Embp is a surface protein and I therefore expected to see signal from the fusion protein at the surface of bacteria. Unfortunately, no labelling was seen in either biofilms or planktonic cultures (Figure 30). In biofilms, there was a background signal in both the wildtype and *snap:embp* mutant, indicating this was non-specific staining and did not arise from staining of the SNAP tag. In planktonic cultures, no staining was seen at all. In retrospect, Embp was probably not expressed in the planktonic experiment because I forgot to include serum when incubating the bacteria, which is thought to be necessary to induce *embp* expression [75]. However, in the biofilm experiment, *embp* expression was expected because bacteria were incubated with plasma, which contains serum. Increasing plasma concentration from 50 % to 75 % or 100 % did not improve the SNAP labelling (data not shown). There is no assay to verify whether Embp is expressed, and I therefore did not know whether fusion to SNAP inhibited Embp expression or function. Therefore my colleague and I visualised SNAP:Embp with an

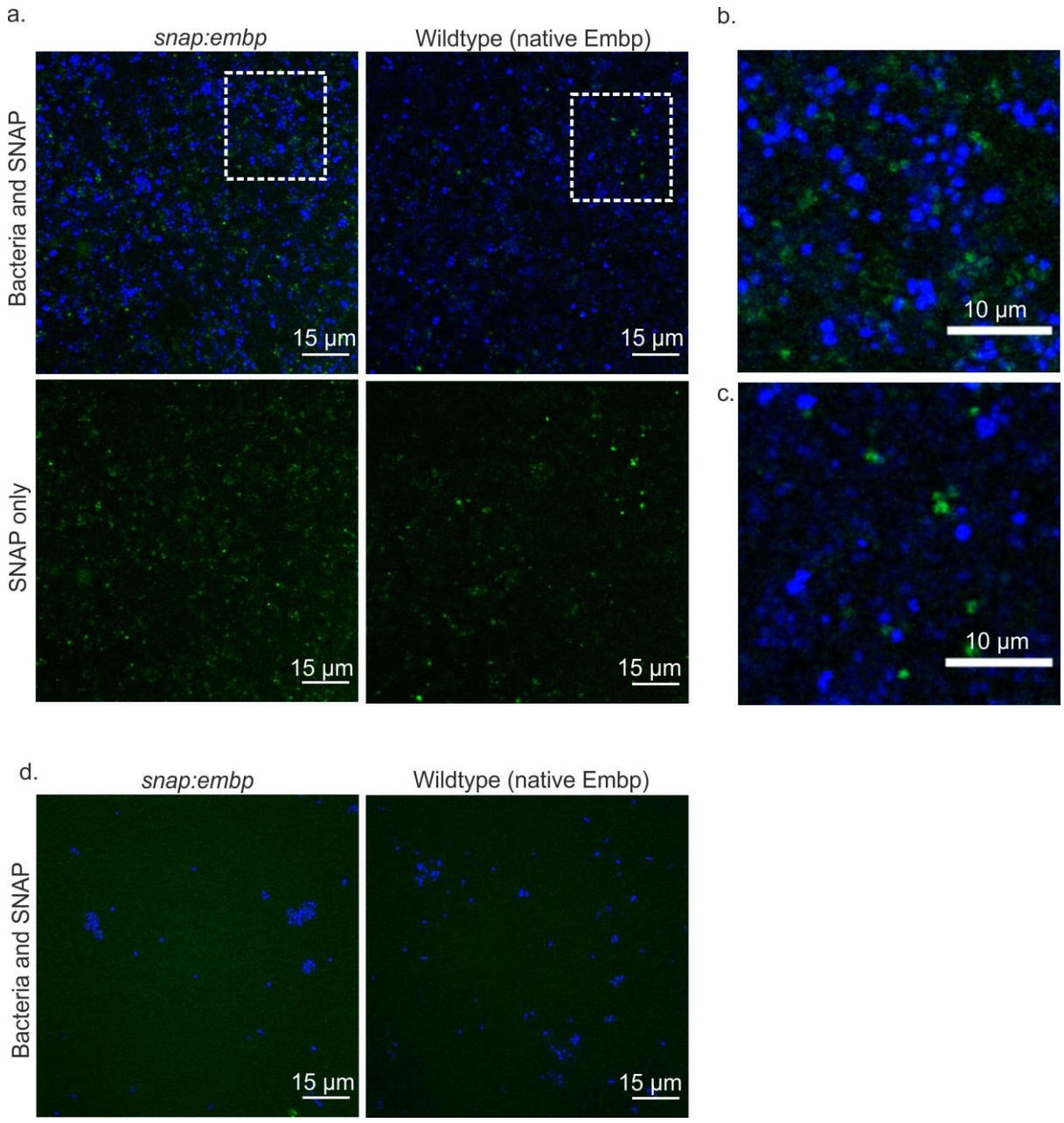

Figure 30 a) *S. epidermidis* 14.1.R1 biofilms that produce either SNAP:Embp or native, unlabelled Embp grown with 50 % plasma. b) and c) Zoomed in images of the highlighted regions in the biofilms with SNAP:Embp and native Embp, respectively. d) Planktonic *S. epidermidis* 14.1.R1 that produce either SNAP:Embp or native Embp. No labelling of the SNAP tag was seen. Cells are blue and SNAP substrate green.

antibody against Embp to verify whether it was produced or not. If we could verify SNAP:Embp expression, we planned to return to this experiment later and optimise the SNAP staining protocol.

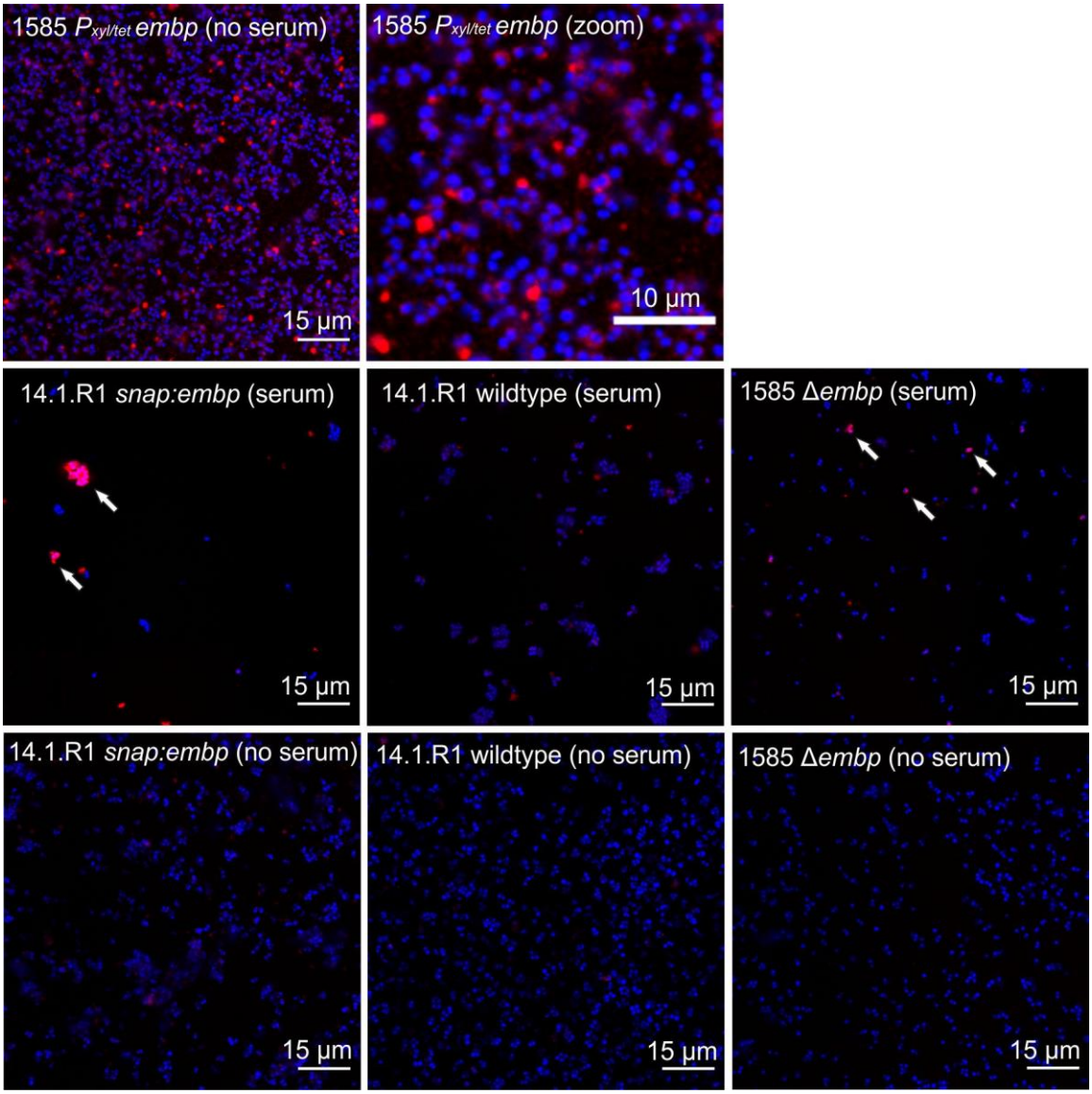

Figure 31 Anti-Embp labelling of *S. epidermidis* strains that produce either native Embp, SNAP:Embp, no Embp, or have inducible Embp expression. Samples were grown in both the presence and absence of serum. Cells are blue and antibody staining is red.

7.5.2 Embp secretion could not be verified by antibody labelling

Because I saw no labelling of SNAP:Embp, we decided to check whether fusion to SNAP prevents Embp expression or secretion. We therefore visualised Embp with an antibody that recognises a recombinant version of Embp. Biofilm group member Nasar Khan verified that this antibody also binds full length Embp prior to our experiments. We visualised Embp in the wildtype and *snap:embp* mutant as well as control samples that either lacked Embp or had inducible *embp* expression. Samples were grown in both the presence and absence of human serum to check if serum was necessary for Embp expression.

In the strain with inducible *embp* expression, signal from Embp was seen as ring-like structures around cell surfaces that were not present at all in the mutant lacking Embp (Figure 31). This provided a benchmark for the signal pattern we expected to see if Embp was secreted in the other strains, albeit that the signal might be lower or not occur in all cells

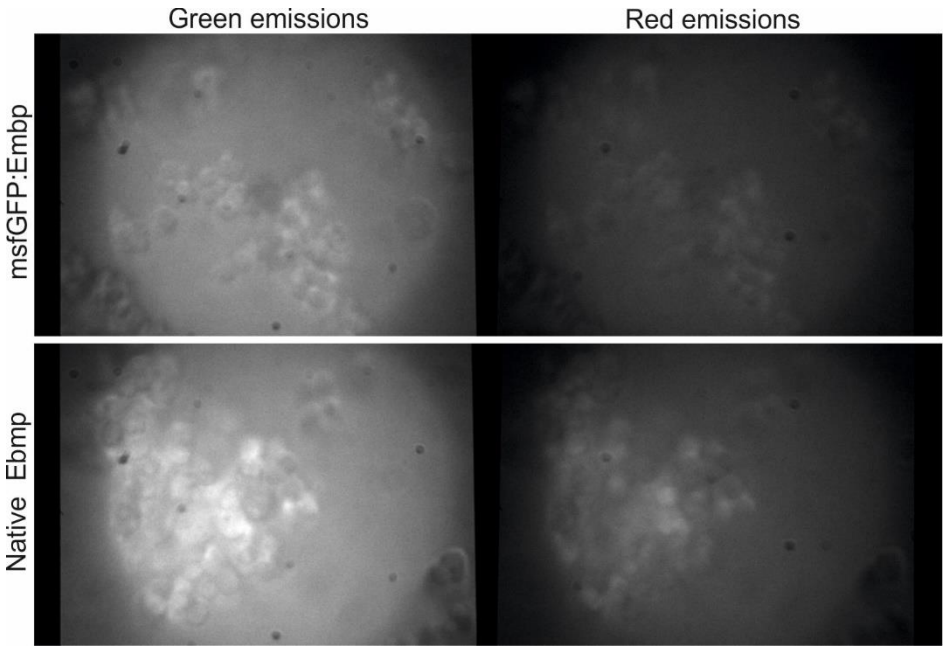

Figure 32 Single molecule fluorescence microscopy images of *S. epidermidis* 14.1.R1 that produce either msfGFP:Embp (top) or native Embp (bottom) when grown in media containing 50 % serum. Fluorescence emissions were split into green and red channels corresponding to the same spatial location within the sample. The green channel shows fluorescence from GFP and autofluorescence. The red channel shows autofluorescence.

under native expression levels. In samples grown with serum, there was strong signal overlapping with some clusters of cells in the *snap:embp* mutant, but not all of them (Figure 31, white arrows). However, this signal was also present on some cells in the mutant lacking Embp (Figure 31, white arrows), so was attributed to non-specific staining by the antibodies. No clear staining of Embp was seen in samples grown in the absence of serum.

While there was no clear staining of Embp, cells appeared to clump more when grown with serum in both the wildtype and *snap:embp* mutant, but not the mutant lacking Embp (Figure 31). Embp causes cells to clump in the presence of serum [75], therefore this clumping might indicate Embp secretion and indicate that it is the antibody labelling that failed, rather than lack of Embp production.

Overall, our results were inconclusive. We were not able to verify Embp secretion in either the wildtype or *snap:embp* mutant via antibody labelling. However, wildtype and *snap:embp* bacteria clumped in the presence of serum, which might indicate that Embp was produced but the antibody labelling failed. Around this time, we learned that msfGFP could be used to label Coa in *S. aureus* (Chapter 6), and decided to change strategy and complete an msfGFP:Embp fusion rather than optimising the antibody and SNAP labelling protocols, which were likely to be lengthy projects with no guarantee of success. Lisbeth Marcussen (Aarhus University) had completed most of the cloning for this fusion already as part of an earlier project, and therefore only a small amount of work was needed to finish the cloning. Additionally we expected that fusion to msfGFP would be a better strategy to visualise Embp because it does not require staining, since the staining procedure was proving difficult.

7.5.3 msfGFP:Embp could not be visualised with single molecule microscopy

I visualised *S. epidermidis* that produce msfGFP:Embp and native, untagged Embp using single molecule HILO microscopy. Attempts to label SNAP tagged Embp had proven difficult, and I hoped that visualising msfGFP tagged Embp would be more successful because firstly, it does not need labelling and thus avoids issues of labelling efficiency and non-specific staining, and secondly, single molecule microscopy is a sensitive technique that would detect even low levels of fluorescence from the fusion protein in the event that expression levels were low. Unfortunately however, there were no differences between images of *S. epidermidis* that produced msfGFP:Embp or native Embp (Figure 32), and therefore I concluded that this fusion protein either did not fluoresce or was not secreted properly. It is likely that the fusion with SNAP had the same issues.

7.6 Discussion

I wanted to visualise Embp in *S. epidermis* biofilms by constructing fusion proteins with SNAP or msfGFP, but unfortunately was unable to visualise any of these fusion proteins. I was unable to verify whether Embp was successfully secreted because there is no assay to verify this. While my colleague and I did attempt to visualise Embp and SNAP:Embp by labelling with an anti-Embp antibody, we were ultimately unsuccessful because we could not label Embp in either the wildtype or the *snap:embp* mutant, and therefore could not conclude whether fusion to SNAP inhibited Embp secretion. We did detect Embp in a mutant that overexpresses *embp*, but the signal was very dim, therefore, one possibility could be that the signal from the strains with native *embp* expression might have simply been too low to detect in our microscope. It is not certain what conditions *embp* is expressed under because it is not produced in regular lab media [75], so it is a possibility that *embp* was not expressed in our experiment, although it was expected upon the addition of serum. I was unable to visualise msfGFP:Embp using single molecule microscopy. If Embp expression was simply too low in our previous experiments, I expected to be able to detect signal from single msfGFP molecules when visualising msfGFP:Embp, but could not. Therefore it is most probably that the fusion protein was not secreted properly or that the protein tag failed to fold correctly to become fluorescent or function normally. Our issues reflect how difficult it can be to troubleshoot problems with fusion proteins when there is no standard test to verify that the fusion protein is secreted and functions correctly.

I realised that the placement of the protein tags may have been poor and thus caused my failure to visualise them after my colleague identified a putative cleavage site in the sequence of Embp in our strain of *S. epidermidis*. The protein tags were placed downstream of the signal peptide, but upstream of the putative cleavage site; this site is highlighted in red in the mutant sequences in Appendix 3. There are several ways that this might have affected the fusion protein. The protein tag might have been cleaved off and therefore did not localise with Embp at cell surfaces where it was expected, the placement could have prevented either protein from folding correctly, or it could have interfered with the signal peptide itself and therefore prevented the secretion of the fusion protein. The full structure of Embp is unknown, so when designing the fusion protein we had to use predictions made by bioinformatics analysis. The sequence was initially analysed assuming that it began with the

usual ATG start codon, however, the gene in the strain that we worked with (*S. epidermidis* 14.1.R1) actually starts with a TTG codon, which is the main non-ATG start codon in prokaryotes [196]. When analysing with the correct start codon, a cleavage site was identified at the N-terminal. Perhaps inserting the protein tag after this cleavage site would provide a better outcome.

Throughout my work with fusion proteins I have learned several things that will help to design an alternative fusion protein with which to visualise Embp. As mentioned above, the next tag should be placed in a different location, probably after the cleavage site. In Chapters 5 and 6, I learned that the SNAP tag and msfGFP can be used to label extracellular proteins in *S. aureus* that are secreted by the Sec pathway, but Embp is exported by a different mechanism where it is directed to the cross wall during cell division. However, in Chapter 5, I successfully visualised *S. aureus snap:lpxtg,* which expresses *snap* fused to a SpA secretion sequence. SpA is also secreted at the cross wall [197], and therefore my success visualising *S. aureus snap:lpxtg* might indicate that SNAP can be exported via this mechanism in *S. epidermidis* too, although it is not possible to be certain of this. Hence, a SNAP:Embp fusion placed after the cleavage site might be successful. The bright signal provided by Alexa Flour conjugated SNAP substrates might be an advantage when detecting Embp because its level of expression is unknown and might be quite low and therefore difficult to detect. Conversely, labelling pre-grown *S. epidermidis* biofilms is difficult because I experienced that they do not adhere to the microwell surface as strongly as *S. aureus*, which results in many cells detaching from the microwell through repeated staining, blocking, and washing steps. Therefore msfGFP might be a better option because it eliminates this problem, and the most optimal strategy going forward is to produce both SNAP:Embp and msfGFP:Embp fusions with the new placement simultaneously. A successful fusion protein will help answer fundamental questions about Embp such as its expression levels, what causes its expression, and its localisation. The more we learn about Embp, the better our understanding will be of why *S. epidermidis* produces it and how it contributes to infection.

8. SINGLE MOLECULE MICROSCOPE DESIGN

8.1 Introduction

Imaging single molecules within biofilms will allow researchers to gain a deeper understanding of biofilms, for example of the molecular mechanisms that they use to form their matrix or interact with host tissues. Imaging single molecules inside biofilms is challenging because the biofilm contains many layers of cells encased in a complex extracellular matrix that contains many biomolecules that autofluoresce and decrease the signal to noise ratio. The biofilm environment is heterogeneous and thus contains areas of varying refractive index that will refract and scatter the excitation light and fluorescence emissions, further decreasing signal to noise ratio. Furthermore, the further light travels through a biofilm, the more obstacles it encounters, and the harder it becomes to image the middle and far away parts of the biofilm. However, it could be possible to design a bespoke microscope that is tailored specifically to help overcome these issues.

I spent the majority of the first year of my PhD in the Leake Group in York designing a single molecule microscope for imaging biofilms. I decided on the main design features and began to assemble parts of the microscope. The process was a combination of reading literature on microscope design, comparing different design features, making calculations to assess whether a particular design feature would work, and taking some preliminary measurements. As my PhD progressed, there became a greater focus on the biological work and I did not complete the microscope build as originally intended. Here I will present the thought processes behind the main design choices, the current progress of the build, and some practical considerations for the future.

8.2 Aim

The aim was to design, build, and test a bespoke fluorescence microscope capable of imaging single molecules inside biofilms with millisecond temporal resolution. The design should be incorporated into an existing inverted single molecule microscope that had pathways to image with TIRF, narrowfield, and widefield microscopy. The existing features could either be utilised in the design, or an additional excitation pathway built with a new design.

8.3 Microscope design concepts and choices

8.3.1 Selective plane illumination reduces out of plane fluorescence and increases imaging depth

It is challenging to achieve single molecule resolution when imaging biofilms because they are thick, heterogeneous samples that attenuate and distort both the excitation and emission signal, and the deeper into the biofilm you image, the higher the background noise due to imaging through many layers of cells and extracellular matrix. *In vivo* biofilms exist in small aggregates of up to approximately 200 µm in diameter, although in some cases they can reach up to 1200 µm [16], and *in vitro* biofilms can be much thicker up to several mm. There are a number of ways to image deep inside samples with high background noise, such as multiphoton excitation (MPE), selective plane illumination microscopy (SPIM), and highly

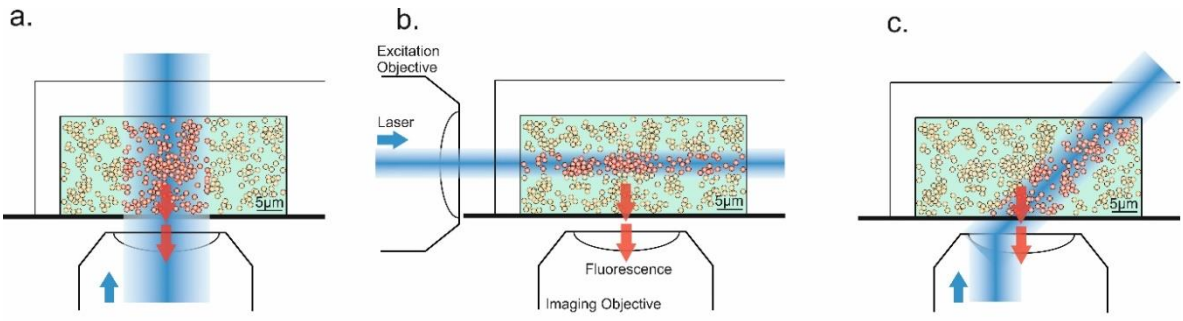

Figure 33 Different configurations for illuminating samples in fluorescence microscopy: a) widefield epifluorescence, b) SPIM, and c) HILO.

inclined and laminated optical sheet microscopy (HILO). These are three design elements that I considered.

In MPE, a laser is focused in the sample and multiple photons are absorbed in a short time window (about 10^{-18} s) to excite the sample [198]. For two photon excitation, each photon requires half the energy and therefore twice the wavelength compared to one photon excitation because the energy E of a photon is related to its wavelength λ by $E \propto 1/\lambda$. Rayleigh scattering, the elastic scattering of light by objects that are smaller than the wavelength (e.g. molecules), has a sensitive $1/\lambda^4$ dependence [199] and is therefore reduced at longer wavelengths. MPE typically uses excitation wavelengths near infrared, resulting in less scattering of the excitation signal in biological tissue and an increased imaging depth [200]. MPE can image deep inside strongly scattering samples like tissue at depths of up to 1.45 mm for two photon absorption [201] and 2.5 mm for three [202]. Background fluorescence and photobleaching outside the focal point are also strongly reduced because multiple photons must be absorbed within a narrow time frame (10^{-18} s) to excite a fluorophore. To achieve this the excitation is highly localised; a high intensity laser is focussed to a point, and the probability of multiple photon absorption is only high at the centre of this point [200]. A drawback of MPE is that it is a slow imaging technique that requires scanning to build up an image, similar to confocal microscopy. This would prevent millisecond imaging of diffusing molecules.

SPIM reduces out of plane fluorescence and photobleaching by only illuminating the focal plane of the sample, typically achieved by illuminating the sample through one objective lens and imaging the sample via another objective lens at a 90 ° angle (Figure 33) and samples can be imaged at greater depths because the illumination is transverse to emission capture. The most common method of SPIM is light sheet microscopy, in which a "light sheet" is formed by focusing a laser through a cylindrical lens to produce a linear focus [203]. The sample or light sheet can be translated to build up a 3D image. Light sheet microscopy has been used to image large samples such as fruit fly [204] and zebrafish embryos [205], but has also been used to track single molecules in tissue from specimens such as *Chironomus tentans* larvae up to a depth of 200 µm [206]. Samples for SPIM are usually mounted in an agarose cylinder, which is suspended between the two objective lenses usually in a specially designed chamber. Biofilms are usually grown for microscopy in microwells or flow cells, so a disadvantage to SPIM is the need to design a specialised sample chamber for growing and imaging biofilms.

HILO illuminates the sample obliquely rather than transversely and allows for mounting the sample on a conventional microscope slide. To achieve this, a laser is directed off-axis through the objective lens and refracts at a large angle to illuminate the sample

(Figure 33) [195]. HILO requires only one objective lens and there is no need to design a special sample mount, however it has a lower signal to noise ratio than SPIM and more limited imaging depth. Nonetheless, HILO still offers an improvement to epifluorescence configurations, and has been used to image single molecules and subcellular features with a 7.6 times improved signal to noise ratio [195].

I chose SPIM as the final design because it reduces background fluorescence and increases imaging depth more than HILO, a significant advantage when imaging strongly scattering samples, and MPE has slower capture rates which prevent millisecond imaging and requires a high cost specialised laser.

8.3.2 Bessel beams create a narrow, collimated beam

To maximise the fluorescence signal, single molecule methods often involve shrinking the diameter of the excitation beam to about 10 µm to give an intensity of a few kW cm^{-2}. Light sheets which are produced by focusing a laser through a cylindrical lens create a beam waist of about 6 µm at the focal point, which diverges on either side [204]. It would be more optimal to image with a narrow, collimated beam, which avoids the divergence at either sides that lowers the intensity of the beam and increases out of plane fluorescence and photobleaching.

Lasers are used for excitation and usually have a Gaussian intensity profile. The intensity I is given by

$$I(r,z) = I(0,z)e^{\frac{-2r^2}{w(z)^2}}, \tag{5}$$

where z is the propagation axis, r is the radial coordinate measured from the beam axis, and $w(z)$ is the beam radius at $1/e^2$ intensity [207]. The intensity profile is bright in the centre where $r = 0$ and falls with distance from the centre (Figure 34). The beam radius is z-dependent, meaning Gaussian beams diffract as they propagate according to the law of beam expansion

$$w(z)^2 = {w_0}^2\left(1 + \frac{\lambda z}{\pi {w_0}^2}\right), \tag{6}$$

where w_0 is the beam waist at $z = 0$ and λ is the wavelength [208]. Therefore, a narrowfield approach with a Gaussian beam would still result in a beam that diverges as it propagates. Gaussian beams also scatter, resulting in a loss of intensity. Since biofilms strongly scatter light, excitation signal will be lost when imaging deep inside a biofilm with a Gaussian beam.

A solution is to image with a Bessel beam instead of a Gaussian beam. They have a bright central core surrounded by lower intensity rings (lobes), with approximately equal energy stored in each lobe [209] (Figure 34). They are non-diffracting beams that propagate along z with an amplitude ψ proportional to the zeroth order Bessel function J_0, and therefore they have an intensity profile I that is proportional to ${J_0}^2$ and is independent of propagation distance [210][211]:

$$\psi(r,\phi,z) = J_0(k_r r)e^{i(k_z z)}, \tag{7}$$

$$I(r,\phi) = {J_0}^2(k_r r). \tag{8}$$

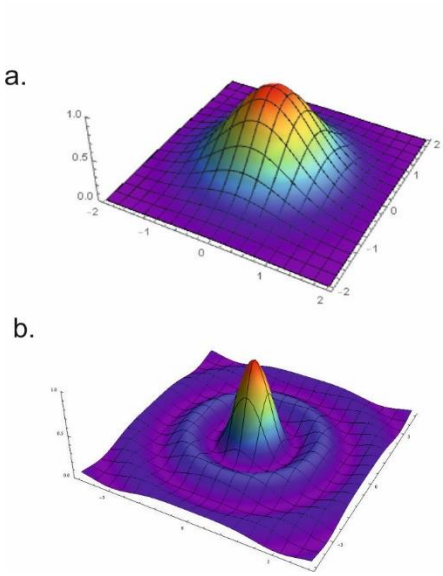

Figure 34 Intensity profiles for a) Gaussian and b) Bessel beams.

r, ϕ, and z are the radial, azimuthal, and longitudinal components in cylindrical polar coordinates, and k_r and k_z are radial and longitudinal wavevectors, related to each other and the wavelength λ by $k = \sqrt{{k_r}^2 + {k_z}^2} = 2\pi/\lambda$. I is independent of z and therefore Bessel beams do not diffract as they propagate. They are also self-reconstructing, which means the beam can reconstruct after scattering and continue to propagate over large distances, an advantage when imaging deep inside scattering samples. This happens because the energy in each lobe is approximately equal, so when the light scatters, the scattered and unscattered parts of the field constructively interfere to reconstruct the beam. Farbach *et al.* (2010) directed Gaussian and Bessel beams through a fluorescing gel containing scattering objects to visualise and compare the paths of the beams. Not only did the Bessel beams reconstruct after scattering, but their intensity dropped by just 5 % compared to 40 % for Gaussian beams [212]. This property makes them ideal for imaging over large distances in biofilms.

Bessel beams have already been applied in SPIM. Purnapatra *et al.* (2012) imaged yeast and reported that the FWHM of the Bessel beam remained constant over large distances and imaged at a depth of 616 µm, compared to 227 µm for confocal imaging [213]. Scanned Bessel beams have also been used in several studies in conjunction with other techniques like two photon excitation to image in living cells with an extended depth of field [214][215][216]. Even though the intensity of the Bessel beam side lobes are low, they can become an issue when scanning the beam to build up a 3D image because they have a cumulative effect on photobleaching and cause out of focus fluorescence which decreases the signal to noise ratio. However, the design here will reduce this problem by imaging with a static beam, with the trade-off of imaging a smaller portion of the sample and not constructing a 3D image.

8.3.3 Objective lens choices for SPIM

The aim was to modify an existing inverted microscope by adding an excitation pathway for SPIM. Therefore, it was important to retain the existing functions of the microscope and consider carefully the choice of objective lenses and how to position them for SPIM. Some other practical considerations were that biofilms are typically grown for microscopy in flow cells or microwells, so the configuration of both objective lenses should accommodate this. Both objective lenses should also be immersed in water. Biological material consists mostly of water, and the mismatch between the refractive index between the objective lens, sample, and air in between causes spherical aberrations which distort the excitation beam and image. Immersing the lens in water removes the mismatch between the lens and air to reduce this.

There are two main designs for mounting objective lenses for SPIM. The first comes from the OpenSPIM project [217], in which two objective lenses are mounted orthogonally in

a specially designed, water filled chamber, and the sample is suspended in a thin agarose cylinder suspended between the lenses. A chamber such as this would not work with samples in flow cells or microwells, but it would be possible to have the excitation objective lens parallel to the sample, and the imaging objective lens perpendicular below the sample in the conventional position. The second design is an inverted SPIM (iSPIM), in which two orthogonal objective lenses are mounted above the sample at a 45 ° angle above it [218]. This allows for mounting the sample on a conventional slide, but requires the construction of a specialised objective lens housing. The objective lenses in iSPIM have long working distances (distance between the lens and sample) and low numerical apertures in order to physically fit the objective lenses without crashing into each other or the sample. Single molecule microscopy requires high numerical aperture objective lenses with values up to 1.4 and above [100][219] to maximise light collection, which typically have short working distances. Water immersion lenses also have shorter working distances than air objective lenses. Even the longest working distance water immersion lens that could be found (3.5 mm working distance) could not tilt at 45 ° without colliding with the sample, and so it was chosen to create a new SPIM configuration with the imaging objective lens below the sample and the excitation objective lens mounted in the horizontal plane. A high numerical aperture water immersion lens was chosen for imaging (Nikon CFI Plan Apochromat VC 60x/1.2W WD 0.27) and a longer working distance water immersion objective lens for excitation (Nikon CFI Plan Apochromat 40x/0.8W WD 3.5).

8.3.4 Lens choices for creating and shaping a Bessel beam

Bessel beams produced in the lab are actually approximations of Bessel beams. A true Bessel beam has an infinite extent and therefore would take an infinite amount of energy to produce, which is not physical. A Gaussian beam can however be shaped to produce a Bessel-Gauss beam, which is possible by several methods. Firstly, an annular mask placed at the back of the objective lens produces a Bessel-Gauss beam at the focus [215], however this method blocks most of the incident light and has a maximum efficiency of about 5 % [220], which could prevent sufficient excitation power for single molecule detection. A second method involves altering the phase of an incoming Gaussian beam with a spatial light modulator to shape the beam [221], which is a useful method for producing single or multiple Bessel-Gauss beams simultaneously, however it incurs a small power loss and requires precise algorithms to manipulate the beam as desired. A third option was chosen, which is to use an axicon to shape the beam. An axicon is a conically shaped lens that shapes a Gaussian beam into a Bessel-Gauss beam by refracting incoming light by an angle β, and the light interferes to produce an approximate Bessel intensity profile along a linear focus (Figure 35a). The beam is approximately diffraction free along the finite linear focus because all rays are at the same angle. Therefore, all transverse planes along this distance look the same regardless of

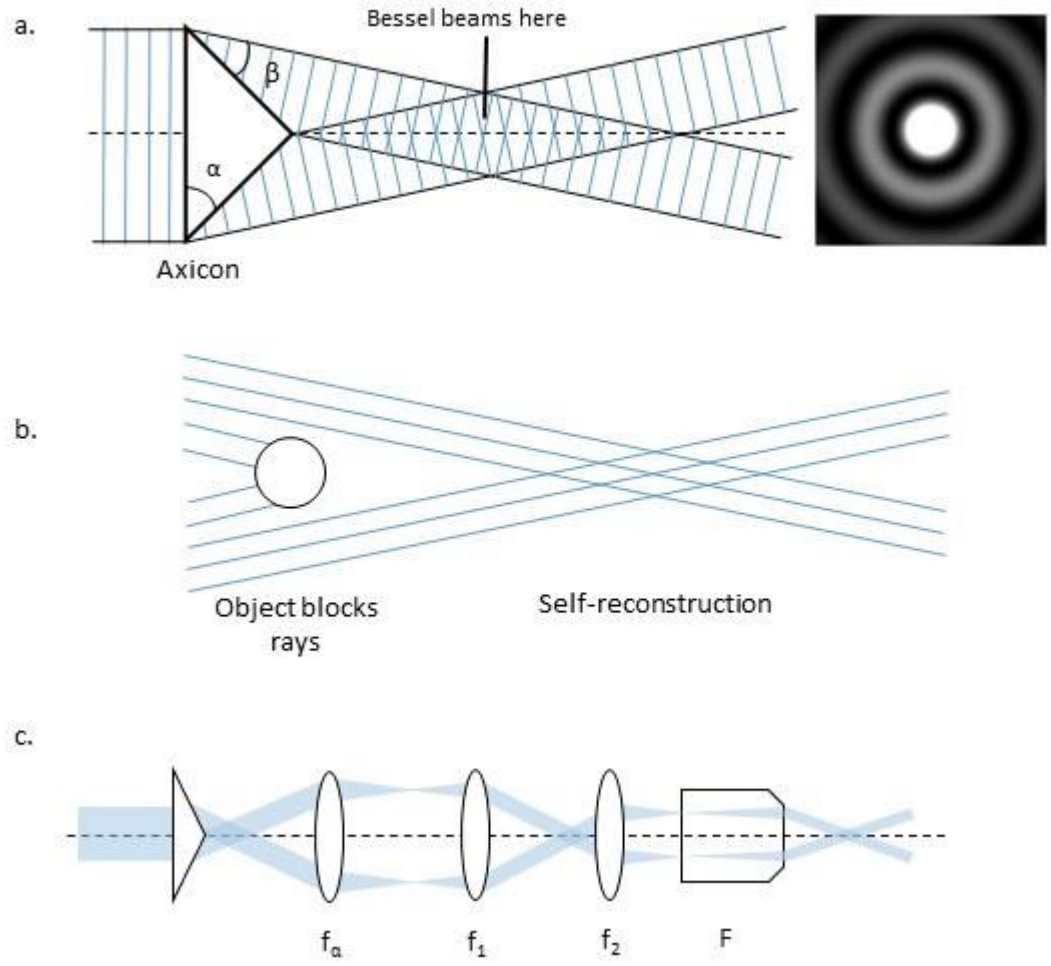

Figure 35 a) Bessel-Gauss beam produced at the focus of an axicon lens, b) Bessel-Gauss beam self-reconstruction after an object blocked it, and c) shaping of a Bessel-Gauss beam with lenses and an objective lens.

position along the axis [222]. These Bessel-Gauss beams are also self-reconstructing over the linear focus because all rays are at the same angle (Figure 35b).

After the linear focus, the beam profile produced by the axicon becomes an annulus with increasing radius with distance, which can be shaped by additional lenses to manipulate the radius and length of Bessel-Gauss beam produced at the focus (Figure 35b). The intensity distribution I of a Bessel-Gauss beam produced by an axicon is

$$I = I_0 \frac{4\pi^2\beta^2 z}{\lambda} e^{-\frac{2\beta^2 z^2}{{w_0}^2}} {J_0}^2\left(\frac{2\pi r\beta}{\lambda}\right), \quad (9)$$

where I_0 is the intensity at the centre of the incident Gaussian beam, λ is the wavelength, w_0 the initial Gaussian beam width, z and r are the transverse and radial coordinates, and β is the deviation angle of the axicon, related to the axicon angle α and axicon refractive index n by $\beta = sin^{-1}(nsin\alpha) - \alpha$ [223][224]. From this equation, the radius r_p of the primary Bessel-Gauss beam produced immediately after the axicon and primary depth of field L_p are [223]

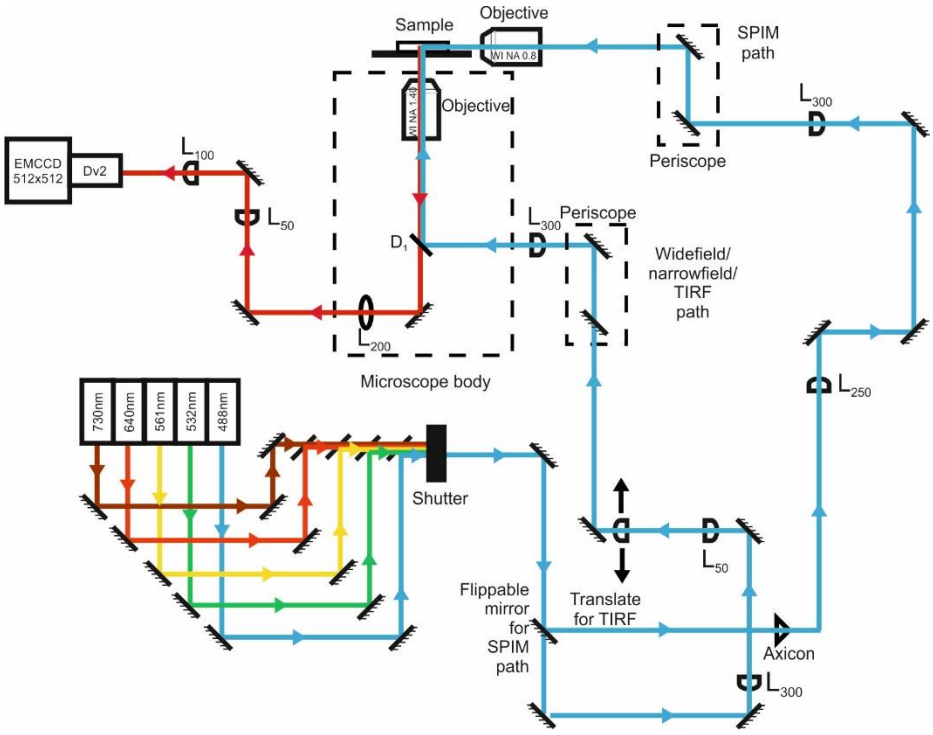

Figure 36 Overall layout for Bessel beam SPIM microscope. The SPIM pathway has a separate excitation pathway to the existing TIRF/widefield pathway and can be selected via a flippable mirror. Lens focal lengths are indicated next to diagrams of lenses and are given in mm.

$$r_p = \frac{2.4048\lambda}{2\pi\beta}, \tag{10}$$

$$L_p = \frac{0.8w_0}{\beta}. \tag{11}$$

When the beam is magnified m times by lenses with focal lengths f such as the configuration inFigure 35c, the resulting secondary radius and depth of field are [223]

$$r_s = \frac{2.4048\lambda}{2\pi\beta}\left(\frac{Ff_1}{f_\alpha f_2}\right), \tag{12}$$

$$L_s = \frac{0.8w_0}{\beta}\left(\frac{Ff_1}{f_\alpha f_2}\right)^2. \tag{13}$$

The equations for r_p, L_p, r_s, and L_s are provided in [223] without derivations. Therefore I have provided derivations in Appendix 4.

These equations were used to predict which values of axicon angle α and focal lengths f would produce a Bessel-Gauss beam with a central lobe of diameter 10 µm at a wavelength of 500 nm and axicon refractive index 1.52. I wrote an algorithm in C that used nested for loops to cycle through possible values for α, f_1, f_2, and f_α, calculating Equation (12) and (13) for each combination, and only outputted combinations with r_s close to 5 µm. F was assumed to equal 2 mm. The code indicated that α = 1 ° was the most versatile and an

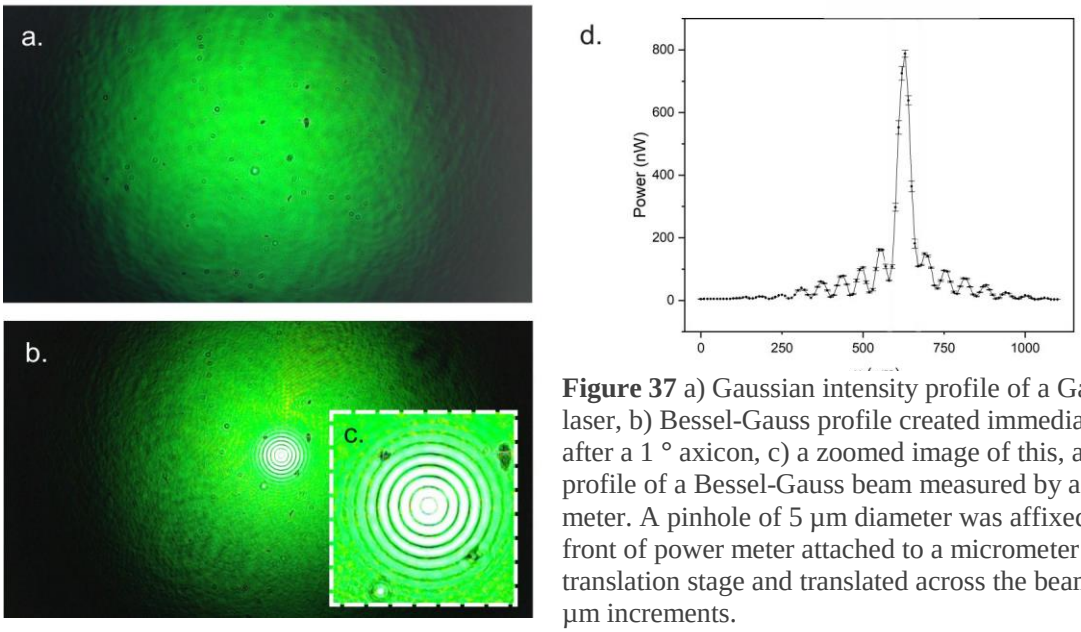

Figure 37 a) Gaussian intensity profile of a Gaussian laser, b) Bessel-Gauss profile created immediately after a 1 ° axicon, c) a zoomed image of this, and d) profile of a Bessel-Gauss beam measured by a power meter. A pinhole of 5 µm diameter was affixed to the front of power meter attached to a micrometer 1D translation stage and translated across the beam in 10 µm increments.

axicon with that angle was bought from Thorlabs (AX251-A). A low angle axicon such as this has the added advantage that it reduces unwanted diffraction effects from an imperfect tip, as it is not possible to manufacture a point that is infinitely sharp. The focal lengths for the other lenses were chosen and the final microscope design drawn by adding a SPIM pathway to the existing microscope layout (Figure 36).

8.4 Microscope construction

8.4.1 Testing the axicon

Images of the Gaussian and Bessel-Gauss beam profiles were taken using a webcam (Logitech HD Pro Webcam C920) to characterise whether the theoretical equations for the Bessel-Gauss beam radius matched experimental measurements (Figure 37). Two ND 1.2 filters and one ND 2 filter were used to attenuate the beam intensity so as not to saturate the camera, but the Bessel-Gauss beam still caused saturation, so no measurements were taken from these images. Instead, power measurements were taken across the x-axis of the beam profile produced by the axicon and followed by 2 x magnification. The laser (Fianium SC400-6) had a wavelength of 500 nm at 48 % power and was attenuated by 2 x ND 1.2 filters. A 5 µm pinhole was affixed to the power meter attached to a micrometer translation stage, which was then translated across the profile of the beam in 10 µm increments and the profile plotted (Figure 37d). The diameter of the central lobe was measured to be approximately 88.6 ± 3.9 µm and the theoretical value was 84.3 µm. While the theoretical value falls slightly outside the error range of the measured value, the value is still very similar. Discrepancies between the two values arose because this was a rough measurement and calculation. The minima of the Bessel-Gauss profile did not reach zero (Figure 37d) when they should have done. It is likely that the incoming Gaussian beam was not incident precisely on the centre of the axicon, and a finer control over the axicon illumination could be achieved by mounting the axicon on an XY translation mount such as CXY1, Thorlabs. There

appeared to be some background light that was not focussed to a Bessel-Gauss profile (Figure 37b) which prevented the minima reaching zero and affected the measured diameter. Discrepancies between theoretical and experimental measurements will also arise due to assumptions made in the theoretical calculations, such as omitting any diffraction of the annulus of light after passing through the axicon, and approximations in the calculations such as the small angle approximation. With these in mind, it is sufficient to use the equations to estimate the final size of the Bessel-Gauss beam and the optics needed to provide the final size, but it is important to experimentally verify it afterwards. The axicon should be mounted in an XY translation mount so that the centre is illuminated and the beam profile is not distorted.

8.4.2 Sample and objective lens mounts

I designed a custom sample mount in AutoCAD and 3D printed in order to accommodate for the space requirements for the orthogonal objective lens setup (Figure 38a). The sample mount could be screwed into the place where the old sample mount was, on top of an XYZ nanostage which allows the sample to be translated in all dimensions. The imaging objective lens was raised using an extender and the excitation objective lens mounted securely in a cage mount with a periscope that directed the laser beam to the sample plane. The excitation objective lens was also mounted in an XY translation mount in order to make small adjustments to the position of the beam incident on the back aperture if required.

Both objective lenses should be immersed in water. The initial idea was to build a chamber whereby both objective lenses and the sample were immersed in water, with O-rings used to provide a leak proof seal between the objective lenses and the chamber. However, this design was discarded because it would prevent translating the sample whilst keeping the seal intact. It was not possible to simply put a drop of water between the excitation objective lens and sample because it would quickly slip away, so it was chosen to use an immersion oil with a refractive index similar to that of water (Immersol W, Zeiss, n = 1.334). The oil is more viscous, so it can be suspended between the lens and sample more easily.

8.4.3 Flow cell system

A flow cell was designed for use with this microscope setup. The sample and excitation objective lens needed to be close together so that the laser could be focused within the sample, so the flow cell needed to be at the end of a microscope cover glass, rather than in the middle like commercially available ones are (Figure 38b). Polydimethylsiloxane (PDMS) is a silicone commonly used to manufacture such devices, which have been used for SPIM [225][226]. PDMS is a suitable material to image through because it is optically transparent, has low autofluorescence [227], and can be moulded with nm precision [228]. To make PDMS flow cells, liquid silicone elastomer was mixed with a curing agent at a 1:10 ratio and poured over a mould that formed the shape of the channels, and baked at 180 ° for 1 – 2 hours to set. The PDMS was removed from the mould and cut into shape with a scalpel, and bonded to a plasma cleaned cover slip. Jose Juan Colas (University of York) kindly helped to make a mould from SU8 on silicon and supervised me while I made the first PDMS flow cell. Because the excitation beam passes through the side of the flow cell, this side must be smooth, otherwise the laser will scatter and power will be lost. Cutting the PDMS with a scalpel does not create a smooth surface, so silicone walls were added to the mould and the

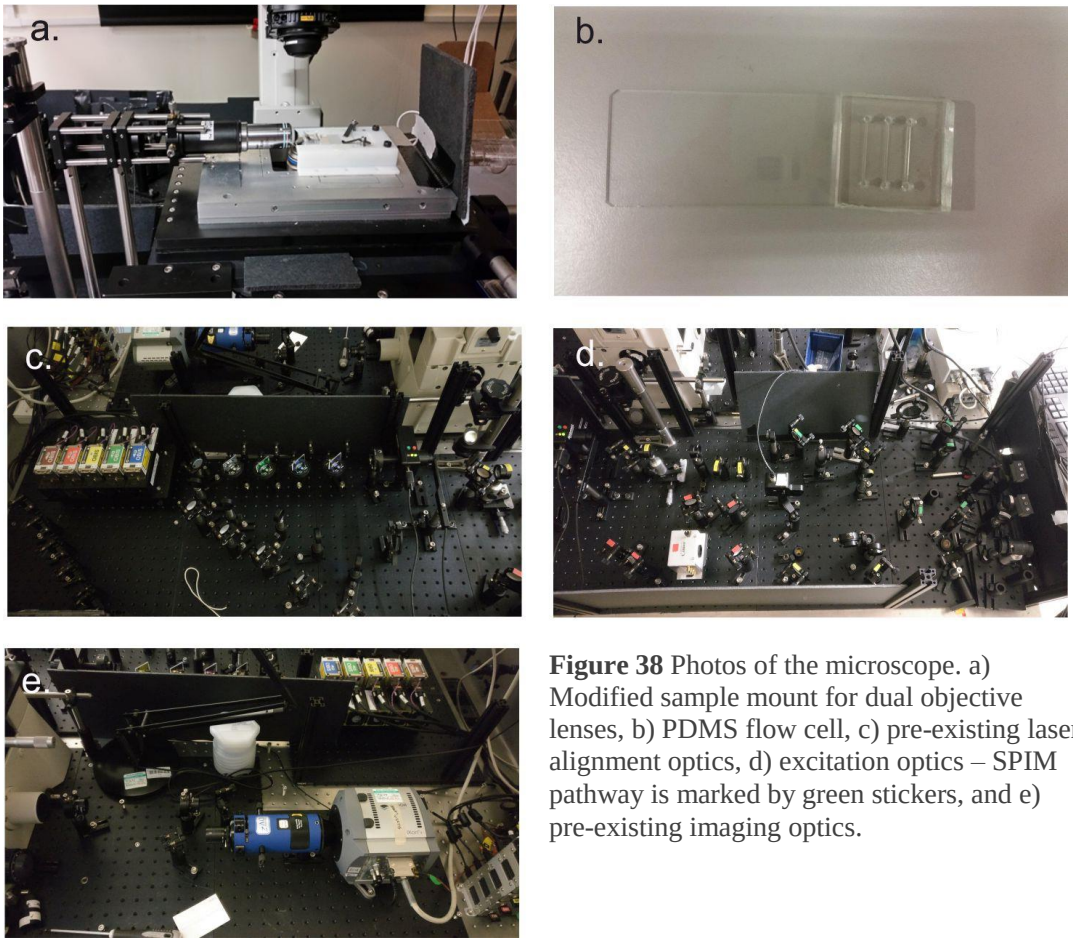

Figure 38 Photos of the microscope. a) Modified sample mount for dual objective lenses, b) PDMS flow cell, c) pre-existing laser alignment optics, d) excitation optics – SPIM pathway is marked by green stickers, and e) pre-existing imaging optics.

PDMS peeled away rather than cutting it. The flow cell could be connected to 23 G needle syringes mounted on a syringe pump (Camtech SPM100) via silicone tubing (Tygon S-54-HL).

It is unlikely that the walls of these flow cells are perfectly perpendicular to the surface, which will result in the laser refracting through the PDMS at an angle, and the excitation beam moving off-camera. To correct for this, the excitation objective lens was mounted on an XY translator, however, perhaps a more reliable sample chamber should be considered in the future. Then a similar chamber for biofilm growth under static conditions could be designed as well.

8.5 Summary of microscope development and future considerations

The main design features for this microscope are Bessel beam excitation combined with SPIM illumination. Bessel beams do not diffract and self-reconstruct after scattering, which makes them ideal for imaging strongly scattering samples like biofilms. SPIM reduces out of plane fluorescence and increases the signal to noise ratio. If the Bessel beam central lobe has a diameter of about 10 µm, this should enable powers of a few kW cm^{-2}, which are sufficient for single molecule detection. The lenses for producing a beam of this diameter have already been selected, including an axicon to create a Bessel-Gauss beam and two objective lenses for orthogonal excitation and imaging. A custom sample mount was made to accommodate the SPIM configuration, whilst still allowing the option of epifluorescence imaging using just

one objective lens below the sample. A SPIM excitation pathway was built into an existing bespoke single molecule microscope, and the imaging optics left unchanged (Figure 36 and Figure 38). The laser now needs aligning through the optics before the system can be tested; however there are some areas of the design that might need further work in the future.

Firstly, there is some light in the background of the image of the Bessel-Gauss beam produced by the axicon (Figure 37a). This would contribute to background fluorescence and photobleaching when imaging a sample. It appears as though a portion of the laser beam did not undergo interference to produce the Bessel-Gauss profile, and so perhaps not all rays were in phase when refracted through the axicon. Maybe this problem arose because the incoming laser beam was not positioned centrally on the axicon, or if there was an issue with the alignment of optics upstream of the axicon that meant the incoming laser beam was not collimated. The alignment should be double checked to see if the problem persists. The side lobes of the Bessel-Gauss beam will also contribute to background fluorescence and photobleaching, however since Bessel beams have already been successfully used in SPIM to track single molecules [213], presumably this does not inhibit single molecule detection. It is a sacrifice that is made in exchange for an improved imaging depth.

The flow cell system needs further development too. The current design has 3 lanes which are some mm away from the edge of the PDMS. The Bessel-Gauss beam is not long enough to span the entire flow cell, and there would be refraction and scattering effects as the beam passes through each subsequent lane. Therefore, the cell should have just one lane, placed closer to the PDMS edge. An alternative could be to grow the sample in a glass capillary tube connected to the syringe pump, however, this would require a complete overhaul of the sample mount design. There is also currently no option for statically grown biofilms in microwells. The easiest solution here could be to rotate the sample in the XY plane by 90 ° and image through the side of commercially available microwells such as the IBIDI µ-Slide 8 wells. It is an advantage to use commercially available microwells because the process of manufacturing homemade microwells could slow down experiments, and there could be inconsistencies between batches of homemade microwells.

Overall, Bessel beam SPIM should enable single molecule detection inside biofilms. The method is perhaps more suited to studying *in vitro* biofilms, which are grown in the lab under artificial conditions in flow cells and microwells, because *in vitro* biofilms are thicker than *in vivo* biofilms, and can be mounted in this microscope with a few tweaks to the design of the sample mount. *In vitro* biofilms may be many hundreds of µm to several mm thick and would benefit from imaging several hundred µm within where current methods cannot reach. *In vivo* biofilms, such as those that form in animal or human infections, tend to be much smaller, generally in clusters of about 5 - 200 µm in diameter and segregated by host material [16], which can be readily imaged by confocal microscopy. However, *in vivo* biofilms on catheters and shunts can grow up to 1.2 mm thick [16], therefore there is potential for applying Bessel beam SPIM specifically for imaging thicker catheter- and shunt-associated biofilms. *In vitro* biofilm models provide essential knowledge into how bacteria produce biofilms, and *in vivo* biofilms teach us how they establish infections and evade treatments or the immune system in a real life environment. The ability to study both biofilm models at the single molecule level would reveal new insights on the molecular interactions and mechanisms that they use to do these things.

9. Conclusions and Outlook

I investigated why *S. aureus* secretes two coagulases, Coa and vWbp, which cause fibrin production in the biofilm extracellular matrix. Fibrin protects *S. aureus* from the host immune system and increases biofilm accumulation on surfaces within the host, such as on implants. It forms a pseudocapsule at cell surfaces surrounded by an extended network of fibers in the wider biofilm matrix. As expected, I demonstrated that Coa is necessary for forming the fibrin pseudocapsule and that it associates to the surface of cells in order to localise fibrin production to the surface. I also demonstrated that vWbp associates to and accelerates the formation of the pseudocapsule, although it cannot form a pseudocapsule on its own. This was contrary to what I expected, as it was previously thought that vWbp just produces the extended fibrin network. However, I did also verify that vWbp and Coa could both produce an extended fibrin network. Therefore, the primary role of Coa is to localise fibrin production to the surface of cells. This provides a first line of defence against immune cells, which has been suggested in the literature as well [41]. Some Coa is secreted into the wider matrix to contribute to forming the extended network. The primary role of vWbp is to cause fibrin production in the extended network, which is a second barrier against immune cells [41], and attaches the biofilm to surfaces within the host like implants or the host extracellular matrix. I observed that both Coa and vWbp could cause the formation of a "fibrin forest" consisting of fibrin fibers extending perpendicular from the biofilm-surface interface, and speculate that Coa and vWbp associate to host proteins, e.g. fibrinogen, or fibronectin in the case of vWbp, to localise fibrin formation close to surfaces. Some vWbp is retained close to the surface of cells in order to accelerate the formation of the pseudocapsule. After the initial colonising bacteria produce a pseudocapsule, they divide within a shared pseudocapsule rather than each producing their own. Therefore, it is advantageous for vWbp to accelerate its formation in order to protect bacteria quickly. By sharing a pseudocapsule, daughter cells share the protection from the immune system and it means that infections can be initiated from only a few adherent bacteria. However, not all bacteria produce a pseudocapsule. Of note, there is a slowly- or non-dividing subpopulation that does not bind fibrin, which might not produce the surface proteins necessary to bind fibrin to their surfaces.

Some unanswered questions about Coa and vWbp remain. The mechanisms that they use to associate to cells to produce the pseudocapsule are unknown. I speculated that Coa associates to cell surfaces via one of *S. aureus* many fibrinogen binding surface proteins, but was unable to pinpoint that interaction to one specific surface protein. Perhaps Coa associates via numerous surface proteins and an appropriate further experiment would be to analyse pseudocapsule formation in a mutant that lacks surface proteins before focussing on which particular proteins are involved. This could be achieved by constructing a mutant lacking Sortase, which would prevent any covalently anchored proteins from attaching to the surface. The mechanism that vWbp associates to the pseudocapsule by is also unknown, and I speculated that it might be via fXIII mediated cross-linking. It is also unknown whether or how Coa and vWbp might interact with host proteins on implant surfaces or in the host extracellular matrix to cause the formation of host surface-attached fibrin. vWbp might play a larger role in directing fibrin formation to host surfaces because it binds a larger number of host proteins than Coa. It is particularly interesting that vWbp binds fibronectin [53], a host

protein that exists in a fibrillar conformation in the host extracellular matrix and on implant surfaces [77]. I wonder whether vWbp therefore associates to this fibrillar conformation of fibronectin.

The question of why some bacteria in *S. aureus* biofilms do not have a pseudocapsule also remains. These bacteria were non- or slowly- dividing and could be distinguished from other bacteria by their bright fluorescence when expressing GFP. I speculated whether these bacteria were antibiotic-tolerant persister cells, but I did not find any evidence that proves this. In fact, a similar proportion of these bacteria appeared to die when treated with vancomycin compared to the dividing population of bacteria, although the sample size of non-dividing bacteria in this experiment was very small. Therefore it is unlikely that these bacteria are persister cells. It appears that they could be cheaters who benefit from the protection of the extended fibrin network without contributing to its formation, and it is unknown whether they have any particular biological role or why they fail to bind fibrin to their surfaces.

My colleagues and I demonstrated that msfGFP is a good candidate for creating fusion proteins that are exported by the Sec pathway in *S. aureus*. msfGFP was exported successfully and folded and fluoresced in the extracellular space when fused to a Sec signal peptide or when fused to Coa. Fluorescence from Coa:msfGFP could be visualised by confocal and single molecule microscopy, unlike our initial Coa:mCherry and vWbp:GFP(-30) fusions. Coa and vWbp could also be visualised with the SNAP and CLIP tags, albeit that there were some issues with non-specific staining in the biofilm matrix. Most extracellular proteins in Gram positive bacteria are exported by the Sec pathway, and *S. aureus* uses many surface associated and secreted proteins to interact with host components and cause infection, such as the large family of MSCRAMMs. Visualising these proteins is a valuable tool for understanding their contributions to biofilm infections, and msfGFP is a good candidate for labelling them with. msfGFP might be a good candidate for tagging secreted proteins in other species too, such as *S. epidermidis*, which also produces a number of surface proteins that interact with the host and promote infections and disease.

I also aimed to investigate the biological role of Embp in *S. epidermidis* biofilms, a giant surface protein that is involved in attachment to fibronectin coated surfaces, increases biofilm accumulation, and increases protection toward the immune system [74][75][76]. My colleagues and I were unsuccessful in generating fusion proteins with which to visualise Embp, which I realised was likely due to poor fusion protein placement. We inserted the fusion after the Embp signal peptide, but realised later that the insertion was in front of a putative cleavage site. Therefore, the fusion protein could have been cleaved off, or its placement could have inhibited export of Embp or inhibited the folding of the fusion protein itself. Without an assay to verify the successful production of Embp, it was difficult to spot this error sooner. However, our results in generating fusion proteins in *S. aureus* were very promising. Embp is directed to the cross wall during cell division, and is exposed on the surface of *S. epidermidis* once the daughter cells split into two. I successfully visualised the SNAP tag when secreted via the same pathway in *S. aureus*, hence, it may be possible to generate a fusion for Embp with proper placement of the fusion. Placing the fusion after the cleavage site is the most probable solution. Visualising Embp would be a valuable tool for studying the biological role of Embp and mechanisms that it uses to promote biofilm

formation and attachment to surfaces, and it would be particularly relevant to study it under *in vivo* like conditions which mimic the environment of the host.

Bibliography

[1] J. W. Costerton, L. Lewandowski, D. E. Caldwell, D. R. Korber, and H. M. Lappin-Scott, “Microbial biofilms,” *Annu. Rev. Microbiol.*, vol. 49, pp. 711–745, 1995, doi: 10.1201/9780203500224.

[2] H. C. Flemming, J. Wingender, U. Szewzyk, P. Steinberg, S. A. Rice, and S. Kjelleberg, “Biofilms: An emergent form of bacterial life,” *Nat. Rev. Microbiol.*, vol. 14, no. 9, pp. 563–575, 2016, doi: 10.1038/nrmicro.2016.94.

[3] H. C. Flemming and J. Wingender, “The biofilm matrix,” *Nat. Rev. Microbiol.*, vol. 8, no. 9, pp. 623–633, 2010, doi: 10.1038/nrmicro2415.

[4] C. D. Taylor, C. O. Wirsen, and F. Gaill, “Rapid microbial production of filamentous sulfur mats at hydrothermal vents,” *Appl. Environ. Microbiol.*, vol. 65, no. 5, pp. 2253–2255, 1999, doi: 10.1128/aem.65.5.2253-2255.1999.

[5] A. L. Reysenbach and S. L. Cady, “Microbiology of ancient and modern hydrothermal systems,” *Trends Microbiol.*, vol. 9, no. 2, pp. 79–86, 2001, doi: 10.1016/S0966-842X(00)01921-1.

[6] M. Storrs-Mabilat, “Study of a Microbial Detection System for Space Applications,” 2001.

[7] D. Or, S. Phutane, and A. Dechesne, “Extracellular Polymeric Substances Affecting Pore-Scale Hydrologic Conditions for Bacterial Activity in Unsaturated Soils,” *Vadose Zo. J.*, vol. 6, no. 2, pp. 298–305, 2007, doi: 10.2136/vzj2006.0080.

[8] S. J. Pamp, M. Gjermansen, H. K. Johansen, and T. Tolker-Nielsen, “Tolerance to the antimicrobial peptide colistin in Pseudomonas aeruginosa biofilms is linked to metabolically active cells, and depends on the pmr and mexAB-oprM genes,” *Mol. Microbiol.*, vol. 68, no. 1, pp. 223–240, 2008, doi: 10.1111/j.1365-2958.2008.06152.x.

[9] B. P. Conlon, S. E. Rowe, and K. Lewis, “Persister Cells in Biofilm Associated Infections,” in *Advances in experimental medicine and biology*, D. Gianfranco, Ed. Springer, 2015, pp. 1–9.

[10] D. Dufour, V. Leung, and C. M. Lévesque, “Bacterial biofilm: structure, function, and antimicrobial resistance,” *Endod. Top.*, vol. 22, no. 1, pp. 2–16, 2010, doi: 10.1111/j.1601-1546.2012.00277.x.

[11] M. Alhede *et al.*, “Phenotypes of non-attached pseudomonas aeruginosa aggregates resemble surface attached biofilm,” *PLoS One*, vol. 6, no. 11, 2011, doi: 10.1371/journal.pone.0027943.

[12] R. M. Donlon, “Biofilms: Microbial life on surfaces,” *Emerg. Infect. Dis.*, vol. 8, no. 9, pp. 881–890, 2002.

[13] L. Hall-Stoodley, J. W. Costerton, and P. Stoodley, “Bacterial biofilms: From the natural environment to infectious diseases,” *Nat. Rev. Microbiol.*, vol. 2, no. 2, pp. 95–108, 2004, doi: 10.1038/nrmicro821.

[14] J. W. Costerton, P. S. Stewart, and E. P. Greenberg, “Bacterial biofilms: A common cause of persistent infections,” *Science*, vol. 284, no. 5418, pp. 1318–1322, 1999, doi: 10.1126/science.284.5418.1318.

[15] M. A. Cataldo, N. Petrosillo, M. Cipriani, R. Cauda, and E. Tacconelli, “Prosthetic joint infection: Recent developments in diagnosis and management,” *J. Infect.*, vol. 61, no. 6, pp. 443–448, 2010, doi: 10.1016/j.jinf.2010.09.033.

[16] T. Bjarnsholt *et al.*, “The in vivo biofilm,” *Trends Microbiol.*, vol. 21, no. 9, pp. 466–474, 2013, doi: 10.1016/j.tim.2013.06.002.

[17] T. Bjarnsholt *et al.*, “Pseudomonas aeruginosa biofilms in the respiratory tract of cystic fibrosis patients,” *Pediatr. Pulmonol.*, vol. 44, no. 6, pp. 547–558, 2009, doi: 10.1002/ppul.21011.
[18] T. B. Rasmussen and M. Givskov, “Quorum-sensing inhibitors as anti-pathogenic drugs,” *Int. J. Med. Microbiol.*, vol. 296, no. 2–3, pp. 149–161, 2006, doi: 10.1016/j.ijmm.2006.02.005.
[19] W. C. Chiang *et al.*, “Extracellular DNA shields against aminoglycosides in Pseudomonas aeruginosa biofilms,” *Antimicrob. Agents Chemother.*, vol. 57, no. 5, pp. 2352–2361, 2013, doi: 10.1128/AAC.00001-13.
[20] K. K. Jefferson, D. A. Goldmann, and G. B. Pier, “Use of confocal microscopy to analyze the rate of vancomycin penetration through Staphylococcus aureus biofilms,” *Antimicrob. Agents Chemother.*, vol. 49, no. 6, pp. 2467–2473, 2005, doi: 10.1128/AAC.49.6.2467-2473.2005.
[21] K. Lewis, “Persister cells, dormancy and infectious disease,” *Nat. Rev. Microbiol.*, vol. 5, no. 1, pp. 48–56, 2007, doi: 10.1038/nrmicro1557.
[22] N. Høiby *et al.*, “ESCMID* guideline for the diagnosis and treatment of biofilm infections 2014,” *Clin. Microbiol. Infect.*, vol. 21, no. S1, pp. S1–S25, 2015, doi: 10.1016/j.cmi.2014.10.024.
[23] A. Oliver, R. Cantón, P. Campo, F. Baquero, and J. Blázquez, “High frequency of hypermutable Pseudomonas aeruginosa in cystic fibrosis lung infection,” *Science*, vol. 288, no. 5469, pp. 1251–1253, 2000, doi: 10.1126/science.288.5469.1251.
[24] D. Campoccia, L. Montanaro, and C. R. Arciola, “The significance of infection related to orthopedic devices and issues of antibiotic resistance,” *Biomaterials*, vol. 27, no. 11, pp. 2331–2339, 2006, doi: 10.1016/j.biomaterials.2005.11.044.
[25] M. Hermann and M. S. Smeltzer, “Clinical significance in humans,” in *Staphylococcus aureus: Genetics and Physiology*, Caister Academic Press, 2016, pp. 23–44.
[26] C. P. Parlet, M. M. Brown, and A. R. Horswill, “Commensal Staphylococci In fl uence Staphylococcus aureus Skin Colonization and Disease,” *Trends Microbiol.*, vol. 27, no. 6, pp. 497–507, 2019, doi: 10.1016/j.tim.2019.01.008.
[27] S. Y. C. Tong, J. S. Davis, E. Eichenberger, T. L. Holland, and V. G. Fowler, “Staphylococcus aureus infections: Epidemiology, pathophysiology, clinical manifestations, and management,” *Clin. Microbiol. Rev.*, vol. 28, no. 3, pp. 603–661, 2015, doi: 10.1128/CMR.00134-14.
[28] Y. Oogai, M. Matsuo, M. Hashimoto, F. Kato, M. Sugai, and H. Komatsuzawa, “Expression of virulence factors by Staphylococcus aureus grown in Serum,” *Appl. Environ. Microbiol.*, vol. 77, no. 22, pp. 8097–8105, 2011, doi: 10.1128/AEM.05316-11.
[29] S. Ravaioli, I. Cangini, and G. Pietrocola, “Scenery of staphylococcus implant infections in orthopedics,” *Future Microbiol.*, vol. 6, no. 11, pp. 1329–1349, 2011.
[30] M. Otto, “Staphylococcal biofilms,” *Microbiol. Spectr.*, vol. 6, no. 4, pp. 3–23, 2018, doi: 10.1128/microbiolspec.GPP3-0023-2018.Staphylococcal.
[31] T. J. Foster, J. A. Geoghegan, V. K. Ganesh, and M. Höök, “Adhesion, invasion and evasion: The many functions of the surface proteins of Staphylococcus aureus,” *Nat. Rev. Microbiol.*, vol. 12, no. 1, pp. 49–62, 2014, doi: 10.1038/nrmicro3161.
[32] D. Molina-manso, A. Ortiz-pérez, M. Manrubia-cobo, E. Gómez-barrena, J. Cordero-ampuero, and J. Esteban, “In vitro susceptibility to antibiotics of staphylococci in biofilms isolated from orthopaedic infections,” *Int. J. Antimicrob. Agents*, vol. 41, no. 6, pp. 521–523, 2013, doi: 10.1016/j.ijantimicag.2013.02.018.

[33] M. Zapotoczna, E. O. Neill, and J. P. O. Gara, “Untangling the Diverse and Redundant Mechanisms of Staphylococcus aureus Biofilm Formation,” *PLoS Pathog.*, pp. 1–6, 2016, doi: 10.1371/journal.ppat.1005671.

[34] A. P. Cardile *et al.*, “Human plasma enhances the expression of Staphylococcal microbial surface components recognizing adhesive matrix molecules promoting biofilm formation and increases antimicrobial tolerance In Vitro,” *BMC Res. Notes*, vol. 7, no. 457, pp. 1–9, 2014.

[35] H. A. Crosby, J. Kwiecinski, A. R. Horswill, J. Roy, and I. City, “Staphylococcus aureus aggregation and coagulation mechanisms, and their function in host-pathogen interactions,” *Adv. Appl. Microbiol.*, vol. 96, pp. 1–41, 2016, doi: 10.1016/bs.aambs.2016.07.018.Staphylococcus.

[36] D. A. C. Stapels *et al.*, “Staphylococcus aureus secretes a unique class of neutrophil serine protease inhibitors,” *Proc. Natl. Acad. Sci. U. S. A.*, vol. 111, no. 36, pp. 13187–13192, 2014, doi: 10.1073/pnas.1407616111.

[37] M. Hussain, K. Becker, C. Von Eiff, J. Schrenzel, G. Peters, and M. Herrmann, “Identification and characterization of a novel 38.5-Kilodalton cell surface protein of Staphylococcus aureus with extended-spectrum binding activity for extracellular matrix and plasma proteins,” *J. Bacteriol.*, vol. 183, no. 23, pp. 6778–6786, 2001, doi: 10.1128/JB.183.23.6778-6786.2001.

[38] Y. P. Ko *et al.*, “Phagocytosis Escape by a Staphylococcus aureus Protein That Connects Complement and Coagulation Proteins at the Bacterial Surface,” *PLoS Pathog.*, vol. 9, no. 12, pp. 1–13, 2013, doi: 10.1371/journal.ppat.1003816.

[39] M. Palma, S. Nozohoor, T. Schennings, A. Heimdahl, and J. I. Flock, “Lack of the extracellular 19-kilodalton fibrinogen-binding protein from Staphylococcus aureus decreases virulence in experimental wound infection,” *Infect. Immun.*, vol. 64, no. 12, pp. 5284–5289, 1996, doi: 10.1128/iai.64.12.5284-5289.1996.

[40] J. Kwiecinski *et al.*, “Staphylokinase control of staphylococcus aureus biofilm formation and detachment through host plasminogen activation,” *J. Infect. Dis.*, vol. 213, no. 1, pp. 139–148, 2016, doi: 10.1093/infdis/jiv360.

[41] C. Guggenberger, C. Wolz, J. A. Morrissey, and J. Heesemann, “Two distinct coagulase-dependent barriers protect Staphylococcus aureus from neutrophils in a three dimensional in vitro infection model,” *PLoS Pathog.*, vol. 8, no. 1, 2012, doi: 10.1371/journal.ppat.1002434.

[42] A. G. Cheng, M. Mcadow, H. K. Kim, T. Bae, and D. M. Missiakas, “Contribution of Coagulases towards Staphylococcus aureus Disease and Protective Immunity,” *PLoS Pathog.*, vol. 6, no. 8, 2010, doi: 10.1371/journal.ppat.1001036.

[43] T. Vanassche *et al.*, “The Role of Staphylothrombin-Mediated Fibrin Deposition in Catheter-Related Staphylococcus aureus Infections,” *J. Infect. Dis.*, vol. 208, no. 1, pp. 92–100, 2013, doi: 10.1093/infdis/jit130.

[44] J. Weisel and L. R. I., “Fibrin Formation, Structure and Properties,” *Subcell. Biochem.*, vol. 82, no. January, pp. 405–456, 2017, doi: 10.1007/978-3-319-49674-0.

[45] M. M. W., “Fibrinogen and fibrin structure and functions,” *J. Thromb. Haemost.*, vol. 3, pp. 1984–1904, 2005.

[46] R. L. C. Adams and R. J. Bird, “Review article : Coagulation cascade and therapeutics update : Relevance to nephrology . Part 1 : Overview of coagulation , thrombophilias and history of anticoagulants,” *Nephrology*, vol. 14, pp. 462–470, 2009, doi: 10.1111/j.1440-1797.2009.01128.x.

[47] R. Friedrich *et al.*, “Staphylocoagulase is a prototype for the mechanism of cofactor-induced zymogen activation,” *Nature*, vol. 425, no. 6957, pp. 535–539, 2003, doi: 10.1038/nature01962.

[48] H. K. Kroh, P. Panizzi, and P. E. Bock, “Von Willebrand factor-binding protein is a hysteretic conformational activator of prothrombin,” *Proc. Natl. Acad. Sci. U. S. A.*, vol. 106, no. 19, pp. 7786–7791, 2009, doi: 10.1073/pnas.0811750106.
[49] M. Peetermans *et al.*, “Plasminogen activation by staphylokinase enhances local spreading of S. aureus in skin infections,” *BMC Microbiol.*, vol. 14, no. 1, pp. 1–12, 2014, doi: 10.1186/s12866-014-0310-7.
[50] L. Thomer *et al.*, “Antibodies against a secreted product of Staphylococcus aureus trigger phagocytic killing,” *J. Exp. Med.*, vol. 213, no. 3, pp. 293–301, 2016, doi: 10.1084/jem.20150074.
[51] L. Thomer, O. Schneewind, and D. Missiakas, “Pathogenesis of Staphylococcus aureus Bloodstream Infections,” *Annu. Rev. Pathol. Mech. Dis.*, vol. 11, pp. 343–364, 2016, doi: 10.1146/annurev-pathol-012615-044351.
[52] J. Bjerketorp, M. Nilsson, Å. Ljungh, J.-I. Flock, K. Jacobsson, and L. Frykberg, “A novel von Willebrand factor binding protein expressed by Staphylococcus aureus,” *Microbiology*, vol. 148, pp. 2037–2044, 2002.
[53] L. Thomer, O. Schneewind, and D. Missiakas, “Multiple ligands of von willebrand factor-binding protein (vWbp) promote Staphylococcus aureus clot formation in human plasma,” *J. Biol. Chem.*, vol. 288, no. 39, pp. 28283–28292, 2013, doi: 10.1074/jbc.M113.493122.
[54] T. Vanassche *et al.*, “Inhibition of staphylothrombin by dabigatran reduces Staphylococcus aureus virulence,” *J. Thromb. Haemost.*, vol. 9, pp. 2436–2446, 2011, doi: 10.1111/j.1538-7836.2011.04529.x.
[55] S. Thomas, W. Liu, S. Arora, V. Ganesh, Y. P. Ko, and M. Höök, “The complex fibrinogen interactions of the staphylococcus aureus coagulases,” *Front. Cell. Infect. Microbiol.*, vol. 9, no. MAR, pp. 1–11, 2019, doi: 10.3389/fcimb.2019.00106.
[56] N. Jørgensen *et al.*, “Streptokinase Treatment Reverses Biofilm-Associated Antibiotic Resistance in Staphylococcus aureus,” *Microorganisms*, vol. 4, no. 3, p. 36, 2016, doi: 10.3390/microorganisms4030036.
[57] S. Hogan, J. P. O’Gara, and E. O’Neill, “Novel treatment of staphylococcus aureus device-related infections using fibrinolytic agents,” *Antimicrob. Agents Chemother.*, vol. 62, no. 2, pp. 1–9, 2018, doi: 10.1128/AAC.02008-17.
[58] D. Missiakas and O. Schneewind, “Staphylococcus aureus vaccines: Deviating from the carol,” *J. Exp. Med.*, vol. 213, no. 9, pp. 1645–1653, 2016, doi: 10.1084/jem.20160569.
[59] J. Kwiecinski *et al.*, “Tissue plasminogen activator coating on implant surfaces reduces Staphylococcus aureus biofilm formation,” *Appl. Environ. Microbiol.*, vol. 82, no. 1, pp. 394–401, 2016, doi: 10.1128/AEM.02803-15.
[60] M. Otto, “Staphylococcus epidermidis – the ‘accidental’ pathogen,” *Nat Rev Microbiol*, vol. 7, no. 8, pp. 555–567, 2009, doi: 10.1038/nrmicro2182.Staphylococcus.
[61] E. A. Grice *et al.*, “Topographical and temporal diversity of the human skin microbiome,” *Science*, vol. 324, no. 5931, pp. 1190–1192, 2009, doi: 10.1126/science.1171700.
[62] S. Naik *et al.*, “Compartmentalized control of skin immunity by resident commensals,” *Science*, vol. 337, no. August, pp. 1115–1120, 2012.
[63] C. R. Schaeffer *et al.*, “Accumulation-Associated Protein Enhances Staphylococcus epidermidis Biofilm Formation under Dynamic Conditions and Is Required for Infection in a Rat Catheter Model,” *Infect. Immun.*, vol. 83, no. 1, pp. 214–226, 2015, doi: 10.1128/IAI.02177-14.

[64] H. Büttner, D. Mack, and H. Rohde, “Structural basis of Staphylococcus epidermidis biofilm formation: Mechanisms and molecular interactions,” *Front. Cell. Infect. Microbiol.*, vol. 5, no. FEB, pp. 1–15, 2015, doi: 10.3389/fcimb.2015.00014.
[65] T. D. Scherr, C. E. Heim, J. M. Morrison, and T. Kielian, “Hiding in plain sight : interplay between staphylococcal biofilms and host immunity,” *Froniters Immunol.*, vol. 5, no. February, pp. 1–7, 2014, doi: 10.3389/fimmu.2014.00037.
[66] H. Rohde *et al.*, “Polysaccharide intercellular adhesin or protein factors in biofilm accumulation of Staphylococcus epidermidis and Staphylococcus aureus isolated from prosthetic hip and knee joint infections $,” *Biomaterials*, vol. 28, pp. 1711–1720, 2007, doi: 10.1016/j.biomaterials.2006.11.046.
[67] B. Hellmark, B. Söderquist, M. Unemo, and Å. Nilsdotter-augustinsson, “Comparison of Staphylococcus epidermidis isolated from prosthetic joint infections and commensal isolates in regard to antibiotic susceptibility , agr type , biofilm production , and epidemiology,” *Int. J. Med. Microbiol.*, vol. 303, no. 1, pp. 32–39, 2013, doi: 10.1016/j.ijmm.2012.11.001.
[68] T. J. Foster, “Surface Proteins of Staphylococcus epidermidis,” *Front. Microbiol.*, vol. 11, no. July, 2020, doi: 10.3389/fmicb.2020.01829.
[69] B. P. Conlon *et al.*, “Role for the A Domain of Unprocessed Accumulation-Associated Protein (Aap) in the Attachment Phase of the Staphylococcus epidermidis Biofilm Phenotype,” *J. Bacteriol.*, vol. 196, no. 24, pp. 4268–4275, 2014, doi: 10.1128/JB.01946-14.
[70] A. E. Paharik, M. Kotasinska, P. Roy, P. D. Fey, A. R. Horswill, and H. Rohde, “The metalloprotease SepA governs processing of accumulation-associated protein and shapes intercellular adhesive surface properties in Staphylococcus epidermidis,” *Mol. Microbiol.*, vol. 103, no. January, pp. 860–874, 2017, doi: 10.1111/mmi.13594.
[71] Z. Qin *et al.*, “Role of autolysin-mediated DNA release in biofilm formation of Staphylococcus epidermidis,” *Microbiology*, vol. 153, pp. 2083–2092, 2007, doi: 10.1099/mic.0.2007/006031-0.
[72] B. Guo, X. Zhao, Y. Shi, D. Zhu, and Y. Zhang, “Pathogenic Implication of a Fibrinogen-Binding Protein of Staphylococcus epidermidis in a Rat Model of Intravascular-Catheter-Associated Infection □,” *Infect. Immun.*, vol. 75, no. 6, pp. 2991–2995, 2007, doi: 10.1128/IAI.01741-06.
[73] L. F. Milles, K. Schulten, H. E. Gaub, and R. C. Bernardi, “Molecular mechanism of extreme mechanostability in a pathogen adhesin,” *Science*, vol. 359, no. 6383, pp. 1527–1533, 2018.
[74] R. J. Williams, B. Henderson, L. J. Sharp, and S. P. Nair, “Identification of a fibronectin-binding protein from Staphylococcus epidermidis,” *Infect. Immun.*, vol. 70, no. 12, pp. 6805–6810, 2002, doi: 10.1128/IAI.70.12.6805-6810.2002.
[75] M. Christner *et al.*, “The giant extracellular matrix-binding protein of Staphylococcus epidermidis mediates biofilm accumulation and attachment to fibronectin,” *Mol. Microbiol.*, vol. 75, no. 1, pp. 187–207, 2010, doi: 10.1111/j.1365-2958.2009.06981.x.
[76] N. N. Schommer, M. Christner, M. Hentschke, K. Ruckdeschel, M. Aepfelbacher, and H. Rohde, “Staphylococcus epidermidis uses distinct mechanisms of biofilm formation to interfere with phagocytosis and activation of mouse macrophage-like cells 774A.1,” *Infect. Immun.*, vol. 79, no. 6, pp. 2267–2276, 2011, doi: 10.1128/IAI.01142-10.
[77] R. Pankov and K. M. Yamada, “Fibronectin at a glance,” *J. Cell Sci.*, vol. 115, no. 20, pp. 3861–3863, 2002, doi: 10.1242/jcs.00059.

[78] P. Speziale, C. R. Arciola, and G. Pietrocola, “Fibronectin and Its Role in Human Infective Diseases,” *Cells*, vol. 8, no. 12, 2019, doi: 10.3390/cells8121516.
[79] J. C. Linnes, H. Ma, and J. D. Bryers, “Giant extracellular matrix binding protein expression in staphylococcus epidermidis is regulated by biofilm formation and osmotic pressure,” *Curr. Microbiol.*, vol. 66, no. 6, pp. 627–633, 2013, doi: 10.1007/s00284-013-0316-7.
[80] J. Weiser *et al.*, “Sub-inhibitory tigecycline concentrations induce extracellular matrix binding protein Embp dependent Staphylococcus epidermidis biofilm formation and immune evasion,” *Int. J. Med. Microbiol.*, vol. 306, no. 6, pp. 471–478, 2016, doi: 10.1016/j.ijmm.2016.05.015.
[81] H. Lam, A. Kesselly, S. Stegalkina, H. Kleanthous, and J. A. Yethon, “Antibodies to PhnD inhibit staphylococcal biofilms,” *Infect. Immun.*, vol. 82, no. 9, pp. 3764–3774, 2014, doi: 10.1128/IAI.02168-14.
[82] M. Loza-Correa *et al.*, “The peptidoglycan and biofilm matrix of Staphylococcus epidermidis undergo structural changes when exposed to human platelets,” *PLoS One*, vol. 14, no. 1, pp. 1–18, 2019, doi: 10.1371/journal.pone.0211132.
[83] S. Schlafer and R. L. Meyer, “Confocal microscopy imaging of the biofilm matrix,” *J. Microbiol. Methods*, vol. 138, pp. 50–59, 2017, doi: 10.1016/j.mimet.2016.03.002.
[84] P. S. Stewart, W. M. Davison, and J. N. Steenbergen, “Daptomycin rapidly penetrates a Staphylococcus epidermidis biofilm,” *Antimicrob. Agents Chemother.*, vol. 53, no. 8, pp. 3505–3507, 2009, doi: 10.1128/AAC.01728-08.
[85] S. J. Pamp, M. Gjermansen, H. K. Johansen, and T. Tolker-Nielsen, “Tolerance to the antimicrobial peptide colistin in Pseudomonas aeruginosa biofilms is linked to metabolically active cells, and depends on the pmr and mexAB-oprM genes,” *Mol. Microbiol.*, vol. 68, no. 1, pp. 223–240, 2008, doi: 10.1111/j.1365-2958.2008.06152.x.
[86] M. Klausen, A. Aaes-Jørgensen, S. Molin, and T. Tolker-Nielsen, “Involvement of bacterial migration in the development of complex multicellular structures in Pseudomonas aeruginosa biofilms,” *Mol. Microbiol.*, vol. 50, no. 1, pp. 61–68, 2003, doi: 10.1046/j.1365-2958.2003.03677.x.
[87] K. Kjærgaard, M. A. Schembri, C. Ramos, S. Molin, and P. Klemm, “Antigen 43 facilitates formation of multispecies biofilms,” *Environ. Microbiol.*, vol. 2, no. 6, pp. 695–702, 2000, doi: 10.1046/j.1462-2920.2000.00152.x.
[88] D. Dussault and P. Hoess, “Noise performance comparison of ICCD with CCD and EMCCD cameras,” *Infrared Syst. Photoelectron. Technol.*, vol. 5563, p. 195, 2004, doi: 10.1117/12.561839.
[89] M. Leake, *Single-Molecule Cellular Biophysics*, 1st ed. Cambridge University Press, 2013.
[90] N. Billinton and A. W. Knight, “Seeing the wood through the trees: A review of techniques for distinguishing green fluorescent protein from endogenous autofluorescence,” *Anal. Biochem.*, vol. 291, no. 2, pp. 175–197, 2001, doi: 10.1006/abio.2000.5006.
[91] S. J. Pamp, C. Sternberg, and T. Tolker-Nielsen, “Insight into the microbial multicellular lifestyle via flow-cell technology and confocal microscopy,” *Cytom. Part A*, vol. 75, no. 2, pp. 90–103, 2009, doi: 10.1002/cyto.a.20685.
[92] J. Icha, M. Weber, J. C. Waters, and C. Norden, “Phototoxicity in live fluorescence microscopy, and how to avoid it,” *BioEssays*, vol. 39, no. 8, pp. 1–15, 2017, doi: 10.1002/bies.201700003.

[93] S. Waldchen, J. Lehmann, T. Klein, S. Van De Linde, and M. Sauer, “Light-induced cell damage in live-cell super-resolution microscopy,” *Sci. Rep.*, vol. 5, pp. 1–12, 2015, doi: 10.1038/srep15348.
[94] V. Berk *et al.*, “Molecular architecture and assembly principles of Vibrio cholerae biofilms,” *Science*, vol. 337, no. 6091, pp. 236–239, 2012, doi: 10.1126/science.1222981.
[95] A. N. Kapanidis, A. Lepore, and M. El Karoui, “Rediscovering Bacteria through Single-Molecule Imaging in Living Cells,” *Biophys. J.*, vol. 115, no. 2, pp. 190–202, 2018, doi: 10.1016/j.bpj.2018.03.028.
[96] M. C. Leake, J. H. Chandler, G. H. Wadhams, F. Bai, R. M. Berry, and J. P. Armitage, “Stoichiometry and turnover in single, functioning membrane protein complexes,” *Nature*, vol. 443, no. 7109, pp. 355–358, 2006, doi: 10.1038/nature05135.
[97] R. Reyes-Lamothe, D. J. Sherratt, and M. C. Leake, “Stoichiometry and architecture of active DNA replication machinery in escherichia coli,” *Science*, vol. 328, no. 5977, pp. 498–501, 2010, doi: 10.1126/science.1185757.
[98] L. Niu and J. Yu, “Investigating intracellular dynamics of FtsZ cytoskeleton with photoactivation single-molecule tracking,” *Biophys. J.*, vol. 95, no. 4, pp. 2009–2016, 2008, doi: 10.1529/biophysj.108.128751.
[99] B. P. English, V. Hauryliuk, A. Sanamrad, S. Tankov, N. H. Dekker, and J. Elf, “Single-molecule investigations of the stringent response machinery in living bacterial cells,” *Proc. Natl. Acad. Sci. U. S. A.*, vol. 108, no. 31, 2011, doi: 10.1073/pnas.1102255108.
[100] S. Shashkova and M. C. Leake, “Single-molecule fluorescence microscopy review: Shedding new light on old problems,” *Biosci. Rep.*, vol. 37, no. 4, pp. 1–19, 2017, doi: 10.1042/BSR20170031.
[101] D. Axelrod, “Cell-substrate contacts illuminated by total internal reflection fluorescence,” *J. Cell Biol.*, vol. 89, no. 1, pp. 141–145, 1981, doi: 10.1083/jcb.89.1.141.
[102] W. Yang and S. M. Musser, “Visualizing single molecules interacting with nuclear pore complexes by narrow-field epifluorescence microscopy,” *Methods*, vol. 39, no. 4, pp. 316–328, 2006, doi: 10.1016/j.ymeth.2006.06.002.
[103] M. Plank, G. H. Wadhams, and M. C. Leake, “Millisecond timescale slimfield imaging and automated quantification of single fluorescent protein molecules for use in probing complex biological processes,” *Integr. Biol.*, vol. 1, no. 10, pp. 602–612, 2009, doi: 10.1039/b907837a.
[104] M. J. Rust, M. Bates, and X. Zhuang, “Sub-diffraction-limit imaging by stochastic optical reconstruction microscopy (STORM),” *Nat. Methods*, vol. 3, no. 10, pp. 793–795, 2006, doi: 10.1038/nmeth929.
[105] E. Betzig *et al.*, “Imaging intracellular fluorescent proteins at nanometer resolution,” *Science*, vol. 313, no. 5793, pp. 1642–1645, 2006, doi: 10.1126/science.1127344.
[106] E. Snapp, “Design and Use of Fluorescent Fusion Proteins in Cell Biology,” *Curr. Protoc. Cell Biol.*, vol. 27, no. 1, pp. 21.4.1-21.4.13, 2005, doi: 10.1002/0471143030.cb2104s27.
[107] S. Hovmöller and T. Zhou, “Why Are Both Ends of the Polypeptide Chain on the Outside of Proteins?,” *Proteins Struct. Funct. Genet.*, vol. 55, no. 2, pp. 219–222, 2004, doi: 10.1002/prot.20011.
[108] X. Chen, J. L. Zaro, and W. C. Shen, “Fusion protein linkers: Property, design and functionality,” *Adv. Drug Deliv. Rev.*, vol. 65, no. 10, pp. 1357–1369, 2013, doi: 10.1016/j.addr.2012.09.039.

[109] M. A. Rizzo, M. W. Davidson, and D. W. Piston, “Fluorescent protein tracking and detection: Fluorescent protein structure and color variants,” *Cold Spring Harb. Protoc.*, vol. 4, no. 12, pp. 1–22, 2009, doi: 10.1101/pdb.top63.
[110] N. Nakashima and K. Miyazaki, “Bacterial cellular engineering by genome editing and gene silencing,” *Int. J. Mol. Sci.*, vol. 15, no. 2, pp. 2773–2793, 2014, doi: 10.3390/ijms15022773.
[111] M. Ormö, A. B. Cubitt, K. Kallio, L. A. Gross, R. Y. Tsein, and S. J. Remington, “Crystal structure of the Aequorea victoria green fluorescent protein,” *Science*, vol. 273, pp. 1392–1395, 1996.
[112] O. Shimomura, F. H. Johnson, and Y. Saiga, “Extraction, purification and properties of aequorin, a bioluminescent,” *J. Cell. Comp. Physiol.*, vol. 59, no. 165, pp. 223–239, 1962, doi: 10.1002/jcp.1030590302.
[113] M. Chalfie, Y. Tu, G. Euskirchen, W. W. Ward, and D. C. Prasher, “Green fluorescent protein as a marker gene expression,” *Science*, vol. 263, no. 5148, pp. 802–805, 1994.
[114] R. Heim and R. Y. Tsien, “Engineering green fluorescent protein for improved brightness, longer wavelengths and fluorescence resonance energy transfer,” *Curr. Biol.*, vol. 6, no. 2, pp. 178–182, 1996, doi: 10.1016/S0960-9822(02)00450-5.
[115] N. C. Shaner, R. E. Campbell, P. A. Steinbach, B. N. G. Giepmans, A. E. Palmer, and R. Y. Tsien, “Improved monomeric red, orange and yellow fluorescent proteins derived from Discosoma sp. red fluorescent protein,” *Nat. Biotechnol.*, vol. 22, no. 12, pp. 1567–1572, 2004, doi: 10.1038/nbt1037.
[116] R. A. G. Cinelli, A. Ferrari, V. Pellegrini, M. Tyagi, M. Giacca, and F. Beltram, “The Enhanced Green Fluorescent Protein as a Tool for the Analysis of Protein Dynamics and Localization: Local Fluorescence Study at the Single-molecule Level,” *Photochem. Photobiol.*, vol. 71, no. 6, p. 771, 2000, doi: 10.1562/0031-8655(2000)071<0771:tegfpa>2.0.co;2.
[117] J. D. Pédelacq, S. Cabantous, T. Tran, T. C. Terwilliger, and G. S. Waldo, “Engineering and characterization of a superfolder green fluorescent protein,” *Nat. Biotechnol.*, vol. 24, no. 1, pp. 79–88, 2006, doi: 10.1038/nbt1172.
[118] E. A. Rodriguez *et al.*, “The Growing and Glowing Toolbox of Fluorescent and Photoactive Proteins,” *Trends Biochem. Sci.*, vol. 42, no. 2, pp. 111–129, 2017, doi: 10.1016/j.tibs.2016.09.010.
[119] A. Keppler, S. Gendreizig, T. Gronemeyer, H. Pick, H. Vogel, and K. Johnsson, “A general method for the covalent labeling of fusion proteins with small molecules in vivo,” *Nat. Biotechnol.*, vol. 21, no. 1, pp. 86–89, 2003, doi: 10.1038/nbt765.
[120] G. V. Los *et al.*, “HaloTag: A novel protein labeling technology for cell imaging and protein analysis,” *ACS Chem. Biol.*, vol. 3, no. 6, pp. 373–382, 2008, doi: 10.1021/cb800025k.
[121] J. Bordeaux *et al.*, “Antibody validation,” *Biotechniques*, vol. 48, no. 3, pp. 197–209, 2010, doi: 10.2144/000113382.
[122] M. Reth, “Matching cellular dimensions with molecular sizes,” *Nat. Immunol.*, vol. 14, no. 8, pp. 765–768, 2013.
[123] D. Landgraf, B. Okumus, P. Chien, T. A. Baker, and J. Paulsson, “Segregation of molecules at cell division reveals native protein localization,” *Nat. Methods*, vol. 9, no. 5, pp. 480–482, 2012, doi: 10.1038/nmeth.1955.
[124] D. E. Aronson, L. M. Costantini, and E. L. Snapp, “Superfolder GFP Is Fluorescent in Oxidizing Environments When Targeted via the Sec Translocon,” *Traffic*, vol. 12, no. 5, pp. 543–548, 2011, doi: 10.1111/j.1600-0854.2011.01168.x.

[125] E. Balleza, J. M. Kim, and P. Cluzel, “Systematic characterization of maturation time of fluorescent proteins in living cells,” *Nat. Methods*, vol. 15, no. 1, pp. 47–51, 2018, doi: 10.1038/nmeth.4509.
[126] H. Miller, Z. Zhou, A. J. M. Wollman, and M. C. Leake, “Superresolution imaging of single DNA molecules using stochastic photoblinking of minor groove and intercalating dyes,” *Methods*, vol. 88, pp. 81–88, 2015, doi: 10.1016/j.ymeth.2015.01.010.
[127] J. Kwiecinski *et al.*, “Staphylokinase promotes the establishment of staphylococcus aureus skin infections while decreasing disease severity,” *J. Infect. Dis.*, vol. 208, no. 6, pp. 990–999, 2013, doi: 10.1093/infdis/jit288.
[128] S. N. A. Qazi, C. E. D. Rees, K. H. Mellits, and P. J. Hill, “Development of gfp vectors for expression in Listeria monocytogenes and other low G+C gram positive bacteria,” *Microb. Ecol.*, vol. 41, no. 4, pp. 301–309, 2001, doi: 10.1007/s002480000091.
[129] M. R. Grosser and A. R. Richardson, “Method for Preparation and Electroporation of S. aureus and S. epidermidis,” in *The Genetic Manipulation of Staphylococci. Methods in Molecular Biology*, J. Bose, Ed. Humana Press, 2014, pp. 51–57.
[130] D. Bradley and G. Roth, “Adaptive Thresholding using the Integral Image,” *J. Graph. Tools*, vol. 12, no. 2, pp. 13–21, 2007, doi: 10.1080/2151237x.2007.10129236.
[131] Nobuyuki Otsu, “A Threshold Selection Method from Gray-Level Histograms,” *IEEE Trans. Syst. Man Cybern*, vol. 9, no. 1, pp. 62–66, 1979.
[132] M. Alhede *et al.*, “Bacterial aggregate size determines phagocytosis efficiency of polymorphonuclear leukocytes,” *Med. Microbiol. Immunol.*, vol. 209, no. 6, pp. 669–680, 2020, doi: 10.1007/s00430-020-00691-1.
[133] J. Roostalu, A. Jõers, H. Luidalepp, N. Kaldalu, and T. Tenson, “Cell division in Escherichia coli cultures monitored at single cell resolution,” *BMC Microbiol.*, vol. 8, pp. 1–14, 2008, doi: 10.1186/1471-2180-8-68.
[134] E. Kussell, R. Kishony, N. Q. Balaban, and S. Leibler, “Bacterial Persistence : A Model of Survival in Changing Environments,” *Genetics*, vol. 169, no. April, pp. 1807–1814, 2005, doi: 10.1534/genetics.104.035352.
[135] Y. P. Ko and M. J. Flick, “Fibrinogen Is at the Interface of Host Defense and Pathogen Virulence in Staphylococcus aureus Infection,” *Semin. Thromb. Hemost.*, vol. 42, no. 4, pp. 408–421, 2016, doi: 10.1055/s-0036-1579635.
[136] T. Schmitz, C. A. Bäuml, and D. Imhof, “Inhibitors of blood coagulation factor XIII,” *Anal. Biochem.*, vol. 605, no. January, p. 113708, 2020, doi: 10.1016/j.ab.2020.113708.
[137] C. Joukhadar, S. Pillai, C. Wennersten, R. C. Moellering, and G. M. Eliopoulos, “Lack of Bactericidal Antagonism or Synergism In Vitro between Oxacillin and Vancomycin against Methicillin-Susceptible Strains of Staphylococcus aureus □,” *Antimicrob. Agents Chemother.*, vol. 54, no. 2, pp. 773–777, 2010, doi: 10.1128/AAC.00348-09.
[138] P. Panizzi, R. Friedrich, P. Fuentes-Prior, W. Bode, and P. E. Bock, “The staphylocoagulase family of zymogen activator and adhesion proteins,” *Cell. Mol. Life Sci.*, vol. 61, no. 22, pp. 2793–2798, 2004, doi: 10.1007/s00018-004-4285-7.
[139] H. K. Kroh, P. Panizzi, and P. E. Bock, “Von Willebrand factor-binding protein is a hysteretic conformational activator of prothrombin,” *Proc. Natl. Acad. Sci. U. S. A.*, vol. 106, no. 19, pp. 7786–7791, 2009, doi: 10.1073/pnas.0811750106.
[140] D. Landgraf, “Quantifying localizations and dynamics in single bacterial cells,” Doctoral dissertation, Harvard University, 2012.

[141] N. Ke, D. Landgraf, J. Paulsson, and M. Berkmen, “Visualization of periplasmic and cytoplasmic proteins with a self-labeling protein tag,” *J. Bacteriol.*, vol. 198, no. 7, pp. 1035–1043, 2016, doi: 10.1128/JB.00864-15.
[142] M. S. Lawrence, K. J. Phillips, and D. R. Liu, “Supercharging Proteins Can Impart Unusual Resilience,” *J. Am. Chem. Soc.*, vol. 129, no. 33, 2007.
[143] C. M. Winterflood and H. Ewers, “Single-molecule localization microscopy using mCherry,” *ChemPhysChem*, vol. 15, no. 16, pp. 3447–3451, 2014, doi: 10.1002/cphc.201402423.
[144] M. Sarvas, C. R. Harwood, S. Bron, and J. M. Van Dijl, “Post-translocational folding of secretory proteins in Gram-positive bacteria,” *Biochim. Biophys. Acta - Mol. Cell Res.*, vol. 1694, no. 1-3 SPEC.ISS., pp. 311–327, 2004, doi: 10.1016/j.bbamcr.2004.04.009.
[145] M. A. Schallenberger, S. Niessen, C. Shao, B. J. Fowler, and F. E. Romesberg, “Type I signal peptidase and protein secretion in Staphylococcus aureus,” *J. Bacteriol.*, vol. 194, no. 10, pp. 2677–2686, 2012, doi: 10.1128/JB.00064-12.
[146] E. M. Merzlyak *et al.*, “Bright monomeric red fluorescent protein with an extended fluorescence lifetime,” *Nat. Methods*, vol. 4, no. 7, pp. 555–557, 2007, doi: 10.1038/nmeth1062.
[147] N. C. Shaner *et al.*, “A bright monomeric green fluorescent protein derived from Branchiostoma lanceolatum,” *Nat. Methods*, vol. 10, no. 5, pp. 407–409, 2013, doi: 10.1038/nmeth.2413.A.
[148] I. Stockmar *et al.*, “Optimization of sample preparation and green color imaging using the mNeonGreen fluorescent protein in bacterial cells for photoactivated localization microscopy,” *Sci. Rep.*, vol. 8, no. 1, pp. 1–11, 2018, doi: 10.1038/s41598-018-28472-0.
[149] J. N. Bach and M. Bramkamp, “Dissecting the molecular properties of prokaryotic flotillins,” *PLoS One*, vol. 10, no. 1, pp. 11–15, 2015, doi: 10.1371/journal.pone.0116750.
[150] A. Gautier *et al.*, “An Engineered Protein Tag for Multiprotein Labeling in Living Cells,” *Chem. Biol.*, vol. 15, no. 2, pp. 128–136, 2008, doi: 10.1016/j.chembiol.2008.01.007.
[151] I. R. Monk, J. J. Tree, B. P. Howden, T. P. Stinear, and T. J. Foster, “Complete bypass of restriction systems for major staphylococcus aureus lineages,” *MBio*, vol. 6, no. 3, pp. 1–12, 2015, doi: 10.1128/mBio.00308-15.
[152] I. R. Monk, I. M. Shah, M. Xu, M. W. Tan, and T. J. Foster, “Transforming the untransformable: Application of direct transformation to manipulate genetically Staphylococcus aureus and Staphylococcus epidermidis,” *MBio*, vol. 3, no. 2, pp. 1–11, 2012, doi: 10.1128/mBio.00277-11.
[153] M. R. Sadykov, “Restriction–Modification Systems as a Barrier for Genetic Manipulation of Staphylococcus aureus,” in *The Genetic Manipulation of Staphylococci. Methods in Molecular Biology*, vol. 1373, J. Bose, Ed. Humana Press, 2014, pp. 9–23.
[154] M. R. Tock and D. T. F. Dryden, “The biology of restriction and anti-restriction,” *Curr. Opin. Microbiol.*, vol. 8, no. 4, pp. 466–472, 2005, doi: 10.1016/j.mib.2005.06.003.
[155] Thermo Fisher Scientific, “Tm calculator.” [Online]. Available: www.thermofisher.com/tmcalculator. [Accessed: 16-Oct-2019].
[156] D. G. Gibson, L. Young, R. Y. Chuang, J. C. Venter, C. A. Hutchison, and H. O. Smith, “Enzymatic assembly of DNA molecules up to several hundred kilobases,” *Nat. Methods*, vol. 6, no. 5, pp. 343–345, 2009, doi: 10.1038/nmeth.1318.

[157] M. McAdow, D. M. Missiakas, and O. Schneewind, “Staphylococcus aureus secretes coagulase and von willebrand factor binding protein to modify the coagulation cascade and establish host infections,” *J. Innate Immun.*, vol. 4, no. 2, pp. 141–148, 2012, doi: 10.1159/000333447.
[158] Y. Zong, T. W. Bice, H. Ton-That, O. Schneewind, and S. V. L. Narayana, “Crystal structures of Staphylococcus aureus Sortase A and its substrate complex,” *J. Biol. Chem.*, vol. 279, no. 30, pp. 31383–31389, 2004, doi: 10.1074/jbc.M401374200.
[159] I. R. Monk, J. J. Tree, B. P. Howden, T. P. Stinear, and T. J. Foster, “Complete bypass of restriction systems for major staphylococcus aureus lineages,” *MBio*, vol. 6, no. 3, pp. 1–12, 2015, doi: 10.1128/mBio.00308-15.
[160] M. Gross, S. E. Cramton, F. Götz, and A. Peschel, “Key role of teichoic acid net charge in Staphylococcus aureus colonization of artificial surfaces,” *Infect. Immun.*, vol. 69, no. 5, pp. 3423–3426, 2001, doi: 10.1128/IAI.69.5.3423-3426.2001.
[161] T. Klein, A. Löschberger, S. Proppert, S. Wolter, S. Van De Linde, and M. Sauer, “Live-cell dSTORM with SNAP-tag fusion proteins,” *Nat. Methods*, vol. 8, no. 1, pp. 7–9, 2011, doi: 10.1038/nmeth0111-7b.
[162] Z. Liu *et al.*, “Super-resolution imaging and tracking of protein-protein interactions in sub-diffraction cellular space,” *Nat. Commun.*, vol. 5, no. 4443, 2014, doi: 10.1038/ncomms5443.
[163] L. Saujet *et al.*, “Genome-Wide Analysis of Cell Type-Specific Gene Transcription during Spore Formation in Clostridium difficile,” *PLoS Genet.*, vol. 9, no. 10, 2013, doi: 10.1371/journal.pgen.1003756.
[164] F. C. Pereira *et al.*, “The Spore Differentiation Pathway in the Enteric Pathogen Clostridium difficile,” *PLoS Genet.*, vol. 9, no. 10, 2013, doi: 10.1371/journal.pgen.1003782.
[165] P. J. Bosch *et al.*, “Evaluation of fluorophores to label SNAP-Tag fused proteins for multicolor single-molecule tracking microscopy in live cells,” *Biophys. J.*, vol. 107, no. 4, pp. 803–814, 2014, doi: 10.1016/j.bpj.2014.06.040.
[166] D. M. Chudakov, M. V. Matz, S. Lukyanov, and K. A. Lukyanov, “Fluorescent proteins and their applications in imaging living cells and tissues,” *Physiol. Rev.*, vol. 90, no. 3, pp. 1103–1163, 2010, doi: 10.1152/physrev.00038.2009.
[167] E. Linton, M. K. Walsh, R. C. Sims, and C. D. Miller, “Translocation of green fluorescent protein by comparative analysis with multiple signal peptides,” *Biotechnol. J.*, vol. 7, no. 5, pp. 667–676, 2012, doi: 10.1002/biot.201100158.
[168] J. D. Thomas, R. A. Daniel, J. Errington, and C. Robinson, “Export of active green fluorescent protein to the periplasm by the twin-arginine translocase (Tat) pathway in Escherichia coli,” *Mol. Microbiol.*, vol. 39, no. 1, pp. 47–53, 2001, doi: 10.1046/j.1365-2958.2001.02253.x.
[169] S. Y. Li, B. Y. Chang, and S. C. Lin, “Coexpression of TorD enhances the transport of GFP via the TAT pathway,” *J. Biotechnol.*, vol. 122, no. 4, pp. 412–421, 2006, doi: 10.1016/j.jbiotec.2005.09.011.
[170] D. Meissner, A. Vollstedt, J. M. Van Dijl, and R. Freudl, “Comparative analysis of twin-arginine (Tat)-dependent protein secretion of a heterologous model protein (GFP) in three different Gram-positive bacteria,” *Appl. Microbiol. Biotechnol.*, vol. 76, no. 3, pp. 633–642, 2007, doi: 10.1007/s00253-007-0934-8.
[171] J. Wiedenmann, F. Oswald, and G. U. Nienhaus, “Fluorescent proteins for live cell imaging: Opportunities, limitations, and challenges,” *IUBMB Life*, vol. 61, no. 11, pp. 1029–1042, 2009, doi: 10.1002/iub.256.
[172] I. Prabudiansyah and A. J. M. Driessen, “The Canonical and Accessory Sec System of Gram-positive Bacteria,” in *Protein and Sugar Export and Assembly in Gram-positive*

Bacteria, F. Bagnoli and R. Rappuoli, Eds. Cham: Springer International Publishing, 2017, pp. 45–67.
[173] E. R. Green and J. Mecsas, "Bacterial Secretion Systems: An Overview," *Microbiol. Spectr.*, vol. 4, no. 1, pp. 1–19, 2016, doi: 10.1128/microbiolspec.vmbf-0012-2015.
[174] E. Papanikou, S. Karamanou, and A. Economou, "Bacterial protein secretion through the translocase nanomachine," *Nat. Rev. Microbiol.*, vol. 5, no. 11, pp. 839–851, 2007, doi: 10.1038/nrmicro1771.
[175] C. Robinson and A. Bolhuis, "Tat-dependent protein targeting in prokaryotes and chloroplasts," *Biochim. Biophys. Acta - Mol. Cell Res.*, vol. 1694, no. 1-3 SPEC.ISS., pp. 135–147, 2004, doi: 10.1016/j.bbamcr.2004.03.010.
[176] L. Biswas *et al.*, "Role of the twin-arginine translocation pathway in Staphylococcus," *J. Bacteriol.*, vol. 191, no. 19, pp. 5921–5929, 2009, doi: 10.1128/JB.00642-09.
[177] M. Müller, "Twin-arginine-specific protein export in Escherichia coli," *Res. Microbiol.*, vol. 156, no. 2, pp. 131–136, 2005, doi: 10.1016/j.resmic.2004.09.016.
[178] B. C. Berks, T. Palmer, and F. Sargent, "Protein targeting by the bacterial twin-arginine translocation (Tat) pathway," *Curr. Opin. Microbiol.*, vol. 8, no. 2, pp. 174–181, 2005, doi: 10.1016/j.mib.2005.02.010.
[179] D. Landgraf, "Quantifying Localizations and Dynamics in Single Bacterial Cells," Harvard University, 2012.
[180] M. J. J. B. Sibbald *et al.*, "Mapping the Pathways to StaphylococcalPathogenesis by Comparative Secretomics," *Microbiol. Mol. Biol. Rev.*, vol. 70, no. 3, pp. 755–788, 2006, doi: 10.1128/mmbr.00008-06.
[181] R. M. Corrigan and T. J. Foster, "An improved tetracycline-inducible expression vector for Staphylococcus aureus," *Plasmid*, vol. 61, no. 2, pp. 126–129, 2009, doi: 10.1016/j.plasmid.2008.10.001.
[182] I. R. Monk, I. M. Shah, and M. Xu, "Transforming the Untransformable : Application of Direct," *MBio*, vol. 3, no. 2, pp. e00277-11, 2012, doi: 10.1128/mBio.00277-11.Editor.
[183] M. A. Schallenberger, S. Niessen, C. Shao, B. J. Fowler, and F. E. Romesberg, "Type I signal peptidase and protein secretion in Staphylococcus aureus," *J. Bacteriol.*, vol. 194, no. 10, pp. 2677–2686, 2012, doi: 10.1128/JB.00064-12.
[184] T. A. Kunkel, "Rapid and efficient site-specific mutagenesis without phenotypic selection," *Proc. Natl. Acad. Sci. U. S. A.*, vol. 82, no. 2, pp. 488–492, 1985, doi: 10.1073/pnas.82.2.488.
[185] V. Vimberg, A. Tats, M. Remm, and T. Tenson, "Translation initiation region sequence preferences in Escherichia coli," *BMC Mol. Biol.*, vol. 8, pp. 1–13, 2007, doi: 10.1186/1471-2199-8-100.
[186] J. R. McLaughlin, C. L. Murray, and J. C. Rabinowitz, "Unique features in the ribosome binding site sequence of the gram-positive Staphylococcus aureus β-lactamase gene," *J. Biol. Chem.*, vol. 256, no. 21, pp. 11283–11291, 1981.
[187] P. Reed *et al.*, "Staphylococcus aureus Survives with a Minimal Peptidoglycan Synthesis Machine but Sacrifices Virulence and Antibiotic Resistance," *PLoS Pathog.*, vol. 11, no. 5, pp. 1–19, 2015, doi: 10.1371/journal.ppat.1004891.
[188] I. Llorente-Garcia *et al.*, "This is a repository copy of Single-molecule in vivo imaging of bacterial respiratory complexes indicates delocalized oxidative phosphorylation," *Biochim. Biophys. Acta. Bioenerg.*, vol. 1837, pp. 811–824, 2014.
[189] O. Scholz, P. Schubert, M. Kintrup, and W. Hillen, "Tet repressor induction without Mg2+," *Biochemistry*, vol. 39, no. 35, pp. 10914–10920, 2000, doi: 10.1021/bi001018p.

[190] H. Büttner *et al.*, “A Giant Extracellular Matrix Binding Protein of Staphylococcus epidermidis Binds Surface-Immobilized Fibronectin via a Novel Mechanism,” *Am. Soc. Microbiol.*, vol. 11, no. 5, pp. 1–19, 2020.
[191] A. G. Cheng, D. Missiakas, and O. Schneewind, “The giant protein ebh is a determinant of Staphylococcus aureus cell size and complement resistance,” *J. Bacteriol.*, vol. 196, no. 5, pp. 971–981, 2014, doi: 10.1128/JB.01366-13.
[192] P. Giesbrecht, T. Kersten, H. Maidhof, and J. Wecke, “Staphylococcal Cell Wall: Morphogenesis and Fatal Variations in the Presence of Penicillin,” *Microbiol. Mol. Biol. Rev.*, vol. 62, no. 4, pp. 1371–1414, 1998, doi: 10.1128/mmbr.62.4.1371-1414.1998.
[193] A. DeDent, T. Bae, D. M. Missiakas, and O. Schneewind, “Signal peptides direct surface proteins to two distinct envelope locations of Staphylococcus aureus,” *EMBO J.*, vol. 27, no. 20, pp. 2656–2668, 2008, doi: 10.1038/emboj.2008.185.
[194] S. B. Lassen, H. B. Lomholt, and H. Brüggemann, “Complete Genome Sequence of a Staphylococcus epidermidis Strain with Exceptional Antimicrobial Activity,” *Am. Soc. Microbiol.*, vol. 5, no. 10, pp. 4–5, 2017.
[195] M. Tokunaga, N. Imamoto, and K. Sakata-sogawa, “Highly inclined thin illumination enables clear single-molecule imaging in cells,” *Nat. Methods*, vol. 5, no. 2, pp. 159–161, 2008, doi: 10.1038/NMETH.1171.
[196] F. Belinky, I. B. Rogozin, and E. V. Koonin, “Selection on start codons in prokaryotes and potential compensatory nucleotide substitutions,” *Sci. Rep.*, vol. 7, no. 1, pp. 1–10, 2017, doi: 10.1038/s41598-017-12619-6.
[197] W. Yu, D. Missiakas, and O. Schneewind, “Septal secretion of protein a in staphylococcus aureus requires seca and lipoteichoic acid synthesis,” *Elife*, vol. 7, pp. 1–27, 2018, doi: 10.7554/eLife.34092.001.
[198] W. Denk, J. H. Strickler, and W. W. Webb, “Two-photon laser scanning fluorescence microscopy,” *Science*, vol. 248, no. 4951, pp. 73–76, 1990, doi: 10.1126/science.2321027.
[199] E. Hecht, *Optics*, 4th ed. Addison Wesley Longman Inc., 2002.
[200] R. K. P. Benninger and D. W. Piston, “Two-photon excitation microscopy the study of living cells and tissues,” *Curr. Protoc. Cell Biol.*, vol. 59, no. 1, pp. 1–36, 2013, doi: 10.1002/0471143030.cb0411s59.
[201] D. R. Miller *et al.*, “In vivo multiphoton imaging of a diverse array of fluorophores to investigate deep neurovascular structure,” *Biomed. Opt. Express*, vol. 8, no. 7, p. 3470, 2017, doi: 10.1364/boe.8.003470.
[202] N. G. Horton *et al.*, “In vivo three-photon microscopy of subcortical structures within an intact mouse brain,” *Nat. Photonics*, vol. 7, no. 3, pp. 205–209, 2013, doi: 10.1038/nphoton.2012.336.
[203] A. H. Voie, D. H. Burns, and F. A. Spelman, “Orthogonal-plane fluorescence optical sectioning : three- dimensional imaging of macroscopic biological specimens,” vol. 170, no. December 1992, pp. 229–236, 1993.
[204] J. Huisken, J. Swoger, F. Del Bene, J. Wittbrodt, and E. H. K. Stelzer, “Optical Sectioning Deep Inside Live Embryos by Selective Plane Illumination Microscopy,” *Science*, vol. 305, no. 5686, pp. 1007–1010, 2004.
[205] P. J. Keller, A. D. Schmidt, J. Wittbrodt, and E. H. K. Stelzer, “Reconstruction of Zebrafish Early Embryonic Development by Scanned Light Sheet Microscopy,” *Science*, vol. 322, no. November, pp. 1065–1070, 2008.
[206] G. Ritter, R. Veith, A. Veenendaal, J. P. Siebrasse, and U. Kubitscheck, “Light Sheet Microscopy for Single Molecule Tracking in Living Tissue,” *PLoS One*, vol. 5, no. 7, pp. 1–9, 2010, doi: 10.1371/journal.pone.0011639.

[207] E. D. Hirleman and W. H. Stevenson, “Intensity distribution properties of a Gaussian laser beam focus,” *Appl. Opt.*, vol. 17, no. 21, pp. 3496–3499, 1978.
[208] S. A. Self, “Focusing of spherical Gaussian beams,” *Appl. Opt.*, vol. 22, no. 5, pp. 658–661, 1983.
[209] J. Durnin, “Exact solutions for nondiffracting beams. I . The scalar theory,” *Opt. Soc. Am.*, vol. 4, no. 4, pp. 651–654, 1987.
[210] J. Durnin, J. H. Eberly, and J. J. Miceli, “Comparison of Bessel and Gaussian beams,” *Opt. Lett.*, vol. 13, no. 2, p. 79, 1988, doi: 10.1364/ol.13.000079.
[211] R. Dharmavarapu, S. Bhattacharya, and S. Juodkazis, “Diffractive optics for axial intensity shaping of Bessel beams,” *J. Opt. (United Kingdom)*, vol. 20, no. 8, 2018, doi: 10.1088/2040-8986/aad155.
[212] F. O. Fahrbach, P. Simon, and A. Rohrbach, “Microscopy with self-reconstructing beams,” *Nat. Photonics*, vol. 4, no. 11, pp. 780–785, 2010, doi: 10.1038/nphoton.2010.204.
[213] S. B. Purnapatra, S. Bera, and P. P. Mondal, “Spatial Filter based bessel-like beam for improved penetration depth imaging in fluorescence microscopy,” *Sci. Rep.*, vol. 2, pp. 1–11, 2012, doi: 10.1038/srep00692.
[214] G. Thériault, M. Cottet, A. Castonguay, N. McCarthy, and Y. De Koninck, “Extended two-photon microscopy in live samples with Bessel beams: Steadier focus, faster volume scans, and simpler stereoscopic imaging,” *Front. Cell. Neurosci.*, vol. 8, pp. 1–11, 2014, doi: 10.3389/fncel.2014.00139.
[215] T. A. Planchon *et al.*, “Rapid three-dimensional isotropic imaging of living cells using Bessel beam plane illumination,” *Nat. Methods*, vol. 8, no. 5, pp. 417–423, 2011, doi: 10.1038/nmeth.1586.
[216] L. Gao, L. Shao, B. C. Chen, and E. Betzig, “3D live fluorescence imaging of cellular dynamics using Bessel beam plane illumination microscopy,” *Nat. Protoc.*, vol. 9, no. 5, pp. 1083–1101, 2014, doi: 10.1038/nprot.2014.087.
[217] P. G. Pitrone *et al.*, “OpenSPIM : an open-access light-sheet microscopy platform a OpenSpinMicroscopy : an open-source integrated microscopy platform,” *Nat. Methods*, vol. 10, no. 7, pp. 598–599, 2013, doi: 10.1038/nmeth.2507.
[218] Y. Wu *et al.*, “Inverted selective plane illumination microscopy (i SPIM) enables coupled cell identity lineaging and neurodevelopmental imaging in Caenorhabditis elegans,” *Proc. Natl. Acad. Sci. U. S. A.*, vol. 108, no. 43, pp. 17708–17713, 2011, doi: 10.1073/pnas.1108494108/-/DCSupplemental.www.pnas.org/cgi/doi/10.1073/pnas.1108494108.
[219] A. J. M. Wollman, S. Shashkova, E. G. Hedlund, R. Friemann, S. Hohmann, and M. C. Leake, “Transcription factor clusters regulate genes in eukaryotic cells,” *Elife*, vol. 6, pp. 1–36, 2017, doi: 10.7554/eLife.27451.
[220] T. Čižmár and K. Dholakia, “Tunable Bessel light modes: engineering the axial propagation,” *Opt. Express*, vol. 17, no. 18, p. 15558, 2009, doi: 10.1364/oe.17.015558.
[221] R. Bowman, N. Muller, X. Zambrana-Puyalto, O. Jedrkiewicz, P. Di Trapani, and M. J. Padgett, “Efficient generation of Bessel beam arrays by means of an SLM,” *Eur. Phys. J. Spec. Top.*, vol. 199, no. 1, pp. 159–166, 2011, doi: 10.1140/epjst/e2011-01511-3.
[222] D. S. Simon, “Bessel beams, self-healing, and diffraction-free propagation,” in *A Guided Tour of Light Beams: From lasers to optical knots*, Morgan & Claypool Publishers, 2016.

[223] G. Thériault, Y. De Koninck, and N. McCarthy, “Extended depth of field microscopy for rapid volumetric two-photon imaging,” *Opt. Express*, vol. 21, no. 8, p. 10095, 2013, doi: 10.1364/oe.21.010095.
[224] A. T. Friberg, “Stationary-phase analysis of generalized axicons,” *J. Opt. Soc. Am. A*, vol. 13, no. 4, p. 743, 1996, doi: 10.1364/josaa.13.000743.
[225] H. Deschout *et al.*, “On-chip light sheet illumination enables diagnostic size and concentration measurements of membrane vesicles in biofluids,” *Nanoscale*, vol. 6, no. 3, pp. 1741–1747, 2014, doi: 10.1039/c3nr04432g.
[226] R. Regmi, K. Mohan, and P. P. Mondal, “MRT Letter : Light Sheet Based Imaging Flow Cytometry on a Microfluidic Platform,” *Microsc. Res. Tech.*, vol. 1107, no. July, pp. 1101–1107, 2013, doi: 10.1002/jemt.22296.
[227] A. Piruska *et al.*, “The autofluorescence of plastic materials and chips measured under laser irradiation,” *Lab Chip*, vol. 5, no. 12, pp. 1348–1354, 2005, doi: 10.1039/b508288a.
[228] F. Hua *et al.*, “Polymer Imprint Lithography with Molecular-Scale Resolution,” *Nano Lett.*, vol. 4, no. 12, pp. 2467–2471, 2004.

Appendix 1. Coa:SNAP and vWbp:CLIP sequences

Appendix 1.1 Coa:SNAP sequence

GTGAAATATAGAGATGCTGGTACAGGTATCCGTGAATACAACGATGGAACATTTGGATATGAAGCGAGACCAAGATTCAACAAGCCAA
GTGAAACAAATGCATACAACGTAACGACAAATCAAGATGGCACAGTATCATACGGAGCTCGCCCAACACAAAACAA**GCCAAGTGAAAC**
AAACGCATATAACGTAACAACACATGCAAATGGTCAAGTATCATACGGTGCTCGCCCAACACAAAACAAGCCAAGCAAAACAAATGCAT
ACAACGTAACAACACATGCAAATGGTCAAGTATCATATGGCGCTCGCCCGACACAAAAAAAGCCAAGCAAAACAAATGCATATAACGTA
ACAACACATGCAAATGGTCAAGTATCATACGGAGCTCGCCCGACATACAAGAAGCCAAGCGAAACAAATGCATACAACGTAACAACAC
ATGCAAATGGTCAAGTATCATATGGCGCTCGCCCGACACAAAAAAAGCCAAGCGAAACAAACGCATATAACGTAACAACACATGCAGA
TGGTACTGCGACATATGGGCCTAGAGTAACAAAATCAGGTGGTGGAGGAGATAAAGATTGTGAAATGAAACGTACAACATTAGATTC
ACCATTAGGTAAATTAGAATTATCAGGTTGTGAACAAGGTTTACATCGTATTATTTTTTTAGGTAAAGGTACATCAGCAGCAGATGCAGT
TGAAGTTCCAGCACCAGCAGCAGTTTTAGGTGGTCCAGAACCATTAATGCAAGCAACAGCATGGTTAAATGCATATTTTCATCAACCAGA
AGCAATTGAAGAATTTCCAGTTCCAGCATTACATCATCCAGTTTTTCAACAAGAATCATTTACACGTCAAGTTTTATGGAAATTATTAAAA
GTTGTTAAATTTGGTGAAGTTATTTCATATTCACATTTAGCAGCATTAGCAGGTAATCCAGCAGCAACAGCAGCAGTTAAAACAGCATTA
TCAGGTAATCCAGTTCCAATTTTAATTCCATGTCATCGTGTTGTTCAAGGTGATTTAGATGTTGGTGGTTATGAAGGTGGTTTAGCAGTTA
AAGAATGGTTATTAGCACATGAAGGTCATCGTTTAGGTAAACCAGGTTTAGGTTAAATTTATAACTCTATCCAAAGACATACAGTCAAT
ACAAAGAATTATGTATCTATACAACAGTAATCATGCATTCTATGATGCTTCTAACTGAATTAAAGCATCGAACAATCGGAAGCATATTTCT
AAATTATTTATTCATTATAGTCTTAAACATAACATGACCTAATATATTACTAACCTATTAAAATAAACCACGCACATCTAAGTGATATACGA
CAATCACAGCAATAATAATTGCTTTAGAAAGTCGTACCGAACTGGAACTTACAAGTCTAGTTCGAACACACACTGATGTGAGTGGTTTTC
TTTATTTTAAACATGAACAATCAGATAAGTTACTAGCATTAGCAAATATTATTAAATCAAAGGGCTTCGATTCATAAAATTTAAAACAAT
GATTAAAATTAGACGTGTAAATGTTAAATTCTAAAACGGAAATAACCACCATCCCATTAAACCACTTTTTTGTTCAATCACTATATTTCACA
CAGCTTCATTAATAAAACGAAATTGCTTCAACCCGCTTCAACTTCAGCCTACTTCA

Coa gene (partial), linker, SNAP, stop codon, Coa downstream region (partial)

Primers **OutF***, c2F, c2R/c1F, c1R/c3F, c3R, OutR*

Appendix 1.2 vWbp:CLIP sequence

AAAATCTAAAAATGAGTCTGTGGTTTCACTAATCGATGACGAAGACGACAACGAAAACGACAGGCAACTTGTGGTTTCTGCGCCATCA
AAGAAACCAACAACACCGACTACATATACTGAAACAACGACTCAGGTACCAATGCCTACAGTTGAGCGTCAAACTCAGCAACAAATCGT
TTACAAAACACCAAAACCATTAGCTGGATTAAATGGTGAAAGTCATGATTTCACAACAACGCATCAATCACCAACAACTTCAAATCATAC
GCATAATAATGTTGTTGAATTTGAAGAAACGTCTGCTTTACCTGGTAGAAAATCAGGATCACTGGTTGGTATAAGTCAAATTGATTCTTC
TCATCTAACTGAACGTGAGAAGCGTGTAATCAAGCGTGAACACGTTAGAGAAGCTCAAAAGTTAGTTGATAATTATAAAGATACACATA
GTTATAAAGACCGATTAAATGCACAACAAAAAGTAAATACTTTAAGTGAAGGTCATCAAAAACGTTTTAATAAACAAATCAATAAAGTA
TACAATGGCAAATCAGGTGGTGGAGGAGATAAAGATTGTGAAATGAAACGTACAACATTAGATTCACCATTAGGTAAATTAGAATTAT
CAGGTTGTGAACAAGGTTTACATCGTATTATTTTTTTAGGTAAAGGTACATCAGCAGCAGATGCAGTTGAAGTTCCAGCACCAGCAGCA
GTTTTAGGTGGTCCAGAACCATTAATTCAAGCAACAGCATGGTTAAATGCATATTTTCATCAACCAGAAGCAATTGAAGAATTTCCAGTT
CCAGCATTACATCATCCAGTTTTTCAACAAGAATCATTTACACGTCAAGTTTTATGGAAATTATTAAAAGTTGTTAAATTTGGTGAAGTTA
TTTCAGAATCACATTTAGCAGCATTAGTTGGTAATCCAGCAGCAACAGCAGCAGTTAATACAGCATTAGATGGTAATCCAGTTCCAATTT
TAATTCCATGTCATCGTGTTGTTCAAGGTGATTCAGATGTTGGTCCATATTTAGGTGGTTTAGCAGTTAAAGAATGGTTATTAGCACATG
AAGGTCATCGTTTAGGTAAACCAGGTTTAGGTTAATATTAATGCATGGCTGCAAAGCAAATAATGAGTTTGTCGTAAAAATAACAACAT
TTTAAACTAGCAATAAATAATATCAAAGTCATCATTTCAATGATGCAATCTAGTATAGTCCACATTCTAAACAGGTGTGGACTATTACTTT
TTTCACTTTATATTACGAAAAAATTATTATGCTTAACTATCAATATCAATAATTAATTTTAAGCTGAAAAACAATAAAAATGTTAAGACAAC
GTTTACTTCAAGTTAATTATTATACTGAAAATTCTGGTATATAATGCTGTTAGTGAATATAACAGGGAAATTATATTGGTTATAATATTGA
GTCTATATAAAGGAGAAATAACAGATGAAAAAGAAATTATTAGTTTTAACTATGAGCACGCTATTTGCTACACAACTTATCAATTCAAAT
CACGCTAAAGCATCAGTGACAGAGAGTGTTGACAAAAAATTTGTAGTTCCAGAATCAGGAATTAATAAAATTATTCCAGCTTACGATGA
ATTTAAGAATTCGCCAAAAGTAAATGTTAGTAA

vWbp gene (partial), linker, CLIP, stop codon, vWbp downstream region (partial)

Primers **vOutF**, v2F, v2R/v1F, v1R/v3F, v3R, vOutR

Appendix 2. msfGFP fusion sequences

Appendix 2.1 Tat:msfGFP sequence

AGGAGGGTACATGACAAATTATGAACAAGTTAATGATTCAACACAATTTTCACGTCGTACATTTTTAAAAATGTTAGGTATTGGTGGTGCAGGTGTTGCAA
TTGGTGCATCAGGTGGTGGAGGATCAAAAGGTGAAGAATTATTTACAGGTGTTGTTCCAATTTTAGTTGAATTAGATGGTGATGTTAATGGTCATAAATTT
TCAGTTCGTGGTGAAGGTGAAGGTGATGCAACAAATGGTAAATTAACATTAAAATTTATTTGTACAACAGGTAAATTACCAGTTCCATGGCCAACATTAGT
TACAACATTAACATATGGTGTTCAATGTTTTTCACGTTATCCAGATCATATGAAACAACATGATTTTTTTAAATCAGCAATGCCAGAAGGTTATGTTCAAGA
ACGTACAATTTCATTTAAAGATGATGGTACATATAAAACACGTGCAGAAGTTAAATTTGAAGGTGATACATTAGTTAATCGTATTGAATTAAAAGGTATTG
ATTTTAAAGAAGATGGTAATATTTTAGGTCATAAATTAGAATATAATTTTAATTCACATAATGTTTATATTACAGCAGATAAACAAAAAAATGGTATTAAAG
CAAATTTTAAAATTCGTCATAATGTTGAAGATGGTTCAGTTCAATTAGCAGATCATTATCAACAAAATACACCAATTGGTGATGGTCCAGTTTTATTACCAG
ATAATCATTATTTATCAACACAATCAAAATTATCAAAAGATCCAAATGAAAAACGTGATCATATGGTTTTATTAGAATTTGTTACAGCAGCAGGTATTACAC
ATGGTATGGATGAATTATATAAATAA

Shine-Dalgarno sequence, Tat-SP, linker, msfGFP

Appendix 2.2 Sec:msfGFP sequence

AGGAGGGTACATGAAAAAATGTATTAAAACATTATTTTTATCAATTATTTTAGTTGTTATGTCAGGTTGGTATCATTCAGCACATGCATCAGGTGGTGGAG
GATCAAAAGGTGAAGAATTATTTACAGGTGTTGTTCCAATTTTAGTTGAATTAGATGGTGATGTTAATGGTCATAAATTTTCAGTTCGTGGTGAAGGTGAA
GGTGATGCAACAAATGGTAAATTAACATTAAAATTTATTTGTACAACAGGTAAATTACCAGTTCCATGGCCAACATTAGTTACAACATTAACATATGGTGTT
CAATGTTTTTCACGTTATCCAGATCATATGAAACAACATGATTTTTTTAAATCAGCAATGCCAGAAGGTTATGTTCAAGAACGTACAATTTCATTTAAAGAT
GATGGTACATATAAAACACGTGCAGAAGTTAAATTTGAAGGTGATACATTAGTTAATCGTATTGAATTAAAAGGTATTGATTTTAAAGAAGATGGTAATAT
TTTAGGTCATAAATTAGAATATAATTTTAATTCACATAATGTTTATATTACAGCAGATAAACAAAAAAATGGTATTAAAGCAAATTTTAAAATTCGTCATAAT
GTTGAAGATGGTTCAGTTCAATTAGCAGATCATTATCAACAAAATACACCAATTGGTGATGGTCCAGTTTTATTACCAGATAATCATTATTTATCAACACAA
TCAAAATTATCAAAAGATCCAAATGAAAAACGTGATCATATGGTTTTATTAGAATTTGTTACAGCAGCAGGTATTACACATGGTATGGATGAATTATATAA
ATAA

Shine-Dalgarno sequence, Sec-SP, linker, msfGFP

Appendix 2.3 Coa:msfGFP sequence

GTGAAATATAGAGATGCTGGTACAGGTATCCGTGAATACAACGATGGAACATTTGGATATGAAGCGAGACCAAGATTCAACAAGCCAAGTGAAACAAAT
GCATACAACGTAACGACAAATCAAGATGGCACAGTATCATACGGAGCTCGCCCAACACAAAACAAGCCAAGTGAAACAAACGCATATAACGTAACAACAC
ATGCAAATGGTCAAGTATCATACGGTGCTCGCCCAACACAAAACAAGCCAAGCAAAACAAATGCATACAACGTAACAACACATGCAAATGGTCAAGTATC
ATATGGCGCTCGCCCGACACAAAAAAAGCCAAGCAAAACAAATGCATATAACGTAACAACACATGCAAATGGTCAAGTATCATACGGAGCTCGCCCGACA
TACAAGAAGCCAAGCGAAACAAATGCATACAACGTAACAACACATGCAAATGGTCAAGTATCATATGGCGCTCGCCCGACACAAAAAAAGCCAAGCGAA
ACAAACGCATATAACGTAACAACACATGCAGATGGTACTGCGACATATGGGCCTAGAGTAACAAAATCAGGTGGTGGAGGATCAAAAGGTGAAGAATTA
TTTACAGGTGTTGTTCCAATTTTAGTTGAATTAGATGGTGATGTTAATGGTCATAAATTTTCAGTTCGTGGTGAAGGTGAAGGTGATGCAACAAATGGTAA
ATTAACATTAAAATTTATTTGTACAACAGGTAAATTACCAGTTCCATGGCCAACATTAGTTACAACATTAACATATGGTGTTCAATGTTTTTCACGTTATCCA
GATCATATGAAACAACATGATTTTTTTAAATCAGCAATGCCAGAAGGTTATGTTCAAGAACGTACAATTTCATTTAAAGATGATGGTACATATAAAACACGT
GCAGAAGTTAAATTTGAAGGTGATACATTAGTTAATCGTATTGAATTAAAAGGTATTGATTTTAAAGAAGATGGTAATATTTTAGGTCATAAATTAGAATA
TAATTTTAATTCACATAATGTTTATATTACAGCAGATAAACAAAAAAATGGTATTAAAGCAAATTTTAAAATTCGTCATAATGTTGAAGATGGTTCAGTTCA
ATTAGCAGATCATTATCAACAAAATACACCAATTGGTGATGGTCCAGTTTTATTACCAGATAATCATTATTTATCAACACAATCAAAATTATCAAAAGATCC
AAATGAAAAACGTGATCATATGGTTTTATTAGAATTTGTTACAGCAGCAGGTATTACACATGGTATGGATGAATTATATAAATAAATTTATAACTCTATCCA
AAGACATACAGTCAATACAAAGAATTATGTATCTATACAACAGTAATCATGCATTCTATGATGCTTCTAACTGAATTAAAGCATCGAACAATCGGAAGCAT
ATTTCTAAATTATTTATTCATTATAGTCTTAAACATAACATGACCTAATATATTACTAACCTATTAAAATAAACCACGCACATCTAAGTGATATACGACAATC
ACAGCAATAATAATTGCTTTAGAAAGTCGTACCGAACTGGAACTTACAAGTCTAGTTCGAACACACACTGATGTGAGTGGTTTTCTTTATTTTAAACATGAA
CAATCAGATAAGTTACTAGCATTAGCAAATATTATTAAATCAAAGGGCTTCGATTCATAAAATTTAAAACAATGATTAAAATTAGACGTGTAAATGTTAAAT
TCTAAAACGGAAATAACCACCATCCCATTAAACCACTTTTTTGTTCAATCACTATATTTCACACAGCTTCATTAATAAAACGAAATTGCTTCAACCCGCTTCA
ACTTCAGCCTACTTCA

Coa upstream, linker, msfGFP, Coa downstream

Appendix 3. SNAP:Embp and msfGFP:Embp sequences

Appendix 3.1 SNAP:Embp sequence

CTTATCAAAGTCACTCGCAGAAATATATACGAAAGTTCCAATTGAAACAGACAAACTTTTTAAAGAGATGACATATGCTCATACACTAAATGAGATTTTAT
CCATTTGTAATGAACATGAACTATACGTTTCAAGTAAATATATTGCAAGTCACCTCTAACCATAAACCAATGAACATTTCATTTAGATATTGTTCATTGGTTT
TTTTAATATCAATAAGCATCTCCATCAAAAATATAAATATTTTATTAAAACTTTGTGAATTAATTTCACAAAGTTATCTTAAAGTGATATTATTGTTTAGAACA
AATAAATTGTTGTTCAAAATGCTATTGTGATAAATGAAGAGCAAACCGAAATCAAATGGTCGGAACATCTGCTCTTTTTTATTGGGCAAATGTATAAGTTAT
TCATTGTCAAAATTATCAACATTAAATACGTATAATTTTCAAATCACATCAAACAACAAAGAAAAAACATCAAGAATAGGAGTGGCAATAGCTTTGAATAA
TCGTGATAAATTACAAAAATTTAGTATCCGAAAATACGCAATTGGAACATTTTCTACTGTGATTGCAACACTTGTGTTCATGGGTATCAATCCAAAAGATA
AAGATTGTGAAATGAAACGTACAACATTAGATTCACCATTAGGTAAATTAGAATTATCAGGTTGTGAACAAGGTTTACATCGTATTATTTTTTAGGTAAA
GGTACATCAGCAGCAGATGCAGTTGAAGTTCCAGCACCAGCAGCAGTTTTAGGTGGTCCAGAACCATTAATGCAAGCAACAGCATGGTTAAATGCATATT
TTCATCAACCAGAAGCAATTGAAGAATTTCCAGTTCCAGCATTACATCATCCAGTTTTTCAACAAGAATCATTTACACGTCAAGTTTTATGGAAATTATTAAA
AGTTGTTAAATTTGGTGAAGTTATTTCATATTCACATTTAGCAGCATTAGCAGGTAATCCAGCAGCAACAGCAGCAGTTAAAACAGCATTATCAGGTAATC
CAGTTCCAATTTTAATTCCATGTCATCGTGTTGTTCAAGGTGATTTAGATGTTGGTGGTTATGAAGGTGGTTTAGCAGTTAAAGAATGGTTATTAGCACATG
AAGGTCATCGTTTAGGTAAACCAGGTTTAGGTGGAGGAGGTGGTTCACATGCAAGTGCCGACGAGTTGAATCAAAATCAAAAGTTAATTAAACAATTAA
ATCAAACAGATGATGATGATTCGAATACGCATAGTCAAGAAATCGAAAATAACAAACAAAATTCAGCTGGGCAGACTGAATCATTAAGTTCATCAACTAG
TCATAATCAAGCAAATGCACGACTGTCGGATCAAGTCAAAGACCCTAATGAAACATCGCAACAATTACCTACAAATGTTTCTAATGATAGTATCAATCAATC
GCATAATGAAACAAATATGAATAACGAACCATTGCAAGTTGATAATAGTACTATGCAAGCACATAGTAAAAAAGTAAGCGATAGCAATGGAAATACTTCT
GGAAATGAACATCATAAACTAACAGAAAATGTACTTGCGGAAAGCCGAGCAAGTAAAAATGACAAAGAAAAAGAGAATCTACAAGAGAAAGATAAACC
ACAGCAAGTACAGCCACCATTAGATAAAAATGCATTACAAGCTTTTTTTGACGCATCATACTACAATTACAGAATGATTGATAGAGATCGTGCGGATACAA
CAGAATATCAAAAAGTCAAATCTGCTTTTGACTACGTCGGTAC

Upstream of Embp (partial), Embp start codon, Embp upstream of insertion site, SNAP, linker, Cleavage site, Embp downstream insertion site (partial)

Primers 2F, **Embp_IntegrationF**, SNAP_2R, **SNAP_1F**, SNAP_1R, 3F, **Embp_IntegrationR**, 3R

Appendix 3.2 msfGFP:Embp sequence

CTTATCAAAGTCACTCGCAGAAATATATACGAAAGTTCCAATTGAAACAGACAAACTTTTTAAAGAGATGACATATGCTCATACACTAAATGAGATTTTAT
CCATTTGTAATGAACATGAACTATACGTTTCAAGTAAATATATTGCAAGTCACCTCTAACCATAAACCAATGAACATTTCATTTAGATATTGTTCATTGGTTT
TTTTAATATCAATAAGCATCTCCATCAAAAATATAAATATTTTATTAAAACTTTGTGAATTAATTTCACAAAGTTATCTTAAAGTGATATTATTGTTTAGAACA
AATAAATTGTTGTTCAAAATGCTATTGTGATAAATGAAGAGCAAACCGAAATCAAATGGTCGGAACATCTGCTCTTTTTTATTGGGCAAATGTATAAGTTAT
TCATTGTCAAAATTATCAACATTAAATACGTATAATTTTCAAATCACATCAAACAACAAAGAAAAAACATCAAGAATAGGAGTGGCAATAGCTTTGAATAA
TCGTGATAAATTACAAAAATTTAGTATCCGAAAATACGCAATTGGAACATTTTCTACTGTGATTGCAACACTTGTGTTCATGGGTATCAATCCAAAATCAA
AAGGTGAAGAATTATTTACAGGTGTTGTTCCAATTTTAGTTGAATTAGATGGTGATGTTAATGGTCATAAATTTTCAGTTCGTGGTGAAGGTGAAGGTGAT
GCAACAAATGGTAAATTAACATTAAAATTTATTTGTACAACAGGTAAATTACCAGTTCCATGGCCAACATTAGTTACAACATTAACATATGGTGTTCAATGT
TTTTCACGTTATCCAGATCATATGAAACAACATGATTTTTTTAAATCAGCAATGCCAGAAGGTTATGTTCAAGAACGTACAATTTCATTTAAAGATGATGGT
ACATATAAAACACGTGCAGAAGTTAAATTTGAAGGTGATACATTAGTTAATCGTATTGAATTAAAAGGTATTGATTTTAAAGAAGATGGTAATATTTTAGG
TCATAAATTAGAATATAATTTTAATTCACATAATGTTTATATTACAGCAGATAAACAAAAAAATGGTATTAAAGCAAATTTTAAAATTCGTCATAATGTTGA
AGATGGTTCAGTTCAATTAGCAGATCATTATCAACAAAATACACCAATTGGTGATGGTCCAGTTTTATTACCAGATAATCATTATTTATCAACACAATCAAA
ATTATCAAAAGATCCAAATGAAAAACGTGATCATATGGTTTTATTAGAATTTGTTACAGCAGCAGGTATTACACATGGTATGGATGAATTATATAAAGGA
GGAGGTGGTTCACATGCAAGTGCCGACGAGTTGAATCAAAATCAAAAGTTAATTAAACAATTAAATCAAACAGATGATGATGATTCGAATACGCATAGT
CAAGAAATCGAAAATAACAAACAAAATTCAGCTGGGCAGACTGAATCATTAAGTTCATCAACTAGTCATAATCAAGCAAATGCACGACTGTCGGATCAAG
TCAAAGACCCTAATGAAACATCGCAACAATTACCTACAAATGTTTCTAATGATAGTATCAATCAATCGCATAATGAAACAAATATGAATAACGAACCATTGC
AAGTTGATAATAGTACTATGCAAGCACATAGTAAAAAAGTAAGCGATAGCAATGGAAATACTTCTGGAAATGAACATCATAAACTAACAGAAAATGTACT
TGCGGAAAGCCGAGCAAGTAAAAATGACAAAGAAAAAGAGAATCTACAAGAGAAAGATAAACCACAGCAAGTACAGCCACCATTAGATAAAAATGCATT
ACAAGCTTTTTTTGACGCATCATACTACAATTACAGAATGATTGATAGAGATCGTGCGGATACAACAGAATATCAAAAAGTCAAATCTGCTTTTGACTACG
TCGGTAC

Upstream of Embp (partial), Embp start codon, Embp upstream of insertion site, msfGFP, linker, Cleavage site, Embp downstream insertion site (partial)

Primers 2F, **Embp_IntegrationF**, GFP_2R, **GFP_1F**, GFP_1R, 3F, **Embp_IntegrationR**, 3R

Appendix 4. Derivations of Bessel-Gauss beam shape equations

Appendix 4.1 Derivation for $r_p = \frac{2.4048\lambda}{2\pi\beta}$

The radial part of Equation (9) is governed by the zeroth order Bessel function J_0. The radius of the central lobe occurs when $J_0(x)$ first equals zero, which is at $x = 2.4048$. Therefore,

$$J_0\left(\frac{2\pi r_p \beta}{\lambda}\right) = J_0(2.4048), \tag{14}$$

$$\boxed{r_p = \frac{2.4048\lambda}{2\pi\beta}.} \tag{15}$$

Appendix 4.2 Derivation for $L_p = \frac{0.8w_0}{\beta}$

The intensity distribution in Equation (9) varies with z. First it increases, then it decreases. The depth of field is the transverse distance over which the intensity full width half maximum spans at $r = 0$. From (9),

$$I(r = 0, z) = I_0 \frac{4\pi^2\beta^2 z}{\lambda} e^{-\frac{2\beta^2 z^2}{{w_0}^2}} \tag{16}$$

Simplify this by removing some of the constants (this does not affect the calculation):

$$f(z) = ze^{-\frac{2\beta^2 z^2}{{w_0}^2}} \tag{17}$$

Find the maximum value of $f(z)$ and the transverse position it occurs at (z_{max}). Find the maximum by differentiating $f(z)$ using the product rule and setting equal to zero.

$$\frac{df}{dz} = e^{-\frac{2\beta^2 z^2}{{w_0}^2}} - \frac{4\beta^2 z^2}{{w_0}^2} e^{-\frac{2\beta^2 z^2}{{w_0}^2}} = 0 \tag{18}$$

$$z_{max} = \frac{w_0}{2\beta} \tag{19}$$

$$f(z_{max}) = \frac{w_0}{2\beta} e^{-0.5} \tag{20}$$

Then find the values of z at which the half maxima occur ($z_{0.5}$). The depth of field, L_p, is the difference between these values. Find $f(z_{0.5})$, set it equal to $f(z)$, and solve for z to get $z_{0.5}$.

$$f(z_{0.5}) = \frac{f(z_{max})}{2} = \frac{w_0}{4\beta} e^{-0.5} \tag{21}$$

$$f(z_{0.5}) = z_{0.5} e^{-\frac{2\beta^2 {z_{0.5}}^2}{{w_0}^2}} = \frac{w_0}{4\beta} e^{-0.5} \tag{22}$$

Substitute $u = z_{0.5}\beta/w_0$ and solve for u:

$$ue^{-2u^2} = \frac{e^{-0.5}}{4} \tag{23}$$

$$u = 0.960811 \; and \; 0.159553 \tag{24}$$

$$\Delta u = \frac{L_p \beta}{w_0} \approx 0.8 \tag{25}$$

$$\boxed{L_p \approx \frac{0.8 w_0}{\beta}} \tag{26}$$

Appendix 4.3 Derivation of $r_s = \frac{2.4048\lambda}{2\pi\beta}\left(\frac{Ff_1}{f_\alpha f_2}\right)$ and $L_s = \frac{0.8w_0}{\beta}\left(\frac{Ff_1}{f_\alpha f_2}\right)^2$

When magnifying the annulus of light produced by an axicon by m, $\beta \rightarrow \beta_s$ and $w_0 \rightarrow w_s$. To get r_s, and L_s, derive equations for β_s and w_s and substitute these into the equations for r_p and L_p. See Figure 35 for the lens order and focal lengths.

The radius R of the annulus before magnification is

$$R = f_\alpha tan\beta \tag{27}$$

After magnification $m = f_2/f_1$ the annulus radius is

$$R_s = mR = \frac{f_2 f_\alpha}{f_1} tan\beta = F tan\beta_s \tag{28}$$

$$tan\beta_s = \frac{f_2 f_\alpha}{f_1 F} tan\beta \tag{29}$$

The incoming beam radius is w_0. This is also the width of the annular light. w_0 is magnified twice, once by f_1/f_α, and once by F/f_2. Hence

$$w_s = \frac{f_1}{f_\alpha} . \frac{F}{f_2} w_0 \tag{30}$$

Using the small angle approximation $tan\beta \approx \beta$:

$$\boxed{r_s = \frac{2.4048\lambda}{2\pi\beta_s} = \frac{2.4048\lambda}{2\pi\beta}\left(\frac{Ff_1}{f_\alpha f_2}\right)} \tag{31}$$

$$\boxed{L_s = \frac{0.8w_s}{\beta_s} = \frac{0.8w_0}{\beta}\left(\frac{Ff_1}{f_\alpha f_2}\right)^2} \tag{32}$$